Artificial Intelligence Tools for Pulseless Electrical Activity Characterization during Cardiac Arrest

By

Jon Urteaga Urizarbarrena

Supervisors:

Elisabete Aramendi Ecenarro

Andoni Elola Artano

Doctoral Thesis

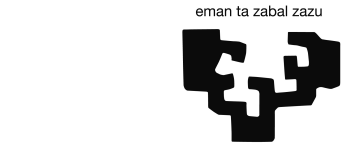

Department of Communications Engineering

To my parents,
all this would not be
possible without their efforts

ACKNOWLEDGEMENTS

Foremost, I would like to thank my supervisors Eli, Unai and Andoni for their unconditional support, guidance and tireless effort. Eli, for offering me the opportunity to embark on my research journey during my bachelor's degree, for all your guidance over the years, and for your dedication. Unai†, for always being willing to help and for your rigorous approach to research; I hope you are proud of the outcome of the thesis. Andoni, for the countless hours you have dedicated to this work, for all your brilliant ideas, and especially for the personal support you have given me. This thesis would not have been possible without your continued encouragement and confidence in my work.

I am also deeply grateful to my group colleagues. Erik, your willingness to lend a hand and your contagious energy have been truly motivating. Iraia, your unwavering support and encouragement during challenging moments have been indispensable. Xabier, for sharing your knowledge and always being willing to help. Diego and Amaia, for the time we spent together in the lab; your jokes and conversations made the long hours of work much more bearable.

I extend my heartfelt gratitude to the numerous individuals and institutions whose contributions have been essential to the completion of this thesis. To the research groups of Ahamed Idris and Lars Wik for sharing clinical data and expertise. In particular, to the group of Eirik Skogvoll at NTNU for hosting me in Trondheim during my research stay and providing an exceptional hospitality. Additionally, I wish to acknowledge the University of the Basque Country, the Basque Government, and the relevant Spanish ministries for their steadfast structural and financial support.

And last but not least, thanks to my family and friends for their unconditional support and for enduring so many hours. I am so grateful to my parents, Juan and Arritxu, for their endless love, support and sacrifices in raising me and preparing for the future. To

my grandmother, Maritxu, you have been a source of strength and comfort throughout my journey. To Leire, my sister, for being my rock in hard moments. To Daniel, for your constant presence and attentive listening whenever I needed it.

ABSTRACT

Sudden cardiac arrest (SCA) is a critical medical condition that abruptly interrupts the function of the heart and often leads to sudden cardiac death (SCD). It is categorized into in-hospital cardiac arrest (IHCA) and out-of-hospital cardiac arrest (OHCA). The incidence of IHCA ranges from 0.78 to 4.60 per 1000 admissions, with survival rates around 25 % in the USA and up to 35 % in Europe. In contrast, the incidence of OHCA varies widely, from 50 to 100 per 100000 person-years, with survival rates below 8 %.

During SCA, pulseless electrical activity (PEA) may occur, in which organized cardiac electrical activity is present, but there are no effective mechanical contractions producing a palpable pulse. Studies of OHCA indicate a prevalence of 20-30 %, whereas studies of IHCA indicate rates of up to 40-60 % as the first rhythm during SCA. Recent data reveal a worrying increase in the prevalence of PEA during IHCA from 36 % in 2000 to 46 % in 2009, reflecting similar trends during OHCA cases.

Researchers and clinicians are actively investigating PEA, focusing on parameters such as heart rate and QRS complex width to obtain prognostic information about the outcome. Despite their efforts, the results remain inconsistent. Furthermore, there is a notable absence of an automated method that leverages biomedical signals for outcome prediction in cases of SCA. This underscores the strong need for further research to fill this gap and improve patient outcomes in cases of IHCA and OHCA.

This thesis presents innovative approaches to monitor the prognosis of PEA in patients with SCA. Predictive models were developed using sophisticated signal processing methodologies and machine learning techniques. The algorithms aimed at distinguishing between favorable and unfavorable PEA rhythms were devised by harnessing the electrocardiogram as well as other biomedical signals such as thoracic impedance and invasive arterial blood pressure. The effec-

tiveness of these algorithms in discriminating the potential outcome of SCA was validated by a retrospective analysis of complete SCA episodes.

Patients experiencing SCA may show signals characterized by higher noise levels and more erratic fluctuations compared to stable patients. Therefore, in this thesis specific delineators adapted to these contexts have been developed. On the one hand, a delineator of the QRS complex based on deep learning architectures was designed. On the other hand, a IBP signal delineator has been devised employing adaptive thresholds and advanced signal processing techniques. This enables the automatic measurement of features derived from these signals during SCA episodes.

This thesis project demanded authentic real-world SCA datasets. To formulate solutions using deep and machine learning algorithms, it was imperative to access carefully annotated datasets with rhythm, outcome, and QRS complexes, ensuring training efficacy. Through collaboration with clinical research cohorts, rigorous evaluation of proposed solutions was made possible, leveraging datasets that encompassed both IHCA and OHCA scenarios.

CONTENTS

1 Introduction 1
1.1 Sudden cardiac arrest . . . 1
1.2 Resuscitation therapy . . . 2
1.3 Monitor Defibrillators . . . 4
1.4 Biomedical Signals . . . 6
1.5 Pulseless Electrical Activity . . . 7
1.6 Prognosis prediction . . . 9
1.7 Motivation . . . 11

2 Background 13
2.1 PEA prognosis prediction . . . 13
2.2 Characterization of ECG, TI and IBP signals . . . 15
2.2.1 Waveform features . . . 16
2.2.2 QRS complex features . . . 18
2.2.3 ABP features . . . 19
2.3 Artificial intelligence models in resuscitation . . . 20
2.3.1 ML Models . . . 21
2.3.2 DL Models . . . 23
2.3.3 Evaluation . . . 26
2.4 ECG delineators . . . 27
2.4.1 Hamilton-Topkins ECG delineator . . . 27
2.4.2 Li et al. ECG delineator . . . 29
2.4.3 Martinez et al. ECG delineator . . . 30
2.4.4 Peimankar et al. ECG delineator . . . 31
2.5 IBP delineators . . . 32
2.5.1 Zong et al. IBP delineator . . . 32
2.5.2 Li et al. IBP delineator . . . 33

3 Hypothesis and objectives 35

4 Results 37
4.1 Results related to objective 1 . . . 37

4.1.1 J1.1: A Machine Learning Model for the Prognosis of Pulseless Electrical Activity during Out-of-Hospital Cardiac Arrest 38
4.1.2 J1.2: Machine learning model to predict evolution of pulseless electrical activity during in-hospital cardiac arrest . . 40
4.1.3 C1.1: A Random Forest Model for Pulseless Electrical Activity Prognosis Prediction During Out-of-Hospital Cardiac Arrest Using Invasive Blood Pressure 43
4.2 Results related to objective 2 45
4.2.1 J2.1: A Deep Learning Model for QRS Delineation in Organized Rhythms during In-Hospital Cardiac Arrest 45
4.2.2 J2.2: Invasive Arterial Blood Pressure Delineator for Cardiopulmonary Resuscitation Patients during Pauses of Chest Compressions 49

5 Conclusions 53
5.1 Main contributions of the thesis 53
5.2 Publications 54
5.2.1 Journals indexed in the JCR science edition 54
5.2.2 National and international conferences 55
5.3 Financial support 56
5.4 Future lines of research 57

Bibliography 59

A Published and submitted studies 79
A.1 Publications associated to objective 1 81
A.1.1 First journal paper 81
A.1.2 First conference paper 99
A.1.3 Second journal paper 103
A.1.4 Second conference paper 123
A.2 Publications associated to objective 2 131
A.2.1 First conference paper 131
A.2.2 First journal paper 137
A.2.3 Second conference paper 149
A.2.4 Second journal paper 155

LIST OF FIGURES

Figure 1.1 SCA rhythms 2
Figure 1.2 Chain of survival 3
Figure 1.3 ZOLL Medical AED 5
Figure 1.4 Physio-Control Lifepak-15 Monitor/Defibrillator 6
Figure 1.5 Example of ECG, TI and IBP signals 8
Figure 1.6 PEA segments 9
Figure 2.1 QRS complex features 19
Figure 2.2 IBP features 20
Figure 2.3 Pooling layer 24
Figure 2.4 Convolutional layer 24
Figure 2.5 Fully Connected Layer 25
Figure 4.1 ECG, TI and ICC segments for faPEA and unPEA 39
Figure 4.2 ModAMSA spectrum 42
Figure 4.3 U-Net architecture 47
Figure 4.4 QRS delineation performance for PEA and PR segments 48
Figure 4.5 IBP delineation example 50

LIST OF TABLES

Table 2.1 Summary of the main references in PEA prognosis prediction. 15
Table 4.1 Performance of J1.1 and SoA algorithms for faPEA/unPEA discriminator 41
Table 4.2 Performance of J1.2 for faPEA/unPEA discriminator 43
Table 4.3 Performance of C1.1 with different signals for faPEA/unPEA discriminator 45
Table 4.4 QRS delineation performance for IHCA dataset 48
Table 4.5 QRS delineation performance for QT dataset . 49
Table 4.6 Performance of IBP delineator for heartbeat detection 51
Table 4.7 Performance of IBP delineator for pulsed segment discrimination 52

LIST OF ABBREVIATIONS

Adam	Adaptive Moment Estimation
AED	Automated external defibrillator
AHA	American Heart Association
AMSA	Amplitude spectrum area
ANN	Artificial neural network
ALS	Advanced life support
ARB	Autoregressive Burg's values
AUC	Area under the curve
BAC	Balanced Accuracy
bpm	Beats per minute
CC	Chest compressions
CNN	Convolutional Neural Network
CPC	Cerebral performance category
CPR	Cardiopulmonary resuscitation
CSL	Complex Systems Laboratory
CV	Cross-validation
DAP	Diastolic arterial pressure
DL	Deep learning
ECG	Electrocardiogram
EMS	Emergency Medical System
ERC	European Resuscitation Council
faPEA	Favorable PEA
FN	False Negative

FP	False Positive
HR	Heart rate
ICC	Thoracic impedance circulation component
IBP	Invasive arterial blood pressure
IHCA	In-hospital cardiac arrest
JCR	Journal Citation Reports
LR	Logistic regression
LSTM	Long short-term memory
MAP	Mean Arterial Pressure
ML	Machine learning
NPV	Negative Predictive Value
OHCA	Out-of-hospital cardiac arrest
PEA	Pulseless electrical activity
PP	Pulse pressure
PPV	Positive Predictive Value
PR	Pulsed rhythm
RF	Random Forest
ROSC	Return of spontaneous circulation
SAP	Systolic arterial pressure
SCA	Sudden cardiac arrest
SCD	Sudden cardiac death
Se	Sensitivity
SNEO	Smoothed Nonlinear Energy Operator

SoA	State of the Art
Sp	Specificity
SSF	Slope sum function
SVM	Support Vector Machines
SWT	Stationary Wavelet Transform
TI	Thoracic impedance
TN	True Negative
TP	True Positive
unPEA	Unfavorable PEA
USA	United States of America
VF	Ventricular fibrillation
VT	Ventricular tachycardia
WT	Wavelet Transforms

1 INTRODUCTION

1.1 Sudden cardiac arrest

Sudden cardiac arrest (SCA) is defined as the abrupt cessation of cardiac system which may result in sudden cardiac death (SCD) [1]. It is typically categorized into two distinct classifications: in-hospital cardiac arrest (IHCA) and out-of-hospital cardiac arrest (OHCA) [2]. The incidence of IHCAs has been noted to vary between 0.78 and 4.60 per 1000 patient admitted in the hospital. Patient survival rates to hospital discharge or within 30 days post-IHCA have been reported to be approximately 25 % in the United States of America (USA) and up to 35 % in European countries [3–6]. The incidence of OHCA is approximately 55 per 100000 person-years in Europe and between 50 and 100 per 100000 person-years in the USA. Despite wide research in protocols and interventions during OHCA, survival rates have exhibited minimal variation, persisting below 8 % [7–9].

Based on the Utstein 2014 categorization of etiology [10], SCAs can be divided into medical and non-medical causes. The vast majority (more than 90 %) fall under the medical category, with approximately 50 to 80 % attributed to cardiac reasons, while the remainder primarily stem from respiratory, neurological, and cancer-related causes. Conversely, slightly less than 10 % of SCAs are non-medical, with notable causes including traumatic incidents, drowning, asphyxiation, electrocution, and drug overdose [11, 12].

During a SCA event, as response to resuscitation therapy, the patient can show different cardiac rhythms, each with distinct implications for patient prognosis and treatment. SCA rhythms

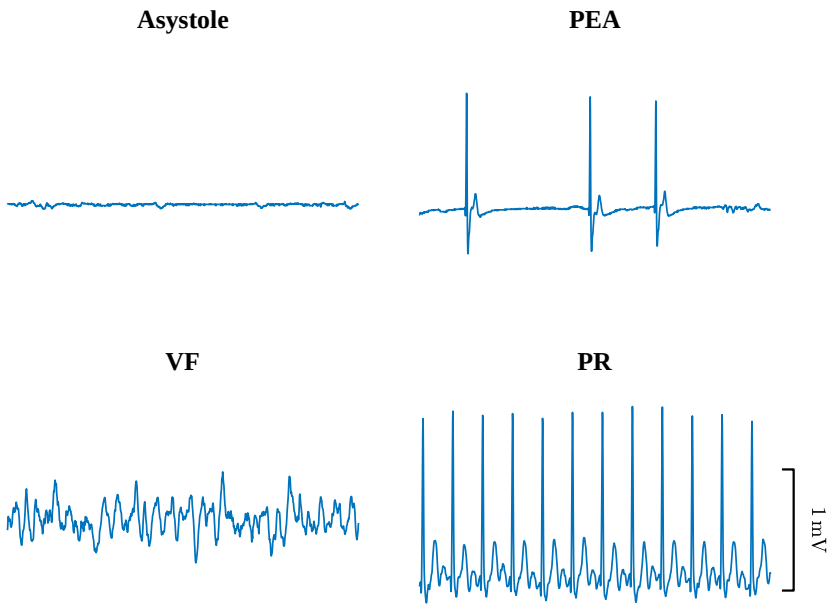

Figure 1.1. Examples of 10 s segments of electrocardiogram (ECG) showing distinct SCA rhythms: asystole, PEA, VF, and PR.

include ventricular fibrillation (VF), occurring in about 20-25 % of cases, pulseless electrical activity (PEA) seen in approximately 30-35 %, and asystole, which constitutes around 35-40 % of cases [13–15]. An illustration of each type of rhythm is available in Figure 1.1. Rapid recognition and appropriate management of these rhythms are crucial for guiding resuscitation efforts and improving the likelihood of successful outcomes in SCA emergencies. The resuscitation manoeuvres should lead the patient towards return of spontaneous circulation (ROSC) characterized by pulsed rhythm (PR).

1.2 Resuscitation therapy

International resuscitation guideline define the framework to systematize and enhance medical emergency interventions during SCA. These guidelines, meticulously compiled and revised approximately every five years, offer evidence-based protocols to ensure consistency and efficacy in resuscitation efforts. Esteemed

organizations such as the European Resuscitation Council (ERC) and the American Heart Association (AHA) are entrusted with the publication and maintenance of these guidelines, with the 2021 and 2020 guidelines in force [16,17].

Resuscitation therapy aims to revive blood flow and oxygen supply leading the patient to ROSC. This involves cardiopulmonary resuscitation (CPR), defibrillation, and advanced life support (ALS) to maintain essential bodily functions until further medical assistance is available [18].

Introduced in 1991 by the AHA [19], the chain of survival (Figure 1.2) outlines critical time-sensitive interventions to maximize survival from OHCA. Though evolving to include additional links, the original four remain fundamental, encompassing essential pre-hospital interventions:

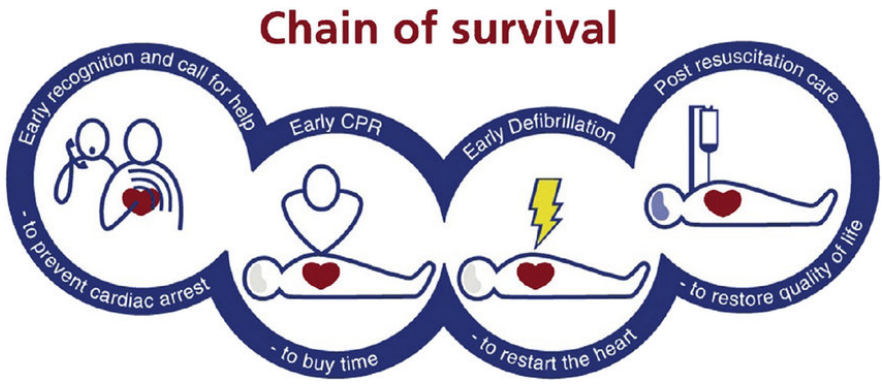

Figure 1.2. The ERC's version of the chain of survival including four main steps: early recognizing, starting CPR quickly, providing defibrillation promptly, and delivering advanced and post-resuscitation cares.

- **Early access:** The first link in the Chain of Survival is early access, which involves rapidly recognizing signs of SCA and promptly calling the local emergency number to activate the Emergency Medical System (EMS). Identifying SCA symptoms before collapse is crucial, as activating EMS prior to the event leads to higher survival rates [20].
- **Early CPR:** Prompt administration of CPR, especially focusing on effective chest compressions (CC), is crucial for patient

survival. Research shows that when bystanders perform CPR, the likelihood of survival rises significantly [21]. This highlights the importance of widespread CPR training programs to educate the general public. The AHA estimates that training 20 % of the population in CPR could notably increase survival rates [22]. Studies indicate that survival rates can double if bystander CPR begins within 4 min of collapse, followed by defibrillation within the first 8 min [23].

- **Early defibrillation:** Defibrillation is essential during SCA, particularly with ventricular arrhythmias like VF or ventricular tachycardia (VT) [24]. These conditions can be corrected with a prompt electrical shock, called defibrillation [25]. Rapid action is crucial as these rhythms deteriorate promptly, leading to SCD if not treated. Shocks administered within 3 to 5 min of collapse have high survival rates of 50 to 70 % [26, 27]. Public access defibrillation programs allow bystanders to use automated external defibrillators (AEDs) before EMS arrival, improving response times [28].
- **Early ALS:** The use of CPR and defibrillation alone may not always be sufficient to regain a normal heart rhythm, and ROSC over an extended period. ALS includes other interventions as intubation or drug administration, and defibrillation [29].

1.3 Monitor Defibrillators

AEDs are fundamental tools utilized in resuscitation scenarios. Their main goal is to facilitate quick defibrillation, making them user-friendly for individuals with minimal training like bystanders [28,30]. Contemporary AEDs offer guidance to the rescuer throughout the process, with features such as audio instructions for pad placement and CPR cessation/resumption. Their ability to swiftly administer essential treatment before professional help arrives can be critical in saving lives [31]. Crucially, they are equipped with algorithms to autonomously assess the patient's heart rhythm and decide if defibrillation is necessary [32].

The standard AED collects two distinct biomedical signals via its defibrillation pads: the electrocardiogram (ECG) and thoracic impedance (TI). Advance AED models, designed for first response professionals like policemen or firefighters, may come equipped with standalone or integrated CPR assist pads (as shown in Figure 1.3). These devices utilize accelerometers and/or force sensors to measure CPR parameters such as CC rate and compression depth, enhancing the effectiveness of resuscitation efforts [33].

Figure 1.3. ZOLL Medical AED 3 BLS defibrillator, which incorporates pads integrated with accelerometers, manufactured in Chelmsford, MA, USA.

More advanced monitor/defibrillators (shown in Figure 1.4), utilized by healthcare providers both pre-hospital and in hospital settings, offer more functionalities than basic AEDs. These devices not only allow manual control of defibrillation but also display real-time continuous waveform data of key physiological parameters. In addition to standard ECG and TI monitoring, these monitor/defibrillators incorporate extra modules for monitoring invasive arterial blood pressure (IBP), pulse oximetry, or capnography. IBP is typically obtained via cannulation of peripheral arteries and it quantifies the pressure exerted by blood on arterial walls [34]. Pulse oximetry, utilizing sensors positioned on the finger, ear, or nose, assesses the oxygen saturation of the blood [35]. Capnography, obtained through sensors placed in the nose or mouth, provides a

measurement of the partial pressure of carbon dioxide in exhaled gases [36].

Figure 1.4. The Physio-Control Lifepak-15 Monitor/Defibrillator is manufactured in Redmond, WA, USA.

Commercial software associated to defibrillators typically enables visualizing and analyzing information and biomedical signals recorded in an electronic file in a proprietary format. Major defibrillator brands like Philips Healthcare (Andover, MA, USA), Stryker/Physio-Control (Redmond, WA, USA), and ZOLL Medical (Chelmsford, MA, USA) play key roles in providing these functionalities. However, converting this data for further examination requires additional tools. Alongside biomedical signal acquisition, comprehensive information about the SCA event is compiled to establish registries. Utstein-style templates ensure consistency in documenting IHCA and OHCA, covering variables such as SCA context, patient demographics, arrest etiology, initial rhythm, CPR and medical intervention specifics, and patient outcomes [10,37].

1.4 Biomedical Signals

ECG provide a non-invasive visual representation of the heart's electrical activity recorded in the resuscitation context through defibrillation pads located in the front-lateral position in the chest of the patient. Of particular interest is the QRS complex, denoting ventricular depolarization and following contraction [38]. Fundamental information such as cardiac rhythm or heart rate

(HR) is obtained from the ECG. Given that the crucial information about cardiac system in an ECG lies within its characteristic wave peaks and boundaries, developing precise methods for automatic ECG delineation is essential [39,40]. Several automatic delineation methods have shown excellent performance in stable patients [40–48], but none have been proposed for patients during SCA.

TI pioneered by Kubicek et al. in 1970 [49], measures the body's resistance to electrical current. It is calculated through Ohm's law using the voltage drop from a high-frequency current passed through pads. Typically operating within a frequency range of 20–100 kHz and a current intensity of $1-5$, mA, TI has been integral in cardiopulmonary research for over five decades, facilitating the measurement of ventilation, respiration, and cardiac output [49–52].

IBP acts as a vital indicator of hemodynamic status, pivotal for monitoring treatment efficacy during SCA therapy [34]. Usually acquired through cannulation in peripheral arteries, IBP waveform analysis holds significance in clinical practice for its ability to delineate cardiac contraction and relaxation, offering essential information on HR, cardiac rhythms, and pressure values [53,54]. IBP waveform reveals distinctive patterns/fiducial-points indispensable for the calculation of physiological parameters. However, during SCA, IBP signals may exhibit distorted waveforms, leading to unreliable fiducial point detection, attributed to factors like patient movement, catheter placement concerns, hemodynamic instability, and high-frequency artifacts [54–56].

In Figure 1.5, a segment is depicted exhibiting the three recorded biomedical signals during an OHCA.

1.5 Pulseless Electrical Activity

PEA is a condition observed during SCA where there is electrical activity in the heart with organized regular ECG as in PR, but no effective mechanical contractions generating a palpable pulse. OHCA studies have recorded a prevalence of 20–30 %, while IHCA studies have reported prevalence of up to 40–60 % [13,57,58]. Over recent decades, there has been an increase in PEA prevalence during IHCA,

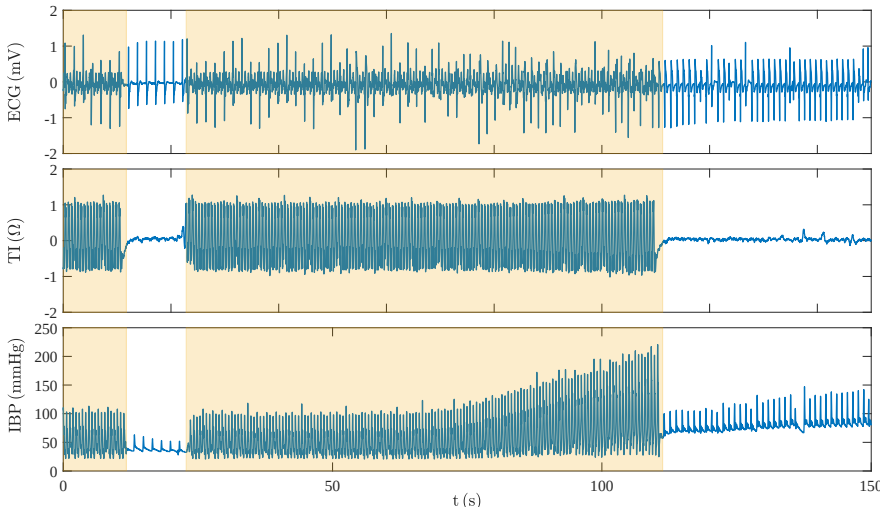

Figure 1.5. Examples of a segment showing the three signals: ECG in the top panel, TI in the central panel, and IBP in the bottom panel. Orange shading indicates the intervals during which CCs are administered.

rising from 36 % in 2000 to 46 % in 2009 [59]. Similar upward trends have been noted during OHCA settings as well [60–62].

In their observational prospective study, Tayal and Kline [63] investigated the distinctions between true-PEA and pseudo-PEA. True-PEA is characterized by the absence of detectable cardiac movement despite the presence of a normal electrical rhythm [64,65]. Conversely, pseudo-PEA exhibits some degree of cardiac movement, albeit insufficient for adequate circulation, often stemming from severe shock states such as hypovolemia or obstruction of cardiac output. Examples of organized PEA, both true and pseudo-PEA, are depicted in Figure 1.6.

The early identification of these reversible etiologies during resuscitation holds significant importance. It enables healthcare professionals to tailor treatment strategies effectively, thereby optimizing the chances of patient survival [65]. As these underlying conditions progress, myocardial contractions may cease entirely, resulting in true-PEA [64,66].

Recent technological advancements have expanded diagnostic tools for SCA, enabling rapid identification of causes and informing clinical

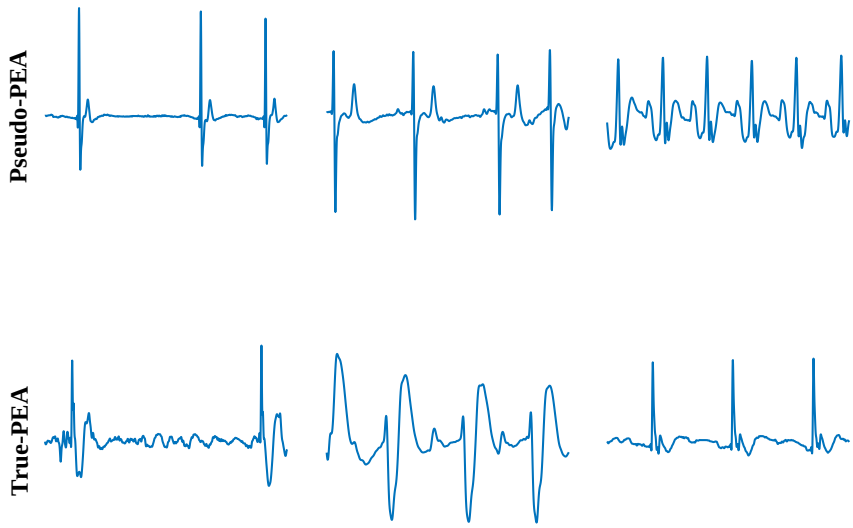

Figure 1.6. Examples of 5 s segments with PEA. In the top row, three pseudo-PEA; in the bottom row, three True-PEA.

decisions. These tools offer vital insights into prognostic outcomes, refining treatment strategies and streamlining SCA management protocols [64, 67, 68]. Numerous studies have investigated the utility of QRS complex characteristics in ECG to differentiate between various causal mechanisms of PEA [69, 70]. Additionally, capnography has gained significant traction as a commonly utilized tool for monitoring OHCA [65].

1.6 Prognosis prediction

Prognosis in medicine entails predicting the likelihood of specific outcomes over a defined period, considering clinical and non-clinical aspects. These outcomes can include events like death or complications, as well as measurable changes such as disease progression or pain levels [71].

In the context of SCA the cardiac rhythm of the patient evolves as response to the resuscitation treatment: defibrillation, CPR, drugs, etc. towards PR in a successful case. Electrical treatment through defibrillation shocks does not guarantee the restoring of PR. It has been proven that unsuccessful shocks may contribute to cardiac

damage and reduce the probability or ROSC. To address this issue, shock prognosis predictors have been proposed [72–77] to optimize the timing of shocks, decrease the number of failed shocks, and minimize myocardial damage.

Predicting rearrest, or the likelihood of a patient experiencing another SCA after regaining a pulse, is essential for improving patient outcomes. Rearrest events are related to poorer outcomes, making prognostic prediction fundamental. Several studies have investigated associated factors [78–80], and automated methods have been proposed to aid in this prediction process [81].

Predicting the prognosis for SCA patients following CPR is pivotal for treatment decisions. Evaluating how patients respond to treatment is vital during SCA to guide resuscitation. Several studies emphasize the necessity of rapid prognosis models to aid clinicians in decision-making. A positive prognosis suggests continuing current efforts unchanged, while a negative prognosis prompts reconsideration, including CPR quality and identifying reversible causes [82–85].

Various prediction models utilize demographic data from the pre-hospital framework to predict survival outcomes or ROSC during SCA. Some employ machine learning (ML) algorithms [86–90] like random forest and support vector machines, while others leverage deep learning (DL) techniques [91–93] such as artificial neural networks (ANN). These models analyze factors like age, gender, event witness or bystander CPR to predict ROSC likelihood, facilitating clinical decision-making. While integration into practice holds promise for enhancing resuscitation outcomes, further research is essential to refine these models and assess their real-world effectiveness [94].

PEA is one of the principal rhythms observed during SCA, which has attracted the attention of researchers and clinicians equally. Among the parameters commonly examined by clinicians are HR and the duration or width of the QRS complex (QRS_w), both of which have been proposed as possible prognostic indicators of SCA. Clinical investigations reveal inconsistency and ambiguity. Whereas some studies have indicated a correlation between initial QRS_w,

HR, and probability of survival [82, 95], others have presented opposing evidence. For instance, certain research has highlighted the prognostic significance of HR alone [96], whereas others have emphasized the importance of QRS_w as an independent predictor of outcome [97]. Notably, there are also studies that have failed to establish a clear association between survival rates and HR or QRS_w [70, 98], further complicating the picture.

Despite much attention to understanding the prognostic factors of PEA, no previous attempts have been made to develop an automated method that leverages biomedical signals to predict its outcomes. This represents a major gap in the current knowledge base, underscoring the need for innovative approaches to unravel the complexities surrounding the prognosis of PEA and potentially improve clinical outcomes.

1.7 Motivation

In recent years, there has been a concerning increase in the incidence of PEA as the initial rhythm in cases of SCA [99]. Despite considerable advancements in studying the prognosis and treatment of that rhythm, the primary parameters correlating with outcome are still calculated manually [82–85]. No automated models have been proposed based on the biomedical signals monitored by monitor defibrillators.

An automated model possesses the capacity to assist rescuers in refining therapeutic approaches, thereby potentially augmenting survival rates. It must discern between PEAs with favorable prognosis (high probability of evolving to ROSC) and those with unfavorable prognosis.

A multimodal approach could include features derived from ECG, TI or IBP have been explored for making alternative predictions and could conceivably be applicable in forecasting the prognosis of PEA [77, 81, 100]. The presently manually computed features could be mechanized to facilitate their integration into automated models [40, 42, 54, 55]. In order to estimate these features, it would be necessary to have the position of the different ECG waves and

the fiducial points of the IBP signal. However, the ECG and IBP delineators have been developed and tested in hemodynamically stable patients; they have not been tested in unstable patients, so their reliability is uncertain.

2 BACKGROUND

2.1 PEA prognosis prediction

In the late nineties, Aufderheide et al. (1989) [95] first analyzed the evolution of patients in PEA during SCA. In that study they compared different ECG patterns in 503 patients attending to OHCA. They observed that successful outcome was linked to fast initial HR, short QRS_w, short QT intervals and high incidence of P waves.

In 2015, Hauck et al. [101] examined how HR and QRS_w relate to survival until hospital discharge in 262 OHCA patients. They focused on patients with a PEA as initial rhythm and analyzed the first 20 s of the episode. Their findings showed no significant difference in survival rates between patients with ”slow” (< 60 beats per minute (bpm)) and ”normal” (60-100 bpm) HR ($p = .16$), nor in survival between patients with ”narrow” (< 120 ms) or ”wide” (> 120 ms) QRS_w ($p = .79$).

Bergum et al. (2016) [70] conducted a retrospective study examining ECG patterns in early PEA and their relation to survival. They analyzed data from 51 IHCA patients, looking at factors like HR, QRS_w, QT interval and presence of P waves. These measurements were taken from three consecutive QRS complexes during the first pause in CC. They classified HR as ”slow”, ”normal”, or ”fast” and QRS complexes as either ”normal” or ”narrow” depending on their width. Them they assessed outcomes like ROSC, 1-hour survival, and hospital discharge. They found no specific patterns linked to the causes of SCA or survival rates.

In Weiser et al.'s study (2018) [96] they examined the initial 60 s of ECG without CC in 504 OHCA patients. Patients were grouped by initial PEA HR (10–24 bpm, 25–39 bpm, 40–59 bpm, $>$ 60 bpm). QRS complexes 120 ms were considered "narrow", while "wide" are $\geq$ 120 ms. Outcomes included 30-day mortality and good neurological outcome (cerebral performance category (CPC) 1 or 2 at day 30). Higher HR was correlated with increased odds of 30-day survival ($p < .0001$ for each frequency category) and good neurological outcome ($p = .001$ for each category). But QRS_w during PEA did not affect outcomes.

Ho et al.'s study (2018) [98] investigated the impact of HR, QRS_w, and the presence of P waves on predicting ROSC. They conducted a retrospective analysis of 332 OHCA patients with PEA rhythm. Survivors showed similar HR (56.8 vs. 52.0 bpm, $p = .53$) and QRS_w (128.7 vs. 129.6 ms, $p = .95$) compared to non-survivors.

Skjeflo et al. (2018) [102] measured the relationship between HR and QRS_w in 74 patients experiencing IHCA. They discovered that increased HR and narrowing of the QRS complex were more common among patients who achieved ROSC. A notable rise in HR was noted in the final 3–6 min preceding ROSC.

In 2021, Kim et al. [97] conducted multivariable logistic regression analyses to examine how the HR and QRS_w relate to hospital discharge. They analyzed data from 3659 patients who experienced OHCA with an initial rhythm of PEA. They found no significant relationship between HR and survival outcomes, however, they found that $QRS_w < 120$ ms increased survival probability (adjusted odds ratio of 3.37).

Our Norwegian collaborators Norvik et al. (2023) [82] investigated 559 segments from 298 patients. Their study aimed to determine how these factors relate to the immediate probability of ROSC during IHCA resuscitation. They found that higher HR and a rising HR were associated with a higher likelihood of ROSC ($p < .0001$), whereas HR was not correlated with the likelihood of transitioning to no-ROSC ($p = .349$). Lower QRS_w and decreasing QRS_w were linked to a higher probability of ROSC ($p < .023$) and a reduced likelihood of no-ROSC ($p = .0002$).

A summary of the references in PEA prognosis prediction is presented in Table 2.1. Between predictors, HR and QRS_w stand out prominently. The conclusions drawn from these studies exhibit some contradictions. While some found correlations between QRS_w, HR, and the outcome [82, 95, 102], others identified correlations only with HR [96] or QRS_w [97]. In the case of Aufderheide et al., no correlation was found between the outcome and any of the predictors [70, 98, 101].

Summary of the studies						
Study	Population type	Number of patients	Inclusion criteria	Features	Outcome	Conclusions
Aufderheide et al. [95]	OHCA	503	Episodes with PEA as the initial rhythm	HR, QRS_w, QT intervals and the presence of P waves	Successful resuscitation	Successfully resuscitated PEA patients showed faster initial HR, shorter QRS_w and QT intervals and more P waves compared to unresponsive patients.
Hauck et al. [101]	OHCA	262	The first 20 s of episodes with PEA as the initial rhythm	HR and QRS_w	Survival until hospital discharge	No significant difference in survival was found based on HR ($<$ 60 vs 60-100 bpm, $p = .16$) or QRS_w ($<$ 120 vs $>$ 120 ms, $p = .79$).
Bergum et al. [70]	IHCA	51	Three consecutive QRS complexes during the first pause in CC	HR, QRS_w, QT intervals and presence of P waves	ROSC, 1-hour survival and hospital discharge	No specific patterns were associated with survival.
Weiser et al. [96]	OHCA	504	Initial 60 s without CC	HR and QRS_w	30-day mortality and good neurological outcome (CPC 1 or 2 at day 30)	Higher HR correlated with increased 30-day survival odds ($p <$ .0001) and better neurological outcomes ($p = .001$). QRS_w had no effect on outcomes.
Ho et al. [98]	OHCA	332	PEA segments	HR, QRS_w, and the presence of P waves	ROSC	Similar HR (56.8 vs. 52.0 bpm, $p =$ .53) and QRS_w (128.7 vs. 129.6 ms, $p = .95$) were observed in survivors compared to non-survivors.
Skjeflo et al. [102]	IHCA	74	QRS complexes during the first pause in CC	HR and QRS_w	ROSC	Higher HR and narrower QRS_w were more prevalent in patients who achieved ROSC compared to those who did not.
Kim et al. [97]	OHCA	3659	PEA segments	HR and QRS_w	Surviving until hospital discharge	No significant link found between HR and survival, but a $QRS_w <$ 120 ms greatly boosted survival chances (adjusted odds ratio: 3.37).
Norvik et al. [82]	IHCA	298	QRS complexes during the first pause in CC	HR and QRS_w	ROSC	Higher and increasing HR were linked to higher chances of ROSC ($p <$ .0001), while lower and decreasing QRS widths increased the likelihood of ROSC ($p <$ .023) and reduced the likelihood of no-ROSC ($p = .0002$).

Table 2.1. Summary of the main references in PEA prognosis prediction.

2.2 Characterization of ECG, TI and IBP signals

In this section the main waveform characteristics of the ECG, the TI and the IBP signals will be presented. Some of them are general features as the QRS metrics of the ECG or the pressure metrics of IBP; others are more specific of SCA as amplitude spectrum area (AMSA) or Fuzzy entropy. They are frequently used in multimodal models for rhythm classification, event detections or predictive purposes in SCA. Features are grouped into three categories according to their origin.

2.2.1 Waveform features

The following features are computed using automatic algorithms and reflect the waveform of the signal on which they are computed.

- The **AMSA** represents the sum of the spectral amplitudes, $A_i(f_i)$, of the signal, with each amplitude weighted by its corresponding frequency (f_i). It is computed following the most extended definition [103, 104] as follows:

$$\text{AMSA} = \sum_i A_i \cdot f_i \tag{1}$$

  It has been highlighted as a shock success predictor, and surrogate measure of coronary perfusion pressure and myocardial energy state [105, 106].

- The **Smoothed Nonlinear Energy Operator (SNEO)** quantifies the local energy content of the signal. The signal $x(n)$ is the convolution between a Kaiser window, $w_L(n)$, and a non-linear Teager-Kaiser Energy Operator, $\psi_k[x(n)]$, [107]:

$$\psi_{S,L}[x(n)] = \psi_k[x(n)] \otimes w_L(n) \tag{2}$$

  $\psi_k[x(n)]$ is computed using the following equation:

$$\psi_k[x(n)] = x^2(n) - x[n-k]x[n+k] \tag{3}$$

  where k is the lag parameter which is associated with the window length (L samples) by $L = 4k + 1$.

  It has generally been used for QRS complex detection [108], identifying circulatory status [100] and predicting shock outcomes [107].

- **ARB** is the error in estimating the spectral power of the signal with a 4th-order autoregressive Burg model. The model yields a lower error in estimating the spectral power for signals whose spectra are centered around a fundamental frequency and its harmonics [109, 110]. The signal $x(n)$ can be modeled as:

$$x(n) = -\sum_{k=1}^{4} a_k s(n-k) + v(n) \tag{4}$$

where $v(n)$ represents an independent white noise sequence with zero mean and variance σ_v^2, and a_k coefficients are the autoregressive coefficients of the model.

This parameter has found applications in identifying circulatory status [100] and classifying cardiac rhythm [110].

- The **cross-power** (**ECGvsTI$_{\text{CrossPower}}$**) measures the cross power between the ECG and TI signals in our applications and it is defined as [111]:

$$\text{ECGvsTI}_{\text{CrossPower}} = \min(P_{c1}, P_{c2}) \tag{5}$$

where P_{ck} power of the k-th half of the sequences, which is calculated as follows:

$$P_{ck} = \frac{1}{N/2} \sum_{n=1}^{N/2} |ecg_k[n]| \cdot |TI_k[n]| \tag{6}$$

considering $ecg_k[n]$ and $TI_k[n]$ as the ECG and the TI samples of the k-th half, respectively.

A high value of ECGvsTI$_{\text{CrossPower}}$ is indicative of pulsatile rhythms, and it has been suggested for automated detection of circulation [111].

- **Fuzzy entropy** was proposed by Chen et al. [112] as a method to determine vector matching in a smooth and gradual way, introducing concepts from fuzzy set theory. The signal samples, denoted as $x(n)$, are divided into sets of vectors, each containing m samples. The total number of vectors created is $N - m + 1$, where N represents the total number of samples in the interval. In the resulting vector structure $x_i^m = \{x(i), x(i+1), \ldots, x(i+m-1)\}$, the baseline is subtracted as follows:

$$x_i^m = \{x(i), x(i+1), \ldots, x(i+m-1)\} - \frac{1}{m}\sum_{l=0}^{m-1} x(i+l) \quad (7)$$

The maximum norm (L_∞-norm) was employed to measure the Chebyshev distance between two vectors, denoted as $\mathbf{x}_i^m$ and $\mathbf{x}_j^m$:

$$d_{ij} = \max_{k=0,\ldots,m-1} (|x(i+k) - x(j+k)|) \quad (8)$$

Matches are computed using a set of functions that decay exponentially with increasing distance. These functions, denoted as $D_{ij}^m(n,r) = \exp\left(-\left(\frac{d_{ij}}{r}\right)^n\right)$, are used with a specific value of $n = 2$ and a Gaussian distance formula $D_{ij}^m(2,r) = \exp\left(-\left(\frac{d_{ij}}{r}\right)^2\right)$, as proposed in previous works in the field of survival prediction [113,114]. The match counts are calculated based on these functions as follows:

$$C_i^m(r) = \frac{1}{N-m-1}\sum_{j=1, j\neq i}^{N-m} D_{ij}^m(2,r) \quad (9)$$

The probability that two vectors of length m match within a tolerance of r is given by the expression:

$$\phi_m(r) = \frac{1}{N-m}\sum_{i=1}^{N-m} C_i^m(r) \quad (10)$$

The same procedure is repeated for the vector of $m+1$ samples to obtain $\phi_{m+1}(r)$, and Fuzzy entropy was computed as:

$$\text{Fuzzy entropy}(m,r,N) = \ln\phi_m(r) - \ln\phi_{m+1}(r) \quad (11)$$

2.2.2 QRS complex features

The following features are estimated based on the characteristic points of the QRS complex. This implies having the QRS onset

(QRS_{on}), end of QRS (QRS_{off}) and R wave peak instants. The graphical illustration of the features is shown in Figure 2.1.

- **HR** and $\mathbf{HR_{var}}$ represents the average and variance of the HR value, calculated as the inverse of consecutive R-R intervals.
- $\mathbf{QRS_w}$ and $\mathbf{QR_w}$ denote the durations between QRS_{on}-QRS_{off} and QRS_{on}-R peak, respectively.
- $\mathbf{QRS_{slope}}$ and $\mathbf{QR_{slope}}$ are computed as the sum of the amplitude values of QRS and QR complexes in the first difference signal divided by QRS_w and QR_width, respectively.
- $\mathbf{R_{amp}}$ is the mean value of the amplitude of the R wave peaks in the segment.

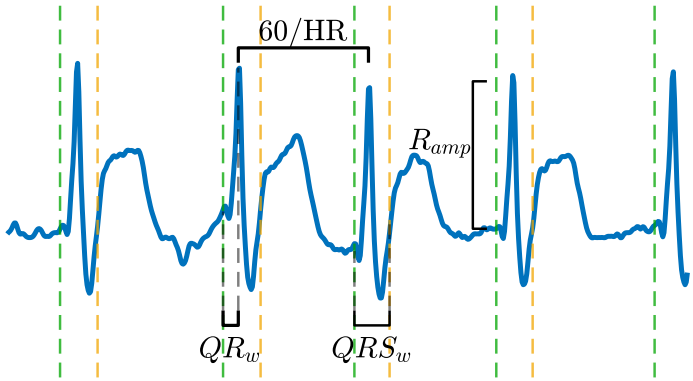

Figure 2.1. A 5 s example of ECG signal, with HR, QR_width, QRS_w and R_{amp} represented. QRS_{on} and QRS_{off} are depicted for each QRS complex with green and orange dashed lines, respectively.

2.2.3 ABP features

The following features are estimated based on the fiducial points of the IBP signal. This implies having the diastolic onset (Dia_{onset}) and systolic peak (Sys_{peak}) instants. The graphical illustration of the features is shown in Figure 2.2.

- Systolic arterial pressure (**SAP**) refers to the value of the IBP signal at the instant of the Sys_{peak}, which represents the maximum pressure in the arteries during heart contraction.
- Diastolic arterial pressure (**DAP**) represents the lowest pressure measured at the Dia_{onset} of heart contraction.
- Pulse pressure (**PP**) is the difference between SAP and DAP readings, reflecting the force exerted on arterial walls during heart contraction.
- The Mean Arterial Pressure (**MAP**) is the average arterial pressure over one cardiac cycle and is calculated using the following formula [115]:

$$\text{MAP} = \text{DAP} + \frac{1}{3}\text{PP} \tag{12}$$

- **HR** can be estimated as the inverse of the distance in time between consecutive Sys_{peak}.

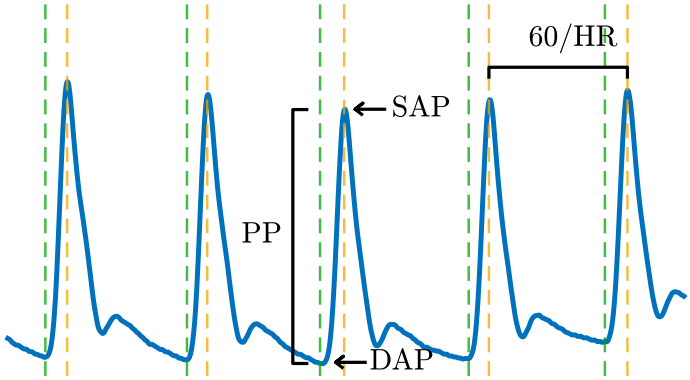

Figure 2.2. A 5 s example of IBP signal, with SAP, DAP, PP and HR represented. Dia_{onset} and Sys_{peak} are depicted for each heartbeat with green and orange dashed lines, respectively.

2.3 Artificial intelligence models in resuscitation

Artificial intelligence (AI) is everywhere, from self-driving cars to fraud detection in finance, virtual assistants, improved customer

service, and optimising manufacturing processes, reshaping modern society. In cardiac resuscitation, AI is widely used in the field of resuscitation monitoring. Many proposals have been made in topics as: shock outcome prediction [107, 116], rhythm classification [110, 117, 118], outcome prediction [119–121], CPR monitoring [122, 123], short term cardiac evolution prediction [124–126], circulation monitoring [100, 111, 127], etc. In this thesis work AI potential is used to predict the evolution of PEA rhythms. ML enables models to improve performance by learning from data without explicit programming, facilitating adaptation and evolution in response to new information. The classical ML approach consist in three steps: feature extraction from the signals, design and training of the ML model, and a final step of evaluation of the model.

2.3.1 ML Models

In ML, input parameters ($\mathbf{X}$) refers to numerical or categorical feature vector, enabling the model to differentiate patterns. The output parameter (Y) is the target variable to predict by the ML model which is known in supervised models. Next three ML models will be described, as they are the key models in the development of thesis work.

Logistic regression (LR), a ML technique for binary classification, predicts outcomes generally labeled as either 0 or 1. This model applies a logistic function to convert real-valued inputs to probabilities within the range of 0 to 1.

$$P(Y = 1|X) = \frac{1}{1 + e^{-(\beta_0+\beta_1 X_1+\beta_2 X_2+...+\beta_n X_n)}} \tag{13}$$

Where:

- $P(Y = 1|X)$ denotes the probability of the outcome Y being 1 given the predictor features $\mathbf{X}$
- e represents the base of the natural logarithm.
- $\beta_0, \beta_1, \ldots, \beta_n$ are the coefficients of the logistic regression model of order n.

- $X_1, X_2, \ldots, X_n$ represent the individual predictors from $\mathbf{X}$ feature vector.

During training, the coefficients are iteratively adjusted to minimize the disparity between the predicted and the actual outcomes. This adjustment process employs optimization techniques such as gradient descent.

LR is particularly effective in scenarios where the relationship between features and the outcome follows a linear pattern on the log-odds scale, making it suitable for binary classification tasks. Its simplicity and interpretability make it valuable for applications where understanding the impact of individual predictors on the outcome is crucial.

In the context of SCA, LR models have been employed, for instance, to predict the probability of survival [128], to predict shock success [77], or to estimate the likelihood of rearrest [80].

Random Forest (RF) is a ML algorithm that builds various decision trees during training and outputs the mode (for classification) or average prediction (for regression) of the individual trees. Each tree is built using a subset of the training data, sampled with replacement [129, 130]. RF optimization entails adjusting hyperparameters like tree count and depth. Moreover, it measures feature importance, identifying influential predictors for accuracy. Optimizing all these variables, the RF model can be enhanced in terms of accuracy [131].

RF works well for handling large and complex datasets with mixed types of features. It is robust against overfitting and noise, making it suitable for classification and regression problems [132, 133]. RF performs well for both linear and nonlinear problems.

In the realm of SCA, RF models have been used to predict outcome probabilities [91, 119], classify cardiac rhythms [134, 135], and detect the pulse presence [104].

Support Vector Machines (SVM) is another typical ML model used for classification problems. It aims to find the best hyperplane $\mathbf{w} \cdot \mathbf{X} + b = 0$ that separates classes in the feature space, where $\mathbf{w}$ is the weighting vector, $\mathbf{X}$ is the input vector, and b is the bias term. The

margin between classes is maximized by solving the optimization problem:

$$\min_{\mathbf{w},b} \frac{1}{2}\|\mathbf{w}\|^2 \tag{14}$$

subject to:

$$y_i(\mathbf{w} \cdot \mathbf{x}_i + b) \geq 1 \text{ for all } i = 1, \ldots, N \tag{15}$$

Here, $(\mathbf{X}_i, Y_i)$ are training samples with their corresponding labels, and N is the number of samples.

SVM excels with high-dimensional data and small or moderate datasets. Moreover, it can be easily extended for nonlinear problems. In cardiology, SVM models trained with diverse features have been proposed to predict SCA outcomes [91], defibrillation outcomes [77, 136], or rearrest probabilities [137].

2.3.2 DL Models

DL is a subfield of ML that uses ANNs with multiple layers (hence the term "deep") to learn complex patterns from data [138, 139].

Warren McCulloch and Walter Pitts [140] introduced the concept of ANN in 1943, which are computational models inspired by the brain's structure. They consist of interconnected nodes that process input data through layers, adjusting connection weights during training to minimize errors.

In the last decades, many types of layers have been proposed. The five main types of layers used during this thesis are the following:

1. **Pooling Layer**: Reduces the size of feature maps while retaining important information, helping summarize features. Two prevalent pooling methods are Max Pooling, picking the highest value in the kernel, and Average Pooling, calculating the average of all values in the kernel [141]. Figure 2.3 illustrates examples of both pooling techniques.
2. **Dropout Layer:** The dropout layer randomly deactivates some neurons during training, preventing overfitting by encouraging

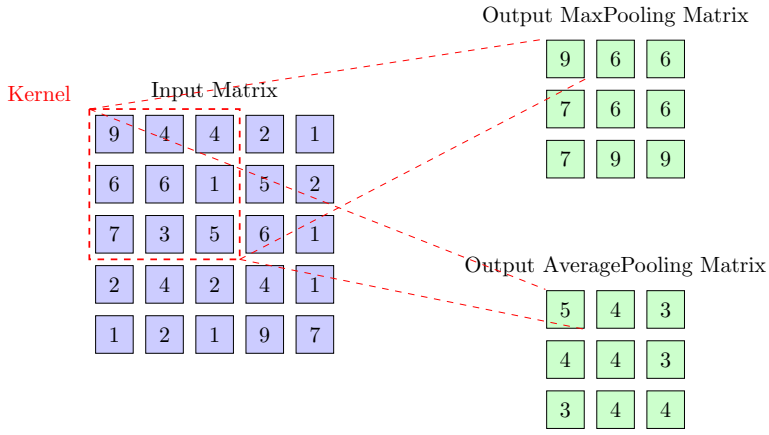

Figure 2.3. The result of pooling process is shown, applying a 3x3 kernel moving across the input data (purple), and providing the Maximum (up, green) or the Average (down, green) values.

independence among them [142]. This enhances the model's capacity to generalize to new data.

3. **Convolutional Layer**: The convolutional layer detects features like edges or textures in the input by applying filters and preserving spatial relationships in the data. Kernels slide over data, performing mathematical operations to compute features at each position [143, 144]. Figure 2.4 provides an illustration of this computation. Convolutional Neural Networks (CNN) consist of multiple layers for feature detection and pattern recognition.

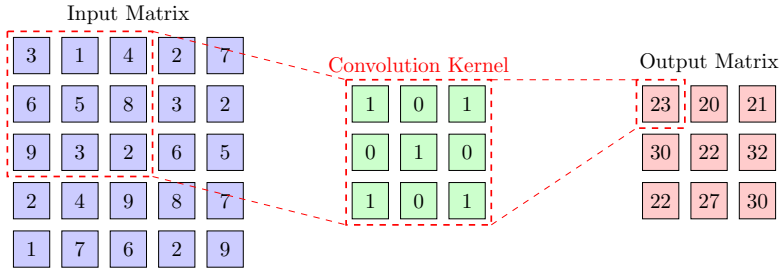

Figure 2.4. The result of convolution process is shown, applying a 3x3 kernel (green) moving across the input data (purple) and computing the output (red).

4. **Long short-term memory (LSTM) layer:** An LSTM layer, a type of recurrent neural network, is adept at capturing long-term dependencies in sequential data like time series or text. Through memory cells and gating mechanisms, it selectively retains and processes relevant information over extended sequences, mitigating the vanishing gradient problem and making it effective for tasks requiring modeling of temporal dependencies [43].
5. **Fully Connected Layer**: Combines features from previous layers for final classification, similar to hidden layers in standard ANNs. Because of its extensive connections and features, this layer requires considerable computational resources [145]. Refer to Figure 2.5 for an illustration of a fully connected classification layer.

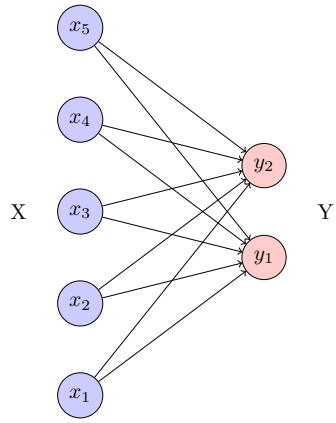

Figure 2.5. The fully connected layer connects the input layer (x1-x5) to the output layer (y1,y2).

These layers work together to learn complex patterns in data, making ANN effective for tasks like image recognition and object detection.

DL enhances medical analysis, specially in image interpretation and patient data analysis. Through techniques like CNNs and Recurrent Neural Networks, it assists in detecting diseases at an early stage from medical images [146–148] and predicts personalized treatments [149–151] using patient records. In the realm of SCA, DL models have been used to predict SCA, predict outcome, classify

cardiac rhythms [152], prognosticating outcomes [152,153] or categorizing arrhythmias [154,155].

2.3.3 Evaluation

Evaluation metrics are crucial to evaluate how effectively classification models perform. For a binary application, with positive and negative cases, key metrics include True Positive (TP) and True Negative (TN) representing instances correctly classified as positive and negative, respectively; while False Positive (FP), and False Negative (FN) denotes instances incorrectly classified as positive and negative, respectively. From these metrics, several additional metrics are calculated:

- Sensitivity (Se) measures the proportion of true positives correctly identified:

$$Se = \frac{TP}{TP + FN} \tag{16}$$

- Specificity (Sp) measures the proportion of true negatives correctly identified:

$$Sp = \frac{TN}{TN + FP} \tag{17}$$

- Positive Predictive Value (PPV) represents the proportion of true positive predictions among all positive predictions:

$$PPV = \frac{TP}{TP + FP} \tag{18}$$

- Negative Predictive Value (NPV) represents the proportion of true negative predictions among all negative predictions:

$$NPV = \frac{TN}{TN + FN} \tag{19}$$

- Balanced Accuracy (BAC) calculates the average of Sensitivity and Specificity:

$$BAC = \frac{Se + Sp}{2} \tag{20}$$

- Accuracy measures the overall correctness of predictions:

$$Accuracy = \frac{TP + TN}{TP + FP + FN + TN} \tag{21}$$

- Area Under the Curve (AUC) quantifies the model's ability to discriminate between positive and negative outcomes across all thresholds.

K-fold cross-validation (CV) is a common technique for developing and evaluating predictive models, especially when limited data sets are available. It divides the data into k subsets. Then it repeats k times the training and evaluation process, using a different subset as the test set in each iteration and the remaining ones as the training set. This allows for a more robust evaluation of the model and helps detecting overfitting [156, 157].

2.4 ECG DELINEATORS

Classical ECG analysis is based on the characterization of the QRS waveform. The main features consist on the detection of QRS complex and the delineation of the different parts as indicated in Subsection 2.2.2. Many classical algorithms were proposed to detect QRS complexes [158–162] and for the delineation of the QRS [40–48]. Most of the algorithms were designed and tested with stable cardiac rhythms. Next the main algorithms are described.

2.4.1 HAMILTON-TOPKINS ECG DELINEATOR

One of the most common algorithms algorithm for peak detection is the one proposed by Hamilton-Tompkins in 1986 [159]. This algorithm is divided into three stages: ECG waveform preprocessing, QRS peak detection and fiducial mark identification.

PREPROCESSING

The signal is band-pass filtered by cascading a low-pass filter and a high-pass filter. This step serves to attenuate noise and emphasize cardiac activity within the 5–11 Hz frequency band. The transfer

functions of the low-pass and high-pass filters, $H(z)_l$ and $H(z)_h$, can be expressed as:

$$H(z)_l = \frac{(1 - z^{-6})^2}{(1 - z^{-1})^2} \tag{22}$$

$$H(z)_h = \frac{(-1 + 32z^{-16} + z^{-32})}{(1 - z^{-1})} \tag{23}$$

Subsequently, a derivative filter is applied to enhance the slope characteristics of the QRS complex. For a 5-point derivative filter with a gain of $1/8$ and a processing delay of 2 samples, the transfer function $H(z)_d$ is given by:

$$H(z)_d = \frac{1}{8}(-z^{-2} - 2z^{-1} + 2z^1 + z^2) \tag{24}$$

Next, the signal is squared to amplify prominent peaks, typically corresponding to QRS complexes. Finally, a moving average filter is applied to compute the QRS complex duration with a average window size of 150 ms.

Peak Detection

The peak detector identifies peaks in the time-averaged signal. It tracks the highest amplitudes and detects a new peak when the signal drops below half the maximum level. The fiducial mark is positioned at the location of the highest peak observed within the preprocessed signal, within 225 to 125 ms prior to the peak detected in the time-averaged signal.

Peak Level Estimation

The method applied to estimate position of the local peak, significantly impacts to QRS detector. The methods are mostly applied, based in the mean, the median or the iterative estimation.

- The mean estimator calculates the local peak level by averaging a specified number of past peaks.

- The median estimator determines the local peak level using the median peak value.
- The 1st-order iterative estimator follows a formula where the current estimate is updated based on a coefficient and the current peak value:

$$\text{Estimate}(n) = (1 - A) \times \text{Estimate}(n-1) + A \times \text{Peak}(n) \quad (25)$$

  A is a positive coefficient less than one.

Peak Estimator Performance

Any peak exceeding the detection threshold (computed using Equation 26) is considered a QRS complex and is used to adapt the detection threshold as:

$$\text{Detection threshold} = B \times \text{Peak level estimate} \quad (26)$$

where the coefficient $B \in [0, 1]$.

2.4.2 Li et al. ECG delineator

Li et al. delineator [41] applies the Wavelet Transforms (WT) to detect characteristic points in ECG signals. WT is a popular time-frequency analysis technique, which decomposes signals into localized building blocks/scales, corresponding to approximation and detail coefficients of the signal in each of the bands of interest.

R peak detection

This algorithm explores different detail coefficients, d_1, d_2, d_3 and d_4 (corresponding to $62.5 - 125$ Hz, $18 - 58.5$ Hz, $8 - 27$ Hz and $4 - 13.5$ Hz for a sampling rate of 250 Hz) to identify "maximum modulus lines" surpassing certain adaptive thresholds (ϵ_1, ϵ_2, ϵ_3 and ϵ_4).

To select the maximum modulus thresholds, the following steps are taken:

1. Identify all maxima points exceeding a threshold ϵ_4 at detail coefficient d_4.

2. Find the largest maxima near each identified point at detail coefficients d_3, d_2 and d_1.
3. If there are multiple peaks exceeding thresholds ϵ_1, ϵ_2, and ϵ_3 in their respective detail coefficients, the highest peak is selected. If there are no peaks exceeding the thresholds, the nearest peak to the original point is chosen. If no peak is found, the location is set to zero.

After the elimination of all isolated and redundant maximum modulus lines, the zero crossing points in the WT within a detail coefficient encompassing a positive maximum-negative minimum pair are identified as a QRS complexes. Additional safeguards are implemented, such as a refractory period or a retrospective search with adjusted thresholds if no QRS is detected in a given time interval.

QRS_{on} and QRS_{off} detection

The QRS_{on} and the QRS_{off}, as shown in Figure 2.1 (Subsection 2.2.2) determine the initial instant of Q wave and the end of S waveform, respectively. Q and S waves typically exhibit high frequency and low amplitude characteristics, with their energies primarily concentrated at smaller detail coefficients.

The algorithm compute the QRS_{on} and QRS_{off} identifying the initial and final maximum modulus lines surrounding the maximum pair of the R wave within a defined time frame. Conducting this detection at detail coefficients d_1 rather than directly on the original signal helps mitigate the impact of baseline drift.

2.4.3 Martinez et al. ECG delineator

Martinez et al. [40] introduced a generalization of the algorithm of Li et al. [41] featuring the delineation of the individual QRS waves for a wide range of QRS morphologies. It consists on the next steps.

R peak detection

The QRS complexes are detected in the R instant, n_{qrs}, through an algorithm grounded in the multiscale approach pioneered by Li et al. [41].

Detection of QRS_{on} and QRS_{off}

Starting from the position identified by the detector secondary waves of the QRS complex are identified based on zero-crossing and local maxima/minima in the d_1 and d_2 detail coefficients of the ECG signal, respectively. Several duration and amplitude thresholds are applied, and any possible QRS morphology with three or less waves is considered. Then, QRS_{on} and QRS_{off} points are selected at the boundaries of the secondary waves, given by either a low-amplitude threshold or a reversed signed maxima/minima in the d_2 detail coefficient.

2.4.4 Peimankar et al. ECG delineator

Peimankar et al. [43] developed a method called DENS-ECG that uses a mix of CNN and LSTM models to accurately identify the start, peak, and end of different heartbeats in the ECG.

Preprocessing

First, each record was filtered and segmented. Signals were filtered using a 3rd-order Butterworth band-pass ($0.5 - 40$ Hz) filter to remove noise. Records were then divided into smaller segments of 1000 samples (6 s segments, sampling frequency is 250 Hz), roughly equivalent to five heartbeats. This aids in capturing a sequence of heartbeats for better model learning.

Delineation Model

The model comprises eight layers, including an input layer, three one-dimension CNN, two bidirectional LSTM layers, a dropout layer, and a dense layer.

The input segments undergo three consecutive CNN to extract temporal patterns from the ECG signals. Each CNN employs a kernel size of 3 and 32, 64, and 128 feature filters, respectively. Zero padding is applied to maintain input dimension.

The output of the final CNN is fed into the first bidirectional LSTM layer, equipped with 250 hidden units, followed by a second bidirectional LSTM layer with 125 hidden units. A dropout layer, set

with a dropout probability of 0.2, is integrated to mitigate overfitting during training.

2.5 IBP DELINEATORS

Delineating the IBP signal means detecting the Dia_{onset} and Sys_{peak} instants that refer to the beginning and peak instant of the IBP signal at each heart contraction. Several algorithms [53–55, 163, 164] have been proposed to delineate the IBP signal, with the primary goal of identifying fiducial points such as the Dia_{onset} and Sys_{peak}, shown in Figure 2.2 of Subsection 2.2.3. Among the most commonly utilized algorithms are those proposed by Zong et al. [55] and Li et al. [54]. They have been widely used to analyze cardiovascular dynamics in hemodinamically stable patients. Nevertheless, they have not been applied to SCA patients, and no validated algorithms are published for the context of this thesis.

2.5.1 ZONG ET AL. IBP DELINEATOR

Zong et al. introduced an algorithm that identifies the start of arterial pressure pulses [55]. It comprises three main steps: a low-pass filter, slope sum function (SSF), and a decision rule:

Low-pass filter: To mitigate potential interference from high-frequency artifacts during Dia_{onset} detection, a 2nd-order recursive filter with a cutoff frequency of 16 Hz was utilized. Its transfer functions can be expressed as:

$$H(z) = \frac{(1 - z^{-6})^2}{(1 - z^{-1})^2} \tag{27}$$

SSF: The SSF amplifies the rising slope of the IBP pulse while reducing other signal components. It is calculated as follows:

$$SSF(i) = \sum_{i=2}^{N} \Delta x_i \qquad \begin{cases} \Delta x_i, & \text{if } \Delta x_i > 0 \\ 0, & \text{if } \Delta x_i \leqslant 0 \end{cases} \tag{28}$$

Where x_i is the filtered IBP signal, N is its length of the IBP signal and $\Delta x_i = x_i - x_{i-1}$.

Normally, the beginning of the SSF pulse matches the start of the IBP pulse.

Decision rule: In this step, two criteria are applied. Firstly, an adaptive threshold is set based on the maximum SSF value for each detected pulse. Then, a local search strategy identifies the Dia_{onset} point by examining SSF minimum and maximum values within a 150 ms window before and after the threshold crossing. The IBP Dia_{onset} is determined when the SSF signal surpasses 1 % of the maximum SSF value, and it is adjusted by 20 ms to compensate the delay caused by the filter. Additionally, a 300 ms refractory period is implemented to avoid double pulse detection.

2.5.2 Li et al. IBP delineator

Li et al. [54] proposed a more comprehensive algorithm that, in addition to detecting the Dia_{onset} like Zong et al. [55], also identifies the Sys_{peak}.

Noise and artifacts in the raw signals are suppressed using a 3rd-order low-pass Bessel filter with a cutoff frequency of 25 Hz.

The delineator uses 1st-order amplitude differences to estimate the derivative of filtered IBP waveforms. It looks for the derivative at pairs of inflection and zero-crossing points. Specifically for Dia_{onset} and Sys_{peak}, the delineator focuses on the zero-crossing points before and after the maximal inflection in each beat of the waveform derivative.

Finally, the delineator assesses these candidate Dia_{onset} and Sys_{peak} in the IBP waveforms based on both amplitude and interval thresholds.

3 HYPOTHESIS AND OBJECTIVES

This thesis work aims to address significant gaps in the automatic characterization and analysis of PEA during resuscitation therapy. The main hypothesis of the thesis is that signal processing and AI techniques designed specifically for PEA rhythms could contribute to monitor resuscitation efforts and the response of the patient. The final aim is to enhance treatment and improve outcome in SCA. The two specific objectives are:

- **Objective 1: Development of models to discriminate between PEAs with favorable and unfavorable prognosis.** In the literature, various automatic models have been designed to discriminate cardiac rhythms with different prognoses during SCA [74, 77, 80, 81, 100]. These algorithms utilize signals recorded by the defibrillator, along with ML models, for the development of predictive models. However, none of them were specifically designed for PEA rhythms. A discriminator of favorable/unfavorable PEA based on features extracted from the defibrillator biosignals could be integrated into AEDs or defibrillator monitors to aid in resuscitation therapy. This thesis work focus on the following three approaches:
  - Development of models to predict PEA prognosis using features automatically extracted from the ECG and the TI recorded by the defibrillation pads, combined in ML models.
  - Development of models to predict PEAs prognosis with ML models that integrate QRS specific features. Various studies have analyzed the potential of some features, such as HR or QRS_w

[82–85]. They used manually annotated QRS features, with no combination with other ECG/TI features. The hypothesis of this thesis work is that a multimodal approach in a ML model would improve accuracy of the predictive models.

  - Development of models to predict PEAs prognosis with ML models that integrate automatic features computed from ECG, TI, and IBP signals. Features from the IBP signal will be included in the previously developed model, which already incorporates ECG and TI features, to provide additional information and enhance its performance.

- **Objective 2: Development of delineation algorithms for the ECG and the IBP of patients in SCA.** Most of the classical algorithms for ECG/IBP delineation were designed for stable patients, and the haven not been tested with unstable patients such as those experiencing SCA. In this context, two partial objectives are defined:

  - ECG delineation algorithm. During SCA, QRS complexes often differ from those observed in healthy and stable patients, both in amplitude and QRS waveform shape. Furthermore, during SCA, the ECG signal may include different artifacts that jeopardize analysis. Delineators proposed in the literature were designed for stable patients [40, 42–48], and their performance may be lower patients in SCA. A delineator that works with patients during SCA could help better characterize the ECG signal and automatically extract features based on duration/amplitude of intra QRS segments.

  - IBP delineation algorithm. The IBP signal during SCA shows the effect of unstable circulation and different circulation states. Even after ROSC the variability and complexity of the IBP signal differs from those of hemodynamically stable patients. Therefore, traditional IBP delineators [53–55, 163, 164] may fail in calculating fiducial-points in every cardiac contraction. An IBP delineator that works in the context of SCA is necessary to calculate physiological parameters such as SAP, DAP, or PP.

4 RESULTS

This section presents an overview of the results obtained in this thesis, in line with the objectives outlined in Section 3. Many of the research studies included a preliminary analysis, which was initially presented at different conferences [165–170]. Afterwards, a more sophisticated approach to the solution was developed, incorporating enhanced and more advanced methodologies and/or additional data, which were later submitted and published in Journal Citation Reports (JCR) journals [171–174]. This section summarizes the main contributions of the thesis work, two journal publications and a conference paper for Objective 1 (J1.1, J1.2 and C1.1), and two journal publications for Objective 2 (J2.1 and J2.2). Original papers are attached in Appendix A.

4.1 Results related to objective 1

During the development of this thesis, three different approaches have been followed to design algorithms that discriminate favorable/unfavorable PEA rhythms. At first, previously known automatic features derived from ECG and TI signals were computed to build support for a ML classifier. Afterwards, ModAMSA and features derived from manual annotations of QRS complexes were integrated into the previous model. Finally, a new model using features extracted from the waveform of ECG, TI and IBP signals was proposed. The first and second methods were published in JCR journals [171, 172], J1.1 and J1.2, respectively. Further, intermedi-

ate results and the last method, C1.1, were presented at a national conference [165] and two international conferences [168, 170].

4.1.1 J1.1: A Machine Learning Model for the Prognosis of Pulseless Electrical Activity during Out-of-Hospital Cardiac Arrest

J1.1 analyzed a subset of OHCA episodes dataset recorded by the Dallas-Fortworth Center for Resuscitation Research. Each episode included ECG and TI signals recorded by a HeartStart MRx defibrillator. A total of 260 episodes of PEA were analyzed, from which 107 recovered ROSC. The beginning of PEA was identified as the first occurrence of an organized rhythm. Segments of PEA of 5 s duration were extracted within the first 10 minute from the start of the first PEA of the episode, avoiding CC artifacts.

A total of 1921 PEA segments were examined, 703 of which were labeled as faPEA from episodes with ROSC and 1218 as unPEA from episodes without ROSC. The faPEA segments showed a more regular ECG with narrower QRS complexes, larger amplitude and faster HR, along with ECG correlated with TI components and TI circulation component (ICC) waveforms.

The ECG signal was denoised using the Stationary Wavelet Transform (SWT) with an 8-level decomposition and Daubechies-4 mother wavelet, focusing on the $0.5 - 31.25$ Hz frequency band. The TI signal was bandpass filtered $0.8 - 10$ Hz to remove baseline fluctuations, respiratory artifacts and high-frequency noise. Subsequently, ICC proposed by Elola et al. [100] was extracted. The ICC signal underwent denoising via 8-level SWT (Daubechies-4) with soft thresholding. Detail coefficients d_5–d_7 were used to reconstruct the denoised ICC, within the 1–8 Hz bandwidth. Figure 4.1 shows the ECG, TI, ICC and its d_5-d_7 coefficients for faPEA and unPEA segments.

Given that faPEA evolves to ROSC, whereas unPEA does not, the hypothesis was that faPEA would be more similar to pulsatile cardiac rhythms than unPEA. Therefore, features previously used to discriminate PEA and PR where proposed. A total of 17 features were computed to characterize the segments:

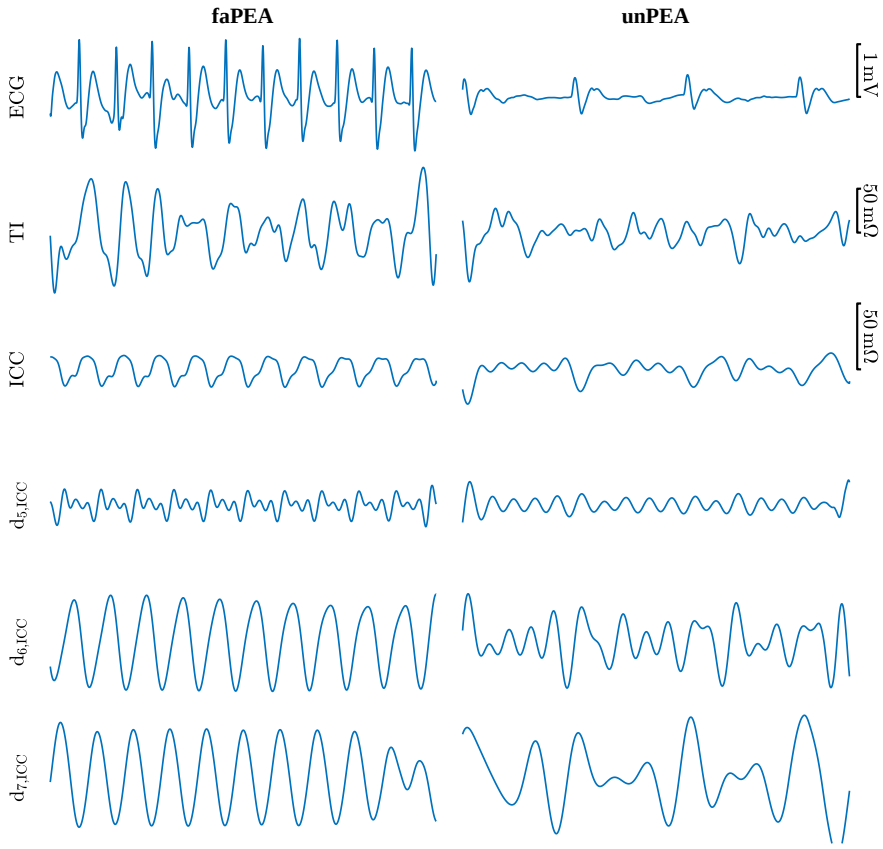

Figure 4.1. 5 s examples of a faPEA segment (left) and an unPEA segment (right). Top to bottom: ECG, TI, ICC and the detailed components, $d5_{ICC}$, $d6_{ICC}$ and $d7_{ICC}$.

- From the ECG:
  - AMSA
  - SNEO_{ECG}
  - ARB_{ECG}
  - Fuzzy entropy
  - IQR values of the ECG d_5, d_6 and d_7 detail coefficients.
  - $\text{High}_{\text{power}}$, ECG power in the $17.5 - 40$ Hz frequency bands.
- From the ICC:

- $SNEO_{ICC}$
- ARB_{ICC}
- IQR values of the ICC d_5, d_6 and d_7 detail coefficients.
- $ECGvsICC_{CrossPower}$ represents the cross power between ECG and ICC. It is similar to $ECGvsTI_{CrossPower}$ explained in Subsection 2.2.1, but using the ICC signal instead of TI.
- The logarithmic power of the ICC signal ($LogPower_{ICC}$) refers to the energy of the ICC in the logarithmic scale. It is computed as follows:

$$\text{LogPower}_{\text{ICC}} = \sum_{n=1}^{N} \log(ICC[n]^2) \tag{29}$$

where N is the length in samples of the ICC signal.

A RF classifier was used for both feature selection and binary classification of the 5 s segments in faPEA/unPEA. Feature selection was analyzed using a 10-fold CV architecture.

The reduced-feature models with 7 features showed the best performance, achieving mean AUC/BAC values of 85.7/78.8 %. Comparisons were made with previous proposals, including a preliminary version of the proposed method based on an RF classifier with a single ECG feature (AMSA) and an ICC feature ($LogPower_{ICC}$), an LR model using ECG-only features proposed by Alonso et al. and single ECG feature models based on HR and QRS_w. The results comparison is shown in Table 4.1.

J1.1 introduces a ML algorithm that effectively distinguishes PEA rhythms with favorable outcomes from those with unfavorable evolution. By taking advantage of the characteristics of both ECG and TI signals it outperforms state of the art (SoA) methods.

4.1.2 J1.2: Machine learning model to predict evolution of pulseless electrical activity during in-hospital cardiac arrest

J1.2 analyzed a subset of 197 IHCA episodes from different hospitals, with 83 from St. Olav University Hospital (Trondheim,

	No. Features	AUC (%)	BAC (%)	Se (%)	Sp (%)
J1.1 (ECG+TI)	17	85.7 (8.6)	77.8 (8.9)	79.8 (11.3)	77.3 (12.1)
J1.1 (ECG)	9	82.1 (9.7)	73.5 (11.2)	79.7 (14.1)	69. (15.9)
J1.1 reduced (ECG+TI)	7	85.7 (9.8)	78.8 (9.8)	80.1 (12.6)	76.7 (13.6)
J1.1 reduced (ECG)	4	83.2 (8.5)	75.7 (10.7)	78.9 (15.9)	75.7 (11.4)
Urteaga et al. [165]	2	82.0 (10.5)	74.8 (11.3)	77.0 (13.9)	73.5 (14.6)
Alonso et al. [175]	6	81.4 (10.3)	74.4 (8.9)	73.2 (15.1)	77.8 (15.3)
HR [96]	1	67.2 (12.9)	62.1 (11.8)	80.2 (14.5)	45.1 (21.1)
QRS_w [102]	1	69.2 (12.9)	67.8 (13.3)	74.8 (20.2)	61.5 (26.6)

Table 4.1. The performance of the proposed algorithm compared to all prior proposals. The table displays median (IQR) values for AUC, BAC, Se, and Sp.

Norway), 90 from the Hospital of the University of Pennsylvania (USA), and 24 from Penn Presbyterian Medical Center (USA). Lifepak-20 defibrillators were used in episodes from Norway (2018-2021), and HeartStart MRx defibrillators for those from Pennsylvania (2008-2010). Sustained ROSC, observed in 120 episodes, was defined as a PR without CC for at least 20 min. Expert clinicians manually annotated rhythm type, QRS complexes, and CC series. PEA segments of 5 s duration, separated by at least 1 s, were extracted for analysis during CC pauses.

The ECG and TI signals were preprocessed using the same method as in J1.1 [171], including denoising the ECG with a band-pass filter (0.5–31.25 Hz) and extracting the ICC component from the TI signal, filtered (1–8 Hz).

The analysis was extended by incorporating seven additional features derived from QRS complex annotations, along with an enhanced version of AMSA called ModAMSA. The features calculated from the QRS complexes are the following:

- HR and HR_{var}
- QR_w and QRS_w
- QR_{slope} and QRS_{slope}
- R_{amp}

ModAMSA calculates spectral content within the frequency range of $20 - 30\,\text{Hz}$. Specifically, ModAMSA values were found to be higher for faPEA rhythms than for unPEA rhythms. Figure 4.2 illustrates a significant overlap in spectral content between $0 - 15\,\text{Hz}$ for both rhythm types, but a clearer distinction emerges between $20 - 30\,\text{Hz}$.

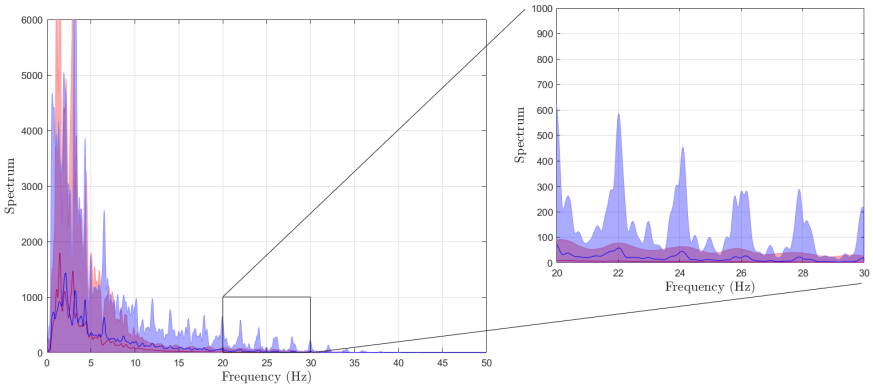

Figure 4.2. ECG signal spectrum for faPEA and unPEA segments. The blue line and shaded area represent the mean (Standard Deviation - SD) of faPEA segments, while the red line indicates the same for unPEA segments. On the left, the spectrum covers frequencies from $0 - 50\,\text{Hz}$, while the right zooms on the $20 - 30\,\text{Hz}$ range used in ModAMSA.

LR binary models were trained and tested using a 10-fold CV and changing the features and the number of features. In the first iteration, all features were individually tested. In the second iteration, the best-performing feature was combined with the remaining features to calculate the best pair. This process continued iteratively, adding one feature at a time in each iteration. LR was chosen because it provides easily interpretable binary classifications.

Table 4.2 shows the results of the first six iterations, training the model from one feature to six features. The analysis reveals that the best performance was achieved with a three-feature model based on: ModAMSA, $\text{LogPower}_{\text{ICC}}$ and QRS_{w}, with AUC/BAC values of 80.3 % and 75.6 %, respectively. No improvement was found when increasing the number of features. It is worth highlighting that each of these features belongs to a different feature family (ECG signal

	No. Features	AUC (%)	BAC (%)	Se (%)	Sp (%)
ModAMSA	1	79.1 (11.3)	71.4 (10.4)	62.9 (13.4)	79.2 (18.5)
Previous feature + $LogPower_{ICC}$	2	79.7 (9.1)	71.5 (13.2)	64.2 (17.1)	78.5 (15.2)
Previous features + QRS_w	3	80.3 (9.9)	75.6 (8.0)	77.4 (15.2)	72.3 (16.4)
Previous features + ARB_{ECG}	4	80.2 (10.0)	75.5 (8.2)	77.5 (15.2)	69.5 (18.3)
Previous features + QR_w	5	79.8 (10.7)	73.1 (9.2)	77.8 (11.1)	66.4 (18.9)
Previous features + $ECGvsICC_{CrossPower}$	6	79.6 (11.2)	72.6 (9.1)	76.4 (9.9)	64.4 (21.2)

Table 4.2. Performance of the LR model in terms of median (IQR) AUC, BAC, Se and Sp. For each number of features only the best one is shown, all possible combinations have been tested using one to six features.

waveform, ICC signal waveform, and QRS complex), this suggests that each family contains valuable information for prediction.

To our knowledge, J1.2 represents the first case of a ML predicting the progression of PEA rhythms that integrates features from both ECG and TI, along with specific QRS metrics. The QRS metrics have been computed from clinicians' manual annotations, an automatic QRS delineator would be necessary for this method to be fully automatic and integrable in a monitor.

4.1.3 C1.1: A Random Forest Model for Pulseless Electrical Activity Prognosis Prediction During Out-of-Hospital Cardiac Arrest Using Invasive Blood Pressure

This research used data from a clinical trial (NCT02479152) on patients in SCA, collected between 2015 and 2017 using the Lifepak-15 monitor/defibrillator. The Air Ambulance Department of the Oslo Medical Emergency System collected the data. ECG, TI, and IBP signals were simultaneously recorded with a sampling rate of 250 Hz.

Segments from episodes with at least 5 min of PR after ROSC were considered faPEA, while those from episodes without ROSC were labelled as unPEA. During CC pauses, PEA segments with at least 5 s of ECG, TI, and IBP signals were extracted to avoid artifacts. From 49 patients, 238 segments (116 min total) were obtained with 172 unPEA segments. PEA segments were divided into 1026 (846 unPEA) non-overlapping 5 s windows for processing and classification.

The ECG and TI signals were preprocessed following the same approach as detailed in references J1.1 and J1.2 [171, 172]. This

involved removing noise from the ECG using SWT and a specific frequency band filter (0.5–31.25 Hz) and isolating the ICC from the TI signal within a frequency range (1–8 Hz). For the IBP signal, a similar filtering was applied, using SWT decomposition into 8-levels and reconstructing it with specific detail coefficients (1–4 Hz).

In addition to the 17 functions proposed in J1.1, 8 new ones were included based on the annotations made using the J2.2 delineator:

- SAP, DAP, PP, HR, and MAP (detailed in Subsection 2.2.3) computed from the IBP signal annotation using the method described in J2.2 (see Figure 2.2).
- $\text{IBP}_{\text{power}}$, reflecting the power of the IBP signal and is estimated as follows:

$$\text{IBP}_{\text{power}} = \sum_{n=1}^{N} IBP[n]^2 \tag{30}$$

  where N is the length in samples of the IBP signal, $250 \cdot 5$ samples per window.
- Cross-correlation measures, $\text{ECGvsIBP}_{\text{CrossPower}}$ and $\text{TIvsIBP}_{\text{CrossPower}}$, similar to $\text{ECGvsICC}_{\text{CrossPower}}$, but for ECG vs. IBP and TI vs. IBP signals, respectively.

A RF classifier was used for feature selection and binary classification of the windows into faPEA and unPEA classes. The classifiers was subjected to 10-fold CV on a per-patient basis. In addition, the RF classifier determined feature importance.

Table 4.3 shows overall performance metrics, including AUC, BAC, Se, Sp, PPV, and NPV. Various models were evaluated using: ECG and TI features, IBP features, all three signal features, and two reduced models (top 4 or 6 features). Results demonstrate superior performance with all IBP features, 20 points higher AUC than ECG & TI alone. Combining all signals improves discrimination by three points, surpassing similar SoA proposals [168, 171]. Reduced feature models outperform full-feature models by 1.5 to 2 AUC points.

This study integrated for first time IBP signals into a ML model for PEA prognosis prediction, significantly enhancing the classifier

	No. Features	AUC (%)	BAC (%)	Se (%)	Sp (%)	PPV (%)	NPV (%)
ECG & TI	17	62.2 (17.3)	69.8 (22.9)	61.1 (47.9)	65.3 (27.4)	49.4 (34.2)	73.2 (35.0)
IBP	6	83.5 (19.8)	73.2 (17.3)	67.1 (38.2)	80.7 (29.7)	69.7 (29.9)	84.4 (23.1)
ECG & TI & IBP	25	86.7 (19.4)	74.7 (14.6)	78.9 (33.3)	69.8 (25.5)	63.5 (30.7)	87.4 (22.7)
C1.1 reduced #1	4	88.9 (14.2)	76.1 (14.4)	94.1 (21.7)	68.1 (30.6)	66.4 (29.5)	95.0 (19.4)
C1.1 reduced #2	6	88.2 (18.0)	78.0 (17.5)	84.9 (22.8)	73.4 (28.7)	66.5 (27.1)	87.5 (21.6)

Table 4.3. The table reports the performance of the methods with different sets of features. in terms of median (IQR) value of AUC, Se, Sp, PPV and NPV.

performance. These results emphasize the value of IBP in assessment of circulation evolution during OHCA and the importance of IBP features to predict cardiac evolution.

4.2 Results related to objective 2

Current biosignal delineators have been designed and tested with hemodynamically stable patients, they have not been tested in unstable patients such as in SCA. ECG and IBP delineators are essential to automate the analysis of IHCA and OHCA patients, because manual annotation is time consuming, cannot be performed in real time and is impractical for long datasets. During this thesis work, two delineators that work in hemodynamically unstable patients have been proposed: an ECG delineator based on DL and a IBP delineator using signal processing and adaptive thresholding. Both methods have resulted in JCR papers [173,174], J2.1 and J2.2, and preliminary results were presented at international conferences [166,167].

4.2.1 J2.1: A Deep Learning Model for QRS Delineation in Organized Rhythms during In-Hospital Cardiac Arrest

The design of the QRS delineator was based on a subset of 332 IHCA episodes from a larger dataset, which included ECG and TI signals. Among these, 124 episodes were from St. Olav's University Hospital, Norway, and 163 from the Hospital of the University of Pennsylvania, USA, along with 45 from the Pennsylvania Presbyterian Medical Center, USA. ECGs were recorded using Lifepak-20 defibrillators in Norway (2018-2021) and HeartStart MRx defibrillators in the USA (2008-2010). Annotation by medical professionals served as the gold standard, including rhythms, QRS

complexes, and CC intervals. ECG segments with organized rhythms (PR/PEA), of at least 6 s, were extracted during CC pauses. 2485 segments were acquired, totaling 30 hours and 151815 QRS complexes.

Additionally, the method was tested on the public QT dataset from PhysioNet [176], with recordings from 105 patients, totalling 1575 min with 112497 annotated QRS complexes.

The raw ECG signal, susceptible to motion noise and baseline drift, was preprocessed using an 8-level SWT with the Daubechies-4 wavelet. Then the signal was reconstructed using only d_3 to d_7 (0.98 − 31.25 Hz) detail coefficients to eliminate undesired components. The signal was divided in 6 s windows with a overlap of 50 %. The AI model used in this study requires input lengths divisible by 16, so padding was applied to achieve the length of 1536 samples.

The used architecture is a modified U-Net engineered for one-dimensional data. The encoding path consists of four downsampling blocks, each comprising convolution, ReLU activation, batch normalization, and dropout layers to avoid overfitting. Maximum clustering reduces the computational burden while emphasizing essential features. After the fourth down-sampling block, two additional convolutional layers are added. The decoding path includes resampling layers with concatenation to skip connections, convolution layers with ReLU activation and dropout. A final convolution with sigmoid activation generates a binary mask indicating inclusion (1) or exclusion (0) of the QRS complex. An overall of the architecture can be seen in Figure 4.3, which also provides more details such as the dropout rate, filter size, and convolution dimensions.

Each processed window is merged to reconstruct the segment with binary values (1/0). Central 3 s (50 % window) of consecutive windows are concatenated, preventing edge effects near the beginning or end of segment and ensuring accurate model handling.

The chosen optimizer was Adaptive Moment Estimation (Adam), widely favored in DL for dynamically adjusting learning rates. The loss function, 1-Dice, was utilized during model training with the aim of reduction of the loss value. A 10-fold patient-wise CV structure

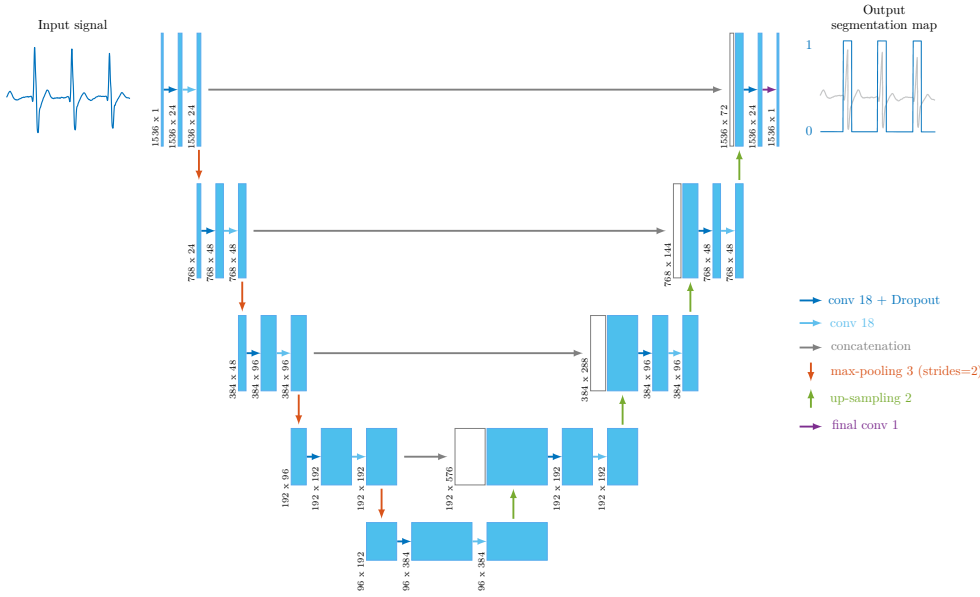

Figure 4.3. Overall architecture of the DL based ECG delineator.

was used to evaluate the model in terms of QRS detection (with a 100 ms tolerance) and time errors in QRS_{on}/QRS_{off} detection (see Figure 2.1).

The suggested method was contrasted with four SoA algorithms. Two of them, Martinez et al. [40] and Pilia et al. [42], utilized advanced signal processing techniques. The other two, Peimankar et al. [43] and Camps et al. [44], applied DL methods.

Table 4.4 shows the results of the method for delineation of the IHCA QRS complex. It is noticeable that the proposed U-Net based algorithm outperforms other SoA proposals, with F1 and IOU scores 1.0-7.5 and 0.9-28.8 points higher, respectively, and QRS_{on}/QRS_{off} errors lower by $0.3 - 14.3/0.3 - 13.9$ ms.

Performance of the algorithm with regular rhythms (PR and PEA) is shown in Figure 4.4 where a slightly higher result is observed for PR.

Model	TP	FP	FN	F1(%)	IOU(%)	QRS_{on}/QRS_{off}(ms)
U-Net	165302	2305	1250	97.0 (8.3)	79.1 (15.8)	8.6 (11.6)/25.1 (25.9)
Martinez et al. [40]	106754	556	59798	93.8 (14.3)	50.3 (38.1)	8.9 (15.4)/32.7 (34.9)
Pilia et al. [42]	162835	2678	3717	93.3 (13.5)	61.9 (18.7)	22.9 (19.3)/39.0 (35.1)
Peimankar et al. [43]	163906	2883	2646	96.0 (9.4)	78.2 (16.6)	9.3 (14.4)/25.4 (26.1)
Camps et al. [44]	156945	10330	9607	89.6 (18.0)	59.3 (28.5)	16.8 (22.3)/35.8 (35.7)

Table 4.4. Performance of QRS delineation methods for the IHCA dataset in terms of mean (SD) values of F1, IOU, and QRS_{on}/QRS_{off} errors.

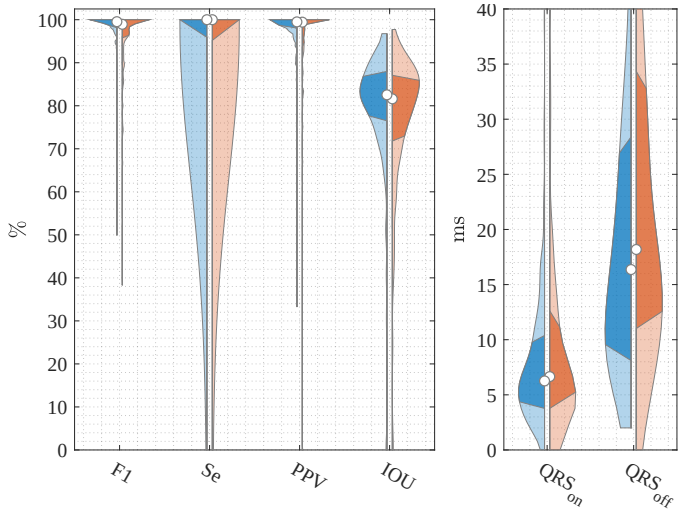

Figure 4.4. Performance of the method for PEA (orange) and PR (blue) segment delineation in terms of F1, Se, PPV, IOU, QRS_{on} and QRS_{off}. The white dot in the center of the distribution defines the median.

The performance analysis of the algorithm on the QT dataset with rhythms from stable patients is presented in the Table 4.5. Martinez et al. shows better performance, surpassing our proposal by 2.2 points in the F1 and IOU metrics, while maintaining comparable QRS_{on}/QRS_{off} error rates. This difference could be attributed to the use of the QT dataset for training SoA algorithms.

The proposed method can accurately delineate the organized rhythms of the patients during SCA. This could assist in automatically computing the features described in Subsection 2.2.2 and greatly facilitate the work of clinicians. In addition, it would be possible to compute these features in real time and therefore could be included in methods such as J1.2 and improve resuscitation therapy.

Model	TP	FP	FN	F1(%)	IOU(%)	QRS_{on}/QRS_{off}(ms)
U-Net	107094	883	3783	97.4 (12.7)	77.1 (16.9)	16.8 (11.8)/11.3 (10.5)
Martinez et al. [40]	110323	172	554	99.6 (1.1)	79.3 (7.0)	16.5 (8.7)/11.3 (9.3)
Pilia et al. [42]	110509	850	368	99.4 (3.4)	72.1 (8.8)	16.9 (9.3)/23.3 (17.1)
Peimankar et al. [43]	90568	1198	20309	92.6 (22.5)	63.0 (32.2)	19.1 (13.2)/14.6 (14.6)
Camps et al. [44]	97912	8608	12965	87.0 (25.6)	61.3 (25.6)	25.3 (18.7)/18.4 (19.7)

Table 4.5. Performance of QRS delineation methods for the QT dataset in terms of mean (SD) values of F1, IOU, and QRS_{on}/QRS_{off} errors.

4.2.2 J2.2: Invasive Arterial Blood Pressure Delineator for Cardiopulmonary Resuscitation Patients during Pauses of Chest Compressions

The designed IBP delineation algorithm applicable to SCA patients, used a OHCA dataset recorded by EMS for traning and testing, and other two hemodynamically stable patients public datasets only for testing. The OHCA dataset, from Oslo (2015-2017), included ECG and IBP signals recorded using Lifepak-15 monitors/defibrillators. 377 segments (1127 min) without CC artifacts were extracted from 81 patients. The fiducial points of the IBP per beat, Sys_{peak} and Dia_{onset}, were manually annotated to be used as gold standards, resulting in 75682 beats. The Polysomnographic[1] and Complex Systems Laboratory (CSL)[2] datasets are composed of 18 sleeping patients and 2 patients, respectively. A total of 20 segments (5257 min) were extracted with Sys_{peak} and Dia_{onset} annotations for CSL dataset and only Dia_{onset} annotations for Polysomnographic dataset.

The raw IBP signal, IBP_{raw}, contained artifacts such as quantization noise and baseline drift. To address this, the signal was preprocessed using the SWT with 8-level decomposition and the Daubechies-4 mother wavelet. Filtered IBP signal, IBP_{filt}, was reconstructed from the sixth and seventh detail coefficients ($1-4$ Hz) as shown in Figure 4.5.

For beat detection, Δ_s was computed as the first difference of IBP_{filt}, followed by low-pass filtering with a 3rd-order Butterworth filter (zero-phase) at 5 Hz. The rectified version, Δs_{rec}, was

1 https://physionet.org/content/slpdb/1.0.0/

2 https://www.pdx.edu/electrical-computer-engineering/biomedical-signal-processing-lab

determined by setting negative values to zero. Sys_{peak} and Dia_{onset} were identified in Δ_{rec} based on changes from positive to zero and zero to positive values, respectively. They were aligned in time within interval of 100 ms before and after the detected points.

Finally, SAP and DAP, as defined in Figure 2.2, values were measured in IBP_{raw} and potential beats were confirmed by adaptive thresholding criteria in those variables.

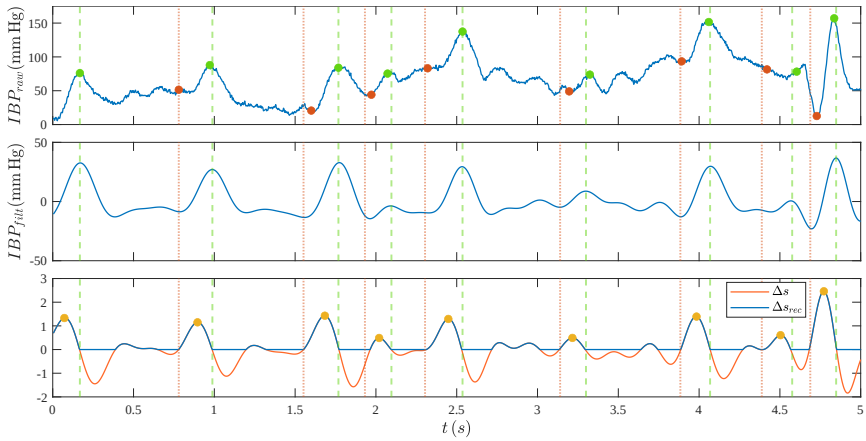

Figure 4.5. From top to button: IBP_{raw}, IBP_{filt}; and the first difference signal, Δs (in orange), and rectified first difference signal, Δs_{rec} (in blue). The yellow dots in the button panel indicate maximums of Δs_{rec}. Green and red dots are Sys_{peak} and Dia_{onset} instants, respectively.

The algorithms by Zong et al. [55] and Li et al. [54], with their scripts accessible on PhysioNet[3] [177] and Matlab File Exchange[4], respectively, were compared to J2.2 IBP delineator.

Performance metrics attending to heartbeat detection included Se_{hb}, PPV_{hb} and $F1_{hb}$. Correct detections were considered within 50 ms interval of the ground truth annotations. Additional analyses focused on Se_s, Sp_s, PPV_s and NPV_s for discriminating pulsatile segments were limited to OHCA segments because all segments in the public dataset were pulsatile.

3 https://physionet.org/content/pcst/1.0.0/

4 https://es.mathworks.com/matlabcentral/fileexchange/29484-pulse-waveform-delineator?s_tid=FX_rc3_behav

A 10-fold CV was used to evaluate the beat delineator. Threshold optimization was performed on the training set to maximize $F1_{hb}$ by uniform grid search.

Table 4.6 compares performance metrics of J2.2 delineator with SoA algorithms for heartbeat detection. Notably, proposed solution exhibits superior performance with the OHCA dataset, while demonstrating comparable performance with the public datasets.

		Heartbeat detection		
		Se_{hb} (%)	PPV_{hb} (%)	$F1_{hb}$ (%)
OHCA dataset	J2.2	96.1 (8.3)	96.1 (7.6)	95.7 (6.4)
	Zong [55]	62.8 (36.3)	93.8 (10.5)	71.9 (29.8)
	Li [54]	94.1 (9.6)	85.4 (23.7)	86.7 (19.6)
Public dataset	J2.2	98.4 (1.5)	98.8 (1.3)	98.6 (1.3)
	Zong [55]	97.9 (3.8)	98.4 (3.2)	98.1 (3.4)
	Li [54]	98.6 (1.3)	99.1 (1.0)	98.6 (1.0)

Table 4.6. Performance of J2.2 delineator compared to SoA algorithms using the OHCA dataset and two public datasets for heartbeat detection. The performance metrics include mean (SD) Se_{hb},PPV_{hb} and $F1_{hb}$.

Table 4.7 shows the performance of J2.2 and SoA delineators for pulsed segment discrimination on OHCA dataset (377 segments, 252 of them with pulse).

A IBP delineator that works with both stable and SCA patients has been developed, which has demonstrated better performance than SoA methods. A delineator of this kind can help to automatically calculate the physiologic variables required by predictive models of Subsection 2.2.3 and thereby can be included in predictors of PEA evolution such as C1.1.

	Pulsatile segment discrimination			
	Se_s (%)	Sp_s (%)	PPV_s (%)	NPV_s (%)
J2.2	98.8 (6.9)	91.6 (20.2)	97.4 (9.7)	98.7 (6.1)
Zong [55]	81.2 (31.0)	75.6 (31.5)	92.4 (20.5)	87.7 (21.8)
Li [54]	99.7 (2.6)	8.9 (23.3)	82.4 (24.4)	88.9 (33.3)

Table 4.7. Performance of J2.2 delineator compared to SoA algorithms using the OHCA dataset for pulsed segment discrimination. The performance metrics include mean (SD) Se_s, Sp_s, PPV_s and NPV_s.

5 CONCLUSIONS

This section provides an overview of the key contributions of the thesis. It begins by emphasizing the most significant findings, followed by a recap of all publications in journals and conferences related to the research. Additionally, it acknowledges the research projects and funding sources that facilitated the thesis development. Lastly, a concise exploration of potential avenues for future research based on the thesis results is presented.

5.1 Main contributions of the thesis

The main objective of this thesis was to contribute to the development of automatic predictors of PEA evolution, as well as ECG and IBP automated delineators that provide physiological parameters to be integrated in the previously mentioned predictors. At the end of the thesis, the main contributions can be synthesized as follows:

- *PEA evolution predicting algorithms based on the ECG and the TI signals:* Machine learning models have been fed with features automatically computed from ECG and TI signals for predicting the evolution of PEA segments during OHCA.
- *PEA evolution predicting algorithms based on models integrating QRS based features:* Features based on QRS complexes have been added to previous models for predicting the evolution of segments with PEA, as well as a modified version of the well known AMSA feature.

- *PEA evolution predicting algorithms based on models integrating IBP signal:* Physiological parameters calculated from the IBP signal have been added to the PEA evolution prediction models. These new features have added significant insight to the model that has improved its performance.
- *ECG delineation algorithms for patients in SCA:* An ECG delineator has been designed using a DL model, accurate to both hemodynamically stable and SCA patients. This delineator has shown better performance than SoA algorithms and might assist in delineating QRS complexes to give rescuers more information to take better decisions. Additionally, it may also be employed to compute automatic features and include them in predictive models of cardiac rhythm evolution.
- *IBP delineation algorithms for patients in SCA:* An IBP delineator accurate with both stable and SCA patients has been developed. This permits the automatic estimation of physiological parameters and provides valuable information to predictive models or to clinicians during the treatment of SCA patients.

5.2 Publications

The thesis has resulted in several significant contributions to the scientific community, formally detailed in Sections 5.2.1 and 5.2.2. These contributions include:

- In relation to Objective 1, two long papers have been published in journals indexed in the JCR Science Edition (A1 and A2), along with presentations at a national and an international conferences (C1 and C4) and one more accepted (C6).
- In relation to Objective 2, one long paper has been published (A3) and another has been submitted (A4) to journals indexed in the JCR Science Edition, along with presentations at three national and international conferences (C2, C3 and C5).

5.2.1 Journals indexed in the JCR science edition

A1 *A machine learning model for the prognosis of pulseless electrical activity during out-of-hospital cardiac arrest*

Jon Urteaga, Elisabete Aramendi, Andoni Elola, Unai Irusta, Ahamed H. Idris
MDPI Entropy 2021 (IF: 2.7, 43/110) [171]

A2 *Machine learning model to predict evolution of pulseless electrical activity during in-hospital cardiac arrest*
Jon Urteaga, Andoni Elola, Anders Norvik, Eirik Unneland, Trygve C Eftestøl, Abhishek Bhardwaj, David Buckler, Benjamin S Abella, Eirik Skogvoll, Elisabete Aramendi
Resuscitation Plus 2024 (IF: 2.4, 28/54) [172]

A3 *Invasive Arterial Blood Pressure Delineator for Cardiopulmonary Resuscitation Patients during Pauses of Chest Compressions*
Jon Urteaga, Andoni Elola, Elisabete Aramendi, Per Olav Berve, Lars Wik
Biomedical Signal Processing and Control 2024 (IF: 5.1, 26/96) [173]

A4 *A Deep Learning Model for QRS Delineation in Organized Rhythms during In-Hospital Cardiac Arrest* (Submitted)
Jon Urteaga, Andoni Elola, Daniel Herráez, Anders Norvik, Eirik Unneland, Abhishek Bhardwaj, David Buckler, Benjamin S. Abella, Eirik Skogvoll, Elisabete Aramend
IEEE Transactions on Biomedical Engineering 2024 (IF: 4.6, 34/96) [174]

5.2.2 National and international conferences

C1 *Modelo predictivo del retorno de circulación espontánea en la parada cardiorrespiratoria utilizando el ECG y la impedancia torácica*
Jon Urteaga, Elisabete Aramendi, Andoni Elola, Unai Irusta, Ahamed H. Idris
XXXVIII Congreso Anual de la Sociedad Española de Ingeniería Biomédica (CASEIB) 2020 [165]

C2 *Automated detection of pulse using continuous invasive arterial blood pressure in patients during cardiopulmonary resuscitation*
Jon Urteaga, Andoni Elola, Elisabete Aramendi, Per Olav Berve, Lars Wik
Computing in Cardiology Conference (CinC) 2021 [166]

C3 *Automated Algorithm for QRS Detection in Cardiac Arrest Patients with PEA*
Jon Urteaga, Andoni Elola, Elisabete Aramendi, Anders Norvik, Eirik Unneland, Eirik Skogvoll
Computing in Cardiology (CinC) 2022 [167]

C4 *The Prediction Of Pulseless Electrical Activity Evolution During In-hospital Cardiac Arrest Using Machine Learning*
Jon Urteaga, Elisabete Aramendi, Andoni Elola, Anders Norvik, Eirik Unneland, Abhishek Bhardwaj, David Buckler, Benjamin S Abella, Eirik Skogvoll
Resuscitation Science Symposium (AHA-ReSS) 2022 [168]

C5 *Detección automática de complejos QRS en pacientes con actividad eléctrica sin pulso durante la parada cardiorrespiratoria*
Jon Urteaga, Andoni Elola, Elisabete Aramend, Daniel Herráez, Anders Norvik, Eirik Unneland, Eirik Skogvoll
XL Congreso Anual de la Sociedad Española de Ingeniería Biomédica (CASEIB) 2022 [169]

C6 *A Random Forest Model for Pulseless Electrical Activity Prognosis Prediction During Out-of-Hospital Cardiac Arrest Using Invasive Blood Pressure* (Accepted)
Jon Urteaga, Andoni Elola, Per Olav Berve, Lars Wik, Elisabete Aramendi
EMBC (Annual International Conference of the IEEE Engineering in Medicine and Biology Society) 2024 [170]

5.3 Financial support

This thesis has been primarily supported by a predoctoral grant (P1) and several national and international grants. All projects and funding sources that have supported financially the development of the thesis are acknowledged in the following:

P1 *Ayuda para la formación de personal investigador* (PRE_2020_1_0177, PRE2021_2_0173, PRE_2022_2_0245 and PRE_2023_2_0101). Basque Government Department of Education, Universities and Research. 2020-2023.

P2 *BioRes (Biomedical Engineering and Resuscitation)* (IT1229-19). Basque Government Department of Education, Universities and Research. February 2019 – December 2022.

P3 *BioRes (Biomedical Engineering and Resuscitation)* (IT1717-22). Basque Government Department of Education, Universities and Research. January 2022 – December 2025.

P4 *Procesado multimodal de señal y aprendizaje automático para la mejora del tratamiento de la parada cardiorrespiratoria extrahospitalaria* (RTI2018-101475-BI00). Spanish Ministry of Economy and Competitiveness. February 2019 – September 2022.

P5 *Inteligencia artificial y nuevas tecnologías para el guiado de la terapia de resucitación en la parada cardiorrespiratoria extrahospitalaria* (PID2021-122727OB-I00). Spanish Ministry of Science, Research and Universities. September 2022 – August 2025.

5.4 Future lines of research

The thesis has advanced the development of AI models for predicting the prognosis of PEA segment and has developed delineators for characterizing ECG and IBP signals for SCA patients. This work has already prompted new research interests and revealed opportunities to improve or enhance existing solutions as the next ones:

- Current ML methods for developing PEA predictors could potentially be replaced by DL based methods, which have demonstrated significant potential. These methods would require access to a larger patient datasets, but they could substantially enhance model performance by capturing details that ML methods may overlook.
- Existing models for PEA evolution prediction using ECG, TI and even IBP signals could improve their performance with additional signals or information. Pulse oximetry and capnography signals are leading candidates to provide relevant information to predictive methods. In addition, demographic information such as the patient's initial heart rhythm, the location of sudden cardiac arrest or bystander response could be incorporated to enrich the model.

- A DL based delineation model like the one proposed in J2.1 could be tested for delineating IBP signals in SCA patients. These models have already demonstrated potential delineating and segmenting biomedical signals. Using them for IBP signals could enhance the performance of the current delineator and potentially calculate physiological parameters more accurately.
- Despite the access to wide international datasets in the development of current thesis work, employing methods to augment the size and variety of datasets would contribute to more accurate models. Synthetic data or data augmentation techniques would contribute to better training processes, reducing the risks of overfitting and allowing a better generalization. Those aspects are especially beneficial in DL, where complex models require large datasets to effectively capture intricate patterns.

BIBLIOGRAPHY

[1] R. J. Myerburg, "Sudden cardiac death," *interface between pathophysiology and epidemiology. Card Electrophysiol Clin*, vol. 9, pp. 515–524, 2017.

[2] M. Høybye, N. Stankovic, M. Holmberg, H. C. Christensen, A. Granfeldt, and L. W. Andersen, "In-hospital vs. out-of-hospital cardiac arrest: patient characteristics and survival," *Resuscitation*, vol. 158, pp. 157–165, 2021.

[3] A. Fuchs, D. Käser, L. Theiler, R. Greif, J. Knapp, and J. Berger-Estilita, "Survival and long-term outcomes following in-hospital cardiac arrest in a swiss university hospital: a prospective observational study," *Scandinavian journal of trauma, resuscitation and emergency medicine*, vol. 29, pp. 1–10, 2021.

[4] J.-T. Gräsner, J. Herlitz, I. B. Tjelmeland, J. Wnent, S. Masterson, G. Lilja, B. Bein, B. W. Böttiger, F. Rosell-Ortiz, J. P. Nolan *et al.*, "European resuscitation council guidelines 2021: epidemiology of cardiac arrest in europe," *Resuscitation*, vol. 161, pp. 61–79, 2021.

[5] L. W. Andersen, M. J. Holmberg, K. M. Berg, M. W. Donnino, and A. Granfeldt, "In-hospital cardiac arrest: a review," *Jama*, vol. 321, no. 12, pp. 1200–1210, 2019.

[6] J. P. Nolan, J. Soar, G. B. Smith, C. Gwinnutt, F. Parrott, S. Power, D. A. Harrison, E. Nixon, K. Rowan *et al.*, "Incidence and outcome of in-hospital cardiac arrest in the united kingdom national cardiac arrest audit," *Resuscitation*, vol. 85, no. 8, pp. 987–992, 2014.

[7] P. S. Chan, B. McNally, F. Tang, and A. Kellermann, "Recent trends in survival from out-of-hospital cardiac arrest in the united states," *Circulation*, vol. 130, no. 21, pp. 1876–1882, 2014.

[8] G. Nichol, E. Thomas, C. W. Callaway, J. Hedges, J. L. Powell, T. P. Aufderheide, T. Rea, R. Lowe, T. Brown, J. Dreyer *et al.*, "Regional

variation in out-of-hospital cardiac arrest incidence and outcome," *Jama*, vol. 300, no. 12, pp. 1423–1431, 2008.

[9] C. Atwood, M. S. Eisenberg, J. Herlitz, and T. D. Rea, "Incidence of ems-treated out-of-hospital cardiac arrest in europe," *Resuscitation*, vol. 67, no. 1, pp. 75–80, 2005.

[10] I. Jacobs, V. Nadkarni, I. T. F. on Cardiac Arrest, C. R. Outcomes, C. Participants, J. Bahr, R. A. Berg, J. E. Billi, L. Bossaert, P. Cassan, A. Coovadia *et al.*, "Cardiac arrest and cardiopulmonary resuscitation outcome reports: update and simplification of the utstein templates for resuscitation registries: a statement for healthcare professionals from a task force of the international liaison committee on resuscitation (american heart association, european resuscitation council, australian resuscitation council, new zealand resuscitation council, heart and stroke foundation of canada, interamerican heart foundation, resuscitation councils of southern africa)," *Circulation*, vol. 110, no. 21, pp. 3385–3397, 2004.

[11] D. Christensen, S. Rajan, K. Kragholm, K. Søndergaard, O. Hansen, T. A. Gerds, C. Torp-Pedersen, G. Gislason, F. K. Lippert, and C. Barcella, "Bystander cardiopulmonary resuscitation and survival in patients with out-of-hospital cardiac arrest of non-cardiac origin," *Resuscitation*, vol. 140, pp. 98–105, 2019.

[12] A. Claesson, T. Djarv, P. Nordberg, M. Ringh, J. Hollenberg, C. Axelsson, A. Ravn-Fischer, and A. Stromsoe, "Medical versus non medical etiology in out-of-hospital cardiac arrest—changes in outcome in relation to the revised utstein template," *Resuscitation*, vol. 110, pp. 48–55, 2017.

[13] P. A. Meaney, V. M. Nadkarni, K. B. Kern, J. H. Indik, H. R. Halperin, and R. A. Berg, "Rhythms and outcomes of adult in-hospital cardiac arrest," *Critical care medicine*, vol. 38, no. 1, pp. 101–108, 2010.

[14] C. Sandroni, J. Nolan, F. Cavallaro, and M. Antonelli, "In-hospital cardiac arrest: incidence, prognosis and possible measures to improve survival," *Intensive care medicine*, vol. 33, pp. 237–245, 2007.

[15] S. P. Keller and H. R. Halperin, "Cardiac arrest: the changing incidence of ventricular fibrillation," *Current treatment options in cardiovascular medicine*, vol. 17, pp. 1–11, 2015.

[16] G. D. Perkins, J.-T. Gräsner, F. Semeraro, T. Olasveengen, J. Soar, C. Lott, P. Van de Voorde, J. Madar, D. Zideman, S. Mentzelopoulos *et al.*, "European resuscitation council guidelines 2021: executive summary," *Resuscitation*, vol. 161, pp. 1–60, 2021.

[17] R. M. Merchant, A. A. Topjian, A. R. Panchal, A. Cheng, K. Aziz, K. M. Berg, E. J. Lavonas, D. J. Magid, and Adult Basic and Advanced Life Support, Pediatric Basic and Advanced Life Support, Neonatal Life Support, Resuscitation Education Science, and Systems of Care Writing Groups, "Part 1: Executive summary: 2020 american heart association guidelines for cardiopulmonary resuscitation and emergency cardiovascular care." *Circulation*, vol. 142, pp. S337–S357, Oct. 2020.

[18] J. Kramer-Johansen, D. P. Edelson, H. Losert, K. Köhler, and B. S. Abella, "Uniform reporting of measured quality of cardiopulmonary resuscitation (cpr)," *Resuscitation*, vol. 74, no. 3, pp. 406–417, 2007.

[19] R. O. Cummins, J. P. Ornato, W. H. Thies, and P. E. Pepe, "Improving survival from sudden cardiac arrest: the" chain of survival" concept. a statement for health professionals from the advanced cardiac life support subcommittee and the emergency cardiac care committee, american heart association." *Circulation*, vol. 83, no. 5, pp. 1832–1847, 1991.

[20] C. Sasson, M. A. Rogers, J. Dahl, and A. L. Kellermann, "Predictors of survival from out-of-hospital cardiac arrest: a systematic review and meta-analysis," *Circulation: Cardiovascular Quality and Outcomes*, vol. 3, no. 1, pp. 63–81, 2010.

[21] R. M. Sutton, B. French, A. Nishisaki, D. E. Niles, M. R. Maltese, L. Boyle, M. Stavland, J. Eilevstjønn, K. B. Arbogast, R. A. Berg *et al.*, "American heart association cardiopulmonary resuscitation quality targets are associated with improved arterial blood pressure during pediatric cardiac arrest," *Resuscitation*, vol. 84, no. 2, pp. 168–172, 2013.

[22] M. L. Selby, J. A. Kautz, T. J. Moore, W. R. Gombeski Jr, A. G. Ramirez, E. J. Farge, and R. N. Forthofer, "Indicators of response to a mass media cpr recruitment campaign." *American journal of public health*, vol. 72, no. 9, pp. 1039–1042, 1982.

[23] M. S. Eisenberg, L. Bergner, and A. Hallstrom, "Cardiac resuscitation in the community: importance of rapid provision and implications for program planning," *jama*, vol. 241, no. 18, pp. 1905–1907, 1979.

[24] M. Hayashi, W. Shimizu, and C. M. Albert, "The spectrum of epidemiology underlying sudden cardiac death," *Circulation research*, vol. 116, no. 12, pp. 1887–1906, 2015.

[25] L. Bossaert, "Fibrillation and defibrillation of the heart," *British journal of anaesthesia*, vol. 79, no. 2, pp. 203–213, 1997.

[26] T. D. Valenzuela, D. J. Roe, G. Nichol, L. L. Clark, D. W. Spaite, and R. G. Hardman, "Outcomes of rapid defibrillation by security officers after cardiac arrest in casinos," *New England Journal of Medicine*, vol. 343, no. 17, pp. 1206–1209, 2000.

[27] M. T. Blom, S. G. Beesems, P. C. Homma, J. A. Zijlstra, M. Hulleman, D. A. Van Hoeijen, A. Bardai, J. G. Tijssen, H. L. Tan, and R. W. Koster, "Improved survival after out-of-hospital cardiac arrest and use of automated external defibrillators," *Circulation*, vol. 130, no. 21, pp. 1868–1875, 2014.

[28] A. H. Association *et al.*, "Guidelines 2000 for cardiopulmonary resusciation and emergency cardiovascular care. part 4: The automated external defibrillator: Key link in the chain of survival: The american heart association in collaboration with the international liaison committee on resuscitation," *Circulation*, vol. 102, pp. I–60, 2000.

[29] J. Soar, B. W. Böttiger, P. Carli, K. Couper, C. D. Deakin, T. Djärv, C. Lott, T. Olasveengen, P. Paal, T. Pellis *et al.*, "European resuscitation council guidelines 2021: adult advanced life support," *Resuscitation*, vol. 161, pp. 115–151, 2021.

[30] M. L. Weisfeldt, R. E. Kerber, R. P. McGoldrick, A. J. Moss, G. Nichol, J. P. Ornato, D. G. Palmer, B. Riegel, and S. C. Smith Jr, "Public access defibrillation: a statement for healthcare professionals from the american heart association task force on automatic external defibrillation," *Circulation*, vol. 92, no. 9, pp. 2763–2763, 1995.

[31] J. Drezner, "Preparing for sudden cardiac arrest—the essential role of automated external defibrillators in athletic medicine: a critical review," *British Journal of Sports Medicine*, vol. 43, no. 9, pp. 702–707, 2009.

[32] R. E. Kerber, L. B. Becker, J. D. Bourland, R. O. Cummins, A. P. Hallstrom, M. B. Michos, G. Nichol, J. P. Ornato, W. H. Thies, R. D. White *et al.*, "Automatic external defibrillators for public access defibrillation: recommendations for specifying and reporting arrhythmia analysis algorithm performance, incorporating new waveforms, and enhancing safety: a statement for health professionals from the american heart association task force on automatic external defibrillation, subcommittee on aed safety and efficacy," *Circulation*, vol. 95, no. 6, pp. 1677–1682, 1997.

[33] S. O. Aase and H. Myklebust, "Compression depth estimation for cpr quality assessment using dsp on accelerometer signals," *IEEE*

Transactions on Biomedical Engineering, vol. 49, no. 3, pp. 263–268, 2002.

[34] R. M. Sutton, S. H. Friess, M. Y. Naim, J. W. Lampe, G. Bratinov, T. R. Weiland III, M. Garuccio, V. M. Nadkarni, L. B. Becker, and R. A. Berg, "Patient-centric blood pressure–targeted cardiopulmonary resuscitation improves survival from cardiac arrest," *American journal of respiratory and critical care medicine*, vol. 190, no. 11, pp. 1255–1262, 2014.

[35] A. Louw, C. Cracco, C. Cerf, A. Harf, P. Duvaldestin, F. Lemaire, and L. Brochard, "Accuracy of pulse oximetry in the intensive care unit," *Intensive care medicine*, vol. 27, pp. 1606–1613, 2001.

[36] C. Pantazopoulos, T. Xanthos, I. Pantazopoulos, A. Papalois, E. Kouskouni, and N. Iacovidou, "A review of carbon dioxide monitoring during adult cardiopulmonary resuscitation," *Heart, Lung and Circulation*, vol. 24, no. 11, pp. 1053–1061, 2015.

[37] J. P. Nolan, R. A. Berg, L. W. Andersen, F. Bhanji, P. S. Chan, M. W. Donnino, S. H. Lim, M. H.-M. Ma, V. M. Nadkarni, M. A. Starks *et al.*, "Cardiac arrest and cardiopulmonary resuscitation outcome reports: update of the utstein resuscitation registry template for in-hospital cardiac arrest: a consensus report from a task force of the international liaison committee on resuscitation (american heart association, european resuscitation council, australian and new zealand council on resuscitation, heart and stroke foundation of canada, interamerican heart foundation, resuscitation council of southern africa, resuscitation council of asia)," *Circulation*, vol. 140, no. 18, pp. e746–e757, 2019.

[38] M. Gardberg and R. Ashman, "The qrs complex of the electrocardiogram," *Archives of Internal Medicine*, vol. 72, no. 2, pp. 210–230, 1943.

[39] A. K. Bhoi and K. S. Sherpa, "Qrs complex detection and analysis of cardiovascular abnormalities: A review." *International Journal Bioautomation*, vol. 18, no. 3, 2014.

[40] J. P. Martínez, R. Almeida, S. Olmos, A. P. Rocha, and P. Laguna, "A wavelet-based ecg delineator: evaluation on standard databases," *IEEE Transactions on biomedical engineering*, vol. 51, no. 4, pp. 570–581, 2004.

[41] C. Li, C. Zheng, and C. Tai, "Detection of ecg characteristic points using wavelet transforms," *IEEE Transactions on biomedical Engineering*, vol. 42, no. 1, pp. 21–28, 1995.

[42] N. Pilia, C. Nagel, G. Lenis, S. Becker, O. Dössel, and A. Loewe, "Ecgdeli-an open source ecg delineation toolbox for matlab," *SoftwareX*, vol. 13, p. 100639, 2021.

[43] A. Peimankar and S. Puthusserypady, "Dens-ecg: A deep learning approach for ecg signal delineation," *Expert systems with applications*, vol. 165, p. 113911, 2021.

[44] J. Camps, B. Rodríguez, and A. Mincholé, "Deep learning based qrs multilead delineator in electrocardiogram signals," in *2018 Computing in Cardiology Conference (CinC)*, vol. 45. IEEE, 2018, pp. 1–4.

[45] G. de Lannoy, B. Frénay, M. Verleysen, and J. Delbeke, "Supervised ecg delineation using the wavelet transform and hidden markov models," in *4th European Conference of the International Federation for Medical and Biological Engineering: ECIFMBE 2008 23–27 November 2008 Antwerp, Belgium*. Springer, 2009, pp. 22–25.

[46] J. M. Bote, J. Recas, F. Rincón, D. Atienza, and R. Hermida, "A modular low-complexity ecg delineation algorithm for real-time embedded systems," *IEEE journal of biomedical and health informatics*, vol. 22, no. 2, pp. 429–441, 2017.

[47] P. Laguna, R. Jané, and P. Caminal, "Automatic detection of wave boundaries in multilead ecg signals: Validation with the cse database," *Computers and biomedical research*, vol. 27, no. 1, pp. 45–60, 1994.

[48] X. Liang, L. Li, Y. Liu, D. Chen, X. Wang, S. Hu, J. Wang, H. Zhang, C. Sun, and C. Liu, "Ecg_segnet: An ecg delineation model based on the encoder-decoder structure," *Computers in Biology and Medicine*, vol. 145, p. 105445, 2022.

[49] W. Kubicek, D. Witsoe, R. Patterson *et al.*, "Development and evaluation of an impedance cardiographic system to measure cardiac output and other cardiac parameters: Final progress report (nasa 9-4500)," *National Aeronautics and Space Administration*, vol. 170, pp. 724–732, 1970.

[50] L. A. Geddes and L. E. Baker, *Principles of applied biomedical instrumentation*. John Wiley & Sons, 1991.

[51] F. S. Stecher, J.-A. Olsen, R. E. Stickney, and L. Wik, "Transthoracic impedance used to evaluate performance of cardiopulmonary resuscitation during out of hospital cardiac arrest," *Resuscitation*, vol. 79, no. 3, pp. 432–437, 2008.

[52] M. Bayram and C. W. Yancy, "Transthoracic impedance cardiography: a noninvasive method of hemodynamic assessment," *Heart failure*

clinics, vol. 5, no. 2, pp. 161–168, 2009.

[53] O. Singh and R. K. Sunkaria, "Empirical wavelet transform-based delineator for arterial blood pressure waveforms," *Bio-Algorithms and Med-Systems*, vol. 12, no. 2, pp. 61–66, 2016.

[54] B. N. Li, M. C. Dong, and M. I. Vai, "On an automatic delineator for arterial blood pressure waveforms," *Biomedical Signal Processing and Control*, vol. 5, no. 1, pp. 76–81, 2010.

[55] W. Zong, T. Heldt, G. Moody, and R. Mark, "An open-source algorithm to detect onset of arterial blood pressure pulses," in *Computers in Cardiology, 2003*. IEEE, 2003, pp. 259–262.

[56] Q. Li, R. G. Mark, and G. D. Clifford, "Artificial arterial blood pressure artifact models and an evaluation of a robust blood pressure and heart rate estimator," *Biomedical engineering online*, vol. 8, no. 1, pp. 1–15, 2009.

[57] D. T. Ko, F. Qiu, M. Koh, P. Dorian, S. Cheskes, P. C. Austin, D. C. Scales, H. C. Wijeysundera, P. R. Verbeek, I. Drennan *et al.*, "Factors associated with out-of-hospital cardiac arrest with pulseless electric activity: a population-based study," *American heart journal*, vol. 177, pp. 129–137, 2016.

[58] T. J. Mader, B. H. Nathanson, S. Millay, R. A. Coute, M. Clapp, and B. McNally, "Out-of-hospital cardiac arrest outcomes stratified by rhythm analysis," *Resuscitation*, vol. 83, no. 11, pp. 1358–1362, 2012.

[59] S. Girotra, B. K. Nallamothu, J. A. Spertus, Y. Li, H. M. Krumholz, and P. S. Chan, "Trends in survival after in-hospital cardiac arrest," *New England Journal of Medicine*, vol. 367, no. 20, pp. 1912–1920, 2012.

[60] L. A. Cobb, C. E. Fahrenbruch, M. Olsufka, and M. K. Copass, "Changing incidence of out-of-hospital ventricular fibrillation, 1980-2000," *Jama*, vol. 288, no. 23, pp. 3008–3013, 2002.

[61] J. Herlitz, E. Andersson, A. Bång, J. Engdahl, M. Holmberg, J. Lindqvist, B. Karlson, and L. Waagstein, "Experiences from treatment of out-of-hospital cardiac arrest during 17 years in göteborg," *European heart journal*, vol. 21, no. 15, pp. 1251–1258, 2000.

[62] A. Norvik, E. Unneland, D. Bergum, D. Buckler, A. Bhardwaj, T. Eftestøl, E. Aramendi, T. Nordseth, B. Abella, J. T. Kvaløy *et al.*, "Pulseless electrical activity in in-hospital cardiac arrest–a crossroad for decisions," *Resuscitation*, vol. 176, pp. 117–124, 2022.

[63] V. S. Tayal and J. A. Kline, "Emergency echocardiography to detect pericardial effusion in patients in pea and near-pea states,"

Resuscitation, vol. 59, no. 3, pp. 315–318, 2003.

[64] J. Rabjohns, T. Quan, K. Boniface, and A. Pourmand, "Pseudo-pulseless electrical activity in the emergency department, an evidence based approach," *The American journal of emergency medicine*, vol. 38, no. 2, pp. 371–375, 2020.

[65] S. Van den Bempt, L. Wauters, and P. Dewolf, "Pulseless electrical activity: detection of underlying causes in a prehospital setting," *Medical Principles and Practice*, vol. 30, no. 3, pp. 212–222, 2021.

[66] D. C. Parish, H. Goyal, and F. C. Dane, "Mechanism of death: there's more to it than sudden cardiac arrest," *Journal of thoracic disease*, vol. 10, no. 5, p. 3081, 2018.

[67] Y.-J. Kim, Y. J. Lee, S. M. Ryoo, C. H. Sohn, S. Ahn, D.-W. Seo, K. S. Lim, and W. Y. Kim, "Role of blood gas analysis during cardiopulmonary resuscitation in out-of-hospital cardiac arrest patients," *Medicine*, vol. 95, no. 25, 2016.

[68] P.-Y. Tsou, J. Kurbedin, Y.-S. Chen, E. H. Chou, M.-t. G. Lee, M. C.-H. Lee, M. H.-M. Ma, S.-C. Chen, and C.-C. Lee, "Accuracy of point-of-care focused echocardiography in predicting outcome of resuscitation in cardiac arrest patients: a systematic review and meta-analysis," *Resuscitation*, vol. 114, pp. 92–99, 2017.

[69] L. Littmann, D. J. Bustin, and M. W. Haley, "A simplified and structured teaching tool for the evaluation and management of pulseless electrical activity," *Medical Principles and Practice*, vol. 23, no. 1, pp. 1–6, 2013.

[70] D. Bergum, G. W. Skjeflo, T. Nordseth, O. C. Mjølstad, B. O. Haugen, E. Skogvoll, and J. P. Loennechen, "Ecg patterns in early pulseless electrical activity-associations with aetiology and survival of in-hospital cardiac arrest," *Resuscitation*, vol. 104, pp. 34–39, 2016.

[71] K. G. Moons, P. Royston, Y. Vergouwe, D. E. Grobbee, and D. G. Altman, "Prognosis and prognostic research: what, why, and how?" *Bmj*, vol. 338, 2009.

[72] T. Eftestøl, K. Sunde, S. Ole Aase, J. H. Husøy, and P. A. Steen, "Predicting outcome of defibrillation by spectral characterization and nonparametric classification of ventricular fibrillation in patients with out-of-hospital cardiac arrest," *Circulation*, vol. 102, no. 13, pp. 1523–1529, 2000.

[73] A. Neurauter, T. Eftestøl, J. Kramer-Johansen, B. S. Abella, K. Sunde, V. Wenzel, K. H. Lindner, J. Eilevstjønn, H. Myklebust, P. A. Steen

et al., "Prediction of countershock success using single features from multiple ventricular fibrillation frequency bands and feature combinations using neural networks," *Resuscitation*, vol. 73, no. 2, pp. 253–263, 2007.

[74] I. Jekova, "Shock advisory tool: Detection of life-threatening cardiac arrhythmias and shock success prediction by means of a common parameter set," *Biomedical Signal Processing and Control*, vol. 2, no. 1, pp. 25–33, 2007.

[75] S. Shandilya, K. Ward, M. Kurz, and K. Najarian, "Non-linear dynamical signal characterization for prediction of defibrillation success through machine learning," *BMC Medical Informatics and Decision Making*, vol. 12, no. 1, pp. 1–9, 2012.

[76] M. D. Ivanović, J. Hannink, M. Ring, F. Baronio, V. Vukčević, L. Hadžievski, and B. Eskofier, "Predicting defibrillation success in out-of-hospital cardiac arrested patients: Moving beyond feature design," *Artificial Intelligence in Medicine*, vol. 110, p. 101963, 2020.

[77] J. Coult, T. D. Rea, J. Blackwood, P. J. Kudenchuk, C. Liu, and H. Kwok, "A method to predict ventricular fibrillation shock outcome during chest compressions," *Computers in Biology and Medicine*, vol. 129, p. 104136, 2021.

[78] S. M. Ryoo, D. H. Lee, B. K. Lee, C. S. Youn, Y.-J. Kim, S. J. Kim, Y. H. Kim, and W. Y. Kim, "Prognostic factors for re-arrest with shockable rhythm during target temperature management in out-of-hospital shockable cardiac arrest patients," *Journal of Clinical Medicine*, vol. 8, no. 9, p. 1360, 2019.

[79] K. S. Han, S. J. Kim, E. J. Lee, and S. W. Lee, "The effect of extracorporeal cardiopulmonary resuscitation in re-arrest after survival event: a retrospective analysis," *Perfusion*, vol. 35, no. 1, pp. 39–47, 2020.

[80] Y. H. Jung, K. W. Jeung, H. Y. Lee, B. K. Lee, D. H. Lee, J. Shin, H. J. Lee, I. S. Cho, Y.-M. Kim, K. H. N. investigators *et al.*, "Rearrest during hospitalisation in adult comatose out-of-hospital cardiac arrest patients: Risk factors and prognostic impact, and predictors of favourable long-term outcomes," *Resuscitation*, vol. 170, pp. 150–159, 2022.

[81] A. Elola, E. Aramendi, E. Rueda, U. Irusta, H. Wang, and A. Idris, "Towards the prediction of rearrest during out-of-hospital cardiac arrest," *Entropy*, vol. 22, no. 7, p. 758, 2020.

[82] A. Norvik, J. Kvaløy, G. Skjeflo, D. Bergum, T. Nordseth, J. Loennechen, E. Unneland, D. Buckler, A. Bhardwaj, T. Eftestøl *et al.*, "Heart rate and qrs duration as biomarkers predict the immediate outcome from pulseless electrical activity," *Resuscitation*, vol. 185, p. 109739, 2023.

[83] A. Norvik, G. W. Skjeflo, E. Unneland, D. Bergum, D. Buckler, A. Bhardwaj, T. Eftestol, E. Aramendi, T. Nordseth, B. Abella *et al.*, "Heart rate and qrs duration predict immediate outcome in pulseless electrical activity (pea) during in-hospital cardiac arrest (ihca)," *Circulation*, vol. 146, no. Suppl_1, pp. A250–A250, 2022.

[84] C. Hassager, K. Nagao, and D. Hildick-Smith, "Out-of-hospital cardiac arrest: in-hospital intervention strategies," *The Lancet*, vol. 391, no. 10124, pp. 989–998, 2018.

[85] J.-m. Kwon, K.-H. Jeon, H. M. Kim, M. J. Kim, S. Lim, K.-H. Kim, P. S. Song, J. Park, R. K. Choi, and B.-H. Oh, "Deep-learning-based out-of-hospital cardiac arrest prognostic system to predict clinical outcomes," *Resuscitation*, vol. 139, pp. 84–91, 2019.

[86] M. Krizmaric, M. Verlic, G. Stiglic, S. Grmec, and P. Kokol, "Intelligent analysis in predicting outcome of out-of-hospital cardiac arrest," *Computer methods and programs in biomedicine*, vol. 95, no. 2, pp. S22–S32, 2009.

[87] N. Al-Dury, A. Ravn-Fischer, J. Hollenberg, J. Israelsson, P. Nordberg, A. Strömsöe, C. Axelsson, J. Herlitz, and A. Rawshani, "Identifying the relative importance of predictors of survival in out of hospital cardiac arrest: a machine learning study," *Scandinavian journal of trauma, resuscitation and emergency medicine*, vol. 28, pp. 1–8, 2020.

[88] Y. H. Lo and Y. C. A. Siu, "Predicting survived events in nontraumatic out-of-hospital cardiac arrest: A comparison study on machine learning and regression models," *The Journal of Emergency Medicine*, vol. 61, no. 6, pp. 683–694, 2021.

[89] Y. Hirano, Y. Kondo, K. Sueyoshi, K. Okamoto, and H. Tanaka, "Early outcome prediction for out-of-hospital cardiac arrest with initial shockable rhythm using machine learning models," *Resuscitation*, vol. 158, pp. 49–56, 2021.

[90] D.-W. Seo, H. Yi, H.-J. Bae, Y.-J. Kim, C.-H. Sohn, S. Ahn, K.-S. Lim, N. Kim, and W.-Y. Kim, "Prediction of neurologically intact survival in cardiac arrest patients without pre-hospital return of spontaneous circulation: Machine learning approach," *Journal of clinical medicine*, vol. 10, no. 5, p. 1089, 2021.

[91] S. Harford, H. Darabi, M. Del Rios, S. Majumdar, F. Karim, T. V. Hoek, K. Erwin, and D. P. Watson, "A machine learning based model for out of hospital cardiac arrest outcome classification and sensitivity analysis," *Resuscitation*, vol. 138, pp. 134–140, 2019.

[92] S. Harford, M. Del Rios, S. Heinert, J. Weber, E. Markul, K. Tataris, T. Campbell, T. Vanden Hoek, and H. Darabi, "A machine learning approach for modeling decisions in the out of hospital cardiac arrest care workflow," *BMC Medical Informatics and Decision Making*, vol. 22, no. 1, pp. 1–9, 2022.

[93] S. J. Shin, H. S. Bae, H. J. Moon, G. W. Kim, Y. S. Cho, D. W. Lee, D. K. Jeong, H. J. Kim, and H. J. Lee, "Evaluation of optimal scene time interval for out-of-hospital cardiac arrest using a deep neural network," *The American Journal of Emergency Medicine*, vol. 63, pp. 29–37, 2023.

[94] J. Toy, N. Bosson, S. Schlesinger, M. Gausche-Hill, and S. Stratton, "Artificial intelligence to support out-of-hospital cardiac arrest care: A scoping review," *Resuscitation Plus*, vol. 16, p. 100491, 2023.

[95] T. P. Aufderheide, R. K. Thakur, H. A. Stueven, C. Aprahamian, Y.-R. Zhu, D. Fark, K. Hargarten, and D. Olson, "Electrocardiographic characteristics in emd," *Resuscitation*, vol. 17, no. 2, pp. 183–193, 1989.

[96] C. Weiser, M. Poppe, F. Sterz, H. Herkner, C. Clodi, C. Schriefl, A. Warenits, M. Vossen, M. Schwameis, A. Nürnberger *et al.*, "Initial electrical frequency predicts survival and neurological outcome in out of hospital cardiac arrest patients with pulseless electrical activity," *Resuscitation*, vol. 125, pp. 34–38, 2018.

[97] J. H. Kim, H. W. Ryoo, J.-y. Kim, J. Y. Ahn, S. Moon, D. E. Lee, Y. H. Mun, and J. W. Son, "Qrs complex characteristics and patient outcomes in out-of-hospital pulseless electrical activity cardiac arrest," *Emergency Medicine Journal*, vol. 38, no. 1, pp. 53–58, 2021.

[98] M. L. Ho, M. Gatien, C. Vaillancourt, V. Whitham, and I. G. Stiell, "Utility of prehospital electrocardiogram characteristics as prognostic markers in out-of-hospital pulseless electrical activity arrests," *Emergency Medicine Journal*, vol. 35, no. 2, pp. 89–95, 2018.

[99] C. Mehta and W. Brady, "Pulseless electrical activity in cardiac arrest: electrocardiographic presentations and management considerations based on the electrocardiogram," *The American journal of emergency medicine*, vol. 30, no. 1, pp. 236–239, 2012.

[100] A. Elola, E. Aramendi, U. Irusta, P. O. Berve, and L. Wik, "Multimodal algorithms for the classification of circulation states during out-of-hospital cardiac arrest," *IEEE Transactions on Biomedical Engineering*, vol. 68, no. 6, pp. 1913–1922, 2020.

[101] M. Hauck, J. Studnek, A. C. Heffner, and D. A. Pearson, "Cardiac arrest with initial arrest rhythm of pulseless electrical activity: do rhythm characteristics correlate with outcome?" *The American Journal of Emergency Medicine*, vol. 33, no. 7, pp. 891–894, 2015.

[102] G. W. Skjeflo, T. Nordseth, J. P. Loennechen, D. Bergum, and E. Skogvoll, "Ecg changes during resuscitation of patients with initial pulseless electrical activity are associated with return of spontaneous circulation," *Resuscitation*, vol. 127, pp. 31–36, 2018.

[103] G. Ristagno, Y. Li, F. Fumagalli, A. Finzi, and W. Quan, "Amplitude spectrum area to guide resuscitation—a retrospective analysis during out-of-hospital cardiopulmonary resuscitation in 609 patients with ventricular fibrillation cardiac arrest," *Resuscitation*, vol. 84, no. 12, pp. 1697–1703, 2013.

[104] A. Elola, E. Aramendi, U. Irusta, J. Del Ser, E. Alonso, and M. Daya, "Ecg-based pulse detection during cardiac arrest using random forest classifier," *Medical & biological engineering & computing*, vol. 57, no. 2, pp. 453–462, 2019.

[105] G. Ristagno, T. Mauri, G. Cesana, Y. Li, A. Finzi, F. Fumagalli, G. Rossi, N. Grieco, M. Migliori, A. Andreassi *et al.*, "Amplitude spectrum area to guide defibrillation: a validation on 1617 patients with ventricular fibrillation," *Circulation*, vol. 131, no. 5, pp. 478–487, 2015.

[106] J. C. Reynolds, D. D. Salcido, and J. J. Menegazzi, "Correlation between coronary perfusion pressure and quantitative ecg waveform measures during resuscitation of prolonged ventricular fibrillation," *Resuscitation*, vol. 83, no. 12, pp. 1497–1502, 2012.

[107] B. Chicote, U. Irusta, E. Aramendi, I. Isasi, D. Alonso, F. Vicente, and M. Sanchez, "Nonlinear energy operators for defibrillation shock outcome prediction," in *2016 Computing in Cardiology Conference (CinC)*. IEEE, 2016, pp. 61–64.

[108] L. El Bouny, M. Khalil, and A. Abdellah, "Qrs complex detection based on smoothed nonlinear energy operator," in *2018 9th International symposium on signal, image, video and communications (ISIVC)*. IEEE, 2018, pp. 191–196.

[109] R. Bos, S. De Waele, and P. M. Broersen, "Autoregressive spectral estimation by application of the burg algorithm to irregularly sampled data," *IEEE Transactions on Instrumentation and Measurement*, vol. 51, no. 6, pp. 1289–1294, 2002.

[110] A. B. Rad, T. Eftestøl, K. Engan, U. Irusta, J. T. Kvaløy, J. Kramer-Johansen, L. Wik, and A. K. Katsaggelos, "Ecg-based classification of resuscitation cardiac rhythms for retrospective data analysis," *IEEE Transactions on Biomedical Engineering*, vol. 64, no. 10, pp. 2411–2418, 2017.

[111] J. M. Ruiz, S. R. de Gauna, D. M. González-Otero, P. Saiz, J. J. Gutiérrez, J. F. Veintemillas, J. M. Bastida, and D. Alonso, "Circulation assessment by automated external defibrillators during cardiopulmonary resuscitation," *Resuscitation*, vol. 128, pp. 158–163, 2018.

[112] W. Chen, Z. Wang, H. Xie, and W. Yu, "Characterization of surface emg signal based on fuzzy entropy," *IEEE Transactions on neural systems and rehabilitation engineering*, vol. 15, no. 2, pp. 266–272, 2007.

[113] W. Chen, J. Zhuang, W. Yu, and Z. Wang, "Measuring complexity using fuzzyen, apen, and sampen," *Medical engineering & physics*, vol. 31, no. 1, pp. 61–68, 2009.

[114] B. Chicote, U. Irusta, E. Aramendi, R. Alcaraz, J. J. Rieta, I. Isasi, D. Alonso, M. d. M. Baqueriza, and K. Ibarguren, "Fuzzy and sample entropies as predictors of patient survival using short ventricular fibrillation recordings during out of hospital cardiac arrest," *Entropy*, vol. 20, no. 8, p. 591, 2018.

[115] D. DeMers and D. Wachs, "Physiology, mean arterial pressure," 2019.

[116] S. Shandilya, K. R. Ward, and K. Najarian, "A time-series approach for shock outcome prediction using machine learning," in *2010 IEEE International Conference on Bioinformatics and Biomedicine Workshops (BIBMW)*. IEEE, 2010, pp. 440–446.

[117] M. Firyulina and I. Kashirina, "Classification of cardiac arrhythmia using machine learning techniques," in *Journal of Physics: Conference Series*, vol. 1479, no. 1. IOP Publishing, 2020, p. 012086.

[118] S. Sager, F. Bernhardt, F. Kehrle, M. Merkert, A. Potschka, B. Meder, H. Katus, and E. Scholz, "Expert-enhanced machine learning for cardiac arrhythmia classification," *PloS one*, vol. 16, no. 12, p. e0261571, 2021.

[119] T. Seki, T. Tamura, M. Suzuki, S.-K. . S. Group *et al.*, "Outcome prediction of out-of-hospital cardiac arrest with presumed cardiac aetiology using an advanced machine learning technique," *Resuscitation*, vol. 141, pp. 128–135, 2019.

[120] V. Brandt, T. Emrich, U. J. Schoepf, D. M. Dargis, R. R. Bayer, C. N. De Cecco, and C. Tesche, "Ischemia and outcome prediction by cardiac ct based machine learning," *The International Journal of Cardiovascular Imaging*, vol. 36, pp. 2429–2439, 2020.

[121] C.-Y. Cheng, I.-M. Chiu, W.-H. Zeng, C.-M. Tsai, C.-H. R. Lin *et al.*, "Machine learning models for survival and neurological outcome prediction of out-of-hospital cardiac arrest patients," *BioMed Research International*, vol. 2021, 2021.

[122] M. Jerkeman, P. Lundgren, E. Omerovic, A. Strömsöe, G. Riva, J. Hollenberg, P. Nivedahl, J. Herlitz, and A. Rawshani, "Association between type of bystander cardiopulmonary resuscitation and survival in out-of-hospital cardiac arrest: A machine learning study," *Resuscitation Plus*, vol. 10, p. 100245, 2022.

[123] S. N. Blomberg, F. Folke, A. K. Ersbøll, H. C. Christensen, C. Torp-Pedersen, M. R. Sayre, C. R. Counts, and F. K. Lippert, "Machine learning as a supportive tool to recognize cardiac arrest in emergency calls," *Resuscitation*, vol. 138, pp. 322–329, 2019.

[124] B. Patel and P. Sengupta, "Machine learning for predicting cardiac events: what does the future hold?" *Expert review of cardiovascular therapy*, vol. 18, no. 2, pp. 77–84, 2020.

[125] E. Donal, A. Hubert, V. Le Rolle, C. Leclercq, R. Martins, P. Mabo, E. Galli, and A. Hernandez, "New multiparametric analysis of cardiac dyssynchrony: machine learning and prediction of response to crt," *JACC: Cardiovascular Imaging*, vol. 12, no. 9, pp. 1887–1888, 2019.

[126] A. Nasim, D. C. Nchekwube, F. Munir, and Y. S. Kim, "An evolutionary-neural mechanism for arrhythmia classification with optimum features using single-lead electrocardiogram," *IEEE Access*, vol. 10, pp. 99 050–99 065, 2022.

[127] E. Alonso, E. Aramendi, M. Daya, U. Irusta, B. Chicote, J. K. Russell, and L. G. Tereshchenko, "Circulation detection using the electrocardiogram and the thoracic impedance acquired by defibrillation pads," *Resuscitation*, vol. 99, pp. 56–62, 2016.

[128] A. Thorén, A. Rawshani, J. Herlitz, J. Engdahl, T. Kahan, L. Gustafsson, and T. Djärv, "Ecg-monitoring of in-hospital cardiac

arrest and factors associated with survival," *Resuscitation*, vol. 150, pp. 130–138, 2020.

[129] L. Breiman, "Random forests," *Machine learning*, vol. 45, pp. 5–32, 2001.

[130] S. J. Rigatti, "Random forest," *Journal of Insurance Medicine*, vol. 47, no. 1, pp. 31–39, 2017.

[131] N. Mohapatra, K. Shreya, and A. Chinmay, "Optimization of the random forest algorithm," in *Advances in Data Science and Management: Proceedings of ICDSM 2019*. Springer, 2020, pp. 201–208.

[132] X. Chen and H. Ishwaran, "Random forests for genomic data analysis," *Genomics*, vol. 99, no. 6, pp. 323–329, 2012.

[133] R. Genuer, J.-M. Poggi, C. Tuleau-Malot, and N. Villa-Vialaneix, "Random forests for big data," *Big Data Research*, vol. 9, pp. 28–46, 2017.

[134] E. Manibardo, U. Irusta, J. Del Ser, E. Aramendi, I. Isasi, M. Olabarria, C. Corcuera, J. Veintemillas, and A. Larrea, "Ecg-based random forest classifier for cardiac arrest rhythms," in *2019 41st Annual International Conference of the IEEE Engineering in Medicine and Biology Society (EMBC)*. IEEE, 2019, pp. 1504–1508.

[135] R. Mahajan, R. Kamaleswaran, J. A. Howe, and O. Akbilgic, "Cardiac rhythm classification from a short single lead ecg recording via random forest," in *2017 Computing in Cardiology (CinC)*. IEEE, 2017, pp. 1–4.

[136] A. Howe, O. J. Escalona, R. Di Maio, B. Massot, N. A. Cromie, K. M. Darragh, J. Adgey, and D. J. McEneaney, "A support vector machine for predicting defibrillation outcomes from waveform metrics," *Resuscitation*, vol. 85, no. 3, pp. 343–349, 2014.

[137] C. J. Sheela and L. Vanitha, "Prediction of sudden cardiac death using support vector machine," in *2014 International Conference on Circuits, Power and Computing Technologies [ICCPCT-2014]*. IEEE, 2014, pp. 377–381.

[138] I. Goodfellow, Y. Bengio, and A. Courville, *Deep learning*. MIT press, 2016.

[139] M. H. Hassoun, *Fundamentals of artificial neural networks*. MIT press, 1995.

[140] W. S. McCulloch and W. Pitts, "A logical calculus of the ideas immanent in nervous activity," *The bulletin of mathematical biophysics*,

vol. 5, pp. 115–133, 1943.

[141] F. Svendsen, "Image processing and deep neural networks for detection of immune cells on histological images of bladder cancer," Master's thesis, University of Stavanger, Norway, 2019.

[142] P. Baldi and P. J. Sadowski, "Understanding dropout," *Advances in neural information processing systems*, vol. 26, 2013.

[143] S. Saha, "A comprehensive guide to convolutional neural networks—the eli5 way," *Towards data science*, vol. 15, p. 15, 2018.

[144] S. M. Anwar, M. Majid, A. Qayyum, M. Awais, M. Alnowami, and M. K. Khan, "Medical image analysis using convolutional neural networks: a review," *Journal of medical systems*, vol. 42, pp. 1–13, 2018.

[145] S. S. Basha, S. R. Dubey, V. Pulabaigari, and S. Mukherjee, "Impact of fully connected layers on performance of convolutional neural networks for image classification," *Neurocomputing*, vol. 378, pp. 112–119, 2020.

[146] K. Sirinukunwattana, S. E. A. Raza, Y.-W. Tsang, D. R. Snead, I. A. Cree, and N. M. Rajpoot, "Locality sensitive deep learning for detection and classification of nuclei in routine colon cancer histology images," *IEEE transactions on medical imaging*, vol. 35, no. 5, pp. 1196–1206, 2016.

[147] X. Jia and M. Q.-H. Meng, "A deep convolutional neural network for bleeding detection in wireless capsule endoscopy images," in *2016 38th annual international conference of the IEEE engineering in medicine and biology society (EMBC)*. IEEE, 2016, pp. 639–642.

[148] Z. Wang, G. Yu, Y. Kang, Y. Zhao, and Q. Qu, "Breast tumor detection in digital mammography based on extreme learning machine," *Neurocomputing*, vol. 128, pp. 175–184, 2014.

[149] L. Lu, L. Dercle, B. Zhao, and L. H. Schwartz, "Deep learning for the prediction of early on-treatment response in metastatic colorectal cancer from serial medical imaging," *Nature communications*, vol. 12, no. 1, p. 6654, 2021.

[150] H. Ahmed, S. Hamad, H. A. Shedeed, and A. S. Hussein, "Enhanced deep learning model for personalized cancer treatment," *IEEE Access*, vol. 10, pp. 106 050–106 058, 2022.

[151] N. Gaur, R. Dharwadkar, and J. Thomas, "Personalized therapy using deep learning advances," *Deep Learning for Targeted Treatments: Transformation in Healthcare*, pp. 171–197, 2022.

[152] J.-m. Kwon, Y. Lee, Y. Lee, S. Lee, and J. Park, "An algorithm based on deep learning for predicting in-hospital cardiac arrest," *Journal of the American Heart Association*, vol. 7, no. 13, p. e008678, 2018.

[153] W.-L. Zheng, E. Amorim, J. Jing, O. Wu, M. Ghassemi, J. W. Lee, A. Sivaraju, T. Pang, S. T. Herman, N. Gaspard *et al.*, "Predicting neurological outcome from electroencephalogram dynamics in comatose patients after cardiac arrest with deep learning," *IEEE transactions on biomedical engineering*, vol. 69, no. 5, pp. 1813–1825, 2021.

[154] S. Parvaneh, J. Rubin, S. Babaeizadeh, and M. Xu-Wilson, "Cardiac arrhythmia detection using deep learning: A review," *Journal of electrocardiology*, vol. 57, pp. S70–S74, 2019.

[155] T.-M. Chen, C.-H. Huang, E. S. Shih, Y.-F. Hu, and M.-J. Hwang, "Detection and classification of cardiac arrhythmias by a challenge-best deep learning neural network model," *Iscience*, vol. 23, no. 3, 2020.

[156] M. Stone, "Cross-validation: A review," *Statistics: A Journal of Theoretical and Applied Statistics*, vol. 9, no. 1, pp. 127–139, 1978.

[157] M. W. Browne, "Cross-validation methods," *Journal of mathematical psychology*, vol. 44, no. 1, pp. 108–132, 2000.

[158] J. Pan and W. J. Tompkins, "A real-time qrs detection algorithm," *IEEE transactions on biomedical engineering*, no. 3, pp. 230–236, 1985.

[159] P. S. Hamilton and W. J. Tompkins, "Quantitative investigation of qrs detection rules using the mit/bih arrhythmia database," *IEEE transactions on biomedical engineering*, no. 12, pp. 1157–1165, 1986.

[160] V. X. Afonso, W. J. Tompkins, T. Q. Nguyen, and S. Luo, "Ecg beat detection using filter banks," *IEEE transactions on biomedical engineering*, vol. 46, no. 2, pp. 192–202, 1999.

[161] Y. H. Hu, W. J. Tompkins, J. L. Urrusti, and V. X. Afonso, "Applications of artificial neural networks for ecg signal detection and classification." *Journal of electrocardiology*, vol. 26, pp. 66–73, 1993.

[162] B. Kohler, C. Hennig, and R. Orglmeister, "Qrs detection using zero crossing counts," *Applied genomics and proteomics*, vol. 2, no. 2, pp. 138–145, 2003.

[163] A. Pachauri and M. Bhuyan, "Wavelet transform based arterial blood pressure waveform delineator," *International journal of biology and biomedical engineering*, vol. 6, no. 1, pp. 15–25, 2012.

[164] M. Aboy, J. McNames, T. Thong, D. Tsunami, M. S. Ellenby, and B. Goldstein, "An automatic beat detection algorithm for pressure signals," *IEEE Transactions on Biomedical Engineering*, vol. 52, no. 10, pp. 1662–1670, 2005.

[165] J. U. Urizarbarrena, E. A. Ecenarro, A. E. Artano, U. I. Zarandona, and A. Idris, "Modelo predictivo del retorno de circulación espontánea en la parada cardiorrespiratoria utilizando el ecg y la impedancia torácica," in *XXXVIII Congreso Anual de la Sociedad Española de Ingeniería Biomédica. CASEIB 2020: Libro de actas*. Grupo de Ingeniería Biomédica, 2020, pp. 426–429.

[166] J. Urteaga, A. Elola, E. Aramendi, U. Irusta, P. O. Berve, and L. Wik, "Automated detection of pulse using continuous invasive arterial blood pressure in patients during cardiopulmonary resuscitation," in *2021 Computing in Cardiology (CinC)*, vol. 48. IEEE, 2021, pp. 1–4.

[167] J. Urteaga, A. Elola, E. Aramendi, A. Norvik, E. Unneland, and E. Skogvoll, "Automated algorithm for qrs detection in cardiac arrest patients with pea," in *2022 Computing in Cardiology (CinC)*, vol. 498. IEEE, 2022, pp. 1–4.

[168] J. Urteaga, E. Aramendi, A. Elola, A. Norvik, E. Unneland, A. Bhardwaj, D. Buckler, B. Abella, and E. Skogvoll, "The prediction of pulseless electrical activity evolution during in-hospital cardiac arrest using machine learning," *Circulation*, vol. 146, no. Suppl_1, pp. A220–A220, 2022.

[169] J. Urteaga, A. Elola, E. Aramendi, D. Herráez, A. Norvik, E. Unneland, and E. Skogvoll, "Detección automática de complejos qrs en pacientes con actividad eléctrica sin pulso durante la parada cardiorrespiratoria," 2022.

[170] J. Urteaga, A. Elola, U. Irusta, P. O. Berve, L. Wik, and E. Aramendi, "A random forest model for pulseless electrical activity prognosis prediction during out-of-hospital cardiac arrest using invasive blood pressure," in *2024 46th Annual International Conference of the IEEE Engineering in Medicine and Biology Society (EMBC)*. IEEE, 2024 (Accepted).

[171] J. Urteaga, E. Aramendi, A. Elola, U. Irusta, and A. Idris, "A machine learning model for the prognosis of pulseless electrical activity during out-of-hospital cardiac arrest," *Entropy*, vol. 23, no. 7, p. 847, 2021.

[172] J. Urteaga, A. Elola, A. Norvik, E. Unneland, T. C. Eftestøl, A. Bhardwaj, D. Buckler, B. S. Abella, E. Skogvoll, and E. Aramendi, "Machine learning model to predict evolution of pulseless electrical

activity during in-hospital cardiac arrest," *Resuscitation Plus*, vol. 17, p. 100598, 2024.

[173] J. Urteaga, A. Elola, E. Aramendi, P. O. Berve, and L. Wik, "Invasive arterial blood pressure delineator for cardiopulmonary resuscitation patients during pauses of chest compressions," *Biomedical Signal Processing and Control*, vol. 94, p. 106349, 2024.

[174] J. Urteaga, A. Elola, D. Herráez, A. Norvik, E. Unneland, A. Bhardwaj, D. Buckler, B. S. Abella, E. Skogvoll, and E. Aramendi, "A deep learning model for qrs delineation in organized rhythms during in-hospital cardiac arrest," *IEEE Transactions on Biomedical Engineering*, (Submitted).

[175] E. Alonso, T. Eftestøl, E. Aramendi, J. Kramer-Johansen, E. Skogvoll, and T. Nordseth, "Beyond ventricular fibrillation analysis: Comprehensive waveform analysis for all cardiac rhythms occurring during resuscitation," *Resuscitation*, vol. 85, no. 11, pp. 1541–1548, 2014.

[176] P. Laguna, R. G. Mark, A. Goldberg, and G. B. Moody, "A database for evaluation of algorithms for measurement of qt and other waveform intervals in the ecg," in *Computers in cardiology 1997*. IEEE, 1997, pp. 673–676.

[177] A. N. Vest, G. Da Poian, Q. Li, C. Liu, S. Nemati, A. J. Shah, and G. D. Clifford, "An open source benchmarked toolbox for cardiovascular waveform and interval analysis," *Physiological measurement*, vol. 39, no. 10, p. 105004, 2018.

A PUBLISHED AND SUBMITTED STUDIES

A.1 Publications associated to objective 1

A.1.1 First journal paper

	Publication in international journal
Reference	Jon Urteaga, Elisabete Aramendi, Andoni Elola, Unai Irusta, Ahamed H. Idris, "A machine learning model for the prognosis of pulseless electrical activity during out-of-hospital cardiac arrest", *Entropy, 2021*, vol. 23, no 7, p. 847.
Quality indices	• **Type of publication**: Journal paper indexed in JCR • **Quartile**: Q2 (42/86) based on Web of Science Rank 2021 • **Impact factor**: 2.738

entropy

MDPI

Article

A Machine Learning Model for the Prognosis of Pulseless Electrical Activity during Out-of-Hospital Cardiac Arrest

Jon Urteaga [1,*], Elisabete Aramendi [1,2], Andoni Elola [3], Unai Irusta [1,2] and Ahamed Idris [4,†]

[1] Department of Communications Engineering, University of the Basque Country, 48013 Bilbao, Spain; elisabete.aramendi@ehu.eus (E.A.); unai.irusta@ehu.eus (U.I.)
[2] Biocruces Bizkaia Health Research Institute, Cruces University Hospital, 48903 Baracaldo, Spain
[3] Department of Mathematics, University of the Basque Country, 48013 Bilbao, Spain; andoni.elola@ehu.eus
[4] Department of Emergency Medicine, University of Texas Southwestern Medical Center, Dallas, TX 75390, USA; ahamed.idris@utsouthwestern.edu
* Correspondence: jon.urteaga@ehu.eus; Tel.: +34-946-01-73-85
† A.I. Serves as an Unpaid Volunteer on the American Heart Association National Emergency Cardiovascular Care Committee and the HeartSine, Inc. Clinical Advisory Board.

Abstract: Pulseless electrical activity (PEA) is characterized by the disassociation of the mechanical and electrical activity of the heart and appears as the initial rhythm in 20–30% of out-of-hospital cardiac arrest (OHCA) cases. Predicting whether a patient in PEA will convert to return of spontaneous circulation (ROSC) is important because different therapeutic strategies are needed depending on the type of PEA. The aim of this study was to develop a machine learning model to differentiate PEA with unfavorable (unPEA) and favorable (faPEA) evolution to ROSC. An OHCA dataset of 1921 5 s PEA signal segments from defibrillator files was used, 703 faPEA segments from 107 patients with ROSC and 1218 unPEA segments from 153 patients with no ROSC. The solution consisted of a signal-processing stage of the ECG and the thoracic impedance (TI) and the extraction of the TI circulation component (ICC), which is associated with ventricular wall movement. Then, a set of 17 features was obtained from the ECG and ICC signals, and a random forest classifier was used to differentiate faPEA from unPEA. All models were trained and tested using patientwise and stratified 10-fold cross-validation partitions. The best model showed a median (interquartile range) area under the curve (AUC) of 85.7 (9.8)% and a balance accuracy of 78.8 (9.8)%, improving the previously available solutions at more than four points in the AUC and three points in balanced accuracy. It was demonstrated that the evolution of PEA can be predicted using the ECG and TI signals, opening the possibility of targeted PEA treatment in OHCA.

Keywords: out-of-hospital cardiac arrest (OHCA); electrocardiogram (ECG); thoracic impedance (TI); pulseless electrical activity (PEA); return of spontaneous circulation (ROSC)

Citation: Urteaga, J.; Aramendi, E.; Elola, A.; Irusta, U.; Idris, A. A Machine Learning Model for the Prognosis of Pulseless Electrical Activity during Out-of-Hospital Cardiac Arrest. *Entropy* **2021**, *23*, 847. https://doi.org/10.3390/e23070847

Academic Editor: Carlos M. Travieso-González

Received: 31 May 2021
Accepted: 28 June 2021
Published: 30 June 2021

1. Introduction

Out-of-hospital cardiac arrest (OHCA) is a major public health problem, with an estimated incidence between 350,000 and 700,000 cases per year in Europe and survival rates below 10% [1,2]. A patient in cardiac arrest abruptly looses respiratory and cardiovascular functions and, if untreated, dies within minutes. An early recognition of OHCA and prompt treatment are therefore key for survival. In the prehospital setting, bystander cardiopulmonary resuscitation (CPR) contributes to maintaining artificial blood flow through ventilation and chest compressions until more advanced therapy is available. For instance, when the presenting heart rhythm is ventricular fibrillation (VF), an electrical defibrillation shock within the first five minutes from OHCA onset raises survival rates by 50–70% [2,3].

The best course of treatment for OHCA depends on the heart rhythm of the patient, which can be determined using an electrocardiogram (ECG) [4]. In the preshopital setting, the heart function is monitored by the emergency medical system (EMS) personnel using

monitor defibrillators. Unfortunately, by the time the EMS personnel arrives on scene, VF is the presenting rhythm in only 11–37% of OHCA cases [5,6]. A frequently presenting rhythm is pulseless electrical activity (PEA), with recorded incidences of 20–30% out of hospital [7–9] and up to 40–60% in hospital [10,11], as well as much lower survival rates [7,12–15]. PEA is characterized by the dissociation of the electrical and mechanical activities of the heart. Therefore, a patient in PEA presents apparent heartbeats in the ECG with discernible QRS complexes, but without effective ventricular wall movement. Thus, there is no palpable pulse and an insufficient blood flow [7]. EMS personnel provide CPR and pharmacological treatment to revert PEA and achieve return of spontaneous circulation (ROSC), but treatment depends on the characteristics of PEA. Consequently, directions for understanding the mechanism and stratification of PEA have been addressed by clinical consortia and efforts to predict, prevent, and manage PEA encouraged [7,13,15,16].

PEA states can grossly be classified into pseudo-PEA or true-PEA [17]. In pseudo-PEA, the electrical activity of the heart produces a small mechanical activity, albeit insufficient for a palpable pulse. In true PEA, there is no mechanical cardiac activity [16,18]. The two stages of PEA have different prognoses and treatments [7,18–20], and their distinction is of great clinical interest to predict the hemodynamic evolution of PEA, as well as whether the patient will recover ROSC.

Several contributions have proposed the use of ECG features to differentiate PEA with favorable evolution to ROSC (faPEA) from PEA with unfavorable evolution to ROSC (unPEA). The heart rate (HR) and the width of the QRS complex during PEA have been extensively investigated in both in- and out-of-hospital cardiac arrest, but with contradictory conclusions [12–15]. In these studies, ECG data were manually annotated, and no automatic method has been proposed yet to discriminate faPEA from unPEA. Additionally, the thoracic impedance (TI) measured through the defibrillation pads reflects changes in tissue density and fluid content in the thoracic region and thus presents a small, but discernible component associated with blood flow [21]. TI has been successfully used to discriminate PEA from rhythms associated with ROSC, by extracting the impedance circulation component (ICC), which reflects blood flow during ROSC [22,23]. In fact, models combining ECG and TI have been proposed to predict immediate rhythm transitions during OHCA [24] and to discriminate rhythms in OHCA [25], and in a preliminary study, a model combining an ECG and a TI feature showed promising results for the discrimination of faPEA and unPEA on a limited dataset [26].

This study introduced a new model to discriminate faPEA from unPEA based on comprehensive automatic feature extraction from the ECG and TI signals using various signal analysis domains. An advanced random forest (RF) classifier was then used to efficiently combine those features and improve the accuracy of the diagnosis. A comprehensive dataset of OHCA episodes was used for the analysis. The results showed that a combination of ECG and TI features substantially improved the accuracy of the models, which could be used to assist EMS personnel in evaluating the hemodynamic state of the patient and deciding the optimum resuscitation treatment.

2. Data Collection

The dataset used in this study was a subset of a larger dataset of OHCA episodes recorded by the Dallas-Fortworth Center for Resuscitation Research (Dallas, TX, USA). Every episode had concurrent ECG (250 Hz, resolution = 1.03 mV) and TI signals (200 Hz, resolution = 0.74 mΩ) recorded by the defibrillation pads of a HeartStart MRx defibrillator (Philips Healthcare, Andover, MA, USA).

The dataset consisted of 260 episodes of patients in PEA, of which 107 recovered ROSC and 153 did not. ROSC recovery was certified by clinicians on site and further revised by visual inspection of the episodes. Cases ending in ROSC had confirmed long periods without CPR after recovery of pulse, while cases without ROSC had CPR until the end of the episode. PEA onset was identified in the episodes as the first occurrence of an organized rhythm (QRS complexes) during CPR. PEA segments of 5 s in duration, separated by at

least 1 s, and including the ECG and the TI were identified during the first 10 min after PEA onset. Segments were extracted in the pauses of chest compressions, identified in the TI [27,28], with no artifacts due to compressions in the signals. Figure 1 shows an example of an episode in which PEA evolved to ROSC (in green). Chest compression activity is visible in the TI signal, and PEA segments (in blue) were only selected during the intervals without chest compressions to avoid artifacts in the ECG.

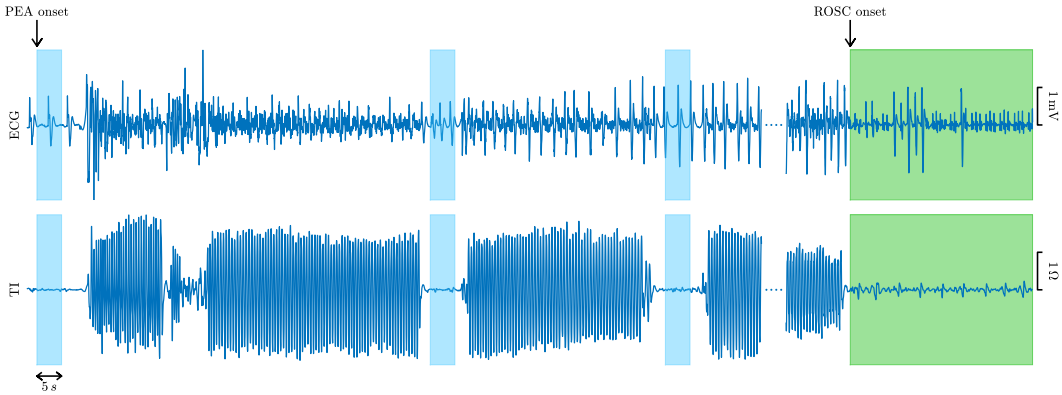

Figure 1. ECG and TI signals of an episode with favorable evolution to ROSC (in green). The 5 s PEA segments extracted from the ECG and the TI are colored in blue.

A total of 1921 PEAs were extracted, a median (interquartile range, IQR) of 4 (6.5) segments per episode. The segments in the ROSC episodes were labeled as faPEA and those in the non-ROSC episodes as unPEA. There were a total of 703 faPEA segments, 4 (5.8) per episode; and 1218 unPEA segments, 5 (7) per episode. Figure 2 shows examples of the faPEA and unPEA segments. As shown in the figure, the faPEA segment presents a more regular ECG with narrower QRS complexes of larger amplitude and a higher heart rate. Moreover, it also presents TI components and an ICC waveform correlated with the heartbeats.

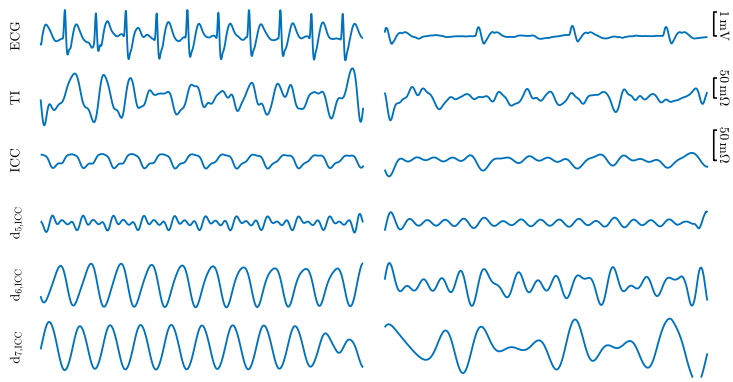

Figure 2. Examples of the signals and components for a 5 s faPEA segment (**left**) and unPEA segment (**right**). From top to bottom: ECG, TI, ICC, and three detail components from the stationary wavelet decomposition of the ICC, $d_{5,ICC}$, $d_{6,ICC}$, and $d_{7,ICC}$

3. Methods

The algorithm to discriminate faPEA from unPEA consisted of the three stages shown in Figure 3. The first stage was an ECG and TI signal-processing stage, where the ECG and TI signals were resampled to a common sampling rate of $f_s = 250$ Hz and then denoised to obtain $\hat{s}_{\mathrm{ECG}}(n)$ and $\hat{s}_{\mathrm{TI}}(n)$. The impedance ICC component, $s_{\mathrm{ICC}}(n)$, was then extracted from $\hat{s}_{\mathrm{TI}}(n)$ by applying adaptive filtering and denoised to obtain $\hat{s}_{\mathrm{ICC}}(n)$. In the second stage, a set of waveform features was computed from the denoised ECG and ICC signals. Finally, in the third stage, these features were fed to an RF classifier to discriminate faPEA from unPEA segments.

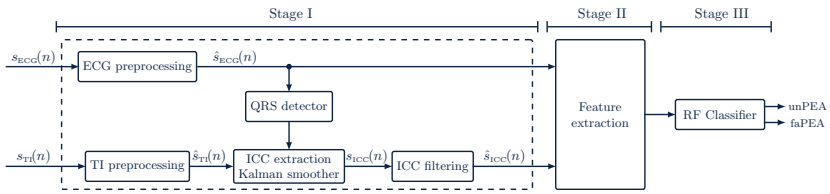

Figure 3. Overview of the faPEA/unPEA classification algorithm. The algorithm consists of three stages: a signal-processing stage, a feature-extraction stage, and a classification stage. The RF classifier uses features from the denoised ECG, $\hat{s}_{ECG}(n)$, and impedance circulation component, $\hat{s}_{ICC}(n)$.

3.1. Processing of ECG and TI Signals

3.1.1. ECG Processing

The ECG signal was denoised using the stationary wavelet transform (SWT) as proposed by Isasi et al. for OHCA rhythms [29,30]. An 8-level SWT decomposition was used with a Daubechies-4 mother wavelet and soft thresholding. Detail coefficients d_3 to d_8 were used to reconstruct the denoised ECG, which corresponds to an analysis band of 0.5–31.25 Hz, a typical band for ECG analysis in OHCA [23,29].

3.1.2. TI Processing and ICC Extraction

The TI measured through the defibrillation pads may show different components due to: baseline wandering, chest compressions and ventilation during CPR, the circulation component in the pulsed rhythm, additional noise/artifacts due to movement, electrode–skin contact, etc. [31]. The segments of the database were extracted during pauses of chest compressions, so the TI signal was bandpass filtered (0.8–10 Hz) to remove baseline fluctuations, respiration artifacts, and other high-frequency noise [22,32]. Then, the ICC component was extracted, that is the TI component correlated with the ECG heartbeats. Heartbeats were detected in the denoised ECG using the Hamilton–Tompkins algorithm [33], and the instantaneous HR was computed as:

$$f(n) = \frac{1}{f_s(r_{i+1} - r_i)} \quad \forall n \in [r_i, r_{i+1}) \tag{1}$$

where r_i is the time instant of the i-th QRS complex (R-peak). Using this information, the ICC can be modeled as a Fourier series of K harmonics [22,31]:

$$s_{\mathrm{ICC}}(n) = \sum_{k=1}^{K} a_k(n)\cos(k\,2\pi f(n)\,n) + b_k(n)\sin(k\,2\pi f(n)\,n) \tag{2}$$

The time-varying Fourier coefficients, $a_k(n)$ and $b_k(n)$, were estimated using a Kalman smoother [23]. The Kalman observation and state vectors are then [23,34]:

$$\boldsymbol{x}_n = [a_1(n), \ldots, a_k(n), b_1(n), \ldots, b_k(n)]^T \quad (3)$$

$$\boldsymbol{H}_n = [\cos(2\pi f(n)\, n), \ldots, \cos(K\, 2\pi f(n)\, n), \sin(2\pi f(n)\, n), \ldots, \sin(K\, 2\pi f(n)\, n)] \quad (4)$$

The time-varying Fourier coefficients were assumed to be Gaussian processes with update equations [23,34]:

$$a_k(n) = \psi_n a_k(n-1) + \omega_n \quad (5)$$

$$b_k(n) = \psi_n b_k(n-1) + \omega_n \quad (6)$$

where $\psi_n = \exp(-\frac{\lambda}{fs})$ and ω_n is a zero-mean Gaussian process with σ the standard deviation. The update equations are thus:

$$\boldsymbol{x}_n = \boldsymbol{\Psi}_n \boldsymbol{x}_{n-1} + \boldsymbol{\Omega}_n \quad (7)$$

where $\boldsymbol{\Psi}_n = \psi_n \cdot \boldsymbol{I}_{2K}$, $\boldsymbol{\Omega}_n = \sigma \cdot \boldsymbol{I}_{2K}$ and $\boldsymbol{I}_{2K}$ is the identity matrix of dimension $2K$.

The Fourier coefficients (state vector), a_k and b_k, were computed applying the Rauch–Tung–Striebel smoother, with $K = 5$ harmonics, $\lambda = 0.05$ and $\sigma = 0.01$, as suggested by Elola et al. [23].

Finally, $s_{\mathrm{ICC}}(n)$ was denoised using an 8-level SWT (Daubechies-4) with soft thresholding. The d_5–d_7 detail coefficients were used to reconstruct the denoised $\hat{s}_{\mathrm{ICC}}(n)$, which corresponds to the bandwidth 1–8 Hz. Figure 2 shows the TI, ICC, and d_5–d_7 detail coefficients for faPEA and unPEA.

3.2. Feature Extraction

Since faPEA evolves to ROSC, while unPEA does not, the hypothesis was that faPEA would be more similar to cardiac rhythms with pulse than unPEA. Therefore, faPEA should present more regular interbeat intervals and heart rates, larger ECG amplitudes, wider spectra (narrower QRS complexes), and an ICC with a greater correlation to the heartbeats than unPEA. Therefore, the features used to detect pulse during cardiac arrest were added [23,35,36], as well as the features to quantify signal regularity and spectral dispersion [37,38]. A total of 17 features were computed, 9 from the denoised ECG ($\hat{s}_{\mathrm{ECG}}$) and 8 from the denoised ICC ($\hat{s}_{\mathrm{ICC}}$).

3.2.1. ECG Features

The ECG features were (for the detailed calculations, consult [4,29,35,37,38]):

- The AMSA, the amplitude spectrum area, which is the weighted sum of the amplitudes of the ECG in the spectral domain, and it quantifies the variability and spectral dispersion of the signal. The AMSA was computed as described in [35];
- $\mathrm{High}_{\mathrm{power}}$, the power of the ECG in the higher frequency bands; a 17.5–40 Hz bandwidth was used [35,38];
- FuzzEn, fuzzy entropy, which measures the regularity of the signal, computed as described in [35];
- The SNEO, the smoothed nonlinear energy operator, as described in [37], which measures the local energy content of the ECG;
- The IQR values of the denoised ECG and its SWT detail coefficients d_5–d_7, which are denoted by $d_{k,\,\mathrm{ECG}}$ for $k = 5, 6, 7$ [29];
- $\mathrm{Burg}_{\mathrm{ECG}}$, the variance of the white noise term of an order-four autoregressive (AR) model estimation of the ECG power spectral density. It measures the goodness-of-fit of the power spectral density to that of spectra concentrated around the fundamental component (HR) and its harmonics [4,39].

3.2.2. ICC Features

The ICC features were (for the detailed calculations, consult [4,22,29,36,37]):

- Log_{Power}, the logarithmic energy (time domain) of the denoised ICC, which has been shown to correlate with ventricular wall movement [22];
- The SNEO, the smoothed nonlinear energy operator, as described in [37], which measures the local energy content of the ICC;
- The IQR values of the denoised ICC and its SWT detail coefficients d_5–d_7, which are denoted by $d_{k,ICC}$ for $k = 5, 6, 7$ [29];
- $Burg_{ICC}$, the variance of the white noise term of the AR(4) estimation of the power spectral density of the denoised ICC [4,39];
- $Cross_{Power}$, the cross-power between the denoised ECG and ICC signals, as described in [36].

3.3. Building the Classifier

An RF classifier was used, both for feature selection and binary classification of the 5 s segments into faPEA/unPEA. RF classifiers have demonstrated good performance and robustness with unbalanced datasets and have the advantage of having an embedded feature ranking/selection through feature importance [40,41].

An RF is an ensemble of B decision trees (weak learners), trained using a different bootstrap replica of the original training dataset. The trees are grown using recursive binary splitting, and at each node, D' features are randomly selected from the available D features for the split. The splitting process is carried out until the tree's terminal nodes are fed with less than l_{size} observations [40,42]. The final decision of the RF classifier is obtained through a majority vote of those B trees.

For this study, an RF classifier with $B = 500$ trees was trained and forced the growth of uncorrelated trees by using a 10% bootstrap replica (with replacement) of the training set for each tree. The number of predictors per node was set to the default $D' = \sqrt{D}$, and the minimum number of observations per terminal node was fixed to $l_{size} = 5$, as recommended in [23]. To avoid class imbalance, uniform priors were assigned.

For baseline comparisons, other machine learning classifiers were also trained and evaluated. The RF was compared to a logistic regression (LR) classifier and to two support vector machine classifiers with polynomial kernels of second (SVM2) and third order (SVM3). In these models, class imbalance was addressed by weighting the least prevalent class (faPEA) by a factor of 1.5.

3.4. Evaluation of the Models

All classifiers were trained and tested using 10-fold cross-validation (CV) with patient-wise and stratified data partitions. In this way, training/test data leakage was avoided, and the class imbalance in each fold reflected that of the whole dataset. The CV evaluation of the models was repeated 10 times to statistically characterize the performance of the classifiers.

The classifiers were evaluated using the typical performance metrics for binary classifiers, taking faPEA as the positive class. The following performance metrics were considered: sensitivity (Se), specificity (Sp), balanced accuracy (BAC, the average of Se and Sp), and the area under the receiver operating characteristic curve (AUC).

4. Results

Table 1 shows a summary of the statistical distribution of the 17 features for the faPEA and unPEA segments of the complete dataset. The features are ranked by the AUC obtained by using a single-feature LR classifier (evaluated in the 10-fold CV partitions). All features except FuzzyEn showed significant differences for the distributions of the faPEA and unPEA segments ($p < 0.001$, Wilcoxon test), and moderate to good AUC values in the range of 52.9 to 81.6%.

Table 1. Median (IQR) values of the features for faPEA and unPEA segments grouped by ECG (left) and ICC (right) features. Features are ranked within each group by the AUC (median, IQR) of a single-feature LR classifier.

ECG Features				ICC Features			
Feature	**faPEA**	**unPEA**	**AUC (%)**	**Feature**	**faPEA**	**unPEA**	**AUC (%)**
Burg	2.4×10^{-6} (3.8×10^{-6})	5.6×10^{-7} (1.1×10^{-6})	81.6 (5.6)	$Cross_{Power}$	1310 (2151)	425 (1083)	71.6 (3.4)
AMSA	31.2 (22.3)	13.1 (14.1)	81.3 (4.9)	$IQR(d_5)$	22.1 (36.3)	10.5 (30.2)	66.5 (1.6)
$High_{Power}$	74.3 (166.0)	8.3 (24.8)	80.3 (8.1)	SNEO	2930 (10,001)	445 (4427)	65.7 (7.8)
$IQR(d_6)$	1.1 (1.2)	0.5 (0.6)	72.6 (15.0)	Log_{Power}	5131 (2783)	2822 (5259)	64.4 (7.5)
$IQR(d_5)$	0.31 (0.65)	0.17 (0.29)	71.0 (11.1)	$IQR(d_6)$	84.2 (136.1)	32.5 (88.9)	64.3 (5.2)
SNEO	0.21 (0.82)	0.06 (0.20)	71.0 (14.4)	IQR	18.6 (26.9)	7.2 (30.5)	61.5 (10.3)
IQR	0.17 (0.17)	0.10 (0.10)	68.8 (14.4)	$IQR(d_7)$	150.9 (253.8)	66.3 (247.5)	54.9 (13.0)
$IQR(d_7)$	1.3 (1.5)	1.0 (1.0)	65.2 (12.6)	Burg	0.21 (1.9)	0.05 (0.8)	54.6 (14.4)
FuzzEn	0.22 (0.13)	0.23 (0.14)	52.9 (20.4)				

4.1. Performance of the RF Classifier

The overall performance of the method is reported in Table 2 in terms of AUC, BAC, and Se/Sp. Two model types were evaluated, those using ECG-only features and those combining ECG and ICC features. For each model, the complete feature set and a reduced optimal feature set based on RF feature importance (see Section 4.2) were used. The models with reduced feature sets showed the best performance, with median (IQR) values of 85.7 (9.8)/78.8 (9.8)% for AUC/BAC for the ECG+ICC model and 83.2 (8.5)/75.7 (10.7)% for the ECG-only model. Adding information derived from the impedance (ICC signal) improved the AUC and BAC of the ECG-only models at 2.5 and three points, respectively.

Table 2 also shows the performance of all previous proposals in the literature for the prognosis of the evolution of PEA. All the methods were implemented in MATLAB and then evaluated using this study's dataset and data partitions. The previous proposals included: (1) a preliminary version of the proposed method based on an RF classifier, but using only one ECG feature (AMSA) and one ICC feature (Log_{Power}) [26]; (2) an LR model using ECG-only features proposed by Alonso et al. [24] for the immediate prediction of the evolution of cardiac arrest rhythms, including PEA; (3) single-ECG feature models based on the heart rate [12] and the width of the QRS complexes [14]. In the original studies [12,14], the HR and QRS widths were manually measured, but in an automatic system, these values have to be automatically computed from the ECG. The *wavedec* wavelet-based algorithm was applied both for QRS detection and HR calculations, and for ECG delineation and QRS width calculations [43], and then, we used these features in a single-feature LR classifier. The best solution outperformed all previous proposals by 4–19 points in the AUC and by 3–16 points in BAC. Moreover, the ECG-only solution also outperformed all previous ECG-only solutions by 2–16 points in the AUC and 1.5–14 points in BAC and used a reduced feature set compared to the second-best ECG only model by Alonso et al. [24] (four vs. six).

Table 2. Performance of the methods introduced in this study compared to all previous proposals for faPEA/unPEA discrimination. The table shows the median (IQR) values for AUC, BAC, Se, and Sp.

	No. Features	**AUC (%)**	**BAC (%)**	**Se (%)**	**Sp (%)**
This study (ECG+TI)	17	85.7 (8.6)	77.8 (8.9)	79.8 (11.3)	77.3 (12.1)
This study (ECG)	9	82.1 (9.7)	73.5 (11.2)	79.7 (14.1)	69.0 (15.9)
This study, reduced (ECG+TI)	7	85.7 (9.8)	78.8 (9.8)	80.1 (12.6)	76.7 (13.6)
This study, reduced (ECG)	4	83.2 (8.5)	75.7 (10.7)	78.9 (15.9)	75.7 (11.4)
Urteaga et al. [26]	2	82.0 (10.5)	74.8 (11.3)	77.0 (13.9)	73.5 (14.6)
Alonso et al. [24]	6	81.4 (10.3)	74.4 (8.9)	73.2 (15.1)	77.8 (15.3)
HR [12]	1	67.2 (12.9)	62.1 (11.8)	80.2 (14.5)	45.1 (21.1)
QRS width [14]	1	69.2 (12.9)	67.8 (13.3)	74.8 (20.2)	61.5 (26.6)

4.2. Feature Selection and Feature Analysis

To analyze how features were ranked, the RF feature importance was used, and the feature selection probability was estimated by adjusting the models of a decreasing number of features (N_f), from $N_f = 17, \cdots, 1$. The selection probability for each feature was measured as the percentage of times it was selected. For each 10-fold CV partition, features were iteratively discarded (in steps of one) by removing the feature with the lowest importance, and the RF models were retrained to rerank the features for the remaining N_f features. The process was carried out until a single feature was left. The proportion of times a feature was included for each value of N_f is shown in Figure 4.

The most frequently selected features included both ECG and ICC features. The features in the top seven positions were ECG spectral features such as AMSA, Burg, and $\text{High}_{\text{Power}}$ and the ICC amplitude/power features such as SNEO_{ICC}, $\text{IQR}(\text{d}_{6,\text{ICC}})$, IQR(ICC), and $\text{Log}_{\text{Power}}$.

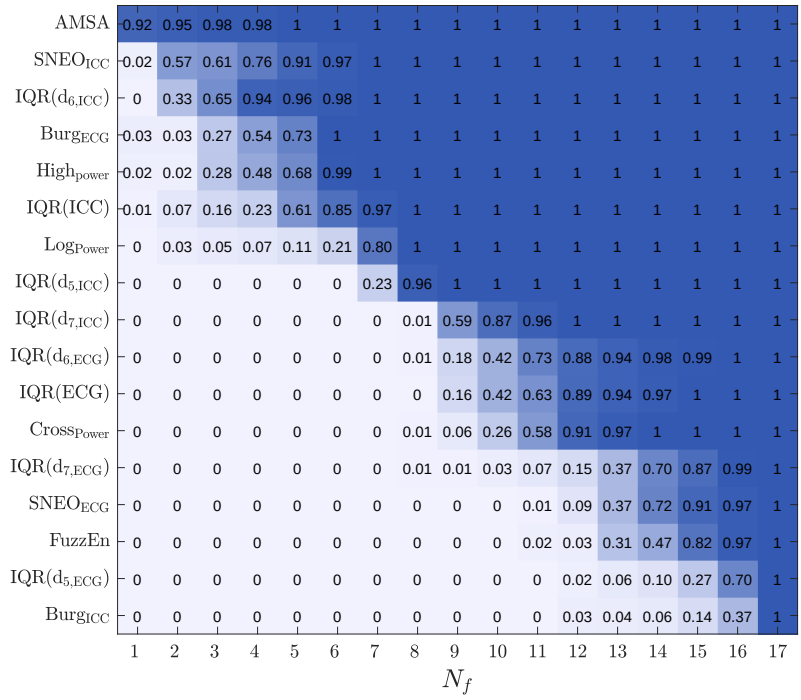

Figure 4. The selection probability for the 17 features, as a function of N_f, the number of features included in the RF classifier.

Another important aspect is the performance of the model as a function of N_f, both to obtain more accurate models by selecting an optimal feature subset, but also to lower the complexity, improve the interpretability, and lower the computational cost of the model. Figure 5 shows the performance of all the classification models (baseline models and the RF classifier) as a function of N_f, the number of features used in the model. The features included for each N_f were those with a higher selection probability (see Figure 4). The best results were obtained for the RF classifier, both in the AUC and BAC, and the RF models showed a stable performance for $N_f \geq 6$. As shown in Table 2, the RF classifier with $N_f = 7$ had the same performance as the RF classifier with the complete set of features.

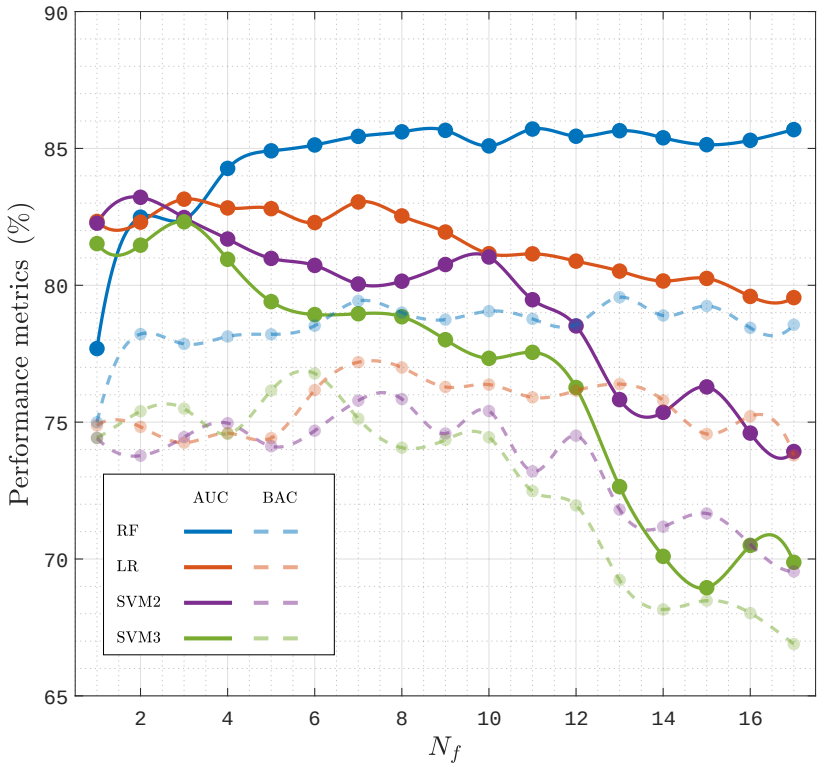

Figure 5. Performance of the classifiers, AUC and BAC, in terms of the number of features, N_f, considered in the model.

4.3. Time Interval for a Prediction

The time needed from PEA onset to a reliable prognosis is key for a prompt initiation of specific therapies. To analyze the time needed for a prognosis, the faPEA/unPEA classification was performed using only the ECG and TI segments in an interval of t_w (min) from PEA onset, then changing t_w from 1 min to 10 min in 1 min steps. Figure 6 shows the AUC and BAC for the different classifiers as a function of t_w. The RF classifier had the best performance for all time intervals, with AUC and BAC values above 80% and 75%, even for the first minute after PEA onset. As expected, as t_w grew as the accuracy of the classifiers improved, since PEA with favorable evolution is closer to conversion to ROSC; however, the improvement in the AUC and BAC was only five points and four points when the interval was extended from 1 min to 10 min; that is, a prompt reliable diagnosis can be obtained, and a specific therapy can be initiated even in the first minute after PEA onset.

Figure 7 shows a combined analysis of the RF performance as a function of N_f and t_w. As shown in the figure, the AUC and BAC increased as the number of features in the model and the analysis interval increased, with AUC values above 85% and BAC values above 78% for $t_w \geq 7$ min and $N_f \geq 4$.

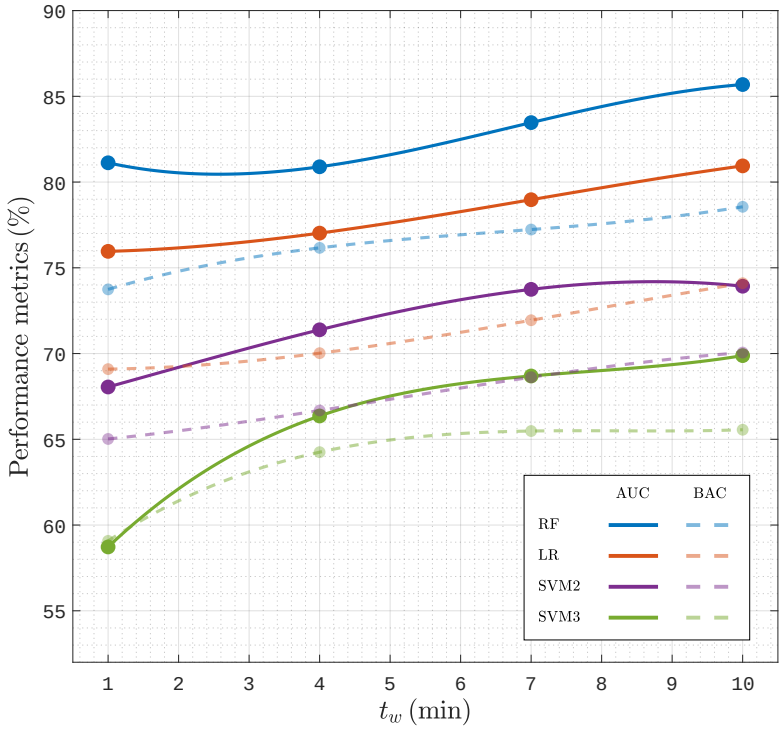

Figure 6. Performance of classifiers in terms of the AUC and BAC as a function of for analysis intervals of t_w duration after the onset of PEA.

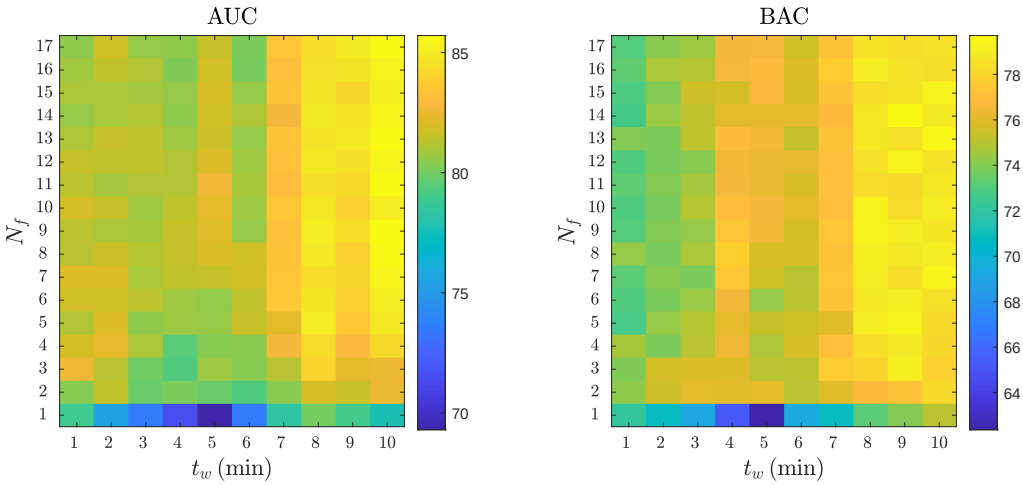

Figure 7. The AUC and BAC of the RF classifier for different analysis intervals, t_w, and number of features, N_f.

4.4. Analysis of the Classification Errors

The classification errors of the best RF model were analyzed to better understand the limitations and potential future improvements of faPEA/unPEA classification. Figure 8 shows the ECG, TI, and ICC signals for segments with correct classifications and segments with typical patterns leading to classification errors. The top panels show correctly classified

segments, despite faPEA having a much lower heart rate than unPEA. In the examples, the TI/ICC signals showed no evidence of mechanical activity for unPEA and activity correlated with the heartbeats in faPEA. The bottom panels show examples of misclassified segments. In the case of faPEA, both the heart rate and the TI/ICC activity were very low, and they corresponded to an episode in which ROSC occurred 38 min after PEA onset. In this episode, at the initial stage of PEA, the mechanical activity of the heart was closer to that of unPEA than faPEA. In the case of unPEA, the ECG had a low amplitude and heart rate, as expected for unPEA, but there was noise in the ECG and TI signals in the last part of the segment, which produced a pulse-like ICC signal estimation by the Kalman smoother.

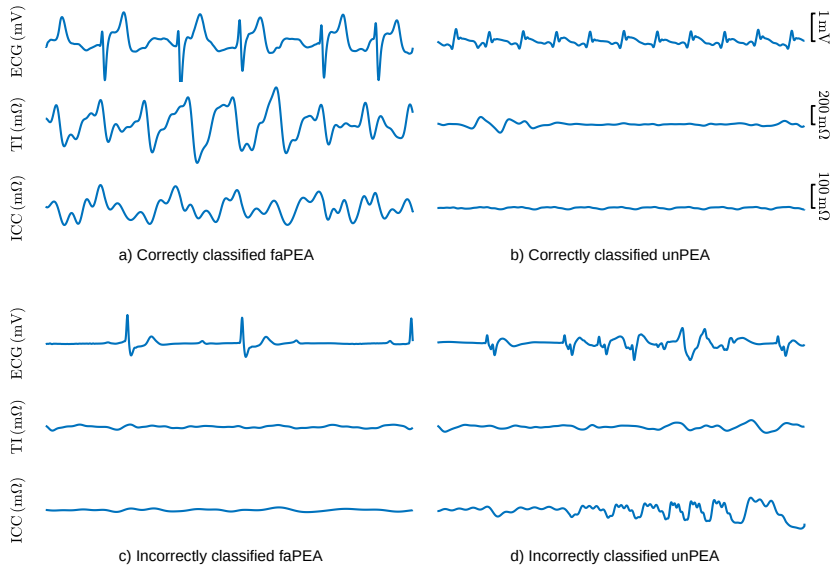

Figure 8. ECG, TI, and ICC signals for 5 s segments of correctly (**top**) and incorrectly (**bottom**) classified faPEA and unPEA segments.

5. Discussion

To the best of our knowledge, the proposed method is the first automated method to discriminate PEA rhythms with favorable evolution to ROSC in OHCA data. The algorithm consisted of the extraction of the ICC component of the TI (associated with mechanical wall movement), an ECG and ICC feature extraction phase, and an RF classifier. The solution outperformed previous solutions both in the AUC (four to nineteen points) and BAC (three to sixteen points) [12,14,23,24,26]. Several aspects of the solution explained the better performance. First, the ECG and TI feature set was larger than in previous studies, and the features were carefully selected to reflect or be associated with ventricular wall movement or ROSC. Second, the features obtained from QRS complex segmentation were not used. In nonarrest patients, QRS detection and segmentation are very accurate [43], but their accuracy substantially decreases for cardiac arrest rhythms [35]. For instance, it was observed that the methods based on HR and QRS width presented the lowest performance in part because of the inaccuracies of the automatic algorithms for cardiac arrest data. Third, features obtained from the ICC were added, and these features revealed information on the incipient mechanical activity of the heart in PEA rhythms that converted to ROSC.

The models with reduced the feature sets (seven features for ECG and ICC and four features for ECG-only) had better or comparable performance to those with the complete feature set. Moreover, adding ICC features improved the ECG-only methods by 2.5 points in AUC and 3.1 points in BAC, demonstrating the utility of the TI signal as a surrogate measure of ventricular wall movement [23,26]. A high correlation between the features from

the detail components of the ECG and ICC (mean $\rho = 0.9$) and between the spectral features of the ECG (mean $\rho = 0.7$) was observed. An effective feature selection process improves the models, particularly when an exhaustive feature extraction process is carried out [23,29]. More importantly, models with fewer features are computationally less expensive and more explainable. For the RF classifier, using an embedded feature selection based on RF feature importance is an efficient way to obtain close-to-optimal feature subsets.

The time from PEA onset to an accurate prognosis of its evolution is key for the prompt implementation of efficient therapies. In the dataset used in this study, the mean time from PEA onset to outcome (ROSC or no ROSC) was 22 min, and the proposed solution had an AUC and BAC of 81% and 74% within the first minute from PEA onset. Evidently, as time evolved, the accuracy of the prognosis improved, and the AUC and BAC rose to 86% and 79% for an analysis interval of 10 min. In cases in which PEA onset was far from ROSC, errors were more frequent, as shown in Figure 8c for a patient that recovered ROSC 38 min after PEA onset. In any case, there is a clinical tradeoff between the accuracy of the prognosis and the prompt implementation of specific therapies. An alternative approach may be to report the probability of conversion to ROSC as a clinical support tool. Such a probability can be obtained from most machine learning models and in particular in the RF model by computing the proportion of trees with positive faPEA classification [35,41].

The solutions proposed in this study were based on the ECG only and on combined features from ECG and TI (the ICC was derived from TI). In both cases, reasonable tradeoffs between time-to-prognosis and accuracy can be reached. The reason for using these signals is that they are universally available in defibrillators and monitor defibrillators, the equipment used by EMS crews to monitor OHCA patients. All these devices have an ECG channel through the defibrillation pads [35], but not all include a TI signal with sufficient resolution to implement these algorithms [22,23]. Since the proposed algorithms are fully automatic, this means they could be integrated into this equipment as decision support tools for the management of OHCA patients in PEA; that is, they would contribute to a personalized resuscitation treatment, as proposed in the latest resuscitation guidelines [44].

The availability of signals during resuscitation is key to improve the accuracy of automatic algorithms. In particular, the prognosis of ROSC during resuscitation (for all rhythms, not only PEA) is a very active field of research. New and established technologies such as capnography [23,45], cerebral oximetry [46,47], echocardiography [18,48], or point-of-care testing (blood gas analysis) [49] have been explored. A complete up-to-date review is available in [17]. These are, in general, emerging technologies to monitor and guide treatment during OHCA, and only echocardiography and, more recently, capnography have been specifically used to stratify PEA during OHCA [18,23]. In the future, combined algorithms integrating information from all these sources should be explored to improve the prognosis of the evolution of PEA. However, acquiring multimodal OHCA datasets with all these sources of information is complex because OHCA is a critical chronodependent clinical situation treated in a prehospital setting. Therefore, these types of datasets are very scarce and have a limited amount of patients [23].

This study had some limitations. First, the data came from a single type of device, the HeartStart MRx defibrillator. Although the ECGs acquired by different commercial devices have slight differences in bandwidth and resolution, no substantial differences would be expected in the ECG-based model for other devices. Conversely, the TI is acquired by proprietary circuitry, with very different amplitude resolutions and sampling rates. The ICC has a very small amplitude rarely exceeding 100 mΩ, so how well the ICC can be estimated from the TI recorded in other devices needs to be tested. Second, the number of cases included in the study was substantial, but augmenting the dataset's size would allow the development of more accurate models. In particular, advanced solutions based on deep learning algorithms could also be developed based on features extracted by neural network architectures [50–52].

6. Conclusions

This study introduced the first machine learning algorithm that discriminates PEA rhythms with favorable evolution to ROSC from those with unfavorable evolution. The proposed algorithm was based on features automatically extracted from the ECG and the TI signal after PEA onset. The RF model proposed outperformed previous solutions, and it demonstrated that both ECG and TI signals contain relevant information for the prognosis of PEA evolution. The results also encourage the development of improved solutions tested on larger datasets. This may lead to decision support tools that assist rescuers in the definition of the best resuscitation treatment during PEA in OHCA, increasing the chances of survival and good neurological outcome. Current commercial defibrillators could benefit from advances in signal processing and machine learning techniques, improving their impact in the course of cardiac arrest resuscitation.

Author Contributions: Conceptualization, J.U., E.A., A.E., U.I. and A.I.; data curation, J.U.; formal analysis, J.U., E.A., A.E. and U.I.; funding acquisition, E.A. and U.I.; investigation, J.U., E.A., A.E., U.I. and A.I.; methodology, J.U., E.A. and A.E.; project administration, E.A. and U.I.; resources, A.I.; software, J.U. and A.E.; supervision, E.A. and U.I.; visualization, J.U.; writing—original draft, J.U. and E.A.; writing—review and editing, J.U., E.A., A.E., U.I. and A.I. All authors read and agreed to the published version of the manuscript.

Funding: This work was supported by the Spanish Ministerio de Ciencia, Innovacion y Universidades through Grant RTI2018-101475-BI00, jointly with the Fondo Europeo de Desarrollo Regional (FEDER), by the Basque Government through Grant IT1229-19 and Grant PRE2020_1_0177, and by the university of the Basque Country (UPV/EHU) under Grant COLAB20/01.

Institutional Review Board Statement: Not applicable.

Informed Consent Statement: Not applicable.

Data Availability Statement: Restrictions apply to the availability of these data. Data was obtained from Dallas-Fortworth Center for Resuscitation Research and are available on request from the corresponding author with the permission of Dr. Idris (Dallas-Fortworth Center for Resuscitation Research).

Conflicts of Interest: The funders had no role in the design of the study; in the collection, analyses, or interpretation of data; in the writing of the manuscript; nor in the decision to publish the results.

Abbreviations

The following abbreviations are used in this manuscript.

OHCA	out-of-hospital cardiac arrest
ROSC	return of spontaneous circulation
CPR	cardiopulmonary resuscitation
EMS	emergency medical services
PEA	pulseless electrical activity
faPEA	pulseless electrical activity with favorable evolution
unPEA	pulseless electrical activity with unfavorable evolution
VF	ventricular fibrillation
ECG	electrocardiogram
TI	thoracic impedance
ICC	impedance circulation component
RF	random forest
LR	logistic regression
SVM	support vector machine
AUC	area under the curve
BAC	balanced accuracy
Se	sensitivity
Sp	specificity

References

1. Atwood, C.; Eisenberg, M.S.; Herlitz, J.; Rea, T.D. Incidence of EMS-treated out-of-hospital cardiac arrest in Europe. *Resuscitation* **2005**, *67*, 75–80. [CrossRef]
2. Berdowski, J.; Berg, R.A.; Tijssen, J.G.; Koster, R.W. Global incidences of out-of-hospital cardiac arrest and survival rates: Systematic review of 67 prospective studies. *Resuscitation* **2010**, *81*, 1479–1487. [CrossRef] [PubMed]
3. Perkins, G.D.; Handley, A.J.; Koster, R.W.; Castrén, M.; Smyth, M.A.; Olasveengen, T.; Monsieurs, K.G.; Raffay, V.; Gräsner, J.T.; Wenzel, V.; et al. European Resuscitation Council Guidelines for Resuscitation 2015: Section 2. Adult basic life support and automated external defibrillation. *Resuscitation* **2015**, *95*, 81–99. [CrossRef]
4. Rad, A.B.; Eftestøl, T.; Engan, K.; Irusta, U.; Kvaløy, J.T.; Kramer-Johansen, J.; Wik, L.; Katsaggelos, A.K. ECG-based classification of resuscitation cardiac rhythms for retrospective data analysis. *IEEE Trans. Biomed. Eng.* **2017**, *64*, 2411–2418. [CrossRef] [PubMed]
5. Gräsner, J.T.; Wnent, J.; Herlitz, J.; Perkins, G.D.; Lefering, R.; Tjelmeland, I.; Koster, R.W.; Masterson, S.; Rossell-Ortiz, F.; Maurer, H.; et al. Survival after out-of-hospital cardiac arrest in Europe-Results of the EuReCa TWO study. *Resuscitation* **2020**, *148*, 218–226. [CrossRef]
6. Oving, I.; de Graaf, C.; Karlsson, L.; Jonsson, M.; Kramer-Johansen, J.; Berglund, E.; Hulleman, M.; Beesems, S.G.; Koster, R.W.; Olasveengen, T.M.; et al. Occurrence of shockable rhythm in out-of-hospital cardiac arrest over time: A report from the COSTA group. *Resuscitation* **2020**, *151*, 67–74. [CrossRef] [PubMed]
7. Myerburg, R.J.; Halperin, H.; Egan, D.A.; Boineau, R.; Chugh, S.S.; Gillis, A.M.; Goldhaber, J.I.; Lathrop, D.A.; Liu, P.; Niemann, J.T.; et al. Pulseless electric activity: Definition, causes, mechanisms, management, and research priorities for the next decade: Report from a National Heart, Lung, and Blood Institute workshop. *Circulation* **2013**, *128*, 2532–2541. [CrossRef]
8. Mader, T.J.; Nathanson, B.H.; Millay, S.; Coute, R.A.; Clapp, M.; McNally, B. Out-of-hospital cardiac arrest outcomes stratified by rhythm analysis. *Resuscitation* **2012**, *83*, 1358–1362. [CrossRef]
9. Ko, D.T.; Qiu, F.; Koh, M.; Dorian, P.; Cheskes, S.; Austin, P.C.; Scales, D.C.; Wijeysundera, H.C.; Verbeek, P.R.; Drennan, I.; et al. Factors associated with out-of-hospital cardiac arrest with pulseless electric activity: A population-based study. *Am. Heart J.* **2016**, *177*, 129–137. [CrossRef]
10. Meaney, P.A.; Nadkarni, V.M.; Kern, K.B.; Indik, J.H.; Halperin, H.R.; Berg, R.A. Rhythms and outcomes of adult in-hospital cardiac arrest. *Crit. Care Med.* **2010**, *38*, 101–108. [CrossRef]
11. Nordseth, T.; Niles, D.E.; Eftestøl, T.; Sutton, R.M.; Irusta, U.; Abella, B.S.; Berg, R.A.; Nadkarni, V.M.; Skogvoll, E. Rhythm characteristics and patterns of change during cardiopulmonary resuscitation for in-hospital paediatric cardiac arrest. *Resuscitation* **2019**, *135*, 45–50. [CrossRef] [PubMed]
12. Weiser, C.; Poppe, M.; Sterz, F.; Herkner, H.; Clodi, C.; Schriefl, C.; Warenits, A.; Vossen, M.; Schwameis, M.; Nürnberger, A.; et al. Initial electrical frequency predicts survival and neurological outcome in out of hospital cardiac arrest patients with pulseless electrical activity. *Resuscitation* **2018**, *125*, 34–38. [CrossRef]
13. Hauck, M.; Studnek, J.; Heffner, A.C.; Pearson, D.A. Cardiac arrest with initial arrest rhythm of pulseless electrical activity: Do rhythm characteristics correlate with outcome? *Am. J. Emerg. Med.* **2015**, *33*, 891–894. [CrossRef]
14. Skjeflo, G.W.; Nordseth, T.; Loennechen, J.P.; Bergum, D.; Skogvoll, E. ECG changes during resuscitation of patients with initial pulseless electrical activity are associated with return of spontaneous circulation. *Resuscitation* **2018**, *127*, 31–36. [CrossRef] [PubMed]
15. Bergum, D.; Skjeflo, G.W.; Nordseth, T.; Mjølstad, O.C.; Haugen, B.O.; Skogvoll, E.; Loennechen, J.P. ECG patterns in early pulseless electrical activity-Associations with aetiology and survival of in-hospital cardiac arrest. *Resuscitation* **2016**, *104*, 34–39. [CrossRef] [PubMed]
16. Mehta, C.; Brady, W. Pulseless electrical activity in cardiac arrest: Electrocardiographic presentations and management considerations based on the electrocardiogram. *Am. J. Emerg. Med.* **2012**, *30*, 236–239. [CrossRef]
17. Van den Bempt, S.; Wauters, L.; Dewolf, P. Pulseless Electrical Activity: Detection of Underlying Causes in a Prehospital Setting. *Med. Princ. Pract.* **2021**, *30*, 212–222. [CrossRef]
18. Rabjohns, J.; Quan, T.; Boniface, K.; Pourmand, A. Pseudo-pulseless electrical activity in the emergency department, an evidence based approach. *Am. J. Emerg. Med.* **2020**, *38*, 371–375. [CrossRef] [PubMed]
19. Flato, U.A.P.; Paiva, E.F.; Carballo, M.T.; Buehler, A.M.; Marco, R.; Timerman, A. Echocardiography for prognostication during the resuscitation of intensive care unit patients with non-shockable rhythm cardiac arrest. *Resuscitation* **2015**, *92*, 1–6. [CrossRef]
20. Prosen, G.; Križmarić, M.; Završnik, J.; Grmec, Š. Impact of modified treatment in echocardiographically confirmed pseudo-pulseless electrical activity in out-of-hospital cardiac arrest patients with constant end-tidal carbon dioxide pressure during compression pauses. *J. Int. Med. Res.* **2010**, *38*, 1458–1467. [CrossRef]
21. Losert, H.; Risdal, M.; Sterz, F.; Nysæther, J.; Köhler, K.; Eftestøl, T.; Wandaller, C.; Myklebust, H.; Uray, T.; Aase, S.O.; et al. Thoracic-impedance changes measured via defibrillator pads can monitor signs of circulation. *Resuscitation* **2007**, *73*, 221–228. [CrossRef] [PubMed]
22. Alonso, E.; Aramendi, E.; Daya, M.; Irusta, U.; Chicote, B.; Russell, J.K.; Tereshchenko, L.G. Circulation detection using the electrocardiogram and the thoracic impedance acquired by defibrillation pads. *Resuscitation* **2016**, *99*, 56–62. [CrossRef]
23. Elola, A.; Aramendi, E.; Irusta, U.; Berve, P.O.; Wik, L. Multimodal algorithms for the classification of circulation states during out-of-hospital cardiac arrest. *IEEE Trans. Biomed. Eng.* **2021**, *68*, 1913–1922. [CrossRef] [PubMed]

24. Alonso, E.; Eftestøl, T.; Aramendi, E.; Kramer-Johansen, J.; Skogvoll, E.; Nordseth, T. Beyond ventricular fibrillation analysis: Comprehensive waveform analysis for all cardiac rhythms occurring during resuscitation. *Resuscitation* **2014**, *85*, 1541–1548. [CrossRef]
25. Lasa, H.; Irusta, U.; Eftestol, T.; Aramendi, E.; Rad, A.B.; Kramer-Johansen, J.; Wik, L. Multimodal Biosignal Analysis Algorithm for the Classification of Cardiac Rhythms During Resuscitation. In Proceedings of the 2020 Computing in Cardiology, Rimini, Italy, 13–16 September 2020; pp. 1–4.
26. Urteaga Urizarbarrena, J.; Aramendi Ecenarro, E.; Elola Artano, A.; Irusta Zarandona, U.; Idris, A. Modelo predictivo del retorno de circulación espontánea en la parada cardiorrespiratoria utilizando el ECG y la impedancia torácica. In Proceedings of the Libro de Actas del XXXVIII Congreso Anual de la Sociedad Española de Ingeniería Biomédica CASEIB, Madrid, Spain, 25–27 November 2020.
27. Ayala, U.; Eftestøl, T.; Alonso, E.; Irusta, U.; Aramendi, E.; Wali, S.; Kramer-Johansen, J. Automatic detection of chest compressions for the assessment of CPR-quality parameters. *Resuscitation* **2014**, *85*, 957–963. [CrossRef]
28. Stecher, F.S.; Olsen, J.A.; Stickney, R.E.; Wik, L. Transthoracic impedance used to evaluate performance of cardiopulmonary resuscitation during out of hospital cardiac arrest. *Resuscitation* **2008**, *79*, 432–437. [CrossRef] [PubMed]
29. Isasi, I.; Irusta, U.; Elola, A.; Aramendi, E.; Ayala, U.; Alonso, E.; Kramer-Johansen, J.; Eftestøl, T. A machine learning shock decision algorithm for use during piston-driven chest compressions. *IEEE Trans. Biomed. Eng.* **2018**, *66*, 1752–1760. [CrossRef]
30. Isasi, I.; Irusta, U.; Elola, A.; Aramendi, E.; Eftestøl, T.; Kramer-Johansen, J.; Wik, L. A Robust Machine Learning Architecture for a Reliable ECG Rhythm Analysis during CPR. In Proceedings of the 2019 41st Annual International Conference of the IEEE Engineering in Medicine and Biology Society (EMBC), Berlin, Germany, 23–27 July 2019; pp. 1903–1907.
31. Ruiz, J.; Alonso, E.; Aramendi, E.; Kramer-Johansen, J.; Eftestøl, T.; Ayala, U.; González-Otero, D. Reliable extraction of the circulation component in the thoracic impedance measured by defibrillation pads. *Resuscitation* **2013**, *84*, 1345–1352. [CrossRef]
32. Risdal, M.; Aase, S.O.; Kramer-Johansen, J.; Eftestol, T. Automatic identification of return of spontaneous circulation during cardiopulmonary resuscitation. *IEEE Trans. Biomed. Eng.* **2007**, *55*, 60–68. [CrossRef]
33. Hamilton, P.S.; Tompkins, W.J. Quantitative investigation of QRS detection rules using the MIT/BIH arrhythmia database. *IEEE Trans. Biomed. Eng.* **1986**, *12*, 1157–1165. [CrossRef]
34. Zhao, Z.; Särkkä, S.; Rad, A.B. Spectro-temporal ECG analysis for atrial fibrillation detection. In Proceedings of the 2018 IEEE 28th International Workshop on Machine Learning for Signal Processing (MLSP), Aalborg, Denmark, 17–20 September 2018; pp. 1–6.
35. Elola, A.; Aramendi, E.; Irusta, U.; Del Ser, J.; Alonso, E.; Daya, M. ECG-based pulse detection during cardiac arrest using random forest classifier. *Med. Biol. Eng. Comput.* **2019**, *57*, 453–462. [CrossRef]
36. Ruiz, J.M.; de Gauna, S.R.; González-Otero, D.M.; Saiz, P.; Gutiérrez, J.J.; Veintemillas, J.F.; Bastida, J.M.; Alonso, D. Circulation assessment by automated external defibrillators during cardiopulmonary resuscitation. *Resuscitation* **2018**, *128*, 158–163. [CrossRef]
37. Chicote, B.; Irusta, U.; Aramendi, E.; Isasi, I.; Alonso, D.; Vicente, F.; Sanchez, M. Nonlinear energy operators for defibrillation shock outcome prediction. In Proceedings of the 2016 Computing in Cardiology Conference (CinC), Vancouver, BC, Canada, 11–14 September 2016; pp. 61–64.
38. Jekova, I.; Krasteva, V. Real time detection of ventricular fibrillation and tachycardia. *Physiol. Meas.* **2004**, *25*, 1167. [CrossRef]
39. Bos, R.; De Waele, S.; Broersen, P.M. Autoregressive spectral estimation by application of the Burg algorithm to irregularly sampled data. *IEEE Trans. Instrum. Meas.* **2002**, *51*, 1289–1294. [CrossRef]
40. Elola, A.; Aramendi, E.; Rueda, E.; Irusta, U.; Wang, H.; Idris, A. Towards the Prediction of Rearrest during Out-of-Hospital Cardiac Arrest. *Entropy* **2020**, *22*, 758. [CrossRef]
41. Breiman, L. Random forests. *Mach. Learn.* **2001**, *45*, 5–32. [CrossRef]
42. Isasi, I.; Irusta, U.; Rad, A.B.; Aramendi, E.; Zabihi, M.; Eftestøl, T.; Kramer-Johansen, J.; Wik, L. Automatic cardiac rhythm classification with concurrent manual chest compressions. *IEEE Access* **2019**, *7*, 115147–115159. [CrossRef]
43. Martínez, J.P.; Almeida, R.; Olmos, S.; Rocha, A.P.; Laguna, P. A wavelet-based ECG delineator: Evaluation on standard databases. *IEEE Trans. Biomed. Eng.* **2004**, *51*, 570–581. [CrossRef]
44. Soar, J.; Böttiger, B.W.; Carli, P.; Couper, K.; Deakin, C.D.; Djärv, T.; Lott, C.; Olasveengen, T.; Paal, P.; Pellis, T.; et al. European Resuscitation Council Guidelines 2021: Adult advanced life support. *Resuscitation* **2021**, *161*, 115–151. [CrossRef] [PubMed]
45. Sandroni, C.; De Santis, P.; D'Arrigo, S. Capnography during cardiac arrest. *Resuscitation* **2018**, *132*, 73–77. [CrossRef]
46. Sanfilippo, F.; Serena, G.; Corredor, C.; Benedetto, U.; Maybauer, M.O.; Al-Subaie, N.; Madden, B.; Oddo, M.; Cecconi, M. Cerebral oximetry and return of spontaneous circulation after cardiac arrest: A systematic review and meta-analysis. *Resuscitation* **2015**, *94*, 67–72. [CrossRef] [PubMed]
47. Takegawa, R.; Hayashida, K.; Rolston, D.M.; Li, T.; Miyara, S.J.; Ohnishi, M.; Shiozaki, T.; Becker, L.B. Near-infrared spectroscopy assessments of regional cerebral oxygen saturation for the prediction of clinical outcomes in patients with cardiac arrest: A review of clinical impact, evolution, and future directions. *Front. Med.* **2020**, *7*, 736. [CrossRef]
48. Breitkreutz, R.; Price, S.; Steiger, H.V.; Seeger, F.H.; Ilper, H.; Ackermann, H.; Rudolph, M.; Uddin, S.; Weigand, M.A.; Müller, E.; et al. Focused echocardiographic evaluation in life support and peri-resuscitation of emergency patients: A prospective trial. *Resuscitation* **2010**, *81*, 1527–1533. [CrossRef]

49. Kim, Y.J.; Lee, Y.J.; Ryoo, S.M.; Sohn, C.H.; Ahn, S.; Seo, D.W.; Lim, K.S.; Kim, W.Y. Role of blood gas analysis during cardiopulmonary resuscitation in out-of-hospital cardiac arrest patients. *Medicine* **2016**, *95*, e3960. [CrossRef]
50. Elola, A.; Aramendi, E.; Irusta, U.; Picón, A.; Alonso, E.; Owens, P.; Idris, A. Deep neural networks for ECG-based pulse detection during out-of-hospital cardiac arrest. *Entropy* **2019**, *21*, 305. [CrossRef] [PubMed]
51. Isasi, I.; Irusta, U.; Aramendi, E.; Eftestøl, T.; Kramer-Johansen, J.K.J.; Wik, L. Rhythm Analysis during Cardiopulmonary Resuscitation Using Convolutional Neural Networks. *Entropy* **2020**, *22*, 595. [CrossRef]
52. Jaureguibeitia, X.; Zubia, G.; Irusta, U.; Aramendi, E.; Chicote, B.; Alonso, D.; Larrea, A.; Corcuera, C. Shock Decision Algorithms for Automated External Defibrillators Based on Convolutional Networks. *IEEE Access* **2020**, *8*, 154746–154758. [CrossRef]

A.1.2 First conference paper

	Publication in international conference
Reference	Jon Urteaga, Elisabete Aramendi, Andoni Elola, Anders Norvik, Eirik Unneland, Abhishek Bhardwaj, David Buckler, Benjamin S Abella, Eirik Skogvoll, "The Prediction Of Pulseless Electrical Activity Evolution During In-hospital Cardiac Arrest Using Machine Learning", *Resuscitation Science Symposium (AHA-ReSS), 2022*
Quality indices	• **Type of publication**: International conference

Circulation

FREE ACCESS | ABSTRACT

RESUSCITATION SCIENCE SYMPOSIUM 2022
SESSION TITLE: POSTER ABSTRACT SESSIONS

Abstract 220: The Prediction Of Pulseless Electrical Activity Evolution During In-hospital Cardiac Arrest Using Machine Learning

Jon Urteaga, Elisabete Aramendi, Andoni Elola, Anders Norvik, Eirik Unneland, Abhishek Bhardwaj, David Buckler, Benjamin Abella and Eirik Skogvoll

Originally published 30 Oct 2022 | https://doi.org/10.1161/circ.146.suppl_1.220 | Circulation. 2022;146:A220

Abstract

Background: Pulseless electrical activity (PEA) is the most common rhythm during in-hospital cardiac arrest (IHCA) with a prevalence around 50%. Knowing the prognosis of PEA evolution towards return of spontaneous circulation (ROSC) could help optimizing both resuscitation maneuvers and pharmacological therapy. The aim of this study was to develop an automatic method to predict the evolution of PEA during resuscitation based on the ECG-waveform.

Materials and Methods: The dataset consists of 164 IHCA cases recorded by St. Olav University Hospital (Norway), Hospital of the University of Pennsylvania (USA) and Penn Presbyterian Medical Center (USA). ROSC was verified in 108 cases of the patients by physicians and bioengineers based on episode waveforms and clinical data. PEA segments of 5 sec were extracted from the last 10 min before ROSC or the end of resuscitation therapy. Three machine learning models were designed for segment binary classification based on an SVM (Gaussian) model using: 1) ECG-waveform features (9); 2) QRS-features (8); and 3) both ECG-waveform and QRS-features (17). Ten-fold cross validation was applied to train and test the models, and the performance was given in terms of area under the curve (AUC), sensitivity (Se) to correctly detect cases evolving to ROSC, specificity (Sp) and balanced accuracy (BAC).

Results: A total of 780 segments were extracted (472 with ROSC). The median (IQR) for the models with the best feature combination are shown in the Table. The most important ECG-waveform features are associated to the ECG spectral distribution. QRS features that showed relevant information about the evolution of PEA were heart rate median and standard deviation, and QRS width, slope and amplitude.

Conclusions: ROSC/no ROSC prediction of PEA segments is feasible using ECG signal information. The combination of ECG-waveform and QRS features enhances performance of predictive model.

Model	AUC (%)	Se (%)	Sp (%)	BAC (%)
ECG-waveform	80.85 (10.91)	63.68 (20.62)	91.45 (29.34)	72. 27(19.11)
QRS	80.17 (11.34)	67.78 (20.08)	74.61 (25.71)	69.87 (9.26)
ECG-waveform & QRS	84.07 (8.73)	63.68 (23.24)	79.61 (27.05)	72.19 (7.95)

Download figure

Footnotes

Author Disclosures: For author disclosure information, please visit the AHA Resuscitation Science Symposium 2022 Online Program Planner and search for the abstract title.

Back to top

A.1.3 Second journal paper

	Publication in international journal
Reference	Jon Urteaga, Andoni Elola, Anders Norvik, Eirik Unneland, Trygve C Eftestøl, Abhishek Bhardwaj, David Buckler, Benjamin S Abella, Eirik Skogvoll, Elisabete Aramendi "Machine learning model to predict evolution of pulseless electrical activity during in-hospital cardiac arrest". *Resuscitation Plus, 2024*, vol. 17, p. 100598.
Quality indices	• **Type of publication**: Journal paper indexed in JCR • **Quartile**: Q2 (23/53) based on Web of Science Rank 2022 • **Impact factor**: 2.4

Available online at www.sciencedirect.com

Resuscitation Plus

journal homepage: www.elsevier.com/locate/resuscitation-plus

Clinical paper

Machine learning model to predict evolution of pulseless electrical activity during in-hospital cardiac arrest

Jon Urteaga[a], *Andoni Elola*[b], *Anders Norvik*[c], *Eirik Unneland*[c], *Trygve C. Eftestøl*[d], *Abhishek Bhardwaj*[e], *David Buckler*[f], *Benjamin S. Abella*[g], *Eirik Skogvoll*[c], *Elisabete Aramendi*[a,h,*]

Abstract

Background: During pulseless electrical activity (PEA) the cardiac mechanical and electrical functions are dissociated, a phenomenon occurring in 25–42% of in-hospital cardiac arrest (IHCA) cases. Accurate evaluation of the likelihood of a PEA patient transitioning to return of spontaneous circulation (ROSC) may be vital for the successful resuscitation.

The aim: We sought to develop a model to automatically discriminate between PEA rhythms with favorable and unfavorable evolution to ROSC.

Methods: A dataset of 190 patients, 120 with ROSC, were acquired with defibrillators from different vendors in three hospitals. The ECG and the transthoracic impedance (TTI) signal were processed to compute 16 waveform features. Logistic regression models where designed integrating both automated features and characteristics annotated in the QRS to identify PEAs with better prognosis leading to ROSC. Cross validation techniques were applied, both patient-specific and stratified, to evaluate the performance of the algorithm.

Results: The best model consisted in a three feature algorithm that exhibited median (interquartile range) Area Under the Curve/Balanced accuracy/Sensitivity/Specificity of 80.3(9.9)/75.6(8.0)/ 77.4(15.2)/72.3(16.4) %, respectively.

Conclusions: Information hidden in the waveforms of the ECG and TTI signals, along with QRS complex features, can predict the progression of PEA. Automated methods as the one proposed in this study, could contribute to assist in the targeted treatment of PEA in IHCA.

Keywords: Pulseless electrical activity (PEA), Machine Learning models, Cardiopulmonary resuscitation (CPR), Evolution prediction

Introduction

The cardiac electrical activity with no effective mechanical contractions (PEA) is a rhythm frequently present in cardiac arrest, with recorded prevalence of 20–30% in out-of-hospital (OHCA) and up to 40–60% in in-hospital cardiac arrest (IHCA).[1–3] In recent decades, PEA prevalence in IHCA increased from 36% in 2000 to 46% in 2009,[4] and similar increasing trends were observed in out-of-hospital studies.[5–7]

In the context of cardiopulmonary resuscitation (CPR), biosignals as electrocardiogram (ECG) and thoracic impedance (TTI) provide valuable information that can assist identifying the prognosis of PEA and guide the appropriate treatment towards the return of spontaneous circulation (ROSC).[8,9] Knowledge of the prognosis of PEA can help clinicians make informed decisions about the appropriate treatment and management of patients, [10,11] discriminating favorable from unfavorable PEA. Pseudo-PEA rhythms show small mechanical activity, albeit insufficient for a palpable pulse, in contrast to

* Corresponding author at: Communications Engineering Department, niversity of the Basque Country UPV/EHU, Escuela de Ingenier´ıa de Billbao, Plaza Ingeniero Torres Quevedo 1, 48013 Bilbao, Spain.

E-mail addresses: jon.urteaga@ehu.eus (J. Urteaga), andoni.elola@ehu.eus (A. Elola), anders.norvik@ntnu.no (A. Norvik), eirik.unneland@ntnu.no (E. Unneland), trygve.eftestol@uis.no (T.C. Eftestøl), drabhishekbhardwaj66@gmail.com (A. Bhardwaj), david.buckler@mountsinai.org (D. Buckler), Benjamin.Abella@pennmedicine.upenn.edu (B.S. Abella), eirik.skogvoll@ntnu.no (E. Skogvoll), elisabete.aramendi@ehu.eus (E. Aramendi).

https://doi.org/10.1016/j.resplu.2024.100598

Received 28 November 2023; Received in revised form 21 February 2024; Accepted 22 February 2024

true-PEA with no mechanical cardiac activity.[8,12,13] The two types of PEA have different prognosis and treatment,[13–16] and their distinction is of great clinical interest to predict the hemodynamical evolution of PEA and their outcome.

Both heart rate (HR) and QRS complex duration are biomarkers that are readily accessible during both the initial and subsequent rhythm assessments. Recent studies have indicated their relation with the outcome and suggest that HR increase and QRS duration decrease indicate a higher probability of ROSC.[10,17–19] More sophisticated features of the ECG and the TTI computed in the frequency domain, as AMSA and the cross-power between ECG and TTI signals, have also shown the potential to predict ROSC.[9] Their combinations in machine learning (ML) models have been proposed to predict the immediate rhythm transition during cardiac arrest,[20] to classify different types of rhythm,[21] and to distinguish between favorable (faPEA) and unfavorable (unPEA) PEA, the former denoting instances of PEA evolving into sustained ROSC (minimum 20 min), while the latter pertaining to PEA cases wherein pulse is not regained.[9,22]

In this study multivariable machine learning models have been proposed to discriminate PEAs with favorable prognosis in IHCA. Features based on different signals and QRS complexes have been included in an automated model, in addition to a new version of the Amplitude Spectrum Area. The potential of the ECG and TTI features, hidden in the biosignal waveforms, were analyzed and combined in a sophisticated regression based classifier. Retrospective analysis of IHCA episodes permitted the evaluation of the accuracy of the models.

Materials and methods

Data materials

The data used in this study was a subset of a larger database containing IHCA episodes from different hospitals. The subset comprised of 197 episodes recorded by emergency services: 83 episodes from St. Olav University Hospital (Trondheim,Norway), 90 episodes from the Hospital of the University of Pennsylvania (USA) and 24 episodes from Penn Presbyterian Medical Center (USA). The episodes from Norway, captured between 2018 and 2021, were recorded using Lifepak- 20 defibrillators (Stryker, Redmond, USA), whereas the episodes from Pennsylvania, captured between 2008 and 2010, were recorded using HeartStart MRx-defibrillators (Philips Medical Systems, Andover, Massachusetts, USA). Out of 197 episodes, 190 came from different patients, and a summary of the patient cohort's characteristics is presented in Table 1.

The median (Interquartile range, IQR) duration of the episodes was 17.1 (9.1–32.2) min from the start of the episode to the ROSC/end-of-CPR, and in 120 episodes sustained ROSC was achieved, 8.2(5.3–19.9) min after switching on the defibrillator. Sustained ROSC was defined as a pulsed rhythm with no chest compressions at least during 20 min.[7]

Expert clinicians reviewed and manually annotated all episodes. They annotated rhythm type and QRS complexes in the ECG signal, and identified chest compression series in the TTI. For the analysis, PEA segments of 5 s duration, separated by at least 1 s, were extracted during chest compression pauses. As rates below 12 bpm during longer than 5 s are considered asystole, a minimum duration of 5 s and 12 bpm were demanded to guarantee that all segments were PEA rhythms.[23–25] Fig. 1 shows two examples of the dataset, where both the ECG and the TTI signals are represented with some meaningful features.

Table 1 – Summary of patient and episode statistics. Data are presented as percentage or median (Interquartile range, IQR).

Patient Summary (*n* = 190)	
Metric	Value
Age (years)	69.5 (57.8–77.3)
Male gender	54.2%
Survived to discharge	17%
Episode Summary (*n* = 197)	
Metric	Value
Monitored CA	78%
Assumed cardiac cause	55%
Received adrenaline	84%

Methods

This section described the procedure to define the PEA analysis based on ML models. The method is divided in three stages consisting of: 1) Preprocessing of ECG and TTI signals, 2) Feature characterization of the signals, and 3) Design of feature-based ML models for binary classification. This last stage includes the training/validation of the models as well as their statistical characterization.

ECG and TTI preprocessing

ECG and TTI signals were preprocessed following the scheme proposed in a previous study.[9,22] The ECG signal was denoised using a stationary wavelet transform (SWT) technique. This involved applying a band-pass filter in the band of 0.5–31.25, Hz to remove baseline noise, high-frequency noise, motion artifacts, and ventilation artifacts. The impedance circulation component (ICC), which reflects the ventricular contractions in the TTI signal correlated with ECG heartbeats,[22,26] was extracted from the TTI signal and filtered 1–8 Hz.[9,22] In Fig. 1, it can be observed how the ICC component of TTI signal correlated with the QRS complexes in the ECG.

Feature extraction

The sets of features considered in this study were gathered in three groups: The ECG and ICC waveform features, previously proposed in cardiac arrest studies, and new additional QRS related features.

ECG waveform features

The main ECG waveform computed, non QRS specific features, were the following:

- The Amplitude Spectrum Area (AMSA) was calculated by summing the product of the spectral amplitudes and corresponding frequencies in the band of 2–48 Hz of the ECG signal as proposed in.[27] It has been widely reported as a reliable predictor for successful defibrillation, and it is indicative of both coronary perfusion pressure and myocardial energy state.[9,28,29]
- ModAMSA is a modified version of AMSA that calculates the spectral content in the frequency range of 20–30 Hz. The ModAMSA associated to faPEA rhythms was observed to be higher than the value for unPEA. The Figure in Appendix A shows

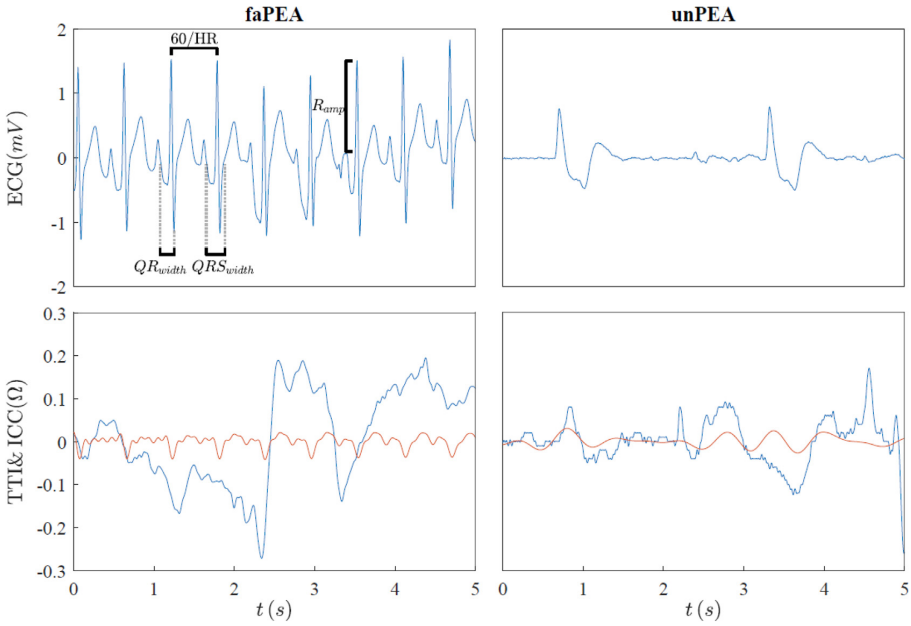

Fig. 1 – Two PEA cases corresponding to faPEA (left) and unPEA (right) are shown. On the top the ECG signals, with HR_{mean}, QR_{width}, QRS_{width}, and R_{amp} represented. On the bottom the TTI and the computed impedance circulation component, ICC, in red.

how the spectral content of both types of rhythms overlaps considerably between 0 and 15 Hz but becomes more distinct between 20 and 30 Hz.

- The Smoothed Nonlinear Energy Operator(SNEO) computed in the ECG, $SNEO_{ECG}$, measures the local energy content of the ECG signal as described in.[30] It has been classically applied for QRS complex detection, [31] shock outcome prediction[30] and identification of circulatory status.[22]
- The Autoregressive Burg's value (ARB) computed in the ECG signal, ARB_{ECG}, evaluates the similarity between the power spectral density of the signal with an autoregressive model of the spectrum.[32] It has been used for identification of circulatory status[22], cardiac rhythm classification[33] and prediction of prognosis of PEA during OHCA.[9]
- Entropy is a complexity measure that quantifies the regularity of the ECG.[34]

ICC waveform features

The ICC of the TTI was computed as described in[9,22] and features computed as follows:

- $Cross_{Power}$ is the cross power between the ECG and ICC signals. High $Cross_{Power}$ indicates pulsatile rhythms, and it has been proposed for automatic circulation detection in OHCA. [35]
- $LogPower_{ICC}$ is the logarithmic energy of the ICC signal, which is related to the ventricular wall movement.[36]
- $SNEO_{ICC}$ is the SNEO value of the ICC signal, computed as described in section 3.2.1.
- ARB_{ICC} is the ARB of the ICC signal, computed as described in section 3.2.1.

QRS waveform features

Additionally to ECG waveform features, several metrics related to the QRS waveform were computed using the manual annotations of the Q, R, and S waves made by clinicians.

- HR_{mean} and HR_{var} are the mean and variance values of HR, respectively, computed as the inverse of consecutive R-R intervals.
- QRS_{width} and QR_{width} correspond to the durations of Q-S and Q-R complex, respectively.
- QRS_{slope} and QR_{slope} are computed as the sum of the amplitude values of QRS and QR complexes in the first difference signal divided by QRS_{width} and QR_{width}, respectively.
- R_{amp} is the mean value of the amplitude of the R wave peaks in the segment.

A detailed description of the algorithms applied to compute the features can be found in Appendix B.

LR classifier

A logistic regression model (LR) was used to classify PEA segments into faPEA or unPEA. The models were trained and tested combining multiple variables. LR was the best option to make understandable binary classifications. The probability of a segment to be a faPEA was computed following the next equation[36]:

$$p = \frac{1}{1 + e^{-z}}$$

where z is the linear combination of the independent features weighted by their coefficients:

$$z = \beta_0 + \beta_1 x_1 + \beta_2 x_2 + \ldots + \beta_n x_n$$

In this equation, β_0, β_1, β_2, ..., β_n are the regression coefficients estimated during the model fitting process, and x_1, x_2, ..., x_n are the features of the PEA segment.

The maximum Area Under the ROC Curve (AUC) was applied as the optimization criteria in the design process.

Feature selection has been performed using forward feature selection. This means that we started with the feature with the highest AUC, and at each step, we added the feature that, when combined, provided the best AUC.

Validation

A 10-fold cross-validation (CV) technique was used for model validation, using different sets of patients for training and testing. This implies that all segments extracted from a patient were used either for training or for testing within each fold; segments from the same patient were never split for training and testing the model. To improve reliability, the partition was done assigning the same weight to all patients, which avoided data leakage between folds.

The performance of the classifiers was evaluated using standard performance metrics for binary classifiers, with faPEA as the positive class. The AUC, Sensitivity (Se), Specificity (Sp) and Balanced Accuracy (BAC, the average of Se and Sp) were considered as the performance metrics.

The performance metric that was primarily focused on optimizing in this study was the AUC.

Time analysis

In previous studies on rhythm evolution or pulse detection in cardiac arrest, predictability was shown to vary over time.[7,9,37,38] In this second analysis segments were separated in four groups (quartiles) depending on their time distance to the ROSC/end-of-CPR, and models analyzed in terms of proximity to the end. While maintaining the 10-fold CV architecture, the models were trained using segments from all quartiles and performance was evaluated in each specific quartile.

Additionally, the evolution of the top three features was analyzed over the last 15 minutes of the episode, and an exponential function adjusted to characterize their evolution.

Results

A total of 1468 PEA segments of 5 s duration were extracted from 197 episodes, with a median (IQR) of 4(1–8) segments per episode. The segments observed during episodes with ROSC were categorized as faPEA, while those without ROSC were categorized as unPEA. There was a total of 767 faPEA segments, median (IQR) 2 (1–9) per episode, and 701 unPEA segments, 5 (3–9) per episode. The 25th, 50th, and 75th percentiles of their time to ROSC/end-of-CPR were 180, 383, and 772 seconds, respectively.

In Table 2, the independent analysis of each feature can be observed for faPEA/unPEA groups. The median (IQR) value of each

Table 2 – Median (IQR) values of each feature for faPEA and unPEA segments are shown, the AUC of the LR classifier. Mann-Whitney U-test was performed considering one value (median among segments) per feature and per patient.

	ECG Features			
Feature	faPEA	unPEA	AUC(%)	*p*-value
AMSA	24.50 (16.56–39.32)	14.00 (9.47–20.50)	75.23 (69.42–81.82)	$3.5{\cdot}10^{-4}$
ModAMSA	4.14 (2.15–6.93)	1.52 (0.94–2.51)	79.13 (74.59–85.72)	$8.3{\cdot}10^{-6}$
$SNEO_{ECG}$	0.16 (0.04–0.65)	0.07 (0.01–0.23)	63.78 (55.81–71.68)	$6.8{\cdot}10^{-5}$
ARB_{ECG}	$2.18{\cdot}10^{-6}$ ($0.71{\cdot}10^{-6}$ –$4.57{\cdot}10^{-6}$)	$0.48{\cdot}10^{-6}$ ($0.26{\cdot}10^{-6}$ –$1.15{\cdot}10^{-6}$)	77.89 (73.47–84.47)	$1.4{\cdot}10^{-9}$
Entropy	0.29 (0.21–0.35)	0.22 (0.16–0.31)	63.06 (57.69–70.45)	$9.6{\cdot}10^{-3}$
	TTI Features			
Feature	faPEA	unPEA	AUC(%)	p-value
$Cross_{Power}$	0.51 (0.14–1.24)	0.30 (0.07–0.80)	58.93 (54.31–64.19)	$4.8{\cdot}10^{-3}$
$LogPower_{ICC}$	4083 (2518–5412)	3308 (1673–4412)	59.54 (55.37–64.83)	$2.1{\cdot}10^{-3}$
$SNEO_{ICC}$	$1.1{\cdot}10^{-3}$ ($0.17{\cdot}10^{-3}$ –$4.65{\cdot}10^{-3}$)	$0.48{\cdot}10^{-3}$ ($0.11{\cdot}10^{-3}$ –$1.80{\cdot}10^{-3}$)	59.99 (55.56–64.34)	$4.3{\cdot}10^{-2}$
ARB_{ICC}	$43.36{\cdot}10^{-9}$ ($4.81{\cdot}10^{-9}$ –$340.91{\cdot}10^{-9}$)	$27.51{\cdot}10^{-9}$ ($5.76{\cdot}10^{-9}$ –$113.21{\cdot}10^{-9}$)	57.53 (54.16–64.93)	$2.4{\cdot}10^{-2}$
	QRS Features			
Feature	faPEA	unPEA	AUC(%)	p-value
HRmean	74.26 (46.57–113.40)	70.83 (38.11–90.40)	56.48 (52.51–62.31)	$2.2{\cdot}10^{-2}$
HR_{var}	5.14 (0.41–157.79)	6.77 (0.06–101.21)	57.75 (55.42–62.98)	$1.2{\cdot}10^{-2}$
QRSwidth	155 (113–195)	205 (160–262)	68.74 (60.92–77.76)	$6.6{\cdot}10^{-5}$
QRwidth	52 (40–77)	67 (50–97)	65.31 (56.35–73.33)	$2.3{\cdot}10^{-3}$
Ramp	0.36 (0.04–0.70)	0.19 (0.23–0.40)	63.29 (57.29–68.74)	$1.0{\cdot}10^{-2}$
QRS_{slope}	0.013 (0.009–0.019)	0.007 (0.005–0.011)	77.63 (68.41–82.08)	$4.3{\cdot}10^{-7}$
QRslope	0.011 (0.008–0.017)	0.007 (0.005–0.096)	72.43 (65.91–78.91)	$2.0{\cdot}10^{-6}$

type of segments was computed using the whole dataset, while AUC was computed following the 10-fold CV model explained in methods section. The results in terms of discrimination power are quite aligned with previous OHCA analysis for ECG and TTI signals,[9] showing AUC values above 75% in several single features.

All the features showed different medians for unPEA and faPEA groups according to Mann-Whitney U-test ($p < 0.05$). However, the features that showed lowest p values, with $p < 0.005$, were ModAMSA, AMSA, $SNEO_{ECG}$, ARB_{ECG}, $LogPower_{ICC}$, $Cross_{Power}$, QRS_{width}, QR_{width}, QRS_{slope} and QR_{slope}.

The performance of the LR classifiers in terms of the number of features, following the criteria of forward feature selection explained in the methods section, is shown in Table 3. The analysis revealed that the best performance was achieved with a three-feature model based on: ModAMSA, $LogPower_{ICC}$, QRS_{width}, with AUC/BAC values of 80.3% and 75.6%, respectively. No improvement was observed increasing the number of features.

In the time analysis, the performance of the three-feature LR model was analyzed in terms of the distance to the ROSC/end-of-CPR and results are shown in Fig. 2. It can be observed that the classifier performs better for segments closer to the end (Q4 compared to Q1). Specifically, the Q4 group with a time-distance of 0–180 s from the end showed an AUC/BAC of 87.3%/BAC of 79.1%, while the Q1 at >772 s from the end presented AUC/BAC of 69.6%/59.9%.

To better understand the results, we analyzed the evolution of the top three features in the last 15 minutes before ROSC. Fig. 3 shows that the values of ModAMSA, QRS_{width} and ICC log Power separate for faPEA(blue) compared to unPEA(red) further as ROSC approaches. These results confirm the potential of these features to evaluate the proximity to ROSC and discriminate between PEA with favorable and unfavorable prognosis.

The study also confirms previous findings[9,10,17–19] that as PEA episodes progress, the predictability of PEA prognosis increases. This is supported by the results in Fig. 2, as well as the observation that features of each type become increasingly distinct over time, as seen in Fig. 3.

Discussion

This work presents a novel predictive model that integrates ECG and TTI features to discriminate PEAs with positive prognosis. This is the first time such a model is designed for IHCA patients and integrates QRS specific features.

The application of ML models to design predictive models for IHCA reinforce previous conclusions of Urteaga et al. with OHCA.[9] Both studies highlight the importance of feature selection and integration of different sources of information to develop accurate tools for PEA state evolution prediction in cardiac arrest patients.

In contrast to previous automated methods, this study integrates QRS complex features that have demonstrated great potential to predict the outcome of PEA.[10,17–19,39,40] The AUC obtained for the QRS complex duration is aligned with previous results, and combining QRS complex features with other ECG/ICC features has improved the overall performance of the model 0.6 points of AUC and 4.1 points of BAC. Fig. 3 showed that QRS complexes are narrower in faPEA segments compared to unPEA, and that they evolve to narrower values as episode progresses towards ROSC. However, the discriminative power of HR does not support its use in this application (see Table 2).

Table 3 – The LR model's performance in terms of median (IQR) AUC, BAC, Se, and Sp. All possible combinations using one to six features have been tested, only the best for each number of features is shown.

	No. Features	AUC (%)	BAC (%)	Se (%)	Sp (%)
ModAMSA	1	79.1 (74.6–85.7)	71.4 (63.9–75.7)	62.9 (56.1–71.9)	79.2 (70.2–89.9)
ModAMSA + $LogPower_{ICC}$	2	79.7 (73.7–85.3)	71.5 (65.2–79.0)	64.2 (57.7–73.9)	78.5 (71.1–88.0)
ModAMSA + $LogPower_{ICC}$ + QRS_{width}	3	80.3 (73.3–85.7)	75.6 (69.6–80.1)	77.4 (70.3–84.2)	72.3 (61.9–79.6)
ModAMSA + $LogPower_{ICC}$ + QRS_{width} + ARB_{ECG}	4	80.2 (73.4–85.7)	75.5 (69.9–80.3)	77.5 (69.9–83.5)	69.5 (60.2–80.0)
ModAMSA + $LogPower_{ICC}$ + QRS_{width} + ARB_{ECG} + QR_{width}	5	79.8 (73.4–85.8)	73.1 (69.0–79.2)	77.8 (69.8–83.8)	66.4 (59.1–78.9)
ModAMSA + $LogPower_{ICC}$ + QRS_{width} + ARB_{ECG} + QR_{width} + $Cross_{Power}$	6	79.6 (73.3–85.7)	72.6 (68.9–72.3)	76.4 (68.7–82.9)	64.4 (58.6–77.7)

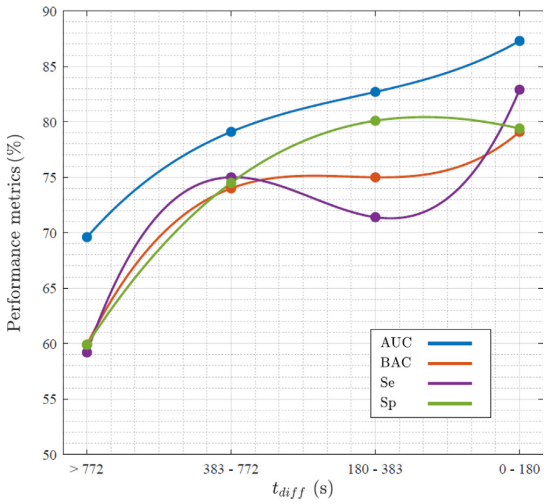

Fig. 2 – Performance of the LR model with three features for segments according to their distance from the ROSC/end-of-episode. The figure shows the median (IQR) values for AUC, BAC, Se and Sp.

The QRS_{width} and the *HR* are the characteristics that have been studied as indicators of PEA prognosis. Norvik et al. and Aufderheide et al. have found a correlation between QRS_{width} and *HR* with survival.[17,19,41] Both studies demonstrated that smaller QRS_{width} and higher *HR* are associated with more favorable outcomes in PEA. On the other hand, Weisser et al. only found a correlation between *HR* and prognosis, not with QRS_{width}.[42] This is in contrast to Kim et al., who found a correlation with the duration of the QRS complex but not with *HR*.[40] In this study, the correlation of QRS_{width} with the prognosis of pulseless electrical activity (PEA) has been demonstrated. In Fig. 2, it can be observed how the mean value of QRS_{width} differs more as it approaches the ROSC/end-of-CPR. This is consistent with the results of Norvik et al.[19]

It is worth highlighting that ModAMSA, which is the independent feature that shows the best performance in Table 2, also exhibits the most significant difference over time in Fig. 2. High values of ModAMSA are associated with more content in the high-frequency spectrum, which is caused by high *HR* and narrow QRS complexes with high amplitude.

The results also demonstrate that ModAMSA, a modified version of the AMSA, has better predictive capabilities than the original feature to differentiate an unPEA from a faPEA. This finding highlights the potential of the frequency range of 20–30 Hz to classify PEA segments according to their prognosis. This frequency band has already shown potential for the detection and classification of cardiac rhythms in previous studies.[9,34,43] Other applications of AMSA[44–47] might benefit from this new definition and provide more accurate predictive models.

Regarding the number of features included in the predictive models, it can be concluded that more features do not necessarily improve the accuracy of the algorithm (see Table 3) because their contribution may result redundant or irrelevant to the model. In our case the best model was reached with three features, one from each group: ECG signal waveform, ICC signal waveform, and QRS complex shape. Each of these features also happens to have the highest AUC value among all the features that showed $p < 0.005$ within their

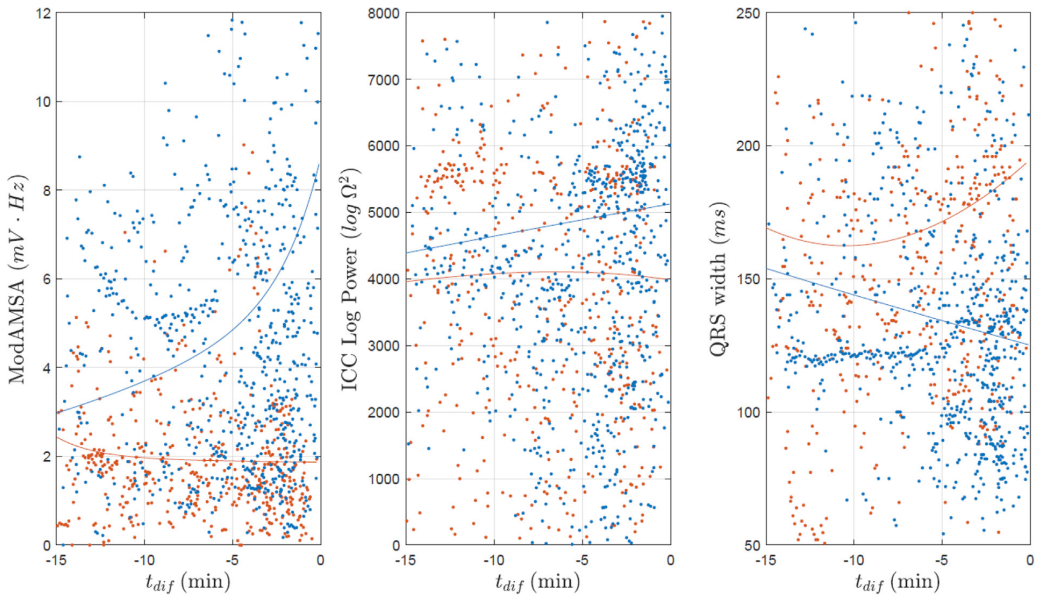

Fig. 3 – The evolution of the top three features (ModAMSA, *ICCLogPower*, and *QRSwidth*) is shown in the figure, representing the last 15 minutes before the ROSC/end-of-episode. Blue and red dots represent the feature values for faPEA and unPEA cases, respectively. The fitted exponential line is also shown for each group.

respective group. This can explain the reason behind the selection of those features. Adding new features does not include relevant information in the model, probably because they are correlated with features already present in the model, as seen for ARB_{ECG} (Pearson correlation coefficient of 0.78 with ModAMSA) and for QRS_{width} (Pearson correlation coefficient of 0.76 with QR_{width}). The correlation matrix can be found in Appendix C.

Another critical consideration lies in the database's heterogeneity. In this context, it is noteworthy that 83 entries originate from Norway, while 114 emanate from Pennsylvania. Beyond mere geographical disparities, distinctions exist in the types of defibrillator equipment utilized and the dates of data collection, potentially engendering divergent treatment modalities. To ascertain the consequential influence of these factors, Appendix D delineates the model's performance across each country. The analysis demonstrated a good performance of the model for both cases (AUC $\approx$ 80% and BAC $\approx$ 75%) and did not reveal a significant difference between them ($p > 0.05$ for both AUC and BAC). Nevertheless, to comprehensively validate the model's robustness, further experimentation incorporating additional countries and diverse defibrillator apparatuses is warranted.

When comparing the results with similar studies with OHCA,[9] the proposed algorithm performed 5.4-points below the AUC of the best OHCA models. We believe that in-hospital patients' condition might have contributed to this difference. as they are probably affected by other illness or injuries that jeopardize the design of PEA evolution models based exclusively in biosignals. Extra information as clinical/demographic data might contribute to build more complex and accurate predictive models.

Assessment of the patient's response to therapy is crucial in cardiac arrest resuscitation. Many contributions highlight the need of short-time prognosis tools that may assist clinicians in decision making.[10,19] With a favorable prognosis, it is reasonable to continue the ongoing efforts quite unaltered. However, with unfavorable prognosis, one may re-assess the situation from a broad perspective including CPR quality, and/or identification of reversible causes. Further research and prospective studies are needed to address the implications of integrating these tools into clinical practice.

Limitations of the study

The annotation of the QRS complexes to obtain the QRS-features included in the automated model was performed manually by medical experts reviewing the signals with an ad-hoc tool.

Although a completely automated method is desired, existing algorithms for QRS complex delineation were developed for stable patients and are not accurate for patients in cardiac arrest.[39,48–51] Further research is needed to overcome this limitation and develop QRS delineation algorithms robust enough in emergency scenarios.

Conclusions

A machine learning model was characterized to predict the evolution of PEA rhythms in cardiac arrest patient. The innovative LR model included features from the ECG and the TTI, with QRS-specific metrics that boosted the accuracy of the model. This new approach, evaluated with patients in IHCA, contributes to improve our knowledge on biosignal based predictive models in the field of resuscitation.

Ethical Considerations

The study is purely observational and involved no experimental intervention. Data were recorded by defibrillators used by the emergency teams responding to in-hospital emergencies and supplemented by clinical information after each event. Ethical approval was granted by the University of Pennsylvania IRB #7 for the US sites (Sept. 6th, 2017, PROTOCOL # 828086) and the regional committee for medical ethics in Central ("Midt") Norway (ref. 2019/785).

CRediT authorship contribution statement

Jon Urteaga: Writing – review & editing, Writing – original draft, Supervision, Software, Investigation, Data curation, Conceptualization. **Andoni Elola:** Writing – review & editing, Writing – original draft, Supervision, Software, Investigation, Data curation, Conceptualization. **Anders Norvik:** Writing – review & editing, Data curation, Conceptualization. **Eirik Unneland:** Writing – review & editing, Investigation, Conceptualization. **Trygve Christian Eftestøl:** Writing – review & editing, Investigation, Conceptualization. **Abhishek Bhardwaj:** Writing – review & editing, Investigation, Conceptualization. **David Buckler:** Writing – review & editing, Investigation, Conceptualization. **Benjamin S. Abella:** Writing – review & editing, Investigation, Data curation, Conceptualization. **Eirik Skogvoll:** Writing – review & editing, Investigation, Conceptualization. **Elisabete Aramendi:** Writing – review & editing, Supervision, Investigation, Data curation, Conceptualization.

Declaration of competing interest

The authors declare that they have no known competing financial interests or personal relationships that could have appeared to influence the work reported in this paper.

Acknowledgments

This research has been partially supported by the MCIN/AEI/10.13039/501100011033/ and by "ERDF A way of making Europe" through grant PID2021-122727OB-I00. Additional support has been provided by the Basque Government through grants IT1717-22 and PRE2021_2_0173, as well as by the University of the Basque Country (UPV/EHU) through COLAB20/01.

Appendix A. Supplementary data

Supplementary data to this article can be found online at https://doi.org/10.1016/j.resplu.2024.100598.

Author details

[a]*Communications Engineering Department, University of the Basque Country (UPV/EHU), Plaza Ingeniero Torres Quevedo 1, 48013 Bilbao, Spain*[b]*Department of Electronic Technology, University of the Basque Country (UPV/EHU), Plaza Ingeniero Torres Quevedo 1, 48013 Bilbao, Spain*[c]*Department of Circulation and Medical Imaging, Norwegian University of Science and Technology (NTNU), Prinsesse Kristinas gate 3, 7030 Trondheim, Norway*[d]*Department of Electrical*

Engineering and Computer Science, University of Stavanger (UiS), Kjell Arholms gate 41, 4021 Stavanger, Norway [e]*University of California, 900 University Ave, Riverside, CA 92521, United State* [f]*Icahn School of Medicine at Mount Sinai, 1 Gustave L. Levy Pl, New York, NY 10029, United States*[g]*University of Pennsylvania, Philadelphia, PA 19104, United State* [h]*Biocruces Bizkaia Health Research Institute, Cruces Plaza, 48903 Barakaldo, Spain*

REFERENCES

1. Ko DT, Qiu F, Koh M, et al. Factors associated with out-of-hospital cardiac arrest with pulseless electric activity: a population-based study. Am Heart J 2016;177:129–37.
2. Mader TJ, Nathanson BH, Millay S, Coute RA, Clapp M, McNally B. Out-of-hospital cardiac arrest outcomes stratified by rhythm analysis. Resuscitation 2012;83:1358–62.
3. Meaney PA, Nadkarni VM, Kern KB, Indik JH, Halperin HR, Berg RA. Rhythms and outcomes of adult in-hospital cardiac arrest. Crit Care Med 2010;38:101–8.
4. Girotra S, Nallamothu BK, Spertus JA, Li Y, Krumholz HM, Chan PS. Trends in survival after in-hospital cardiac arrest. N Engl J Med 2012;367:1912–20.
5. Cobb LA, Fahrenbruch CE, Olsufka M, Copass MK. Changing incidence of out-of-hospital ventricular fibrillation, 1980–2000. JAMA 2002;288:3008–13.
6. Herlitz J, Andersson E, Bang A, et al. Experiences from treatment of out-of-hospital cardiac arrest during 17 years in Goteborg. Eur Heart J 2000;21:1251–8.
7. Norvik A, Unneland E, Bergum D, et al. Pulseless electrical activity in in-hospital cardiac arrest–A crossroad for decisions. Resuscitation 2022;176:117–24.
8. Mehta C, Brady W. Pulseless electrical activity in cardiac arrest: electrocardiographic presentations and management considerations based on the electrocardiogram. Am J Emerg Med 2012;30:236–9.
9. Urteaga J, Aramendi E, Elola A, Irusta U, Idris A. A machine learning model for the prognosis of pulseless electrical activity during out-of-hospital cardiac arrest. Entropy 2021;23:847.
10. Norvik A, Skjeflo GW, Unneland E, et al. heart rate and QRS duration predict immediate outcome in pulseless electrical activity (PEA) during in-hospital cardiac arrest (IHCA). Circulation 2022;146: A250–A.
11. Rabjohns J, Quan T, Boniface K, Pourmand A. Pseudo-pulseless electrical activity in the emergency department, an evidence based approach. Am J Emerg Med 2020;38:371–5.
12. Van den Bempt S, Wauters L, Dewolf P. Pulseless electrical activity: detection of underlying causes in a prehospital setting. Med Princ Pract 2020.
13. Rabjohns J, Quan T, Boniface K, Pourmand A. Pseudo-pulseless electrical activity in the emergency department, an evidence based approach. Am J Emerg Med 2019.
14. Myerburg RJ, Halperin H, Egan DA, et al. Pulseless electric activity: definition, causes, mechanisms, management, and research priorities for the next decade: report from a National Heart, Lung, and Blood Institute workshop. Circulation 2013;128:2532–41.
15. Flato UAP, Paiva EF, Carballo MT, Buehler AM, Marco R, Timerman A. Echocardiography for prognostication during the resuscitation of intensive care unit patients with non-shockable rhythm cardiac arrest. Resuscitation 2015;92:1–6.
16. Prosen G, Krizmaric M, Zavrsnik J, Grmec S. Impact of modified treatment in echocardiographically confirmed pseudo-pulseless electrical activity in out-of-hospital cardiac arrest patients with constant end-tidal carbon dioxide pressure during compression pauses. J Int Med Res 2010;38:1458–67.
17. Chen JY, Huang CH, Chen WJ, et al. QRS duration predicts outcomes in cardiac arrest survivors undergoing therapeutic hypothermia. Am J Emerg Med 2021;50:707–12.
18. Skjeflo GW, Nordseth T, Loennechen JP, Bergum D, Skogvoll E. ECG changes during resuscitation of patients with initial pulseless electrical activity are associated with return of spontaneous circulation. Resuscitation 2018;127:31–6.
19. Norvik A, Kvaløy J, Skjeflo G, et al. Heart rate and QRS duration as biomarkers predict the immediate outcome from pulseless electrical activity. Resuscitation 2023;185 109739.
20. Alonso E, Eftestøl T, Aramendi E, Kramer-Johansen J, Skogvoll E, Nordseth T. Beyond ventricular fibrillation analysis: comprehensive waveform analysis for all cardiac rhythms occurring during resuscitation. Resuscitation 2014;85:1541–8.
21. Lasa H, Irusta U, Eftestol T, et al. Multimodal Biosignal Analysis Algorithm for the Classification of Cardiac Rhythms During Resuscitation. In 2020 Computing in Cardiology. IEEE, 2020, 1–4
22. Elola A, Aramendi E, Irusta U, Berve PO, Wik L. Multimodal algorithms for the classification of circulation states during out-of-hospital cardiac arrest. IEEE Trans Biomed Eng 2020;68:1913–22.
23. Bhat SK, Acosta D, Swartz CM. Postictal asystole during ECT. J ECT 2002;18:103–6.
24. Burd J, Kettl P. Incidence of asystole in electroconvulsive therapy in elderly patients. Am J Geriatr Psychiat 1998;6:203–11.
25. Brown DC, Lewis AJ, Criley JM. Asystole and its treatment: the possible role of the parasympathetic nervous324 system in cardiac arrest. J Am College Emerg Phys 1979;8:448–52.
26. Losert H, Risdal M, Sterz F, et al. Thoracic-impedance changes measured via defibrillator pads can monitor signs of circulation. Resuscitation 2007;73:221–8.
27. Chicote B, Irusta U, Aramendi E, et al. Evolution of AMSA for shock success prediction during the pre-shock pause. Resuscitation 2015;96:21–2.
28. Ristagno G, Mauri T, Cesana G, et al. Amplitude spectrum area to guide defibrillation: a validation on 1617 patients with ventricular fibrillation. Circulation 2015;131:478–87.
29. Reynolds JC, Salcido DD, Menegazzi JJ. Correlation between coronary perfusion pressure and quantitative ECG waveform measures during resuscitation of prolonged ventricular fibrillation. Resuscitation 2012;83:1497–502.
30. Chicote B, Irusta U, Aramendi E, et al. Nonlinear energy operators for defibrillation shock outcome prediction. In 2016 Computing in Cardiology Conference (CinC). IEEE, 2016, 61–64
31. El Bouny L, Khalil M, Abdellah AQRS, complex detection based on smoothed nonlinear energy operator. In,. 9th International symposium on signal, image, video and communications (ISIVC). IEEE 2018;2018:191–6.
32. Bos R, De Waele S, Broersen PM. Autoregressive spectral estimation by application of the Burg algorithm to irregularly sampled data. IEEE Trans Instrum Meas 2002;51:1289–94.
33. Rad AB, Eftestøl T, Engan K, et al. ECG-based classification of resuscitation cardiac rhythms for retrospective data analysis. IEEE Trans Biomed Eng 2017;64:2411–8.
34. Elola A, Aramendi E, Irusta U, Del Ser J, Alonso E, Daya M. ECG-based pulse detection during cardiac arrest using random forest classifier. Med Biol Eng Compu 2019;57:453–62.
35. Ruiz JM, de Gauna SR, Gonzalez-Otero DM, et al. Circulation assessment by automated external defibrillators during cardiopulmonary resuscitation. Resuscitation 2018;128:158–63.
36. Alonso E, Aramendi E, Daya M, et al. Circulation detection using the electrocardiogram and the thoracic impedance acquired by defibrillation pads. Resuscitation 2016;99:56–62.
37. Elola A, Aramendi E, Irusta U, et al. ECG characteristics of pulseless electrical activity associated with return of spontaneous circulation in out-of-hospital cardiac arrest. Resuscitation 2018;130:e54.
38. Elola A, Aramendi E, Irusta U, et al. Capnography: A support tool for the detection of return of spontaneous circulation in out-of-hospital cardiac arrest. Resuscitation 2019;142:153–61.

39. Bergum D, Skjeflo GW, Nordseth T, et al. ECG patterns in early pulseless electrical activity-associations with aetiology and survival of in-hospital cardiac arrest. Resuscitation 2016;104:34–9.
40. Kim JH, Ryoo HW, Jy K, et al. QRS complex characteristics and patient outcomes in out-of-hospital pulseless electrical activity cardiac arrest. Emerg Med J 2021;38:53–8.
41. Aufderheide TP, Thakur RK, Stueven HA, et al. Electrocardiographic characteristics in EMD. Resuscitation 1989;17:183–93.
42. Weiser C, Poppe M, Sterz F, et al. Initial electrical frequency predicts survival and neurological outcome in out of hospital cardiac arrest patients with pulseless electrical activity. Resuscitation 2018;125:34–8.
43. Jekova I, Krasteva V. Real time detection of ventricular fibrillation and tachycardia. Physiol Meas 2004;25:1167.
44. Ristagno G, Gullo A, Berlot G, Lucangelo U, Geheb F, Bisera J. Prediction of successful defibrillation in human victims of out-of-hospital cardiac arrest: a retrospective electrocardiographic analysis. Anaesth Intensive Care 2008;36:46–50.
45. Indik JH, Conover Z, McGovern M, et al. Association of amplitude spectral area of the ventricular fibrillation waveform with survival of out-of-hospital ventricular fibrillation cardiac arrest. J Am Coll Cardiol 2014;64:1362–9.
46. Raymond TT, Pandit SV, Griffis H, et al. Effect of amplitude spectral area on termination of fibrillation and outcomes in pediatric cardiac arrest. J Am Heart Assoc 2021;10:e020353.
47. Gentile FR, Wik L, Isasi I, et al. Amplitude spectral area of ventricular fibrillation and defibrillation success at low energy in out-of-hospital cardiac arrest. Intern Emerg Med 2023:1–9.
48. Martínez JP, Almeida R, Olmos S, Rocha AP, Laguna P. A wavelet-based ECG delineator: evaluation on standard databases. IEEE Trans Biomed Eng 2004;51:570–81.
49. Shaik BS, Naganjaneyulu G, Chandrasheker T, Narasimhadhan A. A method for QRS delineation based on STFT using adaptive threshold. Procedia Comput Sci 2015;54:646–53.
50. Teijeiro T, F´elix P, Presedo J. A noise robust QRS delineation method based on path simplification. In 2015 Computing in Cardiology Conference (CinC). IEEE, 2015, 209–212
51. Berkaya SK, Uysal AK, Gunal ES, Ergin S, Gunal S, Gulmezoglu MB. A survey on ECG analysis. Biomed Signal Process Control 2018;43:216–35.

Appendix A. Spectrum of the ECG signal for faPEA and unPEA segments

In Figure A.1 the ECG signal spectrum is depicted for faPEA and unPEA segments. It illustrates that the spectral characteristics of both rhythm types exhibit significant overlap in the 0 to 15 Hz range, but they become more distinguishable in the 20 to 30 Hz range.

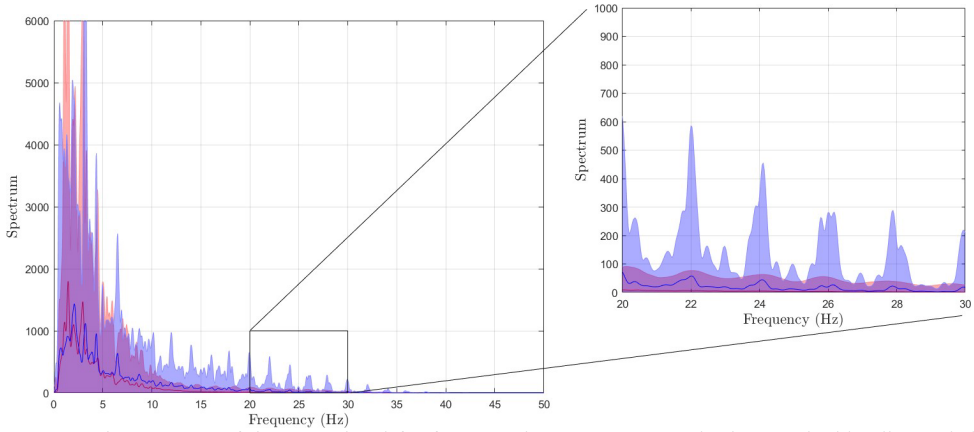

Figure A.1: The spectrum of the ECG signal for faPEA and unPEA segments is shown. The blue line and shaded blue area indicate the mean and standard deviation, respectively, of faPEA segments, while the red line represents the same for unPEA segments. On the left, the spectrum between 0 and 50 Hz is shown, while on the right, it is between 20 and 30 Hz, which is the range used in ModAMSA.

Appendix B. Feature extraction

This section describes the algorithms used to compute the fifteen features of this work: Five were extracted from the ECG signal, four from the IT signal, and six based on the QRS complexes.

The **amplitude spectrum area (AMSA)** represents the sum of the spectral amplitudes of the ECG signal, with each amplitude weighted by its corresponding frequency. To compute AMSA, the spectral amplitudes $A_i(f_i)$ at frequency f_i are needed, which were computed using a 4096-point Fast Fourier Transform (FFT) on the Tuckey windowed ECG segment, following the next equation: [1,2]

$$\mathrm{AMSA} = \sum_i A_i \cdot f_i, \quad 2 < f_i(Hz) < 48 \tag{B.1}$$

The **modified AMSA (ModAMSA)** represents the weighted sum of the spectral amplitudes of the ECG signal, similar to AMSA, but in this case, only within the frequency range of $20-30$Hz.

$$\mathrm{ModAMSA} = \sum_i A_i \cdot f_i, \ 20 < f_i(\mathrm{Hz}) < 30 \tag{B.2}$$

The **Smoothed Nonlinear Energy Operator (SNEO)** has been calculated for both the ECG signal ($\mathbf{SNEO_{ECG}}$) and the ICC signal ($\mathbf{SNEO_{ICC}}$). The SNEO of the signal $x(n)$ is the convolution between a Kaiser window and a non-linear Teager-Kaiser Energy Operator (TKEO):[3]

$$\psi_{S,L}[x(n)] = \psi_k[x(n)] \otimes w_L(n) \tag{B.3}$$

TKEO ($\psi_k[x(n)]$) is computed using the following equation:

$$\psi_k[x(n)] = x^2(n) - x[n-k]x[n+k] \tag{B.4}$$

where k is the lag parameter which is associated to the window length (L) by $L = 4k + 1$.

The **autoregressive Burg's values** (ARB) are the autoregressive parameters of order 4 estimated using Burg's method. [4,5] The signal $x(n)$ can be modelled as:

$$x(n) = -\sum_{k=1}^{4} a_k \, s(n-k) + v(n), \tag{B.5}$$

where $v(n)$ represents an independent identically distributed stochastic sequence with zero mean and variance σ^2, and the a_k coefficients are referred to autoregressive coefficients of the model. $\mathbf{ARB_{ECG}}$ and $\mathbf{ARB_{ICC}}$ are the a_4 coefficients of ECG and ICC signals, respectively.

The overall **cross-power** ($\mathbf{Cross_{Power}}$) was previously defined as: [6]

$$\text{Cross}_{\text{Power}} = min(P_{c1}, P_{c2}), \quad \text{(B.6)}$$

where $P_{c\,k}$ is the k-th half, $k = \{1, 2\}$, cross power of the 2.5 s segment, which is calculated as follows:

$$P_{ck} = \frac{1}{N/2}\sum_{n=1}^{N/2} |\, ecg_k[n]| \cdot |icc_k[n]|, \quad \text{(B.7)}$$

considering $ecg_k[n]$ and $icc_k[n]$ the ECG and the ICC samples of the k-th half, respectively.

The **logarithmic power** of the ICC signal (**LogPower**$_{\text{ICC}}$) refers to the energy of the ICC in the logarithmic scale. [7,8] It is computed as follows:

$$\text{LogPower}_{\text{ICC}} = \sum_{n=1}^{N} \log\ (icc[n]^2), \quad \text{(B.8)}$$

where N is the total sample number.

The **heart rate** (**HR**$_{\text{mean}}$) was computed as the mean value of the inverse of the periods, where the period is defined as the distance between successive R-wave peak instants (R_l vector of length L) within segment. HR_{mean} is calculated using the next equation:

$$\text{HR}_{\text{mean}} = \frac{60}{\frac{1}{L-1}\sum_{l=2}^{K} R_l - R_{l-1}} \quad \text{(B.9)}$$

The **heart rate variability** (**HR_{var}**), computed the variance associated to the R_l vector as follows:

$$\mathrm{HR_{var}} = \frac{60}{\frac{1}{L-1}\sum_{l=2}^{K}((R_l - R_{l-1}) - \mathrm{HR_{mean}})^2} \tag{B.10}$$

The **R-wave amplitudes** (**R_{amp}**) calculates the mean value of the ECG signal at the time instances R_l as follows:

$$\mathrm{R_{amp}} = \frac{1}{L}\sum_{l=1}^{L} ecg(R_l) \tag{B.11}$$

The **width QRS and QR complexes** (**QRS_{width}** and **QR_{width}**) are defined as the average of the QR and QS time intervals respectively (Q_l and S_l vectors of length L):

$$\mathrm{QRS_{width}} = \frac{1}{L}\sum_{l=1}^{L} Q_l - S_l \tag{B.12}$$

$$\mathrm{QR_{width}} = \frac{1}{L}\sum_{l=1}^{L} Q_l - R_l \tag{B.13}$$

To compute a modified **slopes of QRS and QR complexes** (**QRS_{slope}** and **QR_{slope}**), the first difference signal (Δecg) of the ECG was calculated as follows:

$$\Delta ecg[n] = \sum_{n=2}^{N} \mid ecg[n] - ecg[n-1] \mid \tag{B.14}$$

Then the slope of the l-th QRS and QR complex are defined as:

$$\mathrm{QRS_{slope}}[l] = \sum_{n} \Delta ecg[n], Q_l < n < S_l \tag{B.15}$$

$$\mathrm{QR_{slope}}[l] = \sum_{n} \Delta ecg[n], Q_l < n < R_l \tag{B.16}$$

Finally, the mean values of the slopes are computed:

$$\mathrm{QRS_{slope}} = \frac{1}{L}\sum_{l=1}^{L} \mathrm{QRS_{slope}}\,[l] \tag{B.17}$$

$$\mathrm{QR_{slope}} = \frac{1}{L}\sum_{l=1}^{L} \mathrm{QR_{slope}}\,[l] \tag{B.18}$$

Entropy was proposed by Chen et al.[9] as a method to determine vector matching in a smooth and gradual way, introducing concepts from fuzzy set theory. The signal samples within the analysis interval, denoted as $x(n)$, were divided into sets of vectors, each containing m samples. The total number of vectors created was $N - m + 1$, where N represents the total number of samples in the interval. In the resulting vector structure $x_i^m = \{x(i), x(i+1), \ldots, x(i+m-1)\}$, the baseline is subtracted as follows:

$$x_i^m = \{x(i), x(i+1), \dots, x(i+m-1)\} - \frac{1}{m}\sum_{l=0}^{m-1} x(i+l) \quad \text{(B.19)}$$

The maximum norm (L_∞-norm) was employed to measure the Chebyshev distance between two vectors, denoted as $\boldsymbol{x}_i^m$ and $\boldsymbol{x}_j^m$:

$$d_{ij} = \max_{k=0,\dots,m-1}(|x(i+k) - x(j+k)|) \quad \text{(B.20)}$$

Matches were computed using a set of functions that decay exponentially with increasing distance. These functions, denoted as $D_{ij}^m(n,r) = \exp\left(-\left({}^{d_{ij}}/_{r}\right)^n\right)$ were used in this study with a specific value of $n = 2$ and a Gaussian distance formula $D_{ij}^m(2,r) = \exp\left(-\left({}^{d_{ij}}/_{r}\right)^2\right)$, as proposed in a previous work. [10,11] The match counts were calculated based on these functions as follows:

$$C_i^m(r) = \frac{1}{N-m-1}\sum_{j=1, j\neq i}^{N-m} D_{ij}^m(2,r) \quad \text{(B.21)}$$

The probability that two vectors of length m will match within a tolerance of r is given by the expression:

$$\phi_m(r) = \frac{1}{N-m}\sum_{i=1}^{N-m} C_i^m(r) \quad \text{(B.22)}$$

The same procedure was repeated for the vector of $m + 1$ samples to obtain $\phi_{m+1}(r)$ and Entropy was computed as.

$$\text{Entropy}(m,r,N) = \ln\ \phi_m(r) - \ln\ \phi_{m+1}(r) \quad \text{(B.23)}$$

Appendix C. Correlation matrix

Figure C.1 provides a visual representation of the Pearson correlation coefficients that were calculated to examine the relationships between the different features utilized in this study.

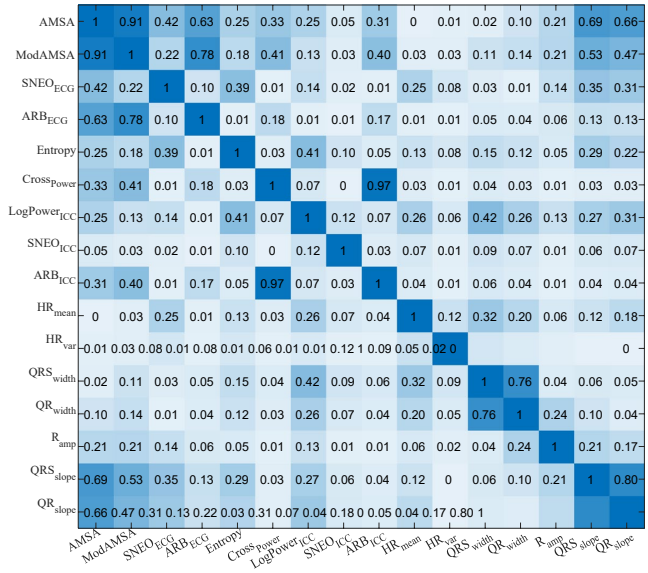

Figure C.1: Correlation matrix for the study features. Each cell indicates the Pearson correlation coefficient for each pair of features.

Appendix D. Model's performance across each country

Tables D.1 and D.2 display the model performance when separately tested on patients from Norway and the USA. Results are reported in terms of AUC, BAC, Se, and Sp.

	No. Features	AUC (%)	BAC (%)	Se (%)	Sp (%)
ModAMSA	1	78.4 (67.0-90.6)	74.7 (64.7-85.0)	68.8 (52.7-78.5)	83.7 (68.1-95.1)
ModAMSA + LogPowerICC	2	79.9 (68.9-91.1)	73.6 (64.8-83.4)	64.0 (50.1-78.7)	87.5 (67.3-97.1)
ModAMSA + LogPowerICC + QRSwidth	3	79.3 (71.1-90.7)	76.0 (67.0-86.2)	72.0 (60.4-85.0)	79.1 (62.9-94.4)
ModAMSA + LogPowerICC + QRSwidth + ARBECG	4	78.6 (71.2-90.2)	75.8 (67.8-83.7)	72.2 (61.1-85.8)	77.3 (62.3-95.0)
ModAMSA + LogPowerICC + QRSwidth + ARBECG + QRwidth	5	78.5 (73.5-87.9)	73.6 (64.3-86.5)	72.6 (60.1-83.4)	75.8 (58.5-95.0)
ModAMSA + LogPowerICC + QRSwidth + ARBECG + QRwidth + CrossPower	6	79.1 (73.3-86.8)	74.4 (64.6-84.3)	72.7 (59.5-83.4)	76.2 (58.5-94.4)

Table 4: he LR model's performance in terms of median (IQR) AUC, BAC, Se, and Sp for patients from Norway. All possible combinations using one to six features have been tested, only the best for each number of features is shown.

	No. Features	AUC (%)	BAC (%)	Se (%)	Sp (%)
ModAMSA	1	79.7 (71.8-90.2)	69.3 (61.6-79.5)	60.7 (51.6-71.7)	80.3 (66.1-93.6)
ModAMSA + LogPowerICC	2	79.4 (73.4-88.2)	68.9 (63.4-79.9)	65.7 (57.6-76.8)	79.6 (66.1-92.5)
ModAMSA + LogPowerICC + QRSwidth	3	81.2 (76.5-91.0)	75.3 (65.3-81.4)	82.5 (74.7-90.0)	66.4 (55.2-78.6)
ModAMSA + LogPowerICC + QRSwidth + ARBECG	4	80.9 (74.2-88.5)	75.4 (65.1-81.4)	84.2 (73.4-90.0)	68.2 (55.2-79.0)
ModAMSA + LogPowerICC + QRSwidth + ARBECG + QRwidth	5	80.7 (72.4-89.3)	73.2 (64.1-78.8)	83.3 (74.8-91.0)	63.1 (50.7-76.3)
ModAMSA + LogPowerICC + QRSwidth + ARBECG + QRwidth + CrossPower	6	80.5 (70.1-89.1)	71.0 (61.0-77.7)	80.7 (71.3-90.3)	65.5 (48.6-82.3)

Table 5: he LR model's performance in terms of median (IQR) AUC, BAC, Se, and Sp for patients from USA. All possible combinations using one to six features have been tested, only the best for each number of features is shown.

References

[1] Ristagno G, Li Y, Fumagalli F, Finzi A, Quan W. Amplitude spectrum area to guide resuscitation—A retrospective analysis during out-of-hospital cardiopulmonary resuscitation in 609 patients with ventricular fibrillation cardiac arrest. Resuscitation 2013;84(12):1697–1703.

[2] Elola A, Aramendi E, Irusta U, Del Ser J, Alonso E, Daya M. ECG-based pulse detection during cardiac arrest using random forest classifier. Medical & biological engineering & computing 2019;57(2):453–462.

[3] Chicote B, Irusta U, Aramendi E, et al. Nonlinear energy operators for defibrillation shock outcome prediction. In 2016 Computing in Cardiology Conference (CinC). IEEE, 2016, 61–64.

[4] Bos R, De Waele S, Broersen PM. Autoregressive spectral estimation by application of the Burg algorithm to irregularly sampled data. IEEE Transactions on Instrumentation and Measurement 2002;51(6):1289–1294.

[5] Rad AB, Eftestøl T, Engan K, et al. ECG-based classification of resuscitation cardiac rhythms for retrospective data analysis. IEEE Transactions on Biomedical Engineering 2017;64(10):2411–2418.

[6] Ruiz JM, de Gauna SR, Gonzalez-Otero DM, et al. Circulation assessment by automated external defibrillators during cardiopulmonary resuscitation. Resuscitation 2018;128:158–163.

[7] Urteaga J, Aramendi E, Elola A, Irusta U, Idris A. A Machine Learning Model for the Prognosis of Pulseless Electrical Activity during Out-of-Hospital Cardiac Arrest. Entropy 2021;23(7):847.

[8] Elola A, Aramendi E, Irusta U, Berve PO, Wik L. Multimodal algorithms for the classification of circulation states during out-of-hospital cardiac arrest. IEEE Transactions on Biomedical Engineering 2020;68(6):1913–1922.

[9] Chen W, Wang Z, Xie H, Yu W. Characterization of surface EMG signal based on fuzzy entropy. IEEE Transactions on neural systems and rehabilitation engineering 2007;15(2):266–272.

[10] Chen W, Zhuang J, Yu W, Wang Z. Measuring complexity using fuzzyen, apen, and sampen. Medical engineering & physics 2009;31(1):61–68.

[11] Chicote B, Irusta U, Aramendi E, et al. Fuzzy and sample entropies as predictors of patient survival using short ventricular fibrillation recordings during out of hospital cardiac arrest. Entropy 2018;20(8):591.

A.1.4 Second conference paper

	Publication in international conference
Reference	Jon Urteaga, Andoni Elola, Per Olav Berve, Lars Wik, Elisabete Aramendi, "A Random Forest Model for Pulseless Electrical Activity Prognosis Prediction During Out-of-Hospital Cardiac Arrest Using Invasive Blood Pressure", *EMBC (Annual International Conference of the IEEE Engineering in Medicine and Biology Society), 2024*
Quality indices	• **Type of publication**: International conference in SJR • **Impact factor**: 0.198 (2023)

A Random Forest Model for Pulseless Electrical Activity Prognosis Prediction During Out-of-Hospital Cardiac Arrest Using Invasive Blood Pressure

Jon Urteaga[1], Andoni Elola[2], Per O. Berve[3], Lars Wik[3] and Elisabete Aramendi[1,4]

***Abstract*— Out-of-hospital cardiac arrest (OHCA) is a major health concern, with an incidence of approximately 55 per 100,000 person-years in the United States. Pulseless electrical activity (PEA) is a cardiac rhythm observed in 20-30% of OHCA cases and it consists on a regular electrical activity presenting disassociation with cardiac mechanical contractions. Discriminating those PEA with favorable prognosis is crucial to decide pre/post resuscitation therapy. A machine learning model is proposed to assist rescuers to predict evolution of PEA. The ECG and the transthoracic impedance recorded using defibrillation pads were integrated in the model, together with the invasive blood pressure. A total of 238 PEA segments were extracted from 49 patients. A Random Forest model was trained with 25 features extracted from the three signals to discriminate between the PEA with favorable prognosis (return of spontaneous circulation). The optimal model showed median (interquartile range) values of 88.9(14.2)% for Area Under the Curve, 94.1(21.7)% for Sensitivity, 68.1(30.6)% for Specificity, 66.4(29.5)% for Positive Predictive Value, and 87.5(21.5)% for Negative Predictive Value.**

***Clinical relevance*— The study concludes that adding IBP based features to models traditionally based on ECG and TTI enhances PEA prognosis prediction during OHCA.**

I. INTRODUCTION

Out-of-hospital cardiac arrest (OHCA) persists as a notable public health concern, resulting in 270,000 annual fatalities in Europe and 420,000 in the United States [1], [2]. Providing effective cardiopulmonary resuscitation (CPR), which involves chest compressions, ventilation, and defibrillation for shockable heart rhythms, is crucial for improving the chances of survival in cases of OHCA [2].

Pulseless electrical activity (PEA), characterized by organized cardiac electrical activity without a discernible pulse, is a frequently observed rhythm during cardiac arrest (CA) [3]. It occurs in approximately 20-30% of OHCA cases and in up to 40-60% of cases within hospital settings [3], [4]. Recognizing the potential outcome of PEA assists healthcare professionals in making well-informed decisions about how to treat and manage patients [5], [6]. Depending to the prognosis of PEA, it may suffice to persist with chest compressions and ventilations, or a specific pharmacological intervention may be deemed necessary [3], [7], [8]. PEA cases with favorable prognosis (faPEA) are those where a return of spontaneous circulation (ROSC) is likely, conversely those with low likelihood are considered unfavorable (unPEA). Recent studies focus on the characterization and classification of PEA rhythms based on the ECG and/or the transthoracic impedance (TTI) recorded through the defibrillation pads, and even integrating additional information as capnography, several proposals have been published for manual and automated classification and prognosis prediction [9], [10], [11], [12].

Invasive arterial blood pressure (IBP) serves as a fundamental hemodynamic variable, holding promise for monitoring treatment and assessing responses during OHCA. The IBP waveform finds extensive application in clinical practice, providing insights into cardiac function. The latest resuscitation guidelines endorse the utilization of IBP in the management of OHCA patients [13], [14]. The established correlation between blood pressure and the survival of patients experiencing cardiac arrest (CA) reinforces the utility of IBP in guiding resuscitation therapy.

In this study, a model grounded in machine learning (ML) is proposed for binary classification of PEA with favorable/unfavorable prognosis. This model leverages features based on the available literature including ECG, TTI, and IBP. Fig. 1 depicts the flowchart of the proposed approach.

II. STUDY DATASET

The data for this study comes from a randomized clinical trial (NCT02479152) investigating the hemodynamics of cardiac arrest patients treated with both manual and mechanical chest compressions. Collected between 2015 and 2017 using the Lifepak 15 (Stryker Ltd.) monitor-defibrillator, the data was obtained by the doctor-manned vehicle associated with the Oslo Emergency Medical System's Air Ambulance Department. The ECG and TTI signals were recorded through the defibrillation pads, while the IBP signal was acquired

*The authors would like to extend our sincere gratitude to Fred W. Champan and Fredrick Arnwald of Stryker Ltd. for their invaluable support and contributions to this study.

*This work was partially supported by the MCIN/AEI/10.13039/501100011033/ and by FEDER Una manera de hacer Europa through grant PID2021-122727OB-I00. Additional support has been provided by the Basque Government through grants IT1717-22 and PRE2021_2_0173.

[1]Jon Urteaga and Elisabete Aramendi are with Department of Communications Engineering, University of the Basque Country, Ingeniero Torres Quevedo Plaza, 1, 48013, Bilbao, Spain (email: jon.urteaga@ehu.eus)

[2]Andoni Elola is with Department of Electronic Technology, University of the Basque Country, Otaola Hiribidea, 29, 20600, Eibar, Spain

[3]Per O. Berve and Lars Wik are with Norwegian National Advisory Unit on Prehospital Emergency Medicine (NAKOS), Oslo University Hospital, Kirkeveien 166, 0450, Oslo, Norway

[4]Elisabete Aramendi is with Biocruces Bizkaia Health Research Institute, Cruces University Hospital, Cruces Plaza, 48903, Barakaldo, Spain

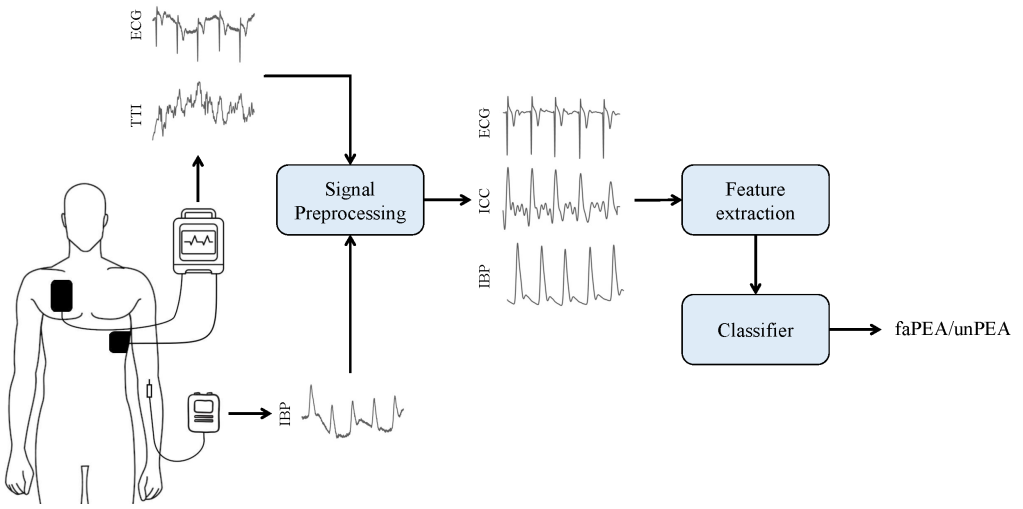

Fig. 1. Comprehensive diagram illustrating the PEA classification procedure, including stages such as measurement, preprocessing, feature extraction, and binary classification of PEA rhythms in both faPEA and unPEA.

through on-site radial/femoral cannulation, all signals with a sampling frequency of 250 Hz.

Segments of PEA lasting a minimum of 5 s, encompassing concurrent ECG, TTI, and IBP signals were extracted during chest compression pauses to avoid compression artifacts. PEA cases leading to significant periods of ROSC lasting a minimum of 5 min without CPR after the pulse was restored were categorized as faPEA; conversely, cases without ROSC were designated as unPEA.

A sum of 238 segments (with a total duration of 116 min) were extracted from 49 patients, with a median (Interquartile range - IQR) of 4 (4) segments per patient and a duration of 13.0 (24.7) s each. 172 segments, amounting to a total duration of 89.9 min, were classified as unPEA, whereas the remaining 66 segments, with a cumulative duration of 26.1 min, were categorized as faPEA. PEA segments were divided into 1026 (846 from unPEA) non-overlapping windows of 5 s for processing and classification. Fig. 2 shows two examples of 5 s segments along with their signals: to the left a unPEA segment and the right a faPEA segment.

III. METHODS

The method for PEA prognosis prediction employing ML models can be segmented into three stages: 1) Preprocessing of ECG, TTI and IBP signals, 2) Feature characterization of the signals, and 3) Formulation of feature-based ML models for the binary classification of the PEA rhythms in faPEA and unPEA. The third stage encompasses training/validation of the models, along with their subsequent statistical characterization.

A. Signal preprocessing

ECG signal was denoised using a stationary wavelet transform (SWT) technique. This included reconstructing the signal with detail components that are in the range of $0.5 - 31.25$ Hz to eliminate baseline noise, high-frequency noise, motion artifacts, and ventilation artifacts [15], [12].

The impedance circulation component (ICC), reflecting ventricular contractions in the TTI signal correlated with ECG heartbeats [16], was isolated from the TTI signal filtered within the $1 - 8$ Hz range [15], [12].

The raw IBP signal exhibited artifacts, high frequency noise and baseline wandering. Using the SWT with 8-level decomposition, noise reduction was achieved by applying soft thresholding in all levels. The threshold was computed from the second detail as follows:

$$\gamma = \sigma\sqrt{2 \cdot ln(N)} \tag{1}$$

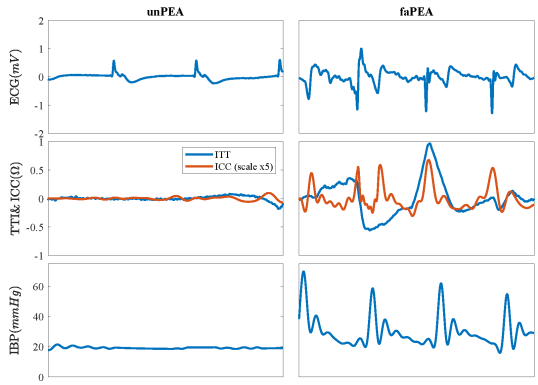

Fig. 2. ECG, TTI, ICC and IBP signals from 5-s windows for unPEA (left) and faPEA (right) segments.

N referring to the duration of the signal and σ computed as follows:

$$\sigma = \frac{\text{Median}\,\{|d_2|\}}{0.6745} \tag{2}$$

The denoised IBP signal was reconstructed using the sixth and seventh detail coefficients to remove undesired components.

B. Feature extraction

In total 25 features were computed for each window according to the following descriptions:

1) ECG features:

- The Amplitude Spectrum Area (AMSA) was calculated by summing the product of spectral amplitudes and frequencies in the 2-48 Hz band of the ECG signal [17].
- Smoothed Nonlinear Energy Operator of the ECG signal (SNEO_{ECG}) is obtained by convolving a Kaiser window ($w_L(n)$) with a non-linear Teager-Kaiser Energy Operator (TKEO) ($\psi_k[x(n)]$) [18]:

$$\psi_{S,L}[x(n)] = \psi_k[x(n)] \otimes w_L(n) \tag{3}$$

  The TKEO ($\psi_k[x(n)]$) is computed using the formula:

$$\psi_k[x(n)] = x^2(n) - x[n-k]x[n+k] \tag{4}$$

  Where, $x(n)$ represents the ECG signal and k the lag parameter, which is linked to the window length (L) through the equation $L = 4k + 1$.
- The autoregressive Burg's values are obtained through Burg's method to describe the autoregressive nature of a signal [19]. Represented as a_k, these values model the signal $x(n)$ by considering its past values and a random component:

$$x(n) = -\sum_{k=1}^{4} a_k s(n-k) + v(n)$$

  Here, $v(n)$ is a random sequence, and the a_k coefficients indicate the autoregressive properties of the model. ARB_{ECG} refers to the error made when estimating spectral power using a 4th order autoregressive Burg model.
- Entropy serves as a measure of complexity, assessing the regularity of the ECG pattern [20].
- $\text{High}_{\text{power}}$ measured the power of the ECG in the bandwidth of $17.5 - 40$ Hz [20].
- IQR values were computed for the denoised ECG and its SWT detail coefficients $\text{d}_{5,\text{ECG}} - \text{d}_{7,\text{ECG}}$.

2) TTI features:

- SNEO_{TTI} is the Smoothed Nonlinear Energy Operator of the TTI signal, calculated as previously explained.
- ARB_{TTI} is the fourth-order autoregressive Burg's coefficient, calculated as previously explained, but for the TTI signal.
- IQR values were computed for the denoised TTI and its SWT detail coefficients $\text{d}_{5,\text{TTI}} - \text{d}_{7,\text{TTI}}$.
- $\text{Log}_{\text{Power}}$ represents the logarithmic energy of the TTI, which is correlated with ventricular wall movement [21].
- $\text{ECGvsTTI}_{\text{CrossPower}}$ denotes the cross power between the denoised ECG and TTI signals [22].

3) IBP features: To compute the features from IBP signal, the instants of systolic peak and diastolic onsets were computed using an automated algorithm [23].

- Systolic arterial pressure (SAP) is the maximum pressure value achieved during the cardiac contraction phase [24].
- Diastolic arterial pressure (DAP) is the minimum pressure measured during the cardiac relaxation phase [24].
- Pulse pressure (PP) is the difference between SAP and DAP [24].
- The Mean Arterial Pressure (MAP) is defined as the average arterial pressure throughout one cardiac cycle and it is calculated with the following formula [25]:

$$\text{MAP} = \text{DAP} + \frac{1}{3}\text{PP} \tag{5}$$

- The Heart Rate (HR) is computed as the inverse of the interval between heartbeats in the IBP signal.
- $\text{IBP}_{\text{Power}}$ represents the energy of the IBP signal.
- $\text{ECGvsIBP}_{\text{CrossPower}}$ denotes the cross power between the ECG and IBP signals.
- $\text{TTIvsIBP}_{\text{CrossPower}}$ denotes the cross power between the TTI and IBP signals.

C. Building the classifier

A Random Forest (RF) classifier was employed for feature selection and binary classification of 5 s windows into faPEA and unPEA. RF, known for robustness with unbalanced datasets, comprises 500 trees, each trained with a bootstrap replica of the dataset. Trees grow via recursive binary splitting with random feature selection. The final decision results from a majority vote. Parameters include a 10 % bootstrap replica and a minimum of 5 observations per terminal node [15].

D. Evaluation

The performance of the RF was analyzed by training with three different sets of features: 1) ECG and TTI features, 2) IBP features, and 3) features from all signals.

Classifiers underwent 10-fold cross-validation with patient-wise, stratified partitions to avoid data leakage and maintain class imbalance consistency. This process was repeated 10 times with different random partitions. Evaluation metrics included Sensitivity (Se), Specificity (Sp), Positive Predictive Value (PPV), Negative Predictive Value (NPV), Balanced Accuracy (BAC) and Area under the curve (AUC).

The importance of features is calculated by the RF classifier based on permuted error. In 10-fold cross-validation, features were iteratively removed (one at a time) based on their importance, and RF models were retrained to re-rank the remaining features for the given N_f. Selection probability for each feature was the percentage of times it was chosen.

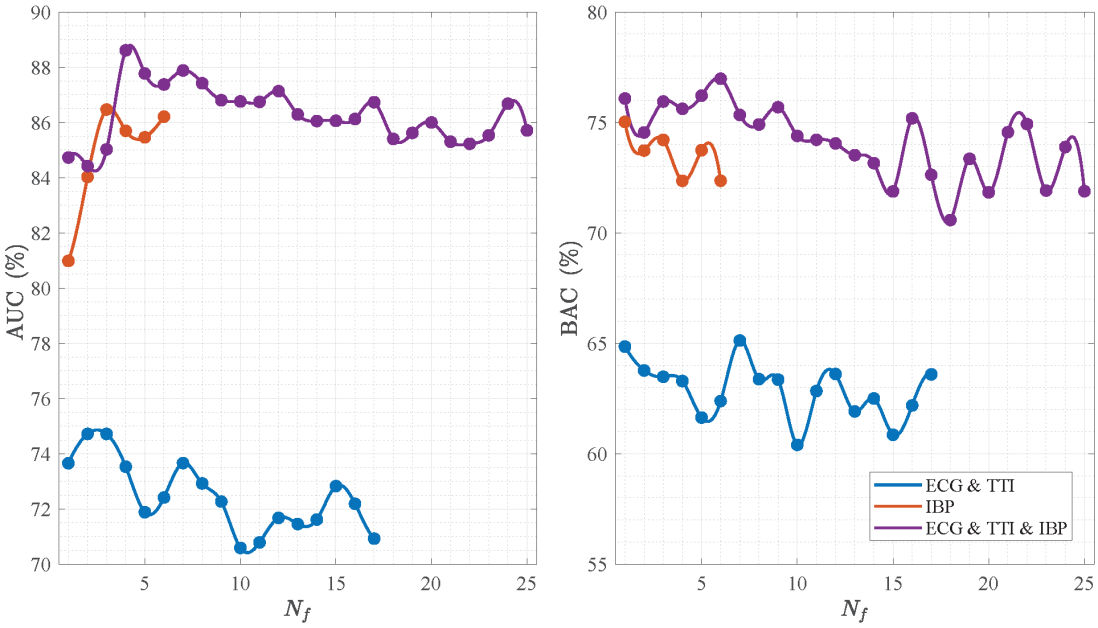

Fig. 3. Performance of the RF models in terms of the AUC (left) and BAC (right) as function of N_f the number of features included in each model using features from the ECG/TTI, the IBP and the ECG/TTI/IBP signals.

IV. RESULTS

Fig. 3 shows the performance of the RF binary classifier. The AUC (left) and BAC (right) are given as function of N_f, the number of features included in each model. Three models were tested using features from 1) ECG/TTI, 2) the IBP and 3) ECG/TTI/IBP signals. Is is noticeable that the inclusion of the IBP improves the models using exclusively the ECG and TTI. The maximum AUC was provided by a 4-feature model, and the maximum BAC by a 6-feature model.

The comprehensive performance of the method is presented in Tab. I, encompassing AUC, BAC, Se, Sp, PPV, and NPV. Various models with different sets of features were evaluated. Using ECG and TTI features; using IBP features, using features of all three signals; and two reduced models, one with the top 4 features (identified as the features most frequently selected by the RF model) and another with the top 6 features. In accordance with the results shown in Fig. 3, it is observed that utilizing all features of the IBP signal yields results with an AUC 20 points higher than when using ECG & TTI. Combining all three signals further enhances the discrimination capability by three points compared to using only the IBP signal. It also outperforms similar state-of-the-art studies that only utilize features computed from ECG and TTI [15], [26]. The models with reduced feature sets showed better performance, between 1.5 and 2 points of AUC, than using all the features.

Fig. 4 shows the proportion of times each feature was included in the N_f-feature model. It can be observed that features with the highest selection probabilities are those utilizing the IBP signal: $\mathrm{TTIvsIBP_{CrossPower}}$, IBPPower, $\mathrm{ECGvsIBP_{CrossPower}}$ and PP. However, it should be noted that $\mathrm{TTIvsIBP_{CrossPower}}$ and $\mathrm{ECGvsIBP_{CrossPower}}$ use the IBP signal in conjunction with the TTI and ECG signals, re-

TABLE I

THE TABLE PRESENTS THE PERFORMANCE OF THE METHODS WITH DIFFERENT SETS OF FEATURES. IT DISPLAYS THE MEDIAN (IQR) VALUES FOR AUC, SE, SP, PPV, AND NPV.

	Feat #	AUC	BAC	SE	SP	PPV	NPV
ECG & TTI	17	62.24 (17.34)	69.77 (22.89)	61.07 (47.89)	65.32 (27.40)	49.44 (34.19)	73.23 (35.05)
IBP	6	83.48 (19.75)	73.19 (17.27)	67.14 (38.18)	80.71 (29.65)	69.65 (29.85)	84.38 (23.14)
ECG & TTI & IBP	25	86.72 (19.38)	74.66 (14.57)	78.87 (33.33)	69.84 (25.50)	63.48 (30.66)	87.35 (22.73)
Reduced #1	4	88.88 (14.23)	76.07 (14.35)	94.11 (21.67)	68.13 (30.62)	66.40 (29.47)	95.01 (19.39)
Reduced #2	6	88.24 (18.00)	77.96 (17.54)	84.94 (22.82)	73.44 (28.70)	66.49 (27.14)	87.53 (21.55)

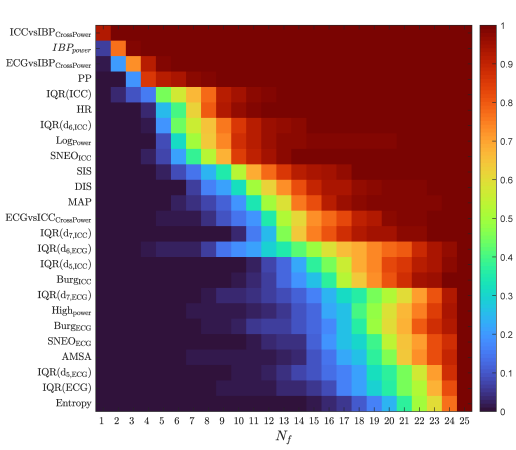

Fig. 4. The frequency of selection for the 25 features, as a function of N_f, the number of features included in the RF classifier.

spectively. These findings are consistent with those presented in Tab. I, where it is demonstrated that by combining various signals, superior results are achieved.

V. CONCLUSIONS

In this study, a ML-based method was introduced for the prediction of PEA prognosis, incorporating the IBP signal. The proposal was compared with previously proposed models based on the ECG and TTI signals. It was demonstrated that features extracted from the IBP are the most discriminative and that they boost the classifier performance of models based on the ECG & TTI. This study emphasizes the value of using IBP monitoring to address PEA OHCA. This underscores the importance of considering IBP alongside other monitoring modalities for a comprehensive approach to managing OHCA and improving patient outcomes.

REFERENCES

[1] Rea, Thomas D., et al. "Incidence of out-of-hospital cardiac arrest." The American journal of cardiology 93.12 (2004): 1455-1460.

[2] Hasselqvist-Ax, Ingela, et al. "Early cardiopulmonary resuscitation in out-of-hospital cardiac arrest." New England Journal of Medicine 372.24 (2015): 2307-2315.

[3] Myerburg, Robert J., et al. "Pulseless electric activity: definition, causes, mechanisms, management, and research priorities for the next decade: report from a National Heart, Lung, and Blood Institute workshop." Circulation 128.23 (2013): 2532-2541.

[4] Meaney, Peter A., et al. "Rhythms and outcomes of adult in-hospital cardiac arrest." Critical care medicine 38.1 (2010): 101-108.

[5] Norvik, Anders, et al. "Heart Rate And QRS Duration Predict Immediate Outcome In Pulseless Electrical Activity (PEA) During In-hospital Cardiac Arrest (IHCA)." Circulation 146.Suppl_1 (2022): A250-A250.

[6] Rabjohns, Jennifer, et al. "Pseudo-pulseless electrical activity in the emergency department, an evidence based approach." The American journal of emergency medicine 38.2 (2020): 371-375.

[7] Rabjohns, J., Quan, T., Boniface, K., & Pourmand, A. (2020). Pseudo-pulseless electrical activity in the emergency department, an evidence based approach. The American journal of emergency medicine, 38(2), 371-375.

[8] Prosen, G., Križmarić, M., Završnik, J., & Grmec, Š. (2010). Impact of modified treatment in echocardiographically confirmed pseudo-pulseless electrical activity in out-of-hospital cardiac arrest patients with constant end-tidal carbon dioxide pressure during compression pauses. Journal of International Medical Research, 38(4), 1458-1467.

[9] Skjeflo, G. W., Nordseth, T., Loennechen, J. P., Bergum, D., & Skogvoll, E. (2018). ECG changes during resuscitation of patients with initial pulseless electrical activity are associated with return of spontaneous circulation. Resuscitation, 127, 31-36.

[10] Bergum, Daniel, et al. "ECG patterns in early pulseless electrical activity-Associations with aetiology and survival of in-hospital cardiac arrest." Resuscitation 104 (2016): 34-39.

[11] Norvik, A., et al. "Heart rate and QRS duration as biomarkers predict the immediate outcome from pulseless electrical activity." Resuscitation 185 (2023): 109739.

[12] Elola, Andoni, et al. "Multimodal algorithms for the classification of circulation states during out-of-hospital cardiac arrest." IEEE Transactions on Biomedical Engineering 68.6 (2020): 1913-1922.

[13] Berg, R. A., Sutton, R. M., Reeder, R. W., Berger, J. T., Newth, C. J., Carcillo, J. A., ... & CPCCRN PICqCPR Investigators. (2018). Association between diastolic blood pressure during pediatric in-hospital cardiopulmonary resuscitation and survival. Circulation, 137(17), 1784-1795.

[14] Bhate, T. D., McDonald, B., Sekhon, M. S., & Griesdale, D. E. (2015). Association between blood pressure and outcomes in patients after cardiac arrest: a systematic review. Resuscitation, 97, 1-6.

[15] Urteaga, Jon, et al. "A machine learning model for the prognosis of pulseless electrical activity during out-of-hospital cardiac arrest." Entropy 23.7 (2021): 847.

[16] Losert, Heidrun, et al. "Thoracic-impedance changes measured via defibrillator pads can monitor signs of circulation." Resuscitation 73.2 (2007): 221-228.

[17] Chicote, Beatriz, et al. "Evolution of AMSA for shock success prediction during the pre-shock pause." Resuscitation 96 (2015): 21-22.

[18] Chicote, Beatriz, et al. "Nonlinear energy operators for defibrillation shock outcome prediction." 2016 Computing in Cardiology Conference (CinC). IEEE, 2016.

[19] Bos, Robert, Stijn De Waele, and Piet MT Broersen. "Autoregressive spectral estimation by application of the Burg algorithm to irregularly sampled data." IEEE Transactions on Instrumentation and Measurement 51.6 (2002): 1289-1294.

[20] Elola, Andoni, et al. "ECG-based pulse detection during cardiac arrest using random forest classifier." Medical & biological engineering & computing 57 (2019): 453-462.

[21] Alonso, Erik, et al. "Circulation detection using the electrocardiogram and the thoracic impedance acquired by defibrillation pads." Resuscitation 99 (2016): 56-62.

[22] Ruiz, Jesus M., et al. "Circulation assessment by automated external defibrillators during cardiopulmonary resuscitation." Resuscitation 128 (2018): 158-163.

[23] Urteaga, Jon, et al. "Invasive arterial blood pressure delineator for cardiopulmonary resuscitation patients during pauses of chest compressions." Biomedical Signal Processing and Control. Vol. 94. pages 106349 Elsevier, 2024.

[24] Barral, Jean-Pierre, and Alain Croibier. Visceral Vascular Manipulations E-Book. Elsevier Health Sciences, 2011.

[25] DeMers, Daniel, and Daliah Wachs. "Physiology, mean arterial pressure." (2019).

[26] Urteaga, Jon, et al. "The Prediction Of Pulseless Electrical Activity Evolution During In-hospital Cardiac Arrest Using Machine Learning." 2022 American Heart Association Resuscitation Science Symposium. Circulation Vol. 146. Suppl_1.

A.2 Publications associated to objective 2

A.2.1 First conference paper

	Publication in international conference
Reference	Jon Urteaga, Andoni Elola, Elisabete Aramendi, Per Olav Berve, Lars Wik, "Automated detection of pulse using continuous invasive arterial blood pressure in patients during cardiopulmonary resuscitation", *Computing in Cardiology Conference (CinC), 2021*
Quality indices	• **Type of publication**: International conference in SJR • **Impact factor**: 0.257

Automated Detection of Pulse Using Continuous Invasive Arterial Blood Pressure in Patients During Cardiopulmonary Resuscitation

Jon Urteaga[1], Andoni Elola[1], Elisabete Aramendi[1,2], Unai Irusta[1,2], Per Olav Berve[3], Lars Wik[3]

[1] Department of Communications Engineering, University of the Basque Country, Bilbao, Spain.
[2] Biocruces Bizkaia Health Research Institute, Cruces University Hospital, Barakaldo, Spain
[3] Norwegian National Advisory Unit on Prehospital Emergency Medicine (NAKOS), Oslo University Hospital, Oslo, Norwey

Abstract

Continuous invasive arterial blood pressure (ABP) and its characteristic waveform features are widely used to monitor cardiovascular health. The invasive ABP signal has been proven useful to guide therapy during cardiopulmonary resuscitation (CPR) of patients in cardiac arrest. Automated algorithms to compute ABP parameters were not designed to work during CPR, so their performance in this scenario is unknown. The aim of this study was to develop automated algorithms to detect pulse and measure physiological ABP variables during CPR. A dataset of 122 segments of invasive ABP were extracted during chest compression pauses from 26 patients with regular ECG during and a total duration of 262 min*. The ABP was denoised using a stationary wavelet decomposition and pulse peaks were detected in the first difference of the ABP by applying adaptive thresholding. The following parameters were computed: systolic blood pressure (SBP), diastolic blood pressure (DBP), pulse pressure (PP) and heart rate (HR). The algorithm presented a median (IQR) Se/PPV/F1 of* $97.6(17.5)/99.3(10.0)/97.2(10.1)\%$ *for diastolic peak detection, 4-points above the F1 obtained with Physionet's wabp algorithm. The absolute and relative errors were* $0.62(1.40)mmHg$ *and* $1.22(1.62)\%$*,* $0.74(1.43)mmHg$ *and* $1.81(2.76)\%$*,* $1.13(1.67)mmHg$ *and* $4.68(4.86)\%$*,* $0.50(1.42)min^{-1}$ *and* $0.58(1.31)\%$ *for SBP, DBP, PP and HR, respectively.*

1. Introduction

Arterial blood pressure (ABP) monitoring is widely used in modern medicine to prevent, detect and evaluate cardiovascular diseases [1–3]. The ABP signal waveform contains valuable information about the cardiovascular system, including heart rate, blood pressure values and pulse waveform [4, 5].

The invasive ABP signal is also used to monitor cardiovascular health during post cardiac arrest care and in intensive care units, and it is recommended to monitor hemodynamically unstable patients [3, 6, 7]. To improve survival rates, the American Heart Association and the Australian Resuscitation guidelines recommended that during post resuscitation care systolic blood pressure (SBP) to be mantained above 90 mmHg and 100 mmHg, respectively [8–10]. Furthermore, invasive ABP has been proven to be useful to guide therapy during cardiopulmonary resuscitation (CPR) [11–14].

Several automatic algorithms have been proposed to denoise and characterize the ABP signal [4, 5, 15], which is usually corrupted by artifacts such as clotting, movement artifacts and high frequency noise [1, 16]. Filters are applied to remove noise and artefact before calculating physiological ABP variables, such as systolic blood pressure (SBP), diastolic blood pressure (DBP), pulse pressure (PP), heart rate (HR) and the dicrotic notch [4, 5, 15].

Known automated algorithms were designed for hemodynamically stable patients, but they have not been tested during CPR. The aim of this study was to develop automated algorithms to detect pulse and measure physiological ABP variables in patients during chest compression pauses in CPR therapy.

2. Materials

The dataset used in this study was recorded by the physician manned rapid response car of the Oslo Emergency Medical System in patients during out-of-hospital cardiac arrest. All episodes were recorded using LifePak 15 defibrillators, and include the ECG and the invasive ABP (radial cannulation) signals, both with a sampling frequency of 250 Hz.

A total of 122 segments with concurrent recordings of ECG and ABP were extracted from 26 patients during chest compression pauses, periods without chest compressions artifacts. The top pannel of Figure 1 shows 5 s of

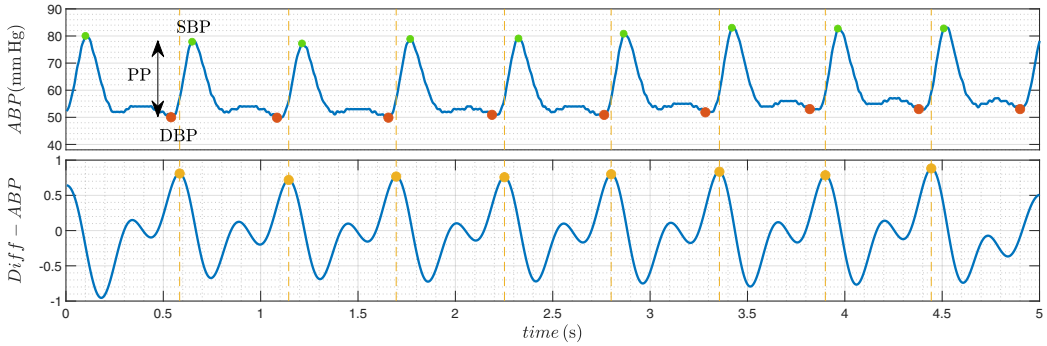

Figure 1. The top panel represents a 5 s segment of the ABP waveform. SBP and DBP, are indicated by green and red dots, respectively. The bottom panel shows the first difference of the ABP signal where yellow dots and dash lines show the peak value and instant of the first difference, respectively.

the ABP waveform, where the main variables, SBP, DBP and PP are annotated. The total duration of the dataset was 262 min, with a mean duration of 2.15 $\pm$ 5 min per segment. The systolic and diastolic peaks of each heartbeat were manually annotated to be used as gold standard.

3. Methods

Figure 2 shows the overall scheme followed in this study to detect peaks in the ABP signal and measure the ABP variables. First, the ABP signal was preprocessed to remove undesired components. Then, an adaptive peak detector was applied to the first difference of the ABP waveform to determine systolic and diastolic peaks. Finally, the physiological variables were computed from the original ABP signal.

3.1. Signal preprocessing

The ABP signal was preprocessed using the stationary wavelet transform (SWT) to remove baseline wandering and high frequency noise. An 8-level SWT decomposition was used with a Daubechies-4 mother wavelet and soft thresholding. Detail coefficients d_6 and d_7 were used to reconstruct the denoised ABP signal, $\mathrm{ABP}_{\mathrm{filt}}$, corresponding to the $1 - 4$ Hz frequency band.

3.2. Pulse peak detection

The systolic peak, corresponding to the maximum pressure value of the heartbeat, and the diastolic peak, corresponding to the inflection just before heartbeat compression phase, were computed for each heartbeat. Heartbeats were detected using the first difference of the ABP signal. Peaks with first difference above a threshold for i-th pulse were considered, and the threshold was adapted according to the following equation:

$$Th_i = \mathrm{median}(P_{i-1} : P_{i-5})/2 \qquad (1)$$

where the median amplitude of the previous 5 peaks were considered. A minimum distance of 300 ms was set between consecutive peaks.

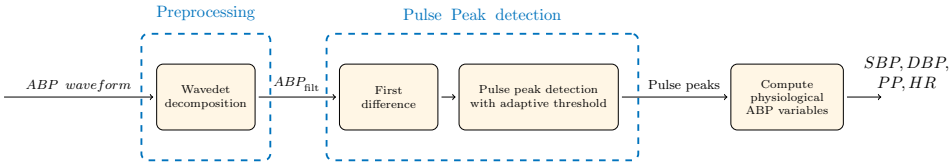

Figure 2. Overall scheme of the automated method applied to the ABP waveform to compute the pulse peaks and the ABP features.

The local maxima of the first difference in each heartbeat correspond to the maximum upslope of the ABP pulse, as shown in Figure 1. The systolic and diastolic peaks were computed by identifying the posterior and previous inflexion points to the instance of the maximum upslope in ABP signal, respectively. At the top panel of Figure 1 the instant of the maximum upslope is shown as a yellow dash line, and the systolic and diastolic peaks by red and green dots, respectively.

3.3. Computation of the physiological ABP variables

Variables used to monitor cardiovascular health were computed from the raw ABP signal using the systolic and diastolic peaks. SBP and DBP were used to compute the PP, their difference. The HR was computed as the inverse of the median distance between consecutive diastolic peaks.

3.4. Statistical evaluation

The ABP heartbeat detector proposed in this study was compared to the wabp algorithm from Physionet, a well known method proposed by Zong et al. [4].

Manually annotated diastolic peaks were considered as ground truth to evaluate the methods. A detected peak was considered a positive heartbeat detection if it fell within $300\,\mathrm{ms}$ of the ground truth. Methods were evaluated in terms of sensitivity (Se): percentage of correctly detected peaks; positive predictive value (PPV): percentage of detected peaks that are actual peaks; and F-score (F1): the harmonic mean of Se and PPV. The performance metrics were computed per patient and the final results were presented as the median (interquartile range, IQR) of all patients.

The absolute error of the physiological ABP variables were computed patient wise so all patients contributed equally.

4. Results

Table 1 shows the Se, PPV and F1 of the proposed heartbeat detector, and results are compared those of the wabp algorithm. It can be observed that the new algorithm outperformed the wabp algorithm in 27-points of Se, 1-point of PPV and 5-points of F1.

In Table 2 the absolute and percentage errors are reported for the SBP, DBP, PP and HR derived from the systolic and diastolic peak detections. It can be observed that absolute errors were below or close to $1\,\%$ for the pressure values, and bellow $5\,\%$ in percentage errors.

Figure 3 shows three examples of ABP segments of the dataset. In the first example the proposed diastolic peak detector and the wabp algorithm correctly identified every diastolic peak. The second and third examples show cases where the wabp algorithm missed several peaks, which were correctly detected by the proposed algorithm.

Table 1. Performance of the method introduced in this study compared to the wabp algorithm for heartbeat detection (using the diastolic peak). The table shows the median (IQR) values for Se, PPV and F1.

	Se (%)	PPV (%)	F1 (%)
This study	97.6 (17.5)	99.3 (10.0)	97.2 (10.1)
Zong et al. [4]	70.2 (85.0)	98.3 (100.0)	92.9 (61.1)

Table 2. Performance of the method to compute physiological ABP variables. The table shows the median (IQR) absolute and percentage errors for SBP, DBP, PP and HR.

	Absolute error	Percentage error
SBP	0.62 (1.40) mmHg	1.22 (1.62) %
DBP	0.74 (1.43) mmHg	1.81 (2.76) %
PP	1.13 (1.67) mmHg	4.68 (4.86) %
HR	0.50 (1.42) min^{-1}	0.58 (1.31) %

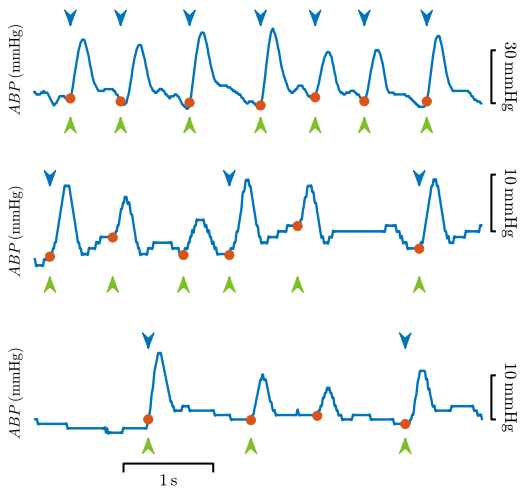

Figure 3. Three examples of the performance of the diastolic peak detection algorithm. The gold standard annotations are shown as red dots, and the annotations of the algorithms in green (this study) and blue (wabp algorithm).

5. Discussion and conclusions

The invasive ABP signal is widely used to monitor cardiovascular health in patients with different diseases. However, current methods to automatically monitor the ABP signal were designed to be used with hemodynamically stable patients. This is, to the best of our knowledge, the first automatic method that detects diastolic and systolic time-stamp during CPR, which could be used thereafter to accurately compute the characteristic ABP variables.

Current ABP algorithms are inaccurate durig CPR due to the irregular waveform and the noise/artifact components of the ABP signal. The wabp algorithm showed low sensitivity compared to the algorithm proposed in this study ($70\,\%$ vs $97\,\%$). During CPR the pulse pressure showed high amplitude variability in short intervals, intrapatient SD of $3.3\,\mathrm{mmHg}$ and interpatient SD of $20.6\,\mathrm{mmHg}$ in this dataset, and the proposed algorithm based on adaptive thresholding outperformed the classical method. Filtering the signal using the SWT was also more efficient than using constant coefficient filters, and improved the accuracy of the heartbeat detector. Consequently the overall F1 score was more than four points above, and the physiological variables were computed with errors below or close to $1\,\%$.

Acknowledgments

This work was supported by the Spanish Ministerio de Ciencia, Innovacion y Universidades through grant RTI2018-101475-BI00, jointly with the Fondo Europeo de Desarrollo Regional (FEDER), by the Basque Government through grant IT1229-19 and grant PRE2020_1_0177, and by the university of the Basque Country (UPV/EHU) under grant COLAB20/01.

References

[1] Marino PL. The ICU book. Lippincott Williams & Wilkins, 2007.

[2] Williams JS, Brown SM, Conlin PR. Blood-pressure measurement. N Engl J Med 2009;360(5):e6.

[3] Muntner P, Shimbo D, Carey RM, Charleston JB, Gaillard T, Misra S, Myers MG, Ogedegbe G, Schwartz JE, Townsend RR, et al. Measurement of blood pressure in humans: a scientific statement from the American Heart Association. Hypertension 2019;73(5):e35–e66.

[4] Zong W, Heldt T, Moody G, Mark R. An open-source algorithm to detect onset of arterial blood pressure pulses. In Computers in Cardiology, 2003. IEEE, 2003; 259–262.

[5] Li BN, Dong MC, Vai MI. On an automatic delineator for arterial blood pressure waveforms. Biomedical Signal Processing and Control 2010;5(1):76–81.

[6] Avolio AP, Butlin M, Walsh A. Arterial blood pressure measurement and pulse wave analysis—their role in enhancing cardiovascular assessment. Physiological Measurement 2009;31(1):R1.

[7] Li-wei HL, Saeed M, Talmor D, Mark R, Malhotra A. Methods of blood pressure measurement in the icu. Critical Care Medicine 2013;41(1):34.

[8] Bray JE, Bernard S, Cantwell K, Stephenson M, Smith K, Committee VS, et al. The association between systolic blood pressure on arrival at hospital and outcome in adults surviving from out-of-hospital cardiac arrests of presumed cardiac aetiology. Resuscitation 2014;85(4):509–515.

[9] Peberdy MA, Callaway CW, Neumar RW, Geocadin RG, Zimmerman JL, Donnino M, Gabrielli A, Silvers SM, Zaritsky AL, Merchant R, et al. Part 9: post–cardiac arrest care: 2010 american heart association guidelines for cardiopulmonary resuscitation and emergency cardiovascular care. Circulation 2010;122(18_suppl_3):S768–S786.

[10] Australian Resuscitation Council NZRC. Post-resuscitation therapy in adult advanced life support. arc and nzrc guideline 2010. Emergency Medicine Australia 2011;23(3):292–296.

[11] Martin GB, Carden DL, Nowak RM, Lewinter JR, Johnston W, Tomlanovich MC. Aortic and right atrial pressures during standard and simultaneous compression and ventilation cpr in human beings. Annals of Emergency Medicine 1986; 15(2):125–130.

[12] Niemann JT, Rosborough JP, Ung S, Criley JM. Coronary perfusion pressure during experimental cardiopulmonary resuscitation. Annals of Emergency Medicine 1982;11(3):127–131.

[13] Sutton RM, French B, Nishisaki A, Niles DE, Maltese MR, Boyle L, Stavland M, Eilevstjønn J, Arbogast KB, Berg RA, et al. American heart association cardiopulmonary resuscitation quality targets are associated with improved arterial blood pressure during pediatric cardiac arrest. Resuscitation 2013;84(2):168–172.

[14] Sutton RM, Friess SH, Naim MY, Lampe JW, Bratinov G, Weiland III TR, Garuccio M, Nadkarni VM, Becker LB, Berg RA. Patient-centric blood pressure–targeted cardiopulmonary resuscitation improves survival from cardiac arrest. American Journal of Respiratory and Critical Care Medicine 2014;190(11):1255–1262.

[15] Navakatikyan MA, Barrett CJ, Head GA, Ricketts JH, Malpas SC. A real-time algorithm for the quantification of blood pressure waveforms. IEEE Transactions on Biomedical Engineering 2002;49(7):662–670.

[16] Li Q, Mark RG, Clifford GD. Artificial arterial blood pressure artifact models and an evaluation of a robust blood pressure and heart rate estimator. Biomedical Engineering Online 2009;8(1):1–15.

Address for correspondence:

Jon Urteaga
Engineering School of Bilbao (UPV/EHU)
jon.urteaga@ehu.eus

A.2.2 First journal paper

	Publication in international journal
Reference	Urteaga, J., Elola, A., Aramendi, E., Berve, P. O., Wik, L., "Invasive arterial blood pressure delineator for cardiopulmonary resuscitation patients during pauses of chest compressions", *Biomedical Signal Processing and Control, 2024*, 94, 106349.
Quality indices	• **Type of publication**: Journal paper indexed in JCR • **Quartile**: Q2 (26/96) based on Web of Science Rank 2022 • **Impact factor**: 5.1

Biomedical Signal Processing and Control 94 (2024) 106349

Contents lists available at ScienceDirect

Biomedical Signal Processing and Control

journal homepage: www.elsevier.com/locate/bspc

Invasive arterial blood pressure delineator for cardiopulmonary resuscitation patients during pauses of chest compressions

Jon Urteaga [a,*], Andoni Elola [b], Elisabete Aramendi [a,c], Per Olav Berve [d], Lars Wik [d]

[a] Department of Communications Engineering, University of the Basque Country, Bilbao, Spain
[b] Department of Electronic Technology, University of the Basque Country, Bilbao, Spain
[c] Biocruces Bizkaia Health Research Institute, Cruces University Hospital, Barakaldo, Spain
[d] Norwegian National Advisory Unit on Prehospital Emergency Medicine (NAKOS), Oslo University Hospital, Oslo, Norway

ARTICLE INFO

Keywords:
Invasive arterial blood pressure
Cardiac arrest
Adaptive thresholding
Wavelet transform

ABSTRACT

Invasive arterial blood pressure (IBP) monitoring is important to assess patient's cardiovascular competence and guide clinical treatment. Besides, international resuscitation guidelines in force suggest its use during Cardiopulmonary Resuscitation (CPR), but current automated algorithms for IBP variables computation were not designed for cardiac arrest patients. A lack of knowledge is detected in the automated processing of IBP signal during CPR.

The aim of this study was to design algorithms for heartbeat detection and for IBP physiological variable computation during CPR, and compare to state-of-the-art (SoA) proposals. The dataset used consists of 81 out-of-hospital-cardiac-arrest (OHCA) patients and two additional public datasets with hemodynamically stable patients. A set of 377 IBP segments, total duration of 1127 min, were extracted from the OHCA dataset during the pauses of chest compressions. The method includes artifact removing from the in IBP using Stationary Wavelet Decomposition and heartbeat detection in the first difference signal. A multicomponent evaluation and two adaptive thresholds were applied to compute IBP physiological variables.

Pulsatile segments with heartbeats were discriminated from pulseless segments with mean (standard deviation) sensitivity(Se)/specificity and positive (PPV)/negative predictive values of 98.8(6.9)/91.6(20.2)% and 97.4(9.7)/98.7(6.1)%, respectively. The heartbeat detection showed 96.1(8.3)% of Se, 96.1(7.6)% of PPV and 95.7(6.4)% of F1-score , with absolute errors of 0.55(2.91)/0.39(4.87)/0.78(6.08) mmHg in systolic, diastolic and pulse pressure values, respectively. The proposed algorithms outperformed SoA solutions with both OHCA and stable patients.

1. Introduction

Cardiac arrest (CA) is defined as cessation of cardiac functions, and out-of-hospital cardiac arrest (OHCA) stands as the predominant cause of annual mortality in Europe and the United States, accounting for respective total death tolls of 275,000 and 420,000 [1–3]. Application of Cardiopulmonary Resuscitation (CPR, chest compressions and ventilations), and defibrillation of shockable heart rhythm increases the survival rates from 4% to above 10% [3]. Many contributions have been proposed to improve CPR quality, to personalize the treatment and to predict the prognosis of the patient. However, the survival rates keep very low worldwide [4–6].

Invasive arterial blood pressure (IBP) is a basic hemodynamic indicator claimed to be promising to monitor treatment and response during OHCA [7]. Blood pressure is defined as the pressure exerted by the blood in the arteries and it is usually monitored through cannulation in a peripheral artery. IBP waveform is widely used in the clinical practice, since it describes the cardiac function of contraction and relaxation, and it contains information about the cardiovascular system, such as heart rate (HR), cardiac rhythms and pressure values [8,9]. That information is essential in modern medicine for cardiovascular disease detection and monitoring in both operating room and intensive care unit [9–13]. There are several techniques to measure the blood pressure signal using, invasive and non-invasive measurement techniques but IBP is the gold standard in cardiovascular health monitoring [14–16].

Recent resuscitation guidelines recommend the use of IBP during treatment of OHCA patients. The association between blood pressure and the survival of patients in CA has been proven, supporting its benefit to guide resuscitation therapy [17,18]. Both European and American guidelines recommend minimum pressure values aligned

* Corresponding author.
E-mail address: jon.urteaga@ehu.eus (J. Urteaga).

https://doi.org/10.1016/j.bspc.2024.106349
Received 19 July 2023; Received in revised form 21 February 2024; Accepted 8 April 2024
Available online 13 April 2024

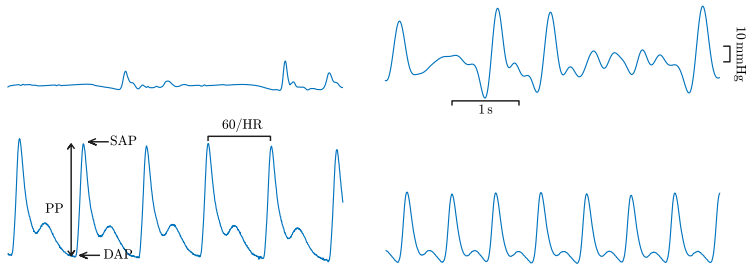

Fig. 1. Four examples of 5 s segments of IBP signals. The two segments at the top correspond to OHCA cases, and the two at the bottom to stable patients from the public datasets. The systolic arterial pressure (SAP), diastolic arterial pressure (DAP), peak pressure (PP) and HR are indicated.

with improved survival rates. During CPR a minimum diastolic arterial pressure (DAP) of 30 mmHg is the goal and a minimum systolic arterial pressure (SAP) of 90 mmHg is recommended before starting post-resuscitation therapy [19–21].

In hemodynamically stable patients, the continuous IBP waveform exhibits systolic peak, diastolic onset and a diastolic notch with each heartbeat [9,22]. SAP is defined as the maximum pressure value achieved during the cardiac contraction phase (ventricular systole), while the DAP is the minimum pressure measured during the cardiac relaxation phase (ventricular diastole). The difference between systolic and diastolic pressures is called pulse pressure (PP) [22,23]. These physiological variables are shown in Fig. 1.

Fiducial points in the IBP are needed to compute main physiological variables as proposed in the literature [8–10,22,24,25]. However, during CA, the IBP signal shows aberrant waveforms with atypical physiological variables. IBP waveform is often distorted by the patient movement, the positioning of the catheter in the artery, the hemodynamic situation or high frequency artifacts, which may lead to unreliable measures of physiological variables. [9,10,26].

Many IBP delineators have shown excellent performance in hemodynamically stable patients, but none has been tested with OHCA patients where a poorer performance is expected. This study proposes new algorithms for heartbeat detection, which permit the discrimination of pulsatile segments, and heartbeat delineation, which permit the calculation of IBP physiological variables. Fig. 2 illustrates the flow chart of the process of pulsatile segment discrimination and the subsequent calculation of physiological variables. The algorithms were tested with both OHCA and hemodynamically stable patients, and compared with state-of-the-art (SoA) algorithms.

2. Materials

Two datasets were used in this study. The first acquired by the emergency medical systems (EMS) during OHCA and the second corresponding to hemodynamically stable patients available in public repositories. To illustrate the differences, examples of continuous IBP waveforms for both datasets are shown in Fig. 1. The greater variability in waveform and amplitude can be observed for the OHCA cases.

2.1. OHCA dataset

The OHCA dataset was extracted from a larger dataset recorded between 2015 and 2017 by physician manned rapid response car of the Oslo EMS. They used Lifepak 15 monitor/defibrillators (Physio-Control, Redmond, United States of America). All episodes included electrocardiogram (ECG) signal recorded through defibrillation pads and IBP waveform signal acquired via onsite radial/femoral cannulation [27].

Segments with concurrent ECG and IBP signals with a sampling frequency of 250 Hz were extracted during the pauses of chest compressions to avoid compression artifacts. A total of 377 segments (total duration of 1127 min) were extracted from 81 patients, median (Interquartile range, IQR) of 4 (4) segments per patient and 39.8 (132.1) s duration.

The instants of systolic peaks (t_{sp}) and diastolic onsets (t_{do}), designated as gold standard, were manually annotated utilizing the IBP and ECG signals with the aid of a ad-hoc created Matlab tool. A minimum PP of 4 mmHg was set for the systolic peaks to consider as heartbeat [28]. A total of 252 segments showed at least one heartbeat and included 75682 systolic peaks. The average values for SAP, DAP and PP were 70.09 (63.90) mmHg, 40.65 (28.00) and 26.01 (38.87) mmHg, respectively.

Fig. 3 illustrates ECG and IBP examples of five different cardiac rhythms from the OHCA dataset [29,30]. Asystole and ventricular fibrillation (VF) are unorganized rhythms, whereas pulsatile rhythm (PR) and pulseless electrical activity (PEA), both true and pseudo PEA, are organized rhythms. Unorganized rhythms and true PEA do not show any fluctuation in the IBP signal as no effective heartbeats are associated with these rhythms. Pseudo PEA shows small fluctuations due to some cardiac mechanical activity, although insufficient to maintain a stable spontaneous circulation as it is the case in PR rhythms.

2.2. Public datasets

The Polysomnographic and the Complex Systems Laboratory (CSL) public datasets were considered to extract the segments from hemodynamically stable patients.

The Polysomnographic dataset, available in PhysioNet,[1] includes ECG and the IBP signal of 18 sleeping patients [31]. Heartbeat annotations in the ECG, fixed with a delay of 200 ms were used to annotate the heartbeats in the IBP signal, as proposed by Zong et al. [10].

The CSL dataset, recorded at Doernbecher Children's Hospital, Oregon Health & Science University, is a standard dataset for the evaluation of IBP delineation algorithms.[2] It contains two episodes of 60 min of IBP signal with systolic peak instants annotated by two expert clinicians [25].

A total of 20 segments (total duration of 5257 min and 381443 annotated heartbeats) were extracted, with a median (IQR) duration of 335 (202.5) s and 22319 (14291) heartbeats per segment.

[1] https://physionet.org/content/slpdb/1.0.0/

[2] https://www.pdx.edu/electrical-computer-engineering/biomedical-signal-processing-lab

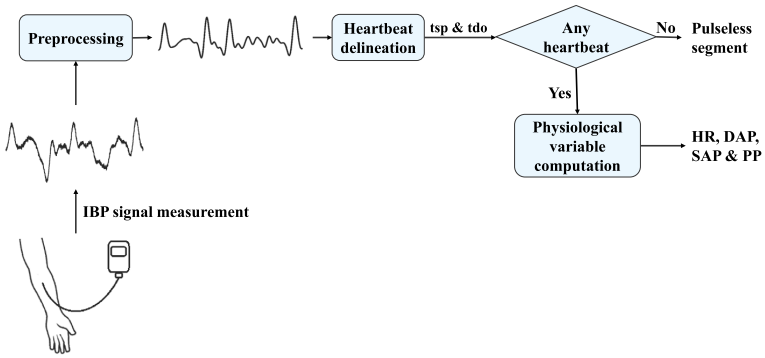

Fig. 2. Detailed flow chart outlining the IBP signal delineation process. It encompasses measurement, preprocessing, heartbeat delineation, discrimination of segments with heartbeats, and computation of IBP physiological variables.

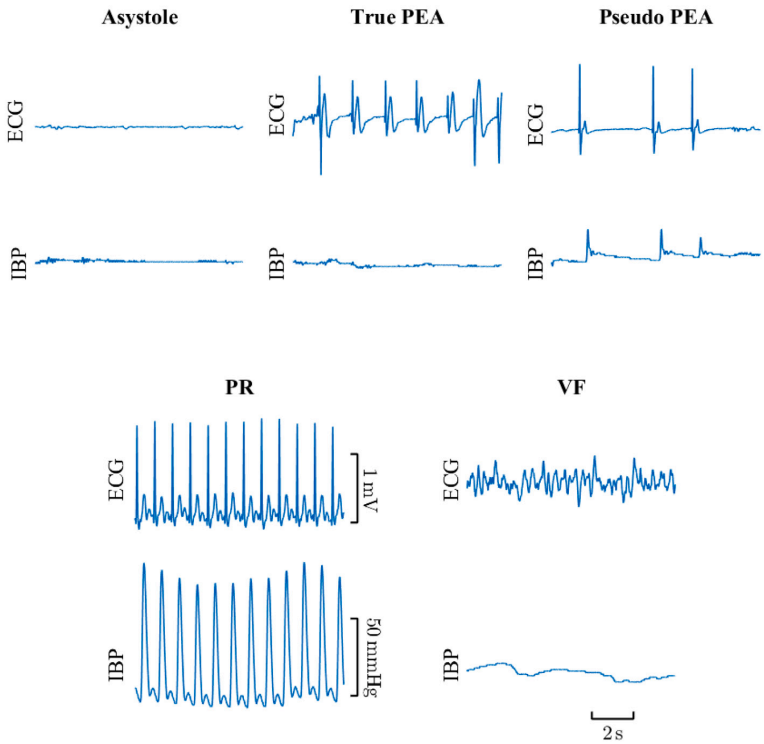

Fig. 3. Examples of 10 s segments of ECG and IBP signals of the dataset, corresponding to different cardiac rhythms. They include rhythms with no heartbeats as asystole, ventricular fibrillation (VF) and true pulseless electrical activity (PEA), and rhythms with heartbeats as pseudo PEA and pulsed rhythms (PR).

3. Methods

This section describes the method proposed to delineate the IBP signal and measure physiological variables. Fig. 4 shows the overall scheme of the method. First, the IBP signal was preprocessed to remove undesired components. Then, a peak detector was applied in the IBP signal's first difference to compute potential heartbeats. Adaptive thresholding was applied based on features associated to each peak to confirm detected heartbeats. Finally, the physiological variables as SAP, DAP, PP and HR were computed in pulsatile segments.

3.1. IBP preprocessing

The raw IBP signal, IBP_{raw}, showed artifacts due to quantification noise, baseline wandering and other high frequency noise. The signal was preprocessed using the stationary wavelet transform (SWT) with 8-level decomposition (Daubechies-4 mother wavelet). In order to reduce noise in the signal, the universal threshold for each segment was calculated in d_2, the 2nd detail coefficients of IBP_{filt}, as follows:

$$\gamma = \sigma\sqrt{2 \cdot ln(N)} \tag{1}$$

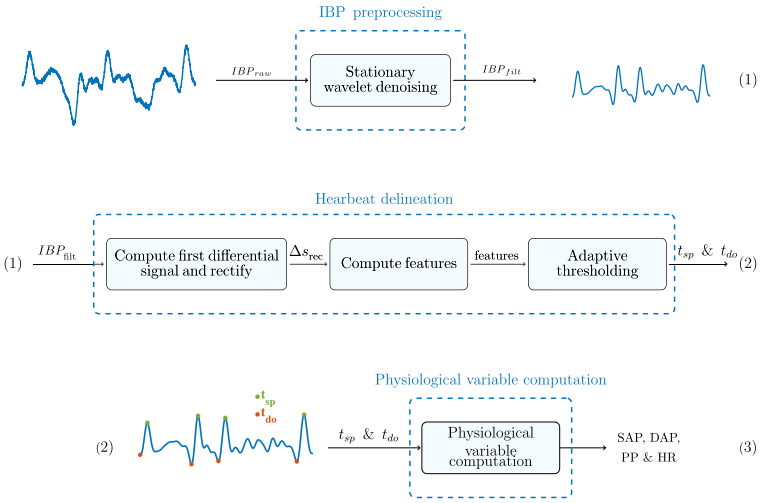

Fig. 4. Overall scheme of the IBP delineator including the preprocessing phase, where original IBP signal (IBP_{raw}) was filtered to obtain IBP_{filt} (1); the heartbeat detection, where t_{sp} and t_{do} were computed from the rectified first difference signal (Δs_{rec}) (2); and the physiological variable computation (3).

when referring to N as the signal's duration and σ is computed as follows:

$$\sigma = \frac{\text{Median}\left\{\left|d_2\right|\right\}}{0.6745} \tag{2}$$

Then, soft thresholding was applied in the rest of the levels for denoising. The filtered IBP signal, IBP_{filt}, was reconstructed using the sixth and seventh detail coefficients.

3.2. Heartbeat detection and delineation

In the heartbeat detection procedure Δs was obtained as the first difference of IBP_{filt} followed by low-pass filtering (zero-phase third order Butterworth filter with a cut-off frequency of 5 Hz). The rectified version, Δs_{rec}, was derived setting to zero the negative values (see Fig. 5).

In Fig. 5, it is noticeable that the peaks of Δs_{rec} are aligned with the maximum slope instants in IBP_{filt}, associated to the heart's contraction which occurs between the diastolic onset and the systolic peak. The t_{sp} instant represents the systolic peak position in the IBP_{filt}, and was located in Δs_{rec} signal detecting the change from positive value to zero (due to rectification). The t_{do} instant represents the diastolic onset position in the IBP_{filt}, and was located in Δs_{rec} signal detecting the change from zero to a positive value.

Local peaks were searched in Δs_{rec} with a minimum distance of 100 ms between consecutive peaks (see Fig. 5). t_{sp} and t_{do} instants of each heartbeat were computed as the first zero value point after and before the peak in Δs_{rec}, respectively. Peaks and onsets were time aligned with the maximum and minimum in a tolerance interval of 100 ms before and after the detected peaks and onsets, respectively. Finally, SAP and DAP values were measured in IBP_{raw}.

The potential heartbeats detected in the previous step were confirmed after applying adaptive thresholding criteria using two physiological variables. Heartbeats with SAP and PP above th_{SAP} and th_{PP}, respectively, were considered as true heartbeats. Thresholds were updated according to the following equations:

$$th_{SAP} = w_{SAP} * \text{median}\{SAP_{i-5}, \ldots, SAP_i\} \tag{3}$$

$$th_{PP} = w_{PP} * \text{median}\{PP_{i-1}, \ldots, PP_{i-5}\} \tag{4}$$

where w_{SAP} and w_{PP} were weights within $[0.05, 0.5]$. The initial value for both thresholds is 5 mmHg and weights were optimized as explained in Section 3.4.

3.3. Computation of physiological variables

For each detected heartbeat SAP and DAP were computed as the values of IBP_{raw} signal at t_{sp} and t_{do} instants, respectively. PP was defined as the difference between SAP and DAP values, and HR was computed as the inverse of the time distance in minutes between consecutive t_{do} instants.

3.4. Statistical evaluation of the methods

3.4.1. Comparison with the SoA algorithms

The IBP delineator proposed in this study was compared to the algorithm proposed by Zong et al. [10] and the delineator proposed by Li et al. [9]. The scripts to implement both methods are public and can be accessed via PhysioNet[3] [32] and Matlab[4] File Exchange, respectively. We used Zong et al.'s function (called *run_wabp*) which takes the IBP signal at a sampling rate of 125 Hz as input and provides the positions of t_{dp} in samples as output. We first resampled our IBP signals from the original sampling rates. In contrast, Li et al.'s function (called *delineator*) requires the IBP signal and the sampling rate as inputs, and delivers both the t_{dp} and t_{sp} instants as outputs.

[3] https://physionet.org/content/pcst/1.0.0/

[4] https://es.mathworks.com/matlabcentral/fileexchange/29484-pulse-waveform-delineator?s_tid=FX_rc3_behav

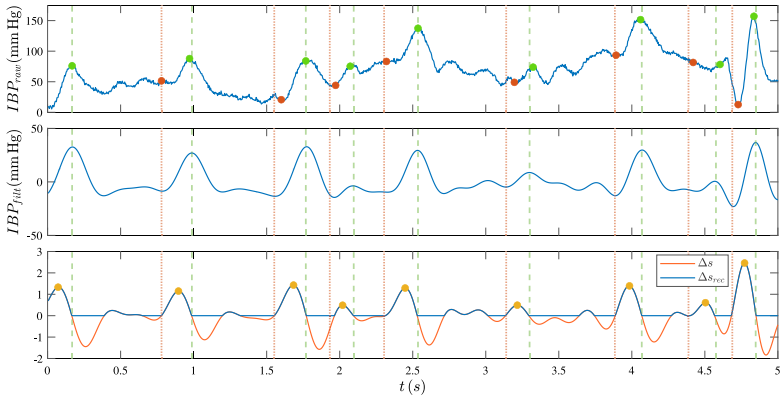

Fig. 5. From top to button: IBP_{raw}, IBP_{filt}; and the first difference signal, Δs (in orange), and rectified first difference signal, Δs_{rec} (in blue). The yellow dots in the button panel indicate maximums of Δs_{rec}. Green and red dots are t_{sp} and t_{do} instants, respectively.

3.4.2. Heartbeat detector

Performance of the detector was given in terms of heartbeat detection sensitivity (Se_{hb}), positive predictive value (PPV_{hb}) and F-score ($F1_{hb}$), harmonic mean of Se_{hb} and PPV_{hb}. Correct detections were defined as those falling within a 50 ms interval around the ground truth annotation, and results were given as patient wise mean (standard deviation, std). This analysis was performed for the segments with at least one heartbeat annotated.

For the OHCA, a 10-fold cross-validation scheme was used to evaluate the heartbeat delineator. The optimization of w_{SAP} and w_{PP} was done in the training set at each iteration to maximize $F1_{hb}$ using a uniform grid search. For public datasets, the weights were set to $w_{SAP} = 0.28$ and $w_{PP} = 0.3$, the mean values of those variables in the OHCA dataset, because the low number of segments made the optimization unfeasible.

3.4.3. Pulsatile segment discrimination

It is essential to correctly discriminate segments with or without heartbeats (see Section 2.1). A secondary analysis was performed to assess the algorithm at discriminating pulsatile segments (segments containing at least one heartbeat). The performance was evaluated in terms of sensitivity (Se_s), specificity (Sp_s), positive predictive value (PPV_s) and negative predictive value (NPV_s); considering as positive class segments with at least one heartbeat. This analysis was only done with OHCA segments, because all segments of the public datasets were pulsatile.

3.4.4. Accuracy of the IBP physiological variables

The physiological variables measured during chest compression pauses from the IBP, i.e., SAP, DAP, PP and HR, were compared to the ground truth. The errors were plotted using Bland-Altman diagrams and the 95% Level of Agreement (LOA).

The measurement of physiological variables by the proposed solution underwent comparison against the SoA in terms of absolute/relative median error LOA. Zong et al. [10] algorithm only computes t_{do}, therefore only DAP and HR were compared. For the method proposed in this study and by Li et al. [9], all physiological variables were compared for the OHCA and CSL datasets. But only DAP and HR were considered in Polysomographic dataset because only t_{do} instants were available.

3.4.5. Signal quality index analysis

For a better interpretation of the performance of our methods, two Signal Quality Indexes (SQI) were applied to the IBP signal: the Non-Binary SQI (NB-SQI) and the jSQI, proposed in [33] and [34], respectively.

Table 1
Overall performance of proposed method compared to SoAs. The OHCA and the two public datasets were used to evaluate the algorithms for heartbeat detection. Performance is provided in terms of mean (std) sensitivity (Se_{hb}),positive predictive value (PPV_{hb}), and F1 ($F1_{hb}$).

		Heartbeat detection		
		Se_{hb} (%)	PPV_{hb} (%)	$F1_{hb}$ (%)
OHCA dataset	Proposed	96.1 (8.3)	96.1 (7.6)	95.7 (6.4)
	Zong [10]	62.8 (36.3)	93.8 (10.5)	71.9 (29.8)
	Li [9]	94.1 (9.6)	85.4 (23.7)	86.7 (19.6)
Public dataset	Proposed	98.4 (1.5)	98.8 (1.3)	98.6 (1.3)
	Zong [10]	97.9 (3.8)	98.4 (3.2)	98.1 (3.4)
	Li [9]	98.6 (1.3)	99.1 (1.0)	98.6 (1.0)

NB-SQI is based on 30-feature vector (computed in time, wavelet and statistical domains) and provides a scalar value between 0–5 for low to excellent heartbeats. jSQI is based on HR, mean pressure and waveform abnormalities, and provides a binary value 0/1 for low/high quality heartbeats.

Every segment was divided into 8 s windows before SQI computation. NB-SQI was normalized (0–1) and jSQI was computed as the fraction of high quality heartbeats in that window. The mean SQI was computed for each segment.

3.5. Time duration analysis

Duration of the pauses with no chest compressions is critical in the survival of a patient in CA, as longer pauses are linked to poorer prognosis. In this study the OHCA segments were extracted from intervals with no chest compressions to avoid artifacts. The effect of the duration of the segment in our algorithms was analyzed. The total segments were split in four groups equally distributed according to their duration, and performance was evaluated in terms of $F1_{hb}$.

4. Results

4.1. Heartbeat detection and pulsatile segment discrimination

Table 1 compares the performance of the proposed heartbeat detection method with SoA algorithms. It can be observed that our solution outperforms previous proposals with the OHCA dataset, and similar performance is reported for the public datasets.

Table 2 provides the performance of the pulsatile segment discriminator for the OHCA consisted of 377 segments (252 pulsatile).

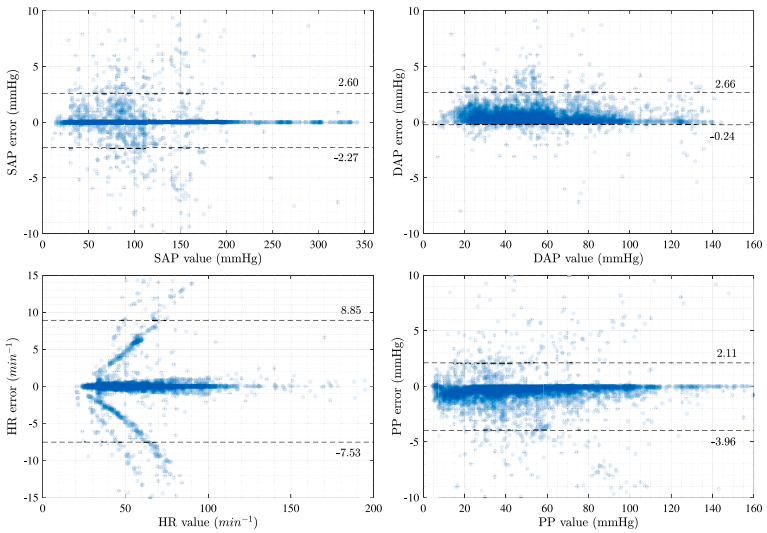

Fig. 6. Blad–Altman diagrams for SAP and DAP in the top panel, and for HR and PP in the panel below. The dashed lines depict the limits of the 95% LOA.

Table 2
Overall performance of proposed method compared to SoAs in OHCA dataset. Performance is provided in terms of sensitivity (Se_s), specificity (Sp_s),positive predictive value (PPV_s), and negative predictive value (NPV_s). All the results were given as patient wise mean (std).

	Pulsatile segment discrimination			
	Se_s (%)	Sp_s (%)	PPV_s (%)	NPV_s (%)
Proposed	98.8 (6.9)	91.6 (20.2)	97.4 (9.7)	98.7 (6.1)
Zong [10]	81.2 (31.0)	75.6 (31.5)	92.4 (20.5)	87.7 (21.8)
Li [9]	99.7 (2.6)	8.9 (23.3)	82.4 (24.4)	88.9 (33.3)

4.2. Accuracy of IBP physiological variables

The comparison of performance between the proposed method and SoA methods in computing physiological variables is presented in Table 3. It can be observed that the proposed algorithm outperforms the SoA algorithms for OHCA dataset. For public datasets, the performance for computing the physiological variables was similar to Li et al. [9] and better than Zong et al. [10].

The detailed error distribution is shown in Fig. 6, where Bland-Altman diagrams report the errors for SAP, DAP, PP and HR. The measured LOA (4.9/2.9/16.4/6.1 mmHg for SAP/DAP/HR/PP) is smaller than using Li et al. (12.8/5.9/45.3/18.2 mmHg) and Zong et al. (-/20.4/-/70.5 mmHg) methods (note that Zong method does not calculate SAP and PP).

4.3. SQI analysis

The values of both indexes, NB-SQI and jSQI, were significantly lower for the OHCA dataset than for the public datasets ($p < 0.05$). The patient wise mean(std) values were 60.42(28.17) vs 91.79(20.88)% for jSQI and 33.47(18.80) vs 75.66(12.10)% for NB-SQI. These results highlight the differences in waveform for the CA IBP compared with stable patients, for which higher SQI are associated attending to current quality measurement methods. OHCA episodes are not hemodynamically stable patients, episodes are noisier and IBP waveform shows more aberrant fluctuations with more variability in peak amplitude.

Fig. 7 shows the violin plots of $F1_{hb}$ for the OHCA dataset segments grouped in quartiles depending on the SQI (highest values in 4th quartile). A clear positive relation can be observed between the performance of the methods and the SQI. Elevated median values and reduced variability were observed in segments of higher quality, varying from median NB-SQI/jSQI values of 0.94/0.92 in Q1 to 0.99/0.99 in 4th quartile.

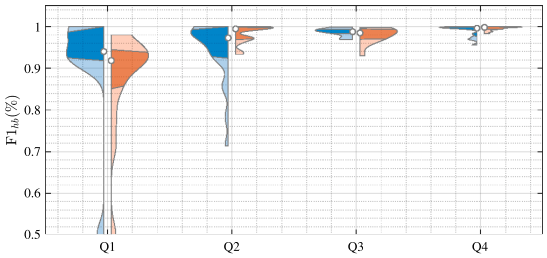

Fig. 7. Violin plots of $F1_{hb}$ for NB-SQI (blue) and jSQI (orange) grouped by SQI quartiles (Q1 the lowest). The white dot indicates the median value, the dark colored areas represent the 25–75 percentile interval, and light colored areas represent values higher than percentile 75 or lower than percentile 25.

4.4. Time duration analysis

The performance of the proposed heartbeat detector for segments of different duration is shown in Fig. 8. Compared to the method by Li et al. [9] it can be observed that both increase performance with longer segments: 97.4%/92.5%, respectively, for 8–16 s segments, and 99.4%/97.9%, respectively, for segments longer than 138 s. The positive correlation between $F1_{hb}$ and the duration of the segment was expected. In OHCA episodes, PR segments (which are the most similar rhythms compared with hemodynamically stable patients) tend to be longer as they were not corrupted by chest compressions, while other organized rhythms such as PEA (more challenging to delineate correctly) need compression therapy and segments without compressions are shorter.

5. Discussion

An automated algorithm for IBP signal delineation and physiological variables computation was proposed. It outperforms SoA solutions

Table 3
Overall performance of proposed method compared to SoAs. The OHCA and public datasets were used to evaluate the algorithms for physiological variable computation. Performance is provided in terms absolute/relative mean (LOA) error.

		IBP physiological variables			
		DAP (mmHg%)	SAP (mmHg%)	PP (mmHg%)	HR (min^{-1}/%)
OHCA	Proposed	0.55(2.89)/1.25(7.05)	0.39(4.87)/0.44(5.74)	0.79(6.07)/2.45(18.91)	1.82(16.39)/2.35(27.54)
	Zong [10]	2.20(20.59)/5.17(47.47)	–(–)/–(–)	–(–)/–(–)	51.50(72.67)/98.24(2.51)
	Li [9]	0.75(5.90)/1.63(13.98)	1.35(12.80)/1.46(15.34)	1.70(16.11)/4.46(45.35)	4.78(45.30)/6.71(69.65)
Public	Proposed	0.19(6.03)/0.26(6.84)	0.35(2.02)/0.39(2.94)[a]	0.78(3.92)/1.63(7.91)[a]	0.17(1.87)/0.08(0.84)
	Zong [10]	0.18(5.98)/0.24(6.88)	–(–)/–(–)	–(–)/–(–)	0.13(14.13)/0.05(8.37)
	Li [9]	0.20(5.87)/0.27(6.56)	0.49(0.64)/0.69(1.03)[a]	0.73(3.68)/1.48(7.81)[a]	0.17(1.66)/0.08(0.80)

[a] In the public dataset, SAP and PP were computed using episodes from CSL dataset because systolic peak annotations were not available in Polysomographic dataset.

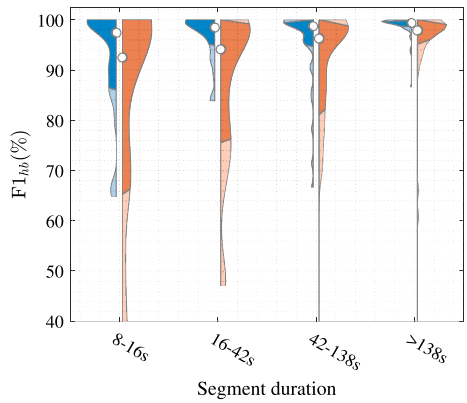

Fig. 8. Violin plots of the proposed heartbeat detector (blue) compared to the method by Li et al. (orange) for segments of different duration. The white dot indicates the median value, the dark colored areas represent the 25–75 percentile interval, and light colored areas represent values higher than percentile 75 or lower than percentile 25.

with OHCA patients in both heartbeat detection and computation of variables as SAP, DAP, PP and HR. To the best of our knowledge, this represents the first proposal tested utilizing the IBP signal of patients suffering CA. The approach was challenging because IBP is not normally available in OHCA and because the waveform highly differs from the IBP signal acquired in hemodynamically stable patients, as those of public datasets.

This study also reports the performance of SoA algorithms with OHCA data. Proposals by Zong et al. and Li et al. exhibit strong performance metrics with stable patients but limited performance with the OHCA database. Both algorithms were designed for stable patients and include low-pass filters (with cutoff frequencies of 16 Hz[10] and 25 Hz[9], respectively). Conversely, the proposed SWT-based filtering in our algorithms applies a more restrictive 1–4 Hz bandpass filter for IBP signals, aligned with the frequency band of interest in OHCA. This more selective filtering effectively removes noise and undesired components during OHCA. Additionally, both SoA algorithms were designed to detect heartbeats in every IBP segment. They compute minimum peak thresholds using either complete or partial segments of the IBP signal, and for pulseless cases as those in CA, they apply a very low minimum threshold. In contrast, our algorithm applies adaptive thresholding, adequate to the variety of IBP signals of both OHCA and public datasets.

Fig. 9 shows the performance of the different algorithms with two examples with different noise levels. In the top example with little noise, all algorithms correctly identify the heartbeats, and the t_{sp}/t_{do} instants. The example in the button with a higher noise level, was more challenging for the SoA algorithms as they incorrectly identify fluctuations as heartbeats (false positives) and miss detecting some heartbeats (false negatives). Mislabeling minor fluctuations as heartbeats distorts physiological variable computation, which jeopardize accurate health assessments in medical algorithms, impacting diagnoses and patient monitoring.

The quality of the signals acquired in out-of-hospital scenario is highly affected by the state of the patients and by external actions that jeopardize the performance of the algorithms. The existing SQIs, such as those for ECG [35–37] or impedance [38,39], have been widely utilized and could serve as the basis for a signal quality control mechanism. The SQIs used in the study were designed for hemodynamically stable patients, and they revealed significantly lower values in OHCA than in the public. It would be beneficial to develop a SQI specifically tailored for the population of hemodynamically unstable patients. By incorporating an appropriate SQI, it would be possible to anticipate the reliability of algorithms, detect low-performance segments, and prevent the occurrence of erroneous values in real applications.

The analysis of IBP during OHCA is associated to many applications in monitoring both the CPR therapy and the patient response. On one hand, goal-directed CPR has shown to improve survival rates in animals [7,40,41], and recent consensus statements from the American Heart Association suggest aiming for a DAP exceeding 25 to 30 mmHg in adult CPR [42]. On the other hand, several blood pressure variables have been associated to post-CA outcomes [20,43]: PP values above 65mmHg happen to be correlated with favorable outcome [43,44], and restoration of PR, in contrast to PEA, can be identified based on IBP metrics avoiding the inaccuracy of pulse palpation [20,43,45,46]. It can be concluded that advanced IBP signal processing might play a crucial role in assisting clinicians and rescue teams in the challenge of enhancing resuscitation treatment. The integration of automated IBP analysis in monitor-defibrillators presents a technological challenge in the development of future resuscitation science.

6. Conclusion

This study proposes an algorithm for the automatic delineation of the IBP signal, which can be used in both hemodynamically stable and OHCA patients. The solution is based on a filtering technique using the STW and adaptive thresholding for peak detection. This method could be employed to automatically calculate physiological variables and assist rescuers in making decisions during OHCA. The progress in this field would ultimately contribute to enhance assessment and care during OHCA, improving patient outcome and survival rates.

7. Limitations

The main limitation of this study relies on the size of the OHCA dataset used. Despite the exceptionality of the IBP records acquired in an out-of-hospital environment, a larger dataset with a variety of defibrillators and more emergency teams and protocols involved, would further support the conclusions of this study.

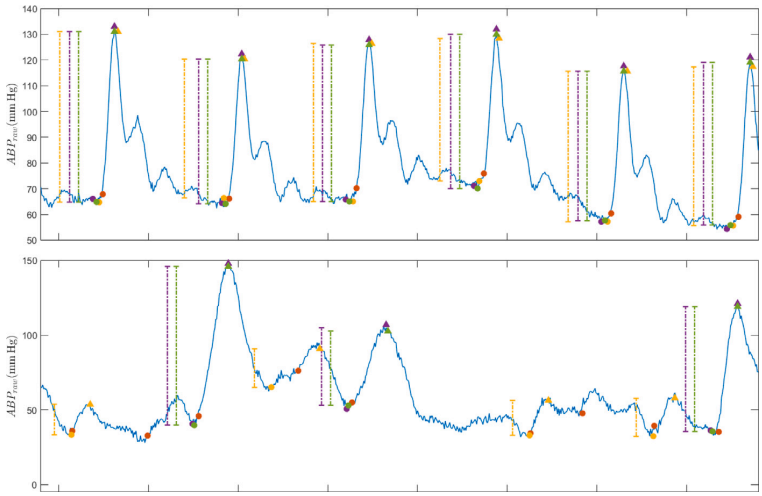

Fig. 9. Two IBP segments of 3 s showing algorithms performance. DAP denoted by dots, SAP by triangles and PP by dash-dotted line. Green, purple, orange, and yellow indicate gold standard, the algorithm proposed in this study, Zong et al.'s algorithm, and Li et al.'s algorithm, respectively.

CRediT authorship contribution statement

Jon Urteaga: Writing – review & editing, Writing – original draft, Visualization, Validation, Software, Methodology, Investigation, Formal analysis, Data curation. **Andoni Elola:** Writing – review & editing, Writing – original draft, Visualization, Validation, Supervision, Software, Methodology, Investigation, Formal analysis, Data curation, Conceptualization. **Elisabete Aramendi:** Writing – review & editing, Writing – original draft, Validation, Supervision, Project administration, Methodology, Investigation, Funding acquisition, Formal analysis, Data curation, Conceptualization. **Per Olav Berve:** Writing – review & editing, Writing – original draft, Resources, Investigation, Data curation, Conceptualization. **Lars Wik:** Writing – review & editing, Writing – original draft, Resources, Investigation, Data curation, Conceptualization.

Declaration of competing interest

The authors declare that they have no known competing financial interests or personal relationships that could have appeared to influence the work reported in this paper.

Data availability

The authors do not have permission to share data.

Acknowledgments

The authors would also like to express our heartfelt gratitude to Fred W. Champan and Fredrick Arnwald (Stryker Ltd.) for their invaluable support and contributions to this study.

This work has been financially supported by the Spanish Ministry of Science, Innovation and Universities through grant PID2021-122727OB-I00, in collaboration with the European Regional Development Fund (FEDER), by the Basque Government, Spain through grants IT1717-22 and PRE2021_2_0173, and by the University of the Basque Country (UPV/EHU), Spain through COLAB20/01.

References

[1] T.D. Rea, R.M. Pearce, T.E. Raghunathan, R.N. Lemaitre, N. Sotoodehnia, X. Jouven, D.S. Siscovick, Incidence of out-of-hospital cardiac arrest, Am. J. Cardiol. 93 (12) (2004) 1455–1460.

[2] S.L. Javan, M.M. Sepehri, H. Aghajani, Toward analyzing and synthesizing previous research in early prediction of cardiac arrest using machine learning based on a multi-layered integrative framework, J. Biomed. Inform. 88 (2018) 70–89.

[3] I. Hasselqvist-Ax, G. Riva, J. Herlitz, M. Rosenqvist, J. Hollenberg, P. Nordberg, M. Ringh, M. Jonsson, C. Axelsson, J. Lindqvist, et al., Early cardiopulmonary resuscitation in out-of-hospital cardiac arrest, N. Engl. J. Med. 372 (24) (2015) 2307–2315.

[4] T.-C. Lu, Y. Chen, T.-W. Ho, Y.-T. Chang, Y.-T. Lee, Y.-S. Wang, Y.-P. Chen, C.-M. Fu, W.-C. Chiang, M.H.-M. Ma, et al., A novel depth estimation algorithm of chest compression for feedback of high-quality cardiopulmonary resuscitation based on a smartwatch, J. Biomed. Inform. 87 (2018) 60–65.

[5] J. Urteaga, A. Elola, E. Aramendi, U. Irusta, E. Alonso, M. Daya, P. Owens, M. Chang, A. Idris, Feasibility of the finger photoplethysmography to give feedback on chest compression rate, Resuscitation 130 (2018) e31.

[6] Y. Maryam, R.M. Sutton, S.H. Friess, G. Bratinov, U. Bhalala, T.J. Kilbaugh, J. Lampe, V.M. Nadkarni, L.B. Becker, R.A. Berg, Blood pressure and coronary perfusion pressure targeted cardiopulmonary resuscitation improves 24-hour survival from ventricular fibrillation cardiac arrest, Crit. Care Med. 44 (11) (2016) e1111.

[7] R.M. Sutton, S.H. Friess, M.Y. Naim, J.W. Lampe, G. Bratinov, T.R. Weiland, III, M. Garuccio, V.M. Nadkarni, L.B. Becker, R.A. Berg, Patient-centric blood pressure–targeted cardiopulmonary resuscitation improves survival from cardiac arrest, Am. J. Respir. Crit. Care Med. 190 (11) (2014) 1255–1262.

[8] O. Singh, R.K. Sunkaria, Empirical wavelet transform-based delineator for arterial blood pressure waveforms, Bio-Algorithms Med-Syst. 12 (2) (2016) 61–66.

[9] B.N. Li, M.C. Dong, M.I. Vai, On an automatic delineator for arterial blood pressure waveforms, Biomed. Signal Process. Control 5 (1) (2010) 76–81.

[10] W. Zong, T. Heldt, G. Moody, R. Mark, An open-source algorithm to detect onset of arterial blood pressure pulses, in: Computers in Cardiology, 2003, IEEE, 2003, pp. 259–262.

[11] H.L. Li-wei, M. Saeed, D. Talmor, R. Mark, A. Malhotra, Methods of blood pressure measurement in the ICU, Crit. Care Med. 41 (1) (2013) 34.

[12] C. Wo, W.C. Shoemaker, P.L. Appel, M.H. Bishop, H.B. Kram, E. Hardin, Unreliability of blood pressure and heart rate to evaluate cardiac output in emergency resuscitation and critical illness., Crit. Care Med. 21 (2) (1993) 218–223.

[13] R. Melamed, K. Johnson, B. Pothen, M.D. Sprenkle, P.J. Johnson, Invasive blood pressure monitoring systems in the ICU: influence of the blood-conserving device on the dynamic response characteristics and agreement with noninvasive measurements, Blood Press. Monitor. 17 (5) (2012) 179–183.

[14] M. Ward, J.A. Langton, Blood pressure measurement, Continuing Educ. Anaesth., Crit. Care Pain 7 (4) (2007) 122–126.

[15] S. Romagnoli, Z. Ricci, D. Quattrone, L. Tofani, O. Tujjar, G. Villa, S.M. Romano, A.R. De Gaudio, Accuracy of invasive arterial pressure monitoring in cardiovascular patients: an observational study, Crit. Care 18 (6) (2014) 1–11.
[16] J. Sende, P. Jabre, B. Leroux, C. Penet, E. Lecarpentier, M. Khalid, A. Margenet, J. Marty, X. Combes, Invasive arterial blood pressure monitoring in an out-of-hospital setting: an observational study, Emerg. Med. J. 26 (3) (2009) 210–212.
[17] R.A. Berg, R.M. Sutton, R.W. Reeder, J.T. Berger, C.J. Newth, J.A. Carcillo, P.S. McQuillen, K.L. Meert, A.R. Yates, R.E. Harrison, et al., Association between diastolic blood pressure during pediatric in-hospital cardiopulmonary resuscitation and survival, Circulation 137 (17) (2018) 1784–1795.
[18] T.D. Bhate, B. McDonald, M.S. Sekhon, D.E. Griesdale, Association between blood pressure and outcomes in patients after cardiac arrest: A systematic review, Resuscitation 97 (2015) 1–6.
[19] R.M. Sutton, B. French, A. Nishisaki, D.E. Niles, M.R. Maltese, L. Boyle, M. Stavland, J. Eilevstjønn, K.B. Arbogast, R.A. Berg, et al., American heart association cardiopulmonary resuscitation quality targets are associated with improved arterial blood pressure during pediatric cardiac arrest, Resuscitation 84 (2) (2013) 168–172.
[20] M.A. Peberdy, C.W. Callaway, R.W. Neumar, R.G. Geocadin, J.L. Zimmerman, M. Donnino, A. Gabrielli, S.M. Silvers, A.L. Zaritsky, R. Merchant, et al., Part 9: post–cardiac arrest care: 2010 American heart association guidelines for cardiopulmonary resuscitation and emergency cardiovascular care, Circulation 122 (18_suppl_3) (2010) S768–S786.
[21] A. Truhlář, C.D. Deakin, J. Soar, G.E.A. Khalifa, A. Alfonzo, J.J. Bierens, G. Brattebø, H. Brugger, J. Dunning, S. Hunyadi-Antičević, et al., European resuscitation council guidelines for resuscitation 2015: section 4. Cardiac arrest in special circumstances, Resuscitation 95 (2015) 148–201.
[22] A. Pachauri, M. Bhuyan, Wavelet transform based arterial blood pressure waveform delineator, Int. J. Biol. Biomed. Eng. 6 (1) (2012) 15–25.
[23] J. Barral, A. Croibier, Circulatory physiology, Visceral Vasc. Manip. (2011) 27–45.
[24] J. Urteaga, A. Elola, E. Aramendi, U. Irusta, P.O. Berve, L. Wik, Automated detection of pulse using continuous invasive arterial blood pressure in patients during cardiopulmonary resuscitation, in: 2021 Computing in Cardiology (CinC), vol. 48, IEEE, 2021, pp. 1–4.
[25] M. Aboy, J. McNames, T. Thong, D. Tsunami, M.S. Ellenby, B. Goldstein, An automatic beat detection algorithm for pressure signals, IEEE Trans. Biomed. Eng. 52 (10) (2005) 1662–1670.
[26] Q. Li, R.G. Mark, G.D. Clifford, Artificial arterial blood pressure artifact models and an evaluation of a robust blood pressure and heart rate estimator, Biomed. Eng. Online 8 (1) (2009) 1–15.
[27] P.O. Berve, B.M. Hardig, T. Skålhegg, H. Kongsgaard, J. Kramer-Johansen, L. Wik, Mechanical active compression-decompression versus standard mechanical cardiopulmonary resuscitation: A randomised haemodynamic out-of-hospital cardiac arrest study, Resuscitation 170 (2022) 1–10.
[28] A. Elola, E. Aramendi, U. Irusta, P.O. Berve, L. Wik, Multimodal algorithms for the classification of circulation states during out-of-hospital cardiac arrest, IEEE Trans. Biomed. Eng. 68 (6) (2020) 1913–1922.
[29] L.F. Polanía, L.K. Mestha, D.T. Huang, J.-P. Couderc, Method for classifying cardiac arrhythmias using photoplethysmography, in: 2015 37th Annual International Conference of the IEEE Engineering in Medicine and Biology Society, EMBC, IEEE, 2015, pp. 6574–6577.
[30] N. Paradkar, S.R. Chowdhury, Cardiac arrhythmia detection using photoplethysmography, in: 2017 39th Annual International Conference of the IEEE Engineering in Medicine and Biology Society, EMBC, IEEE, 2017, pp. 113–116.
[31] Y. Ichimaru, G. Moody, Development of the polysomnographic database on CD-ROM, Psychiatry Clin. Neurosci. 53 (2) (1999) 175–177.
[32] A.N. Vest, G. Da Poian, Q. Li, C. Liu, S. Nemati, A.J. Shah, G.D. Clifford, An open source benchmarked toolbox for cardiovascular waveform and interval analysis, Physiol. Meas. 39 (10) (2018) 105004.
[33] A. Ignácz, S. Földi, P. Sótonyi, G. Cserey, NB-SQI: A novel non-binary signal quality index for continuous blood pressure waveforms, Biomed. Signal Process. Control 70 (2021) 103035.
[34] J. Sun, A. Reisner, M. Saeed, R. Mark, Estimating cardiac output from arterial blood pressurewaveforms: A critical evaluation using the MIMIC II database, in: Computers in Cardiology, 2005, IEEE, 2005, pp. 295–298.
[35] Z. Zhao, Y. Zhang, SQI quality evaluation mechanism of single-lead ECG signal based on simple heuristic fusion and fuzzy comprehensive evaluation, Front. Physiol. 9 (2018) 727.
[36] S. Rahman, C. Karmakar, I. Natgunanathan, J. Yearwood, M. Palaniswami, Robustness of electrocardiogram signal quality indices, J. R. Soc. Interface 19 (189) (2022) 20220012.
[37] U. Satija, B. Ramkumar, M.S. Manikandan, A review of signal processing techniques for electrocardiogram signal quality assessment, IEEE Rev. Biomed. Eng. 11 (2018) 36–52.
[38] X. Jaureguibeitia, E. Aramendi, H.E. Wang, A.H. Idris, Impedance-based ventilation detection and signal quality control during out-of-hospital cardiopulmonary resuscitation, IEEE J. Biomed. Health Inf. (2023).
[39] P.H. Charlton, T. Bonnici, L. Tarassenko, D.A. Clifton, R. Beale, P.J. Watkinson, J. Alastruey, An impedance pneumography signal quality index: Design, assessment and application to respiratory rate monitoring, Biomed. Signal Process. Control 65 (2021) 102339.
[40] A.J. Lautz, R.W. Morgan, M. Karlsson, C.D. Mavroudis, T.S. Ko, D.J. Licht, V.M. Nadkarni, R.A. Berg, R.M. Sutton, T.J. Kilbaugh, Hemodynamic-directed CPR improves neurologic outcomes and mitochondrial function in heart and brain, Crit. Care Med. 47 (3) (2019) e241.
[41] M.Y. Naim, R.M. Sutton, S.H. Friess, G. Bratinov, U. Bhalala, T.J. Kilbaugh, J.W. Lampe, V.M. Nadkarni, L.B. Becker, R.A. Berg, Blood pressure–and coronary perfusion pressure–targeted cardiopulmonary resuscitation improves 24-hour survival from ventricular fibrillation cardiac arrest, Crit. Care Med. 44 (11) (2016) e1111–e1117.
[42] P.A. Meaney, B.J. Bobrow, M.E. Mancini, J. Christenson, A.R. De Caen, F. Bhanji, B.S. Abella, M.E. Kleinman, D.P. Edelson, R.A. Berg, et al., Cardiopulmonary resuscitation quality: improving cardiac resuscitation outcomes both inside and outside the hospital: A consensus statement from the American heart association, Circulation 128 (4) (2013) 417–435.
[43] C.W. Callaway, M.W. Donnino, E.L. Fink, R.G. Geocadin, E. Golan, K.B. Kern, M. Leary, W.J. Meurer, M.A. Peberdy, T.M. Thompson, et al., Part 8: post–cardiac arrest care: 2015 American heart association guidelines update for cardiopulmonary resuscitation and emergency cardiovascular care, Circulation 132 (18_suppl_2) (2015) S465–S482.
[44] J.H. Kilgannon, B.W. Roberts, A.E. Jones, N. Mittal, E. Cohen, J. Mitchell, M.E. Chansky, S. Trzeciak, Arterial blood pressure and neurologic outcome after resuscitation from cardiac arrest, Crit. Care Med. 42 (9) (2014) 2083–2091.
[45] J. Tibballs, P. Russell, Reliability of pulse palpation by healthcare personnel to diagnose paediatric cardiac arrest, Resuscitation 80 (1) (2009) 61–64.
[46] J. Tibballs, C. Weeranatna, The influence of time on the accuracy of healthcare personnel to diagnose paediatric cardiac arrest by pulse palpation, Resuscitation 81 (6) (2010) 671–675.

A.2.3 Second conference paper

	Publication in international conference
Reference	Jon Urteaga, Andoni Elola, Elisabete Aramendi, Anders Norvik, Eirik Unneland, Eirik Skogvoll, "Automated Algorithm for QRS Detection in Cardiac Arrest Patients with PEA", *Computing in Cardiology (CinC), 2022*
Quality indices	• **Type of publication**: International conference in SJR • **Impact factor**: 0.212

Automated Algorithm for QRS Detection in Cardiac Arrest Patients with PEA

Jon Urteaga[1], Andoni Elola[2], Elisabete Aramendi[1,3], Anders Norvik[4], Eirik Unneland[4], Eirik Skogvoll[4]

[1] Department of Communications Engineering, University of the Basque Country, Bilbao, Spain.
[2] Department of Electronic Technology, University of the Basque Country, Bilbao, Spain.
[3] Biocruces Bizkaia Health Research Institute, Cruces University Hospital, Barakaldo, Spain
[4] Department of Circulation and Medical Imaging, Norwegian University of Science and Technology (NTNU), Trondheim, Norway

Abstract

Pulseless electrical activity (PEA) is one of the most common rhythms during a cardiac arrest (CA), and it consists in lack of palpable pulse in presence of electrical activity in the heart. The main treatment for a CA is the cardiopulmonary resuscitation (CPR), including chest compressions and ventilations, together with defibrillation shocks and drugs when necessary. The therapy of PEA depends on its characteristics, mainly the morphology of the QRS complex. Well known algorithms for QRS complex detection and delineation were designed for hemodynamically stable patients with pulsed rhythm (PR). The aim of this study was to develop an automatic method for QRS complex detection in patients with PEA during CA. The database for this study consists of 5128 PEA segments from 264 in-hospital CA patients. The ECG signal was decomposed using the stationary wavelet transform, a peak detector was applied on the third detail component and a multicomponent verification was set to detect the peaks. Finally, a time alignment of the detected QRS complexes was performed using the original ECG signal. The proposed method presents median (IQR) Se/PPV/F1 values of 92.4(15.2)/88.5(15.4)/88.8(15.6) for PEA segments.

1. Introduction

Cardiac arrest (CA) is a main cause of death in the industrialized world, with an average incidence of 55 per 100.000 persons-year and a survival rate below 8.4% [1,2]. An early recognition and a rapid treatment of the CA are essential to enhance survival chance, and the treatment depends on the heart rhythm of the patient [3]. The pulseless electrical activity (PEA) is one of the most frequent rhythms by the time the emergency services arrive, with an incidence between 20-30% and 40-60% in out- and in-hospital CA, respectively [4–6].

PEA is a clinical condition with a electromechanical dissociation, characterized by organized cardiac electrical activity without palpable pulse [7]. The cardiopulmonary resuscitation (CPR) and pharmacological treatment of a PEA during a CA depends on the characteristics of the PEA. Recent studies have shown that PEAs with narrow QRS duration and high slopes have better prognosis and deserve different treatment in contrast to those with wider QRS complex in which immediate pharmacological treatment is advised [8–10].

ECG waves delineation is essential for rhythm characterization. Once ECG is delineated information such as hear rate, and wave segment duration and amplitude features can be computed. The QRS complex is the most characteristic waveform in the ECG and its detection is the most critical step in ECG delineation [11, 12].

Several automatic methods have been proposed in the literature for QRS detection and delineation in patients with pulsed rhythm (PR) [11–15]. Wavelet transform is considered a encouraging technique for QRS detection and delineation. Decomposing ECG in different frequency band details allows discriminating different waves in the ECG avoiding the baseline and high frequency noise [11]. The QRS is usually identified detecting the maximum slope point of the R wave, which is considered the reference point of the QRS complex and it has high amplitude that makes easier to detect [11, 13].

Well known automated QRS detectors have not been evaluated in patients during PEA. In this study an automated algorithm was designed for QRS complex detection in PEA rhythms.

2. Materials

The database used in this study is a subset of a larger in hospital CA episodes database. It consists of 264 episodes, recorded by emergency services and include

ECG, transthoracic impedance (TI) and ventilations signals. 89 of those episodes were from St. Olav University Hospital (Norway), 136 from Hospital of the University of Pennsylvania (USA) and 39 from Penn Presbyterian Medical Center (USA). The 89 episodes from Norway were recorded using LIFEPAK-20 (Stryker, Redmond, USA) defibrillators between 2018 and 2021, while the 175 episodes form USA hospital were recorded using HeartStart MRx-defibrillators (Philips Medical Systems, Andover, Massachusetts, USA) between 2008 and 2010.

All episodes were manually assessed and annotated by expert clinicians. Rhythm type and QRS complexes were annotated in the ECG signal, and the intervals with chest compressions identified in the TI signal. Intervals with duration between 3-6 s were selected in chest compression pauses, and separated in 3 s segments. A total of 5128 segments with a mean duration of $3.47\,\mathrm{s}$ per segment were extracted. The total duration of the database was $335\,\mathrm{min}$, with 19085 heart beats, 3.7 per segment.

3. Methods

Figure 1 shows the overall scheme of the proposed algorithm. First, the ECG signal was decomposed using a 8-level stationary wavelet transform (SWT). Then, possible peaks were searched in the 3rd detail component and a multicomponent evaluation was applied to validate those peaks. Finally, the peak positions were searched in the maximums of the ECG signal.

3.1. SWT decomposition

For the SWT decomposition Daubechies-3 mother wavelet was applied and 8-level decomposition used, following procedures proposed in [2, 15].

3.2. QRS reference point detection

As the energy of the QRS complex is concentrated in 3-40 Hz frequency band [16, 17] the detailed components d3-d5 were analysed to detect the QRS reference points. An example of a PEA segment decomposition in d3, d4 and d5 details is shown in Figure 2.

The QRS reference points were computed in the d3 detail component applying the amplitude threshold given in 1. A minimum peak to peak distance of $100\,\mathrm{ms}$ was established between consecutive peaks.

$$Th_3 = 0.5 * \max(-d3) \tag{1}$$

A multicomponent evaluation was applied in d4 and d5 detail components. Peaks predected in d3 were considered as QRS reference points only if its value in d4 and d5 detail coefficients were above th4 and th5 thresholds:

$$Th_4 = 0.4 * \max(-d4) \tag{2}$$

$$Th_5 = 0.2 * \max(-d5) \tag{3}$$

3.3. Align QRS reference points

Finally, the QRS reference points computed in the previous steps were time aligned with the maximum of the ECG signal in a tolerance interval of $150\,\mathrm{ms}$ before and after the detected peak.

3.4. Statistical evaluation

QRS instants manually annotated by clinicians were considered as ground truth for evaluation purposes. A QRS was considered correct if detected in a range of $100\,\mathrm{ms}$ around the ground truth. Algorithms were evaluated in terms of sensitivity (Se), percentage of correctly detected QRS complexes; positive predictive value (PPV), percentage of detected QRS complexes that are actually QRS; and

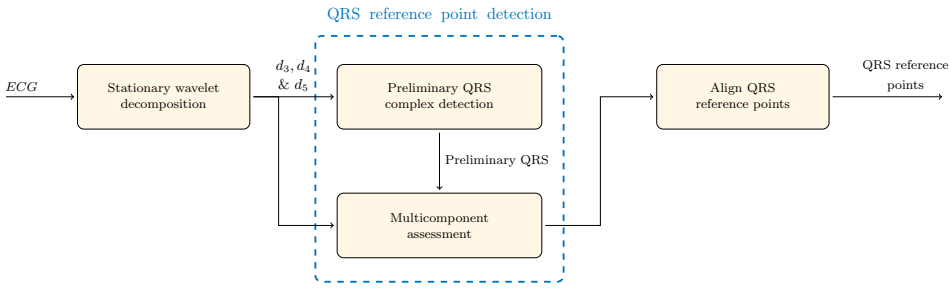

Figure 1. Overall scheme of the automatic algorithm to detect QRS complexes during PEA.

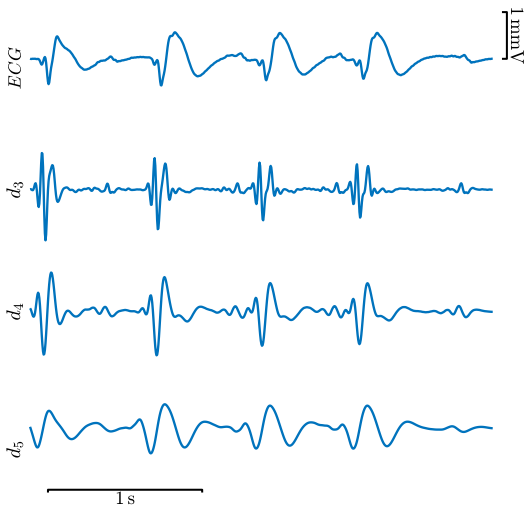

Figure 2. Examples of the ECG signal and its detail components d_3, d_4 and d_5.

F-score (F1), the harmonic mean of Se and PPV. The performance metrics were calculated per patient, and the final results were presented as the median (interquartile range, IQR) for all patients.

The QRS detector proposed in the study was compared with two QRS detection/delineation algorithms proposed in the literature: Martinez et al. [12] and Elola et al. [18].

4. Results

The performance metrics are shown in the Table 1 in terms of Se, PPV and F1. It can be observed that the proposed algorithm outperformed the best literature algorithm in more than 6 points of F1. Its higher Se means that it correctly detects many QRS complexes missed by the other algorithms.

Table 1. Performance metrics for the proposed algorithm and two other methods. The table shows the median (IQR) values for Se, PPV and F1.

	Se (%)	PPV (%)	F1 (%)
This study	92.4 (15.2)	88.5 (15.4)	88.8 (15.6)
Martinez et al. [12]	75.6 (16.4)	89.1 (18.9)	80.0 (16.6)
Elola et al. [18]	82.7 (28.5)	84.5 (28.7)	82.7 (28.3)

5. Discussion and conclusions

The detection and delineation of QRS complexes is widely used in rhythm characterization during CA. However, automated methods proposed in the literature have not been tested with organized PEA rhythms. This study is the fist proposing an automatic algorithm for QRS complex detection in patients in CA presenting PEA.

Comparing to proposals by Martinez et al. [12] and Elola et al. [18], our algorithm outperforms in 10 points of Se with similar PPV values. Two are the main reasons for this improvement. Firstly, the proposed technique is better adapted to the chaotic and variable characteristics of QRS complex during CA. Secondly, CPR therapy implies that the ECG analysis intervals are limited to pauses between compressions, with a duration of 3-10 s. Unlike other published methods, the proposed algorithm was optimized for short-duration segments.

This work is subject to a number of limitations. On the one hand, the database has a limited number of patients, and only in-hospital CA were included in this study. On the other hand, the algorithm assumes that all segments are organized rhythms with PEA, and it would required an adaptation for other organized rhythms or non-organized rhythms.

This study is the first step for the development of automatic algorithms that characterize the QRS complex of PEA patients during a CA. This characterization could assist and guide clinicians in determining the most appropriate resuscitation treatment.

Acknowledgments

This work was supported by the Spanish Ministerio de Ciencia, Innovacion y Universidades through grant RTI2018-101475-BI00, jointly with the Fondo Europeo de Desarrollo Regional (FEDER), by the Basque Government through grant IT1717-22 and grant PRE_2021_2_0173, and by the university of the Basque Country (UPV/EHU) under grant COLAB20/01.

References

[1] Gräsner JT, Bossaert L. Epidemiology and management of cardiac arrest: what registries are revealing. Best practice research Clinical anaesthesiology 2013;27(3):293–306.

[2] Atwood C, Eisenberg MS, Herlitz J, Rea TD. Incidence of ems-treated out-of-hospital cardiac arrest in europe. Resuscitation 2005;67(1):75–80.

[3] Rad AB, Eftestøl T, Engan K, Irusta U, Kvaløy JT, Kramer-Johansen J, Wik L, Katsaggelos AK. Ecg-based classification of resuscitation cardiac rhythms for retrospective data analysis. IEEE Transactions on Biomedical Engineering 2017;64(10):2411–2418.

[4] Urteaga J, Aramendi E, Elola A, Irusta U, Idris A. A machine learning model for the prognosis of pulseless electrical activity during out-of-hospital cardiac arrest. Entropy 2021;23(7):847.

[5] Mader TJ, Nathanson BH, Millay S, Coute RA, Clapp M, McNally B. Out-of-hospital cardiac arrest outcomes stratified by rhythm analysis. Resuscitation 2012;83(11):1358–1362.

[6] Meaney PA, Nadkarni VM, Kern KB, Indik JH, Halperin HR, Berg RA. Rhythms and outcomes of adult in-hospital cardiac arrest. Critical care medicine 2010;38(1):101–108.

[7] Mehta C, Brady W. Pulseless electrical activity in cardiac arrest: electrocardiographic presentations and management considerations based on the electrocardiogram. The American journal of emergency medicine 2012;30(1):236–239.

[8] Bakke M, Borgen A, Norvik A, Skjeflo GW, Irusta U, Dybos Tannvik T, Bergum D, Aramendi E, Eftestol T, Skogvoll E. Physiological effects of adrenaline in human cardiac arrest with pulseless electrical activity: A pilot study. Circulation 2019;140(Suppl_2):A166–A166.

[9] Hauck M, Studnek J, Heffner AC, Pearson DA. Cardiac arrest with initial arrest rhythm of pulseless electrical activity: do rhythm characteristics correlate with outcome? The American Journal of Emergency Medicine 2015;33(7):891–894.

[10] Norvik A, Unneland E, Bergum D, Buckler D, Bhardwaj A, Eftestøl T, Aramendi E, Nordseth T, Abella B, Kvaløy J, et al. Pulseless electrical activity in in-hospital cardiac arrest–a crossroad for decisions. Resuscitation 2022;.

[11] Li C, Zheng C, Tai C. Detection of ecg characteristic points using wavelet transforms. IEEE Transactions on biomedical Engineering 1995;42(1):21–28.

[12] Martínez JP, Almeida R, Olmos S, Rocha AP, Laguna P. A wavelet-based ecg delineator: evaluation on standard databases. IEEE Transactions on biomedical engineering 2004;51(4):570–581.

[13] Zong W, Moody G, Jiang D. A robust open-source algorithm to detect onset and duration of qrs complexes. In Computers in Cardiology, 2003. IEEE, 2003; 737–740.

[14] Vest AN, Da Poian G, Li Q, Liu C, Nemati S, Shah AJ, Clifford GD. An open source benchmarked toolbox for cardiovascular waveform and interval analysis. Physiological measurement 2018;39(10):105004.

[15] Kalidas V, Tamil L. Real-time qrs detector using stationary wavelet transform for automated ecg analysis. In 2017 IEEE 17th International Conference on Bioinformatics and Bioengineering (BIBE). IEEE, 2017; 457–461.

[16] Merah M, Abdelmalik T, Larbi B. R-peaks detection based on stationary wavelet transform. Computer methods and programs in biomedicine 2015;121(3):149–160.

[17] Mahmoodabadi S, Ahmadian A, Abolhasani M, Eslami M, Bidgoli J. Ecg feature extraction based on multiresolution wavelet transform. In 2005 IEEE Engineering in Medicine and Biology 27th Annual Conference. IEEE, 2006; 3902–3905.

[18] Elola A, Aramendi E, Irusta U, Del Ser J, Alonso E, Daya M. Ecg-based pulse detection during cardiac arrest using random forest classifier. Medical biological engineering computing 2019;57(2):453–462.

Address for correspondence:

Jon Urteaga
Engineering School of Bilbao (UPV/EHU)
jon.urteaga@ehu.eus

A.2.4 Second journal paper

	Publication in international journal
Reference	Jon Urteaga, Andoni Elola, Anders Norvik, Eirik Unneland, Trygve C Eftestøl, Abhishek Bhardwaj, David Buckler, Benjamin S Abella, Eirik Skogvoll, Elisabete Aramendi, "A Deep Learning Model for QRS Delineation in Organized Rhythms during In-Hospital Cardiac Arrest", *IEEE Transactions on Biomedical Engineering, 2024* (Submitted)
Quality indices	• **Type of publication**: Journal paper indexed in JCR • **Quartile**: Q2 (34/96) based on Web of Science Rank 2022 • **Impact factor**: 4.6

A Deep Learning Model for QRS Delineation in Organized Rhythms during In-Hospital Cardiac Arrest

Jon Urteaga, Andoni Elola, Daniel Herráez, Anders Norvik, Eirik Unneland, Abhishek Bhardwaj, David Buckler, Benjamin S. Abella, Eirik Skogvoll, Elisabete Aramendi, *Member, IEEE*

***Abstract*— Cardiac arrest (CA) is the sudden cessation of heart function, typically resulting in loss of consciousness and cessation of pulse and breathing. The electrocardiogram (ECG) stands as an essential tool extensively utilized by clinicians, during CA treatment. Within the ECG, the QRS complex reflects the depolarization of the ventricles, yielding valuable perspectives on cardiac health and potential irregularities. The delineation of QRS complexes is crucial for obtaining that information, but classical algorithms have not been tested with CA rhythms. This research aims to introduce a new deep learning-based model for accurately delineating QRS complexes in patients experiencing organized rhythms during in-hospital CA. Two databases have been employed, one comprising 332 episodes of in-hospital CA (151815 QRS complexes) and another consisting of 105 hemodynamically stable patients (112497 QRS complexes). The method comprises three stages: signal preprocessing for noise removal, windowing and sample classification with a U-Net model, and finally, the segmented windows are merged to complete the process. The proposed method exhibited median (interquartile range) F1 score/Sensitivity/Specificity/intersection over union values of 97.03(8.28)/97.69(11.38)/96.47(9.92)/79.09(15.78), and a 8.56(11.62) ms error for $\mathrm{QRS_{on}}$, and 25.11(25.86) ms for $\mathrm{QRS_{off}}$ instant delineation.**

***Index Terms*— Cardiac Arrest, Deep Learning, Delineation, QRS complex, U-Net**

I. Introduction

The electrocardiogram (ECG) is an indispensable tool extensively employed by clinicians to diagnose heart diseases by non-invasively recording the heart's electrical activity. Within the ECG, the QRS complex, consisting of Q, R, and S fiducial points, reflects ventricular depolarization, offering insights into cardiac health and abnormalities [1]–[3].

ECG monitoring is also indispensable during cardiac arrest (CA), which stands as a leading cause of death in industrialized nations. With an average incidence of 55 cases per 100,000 persons-year and a survival rate below 8.4% [4], [5]. Timely recognition and swift intervention are paramount to improve survival rates, with treatment hinging on the patient's heart rhythm [6].

Pulseless electrical activity (PEA) is defined as the electromechanical dissociation between the electrical and mechanical activity of the heart, where the heart shows a organized electrical activity, but lacks a palpable pulse [7]. It is a specific rhythm of CA with a high prevalence as initial rhythm, occurring in 20-30% and 40-60% of out-of-hospital and in-hospital CAs (IHCA), respectively [8]–[10]. The management of PEA during cardiac arrest, including cardiopulmonary resuscitation (CPR) and pharmacological interventions, is contingent upon the specific etiology and characteristics of the PEA. Recent research indicates that PEAs characterized by narrow QRS duration and steep slopes exhibit a more favorable prognosis, while those with wider QRS complexes the prognosis is less favorable. Therefore the latter may require pharmacological intervention or other specific intervention [11]–[13]. Emergency medical services aim to restore spontaneous circulation (ROSC), resulting in a pulsed rhythm (PR).

Both, the PEA and PR, correspond to regular rhythms exhibiting QRS complexes. The delineation of these complexes is crucial for rhythm characterization and essential for computing vital information like heart rate, complex durations, and amplitude features [1], [10]. QRS complex delineation involves precisely identifying the start and end points (QRS_{on} and QRS_{off}) in the waveform, as indicated in Fig. 1, facilitating accurate assessment of the heart's electrical activity and its clinical interpretation [14], [15]. Apart from monitoring patient's vital signs, QRS delineation is a basic preprocessing step for many classification tasks during CA, such as re-arrest prediction, rhythm classification or outcome prediction [16]–[18].

Manually delineating ECG recordings is characterized by a labor-intensive and repetitive task. Consequently, many algorithms have been proposed for ECG signal delineation. These approaches encompass advanced signal processing methodologies [15], [19]–[23] and machine learning techniques or deep learning algorithms [1], [3], [14], [24]–[26]. State of the art (SoA) algorithms have not been assessed within the clinical setting of patients in CA, where irregular, aberrant and uneven QRS complexes are expected [27]. As a result, their applicability in these critical scenarios remain unexplored. As observed in Figure 1, the waveforms of PR and PEA during IHCA differs from the waveform of a stable patient's PR. Hence, the need for a dedicated algorithm for delineation becomes necessary.

The aim of this study is to assess the performance of existing algorithms and propose a new deep learning-based approach for QRS delineation, for both stable and IHCA patients.

II. Materials

This research has been partially supported by the MCIN/AEI/10.13039/501100011033/ and by FEDER Una manera de hacer Europa through grant PID2021-122727OB-I00. Additional support has been provided by the Basque Government through grants IT1717-22 and PRE2021_2_0173, as well as by the University of the Basque Country (UPV/EHU) through COLAB20/01.

Jon Urteaga is with the Communications Engineering Department, University of Basque Country (UPV/EHU), Bilbao, Spain (e-mail: jon.urteaga@ehu.eus).

Andoni Elola is with the Department of Electronic Technology, University of Basque Country (UPV/EHU), Eibar, Spain (e-mail: andoni.elola@ehu.eus).

Daniel Herráez is with Cruces University Hospital, Barkaldo, Spain (e-mail: daniel.herraezmartin@osakidetza.eus).

Anders Norvik, Eirik Unneland and Eirik Skogvoll are with the Department of Circulation and Medical Imaging, Norwegian University of Science and Technology (NTNU), Trondheim, Norway (e-mail: anders.norvik@ntnu.no, eirik.unneland@ntnu.no and eirik.skogvoll@ntnu.no).

Abhishek Bhardwaj is with the University of California, Riverside, USA (e-mail: drabhishekbhardwaj66@gmail.com).

David Buckler is with the Icahn School of Medicine at Mount Sinai, New York, NY, USA (e-mail: David.Buckler@mountsinai.org).

Abella, Benjamin is with the University of Pennsylvania, Philadelphia, Pennsylvania, USA (e-mail: Benjamin.Abella@pennmedicine.upenn.edu).

Elisabete Aramendi is with the Communications Engineering Department, University of Basque Country (UPV/EHU), Bilbao and Biocruces Bizkaia Health Research Institute, Barakaldo, Spain (e-mail: elisabete.aramendi@ehu.eus).

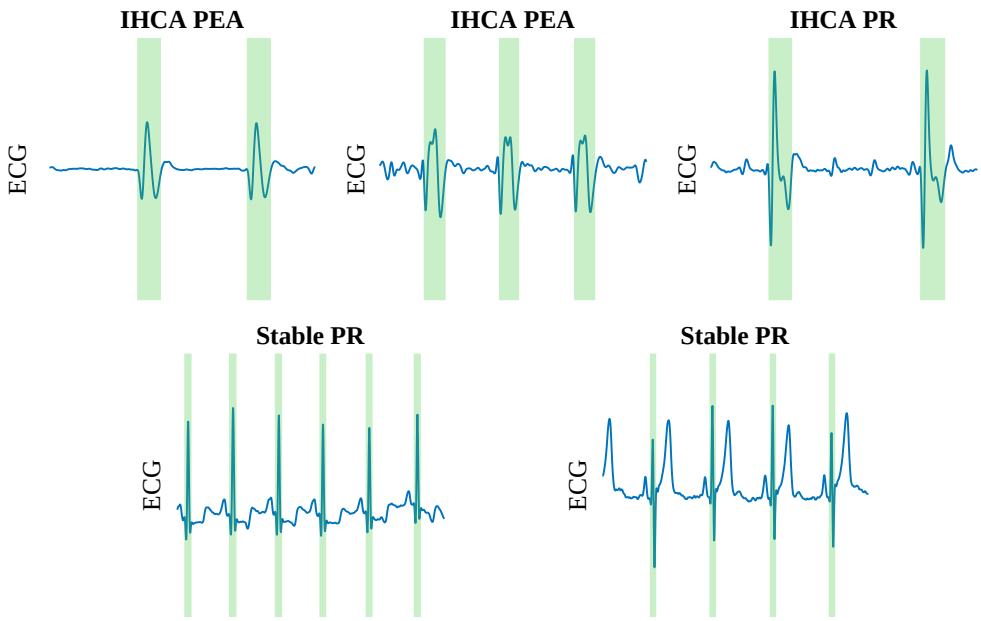

Fig. 1: Examples of 6 s segments of regular rhythms. Two PEA and one PR from IHCA are shown in the upper row. Below, two PR segments from hemodynamically stable patients are presented. QRS complexes are indicated by green shading.

A. IHCA database

The IHCA database utilized in this study is a subset extracted from a larger IHCA database. It comprises a total of 332 episodes that were recorded by emergency services and encompasses ECG and transthoracic impedance (TI). A set of, 124 were from St. Olav University Hospital in Norway, 163 from the Hospital of the University of Pennsylvania in the USA, and 45 from the Penn Presbyterian Medical Center, also in the USA. The 124 episodes from Norway were recorded between 2018 and 2021 using LIFEPAK-20 defibrillators manufactured by Stryker (Redmond, USA). Conversely, the 208 episodes from the US hospitals were captured between 2008 and 2010 using HeartStart MRx defibrillators manufactured by Philips Medical Systems, situated in Andover, Massachusetts, USA. Medical professionals conducted the annotation of rhythms and QRS complexes, which served as the gold standard in this study. Intervals with chest compressions have also been annotated utilizing the transthoracic impedance signal.

ECG segments of organized rhythms (PR/PEA) with a minimum duration of 6 s extracted during pauses in chest compressions, as observed in the transthoracic impedance. In total, 2485 segments were acquired (with mean (standard deviation, SD) duration of 43.6 (188.6) s), amounting to 30 h of data and 151815 QRS complexes. Among these, 978 segments were associated with PR rhythms, totaling 25 h, while the remaining 1507 segments, accounting for 5 h, were associated with PEA rhythms. Three examples of the segments extracted from the IHCA database can be observed in the top row of Figure 1.

B. Public dataset

The dataset of stable patients was extracted from the QT public dataset from Physionet [28], widely used to develop QRS delineation algorithms. The database comprises recordings of 105 patients, resulting in a total duration of 1575 min and 112497 QRS complexes annotated by medical professionals. In Figure 1 two examples of 6 s segments extracted from this database are shown in the lower row.

III. Methods

The method proposed to delineate the QRS complexes is divided into three stages: First, the signal is preprocessed to remove the noise. Next, it is windowed into 6 s overlapping segments to feed the U-Net model dedicated to delineate the QRS complexes, and finally the segmented windows are merged.

A. Preprocessing

The raw ECG signal frequently exhibited movements noise, baseline drift and other high-frequency interferences. The signal (with a sampling frequency of 250 Hz) was decomposed using an 8-level stationary wavelet transform (SWT) with Daubechies-4 mother wavelet. Then the signal was reconstructed using only d_3 (15.62-31.25 Hz), d_4 (7.81-15.62 Hz), d_5 (3.90-7.81 Hz), d_6 (1.95-3.90 Hz) and d_7 (0.98-1.95 Hz) detail coefficients to eliminate undesired components. Details were chosen according to the frequency bands associated to the QRS complexes [2], [10], [29]. The ECG signal was divided into 6 s windows with a 50% overlap to feed the U-Net model. The U-Net model utilized in this study requires the input length to be a multiple of 16. Padding was applied to reach processing segments of 1536 samples.

B. U-Net model

U-NET architecture is a robust deep learning framework widely used in image processing, including medical image segmentation

[30], [31]. It is characterized by the U-shaped encoder-decoder structure, which is able to extract high-level spatial information. The encoder extracts the information from the input data through multiple convolutional layers while employing downsampling blocks to reduce data complexity. The decoder rebuilds the output by employing a combination of convolutional blocks, upsampling techniques, and concatenation operations, restoring the information back to a more detailed and complete state [29], [32], [33].

The architecture employed in this study is a modified version of the U-Net tailored for one-dimensional data (shown in Figure 2).

The encoding path comprises four downsampling blocks, consisting of: Firstly, convolution layers with a filter order of 18 and ReLU activation, batch normalization, and a dropout layer set at a rate of 0.25 to avoid overfitting. Secondly, an additional convolution layer with same filter order, activation and normalization. Finally, a max pooling layer with a pool size of 3 and a stride of 2 is applied, enabling the network to focus on essential features while reducing computational load. This pattern repeats across subsequent blocks, doubling the number of feature maps at each iteration. Following the fourth downsampling block and preceding the first upsampling block, two additional convolutional layers have been incorporated similar to the convolutional layers found within the downsampling block.

The decoding path comprises four blocks, each including: An upsampling layer that duplicates values and concatenation to skip connections (merging the decoder's output with the same-level encoder's feature maps). Convolution layers with a 18 order filter and ReLU activation, followed by a batch normalization layer and a dropout layer with a rate of 0.25. Then, the process is repeated without dropout before passing the feature maps to the next upsampling block. Finally, a convolution of order 18 is applied with sigmoid activation function in order to obtain a single feature map, which is the binary mask. Each element of the obtained binary mask denotes inclusion in the QRS complex (value of 1) or exclusion from the complex (value of 0) as shown in Figure 2.

C. Window merging

Each window processed by the U-net scheme is merged to reconstruct the segment delineated with 1/0 values. Since the overlapping during windowing was 50%, the central 3 s (50% of the window) of consecutive windows were concatenated. This helps avoiding edge effects in cases where the QRS complex is near the beginning or end, providing the model with sufficient information to handle accurately.

D. Training of the Deep Neural Network

The optimizer chosen for this work was the Adaptive Moment Estimation (Adam) method, which is widely used in deep learning due to it capability to dynamically adjusts learning rates for each parameter, resulting in faster convergence and improved model training [34].

The loss function used in the training process of the model was defined as 1-Dice, which is aimed to be reduced during the training. The Dice coefficient measures the similarity between two sets of elements as follows [35], [36]:

$$Dice(A,B) = \frac{2 \cdot |A \cap B|}{|A| + |B|}$$

Where A and B represent the sets being compared, $|A|$ and $|B|$ represent the sizes, and $|A \cap B|$ stands for the number of elements shared between both sets [35]. For this study, A corresponds to the output of the method, and B to the gold standard.

The output of Dice coefficient is a value between 0 and 1, where 0 means no commonality and 1 means complete similarity.

IV. Evaluation

A 10-fold patient wise cross-validation approach was employed to evaluate the model. The dataset was divided into 10 equal parts, enabling the model to be trained and tested 10 times. Each iteration used a different test set, ensuring an impartial evaluation of the model's performance.

A. Metrics

The evaluation of the models was conducted to 1) detect the QRS complexes and 2) delineate the QRS complex detecting the QRS_{on}/QRS_{off}. A tolerance of 100 ms was considered in the QRS detection instant [37], [38], and performance was measured in terms of sensitivity (Se), positive predictive value (PPV), and F1-score, which represents the harmonic mean of Se and PPV. Additionally, time errors in the QRS_{on}/QRS_{off} instant detection were quantified. Lastly, an Intersection over Union (IOU) was calculated, which combines the results in detection and delineation. In cases where the QRS complex was not detected, the IOU value was zero, otherwise, it was calculated using the following formula:

$$IOU(A,B) = \frac{|A \cap B|}{|A \cup B|}$$

Where A and B represent the sets being compared (A corresponds to the QRS gold standard annotations and B to the delineation performed by the method being evaluated), $|A \cap B|$ denotes the overlap area between A and B, and $|A \cup B|$ denotes the total area covered by either A and B, without double-counting.

In each segment, Se, PPV and F1 metrics were calculated for QRS detection. Errors in QRS_{on}/QRS_{off} and IOU were computed as the mean value for all complexes in that segment. The final results are presented in terms of patient wise mean (SD).

Additionally, the error of two physiological parameters were computed: Heart Rate (HR), calculated as the inverse of the mean time difference between consecutive QRS_{on} instants, and the duration of the QRS complex (QRS_{width}), computed as the difference between QRS_{on} and QRS_{off} of each complex.

B. SoA Methods

The proposed method was compared to four SoA algorithms. Two of them, Martinez et al. [15] and Pilia et al. [20], employed advanced signal processing techniques such as Stationary Wavelet Transform and adaptive thresholds. The other two, Peimankar et al. [25] and Camps et al. [14], applied deep learning methods for QRS delineation. The former used convolutional layers and a long short-term memory (LSTM) model, while the latter combined convolutional layers with fully connected neural networks. The source code for the first two methods was available online (PhysioNet[1] and GitHub[2] File Exchange, respectively), and we implemented the other two architectures in accordance with the specifications outlined in their respective papers, adhering to the preprocessing methodologies proposed in this study.

C. Noise analysis

In order to assess the robustness of the proposed algorithm in different contexts where the ECG can be distorted by real-world conditions, a noise analysis was performed. Different types of noise at several signal-to-noise ratio (SNR) levels were added to the ECG, and the QRS detection algorithm performance assessed. The most

[1] https://physionet.org/content/ecgkit/1.0/common/wavedet/

[2] https://github.com/KIT-IBT/ECGdeli/tree/master

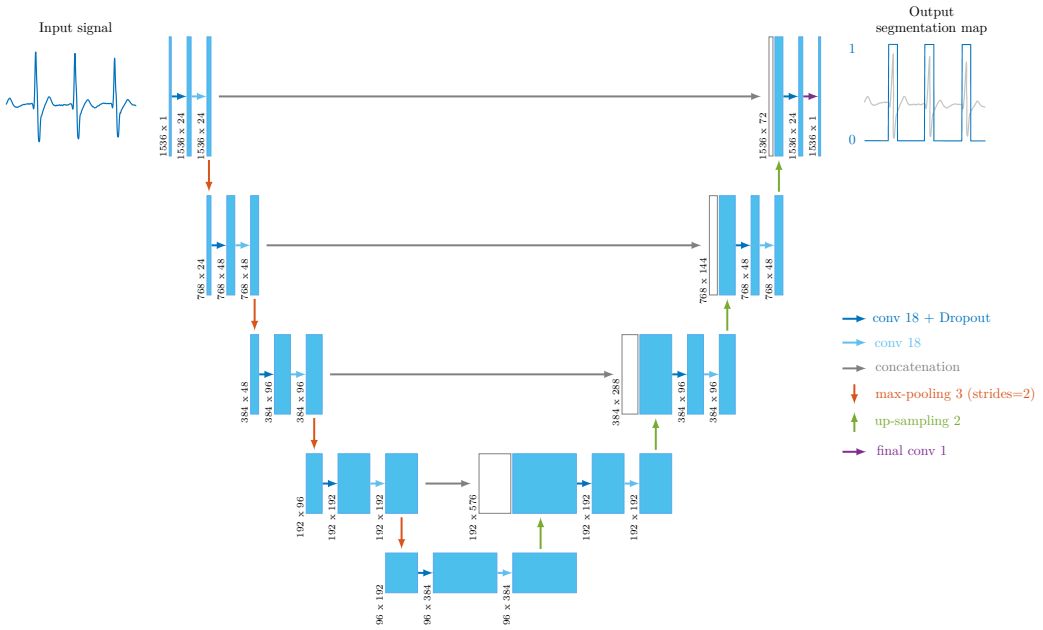

Fig. 2: Overall architecture of the deep learning model for every 6 s window delineation

common noises were artificially generated and added: colored noise, muscular noise, electrode motion noise and baseline wandering.

Colored noise was generated a spectral density function defined by the formula $S(f) \propto \frac{1}{f^{\alpha}}$, where α value sets the variation of the spectral density with frequency: 0 for white and 1 for pink [39]. Noise associated to muscle interference, baseline shifts and electrode movement were extracted from the MIT/BIH open database available in PhysioNet[3].

Aligned with similar analyses in QRS detection robustness [1], [40], [41], SNR values of -6 dB, 0 dB, 6 dB, and 12 dB were tested. The models trained with the clean IHCA dataset, were tested with the segments corrupted with noise.

V. Results

The overall results of the proposed algorithm for the detection and delineation of QRS complexes in the IHCA database can be observed in Table I. The results are reported in the form of the overall True Positive (TP), False Positive (FP), and False Negative (FN) values across the entire dataset. Patient wise mean (SD) values of Se, PPV, F1, IOU and QRS_{on}/QRS_{off} errors are given. It can be observed that the proposed algorithm outperforms other SoA proposals, with F1 and IOU 1.0-7.5 and 0.9-28.8 points higher and QRS_{on}/QRS_{off} errors $0.3-14.3/0.3-13.9$ ms lower. For some segments, the Se was 0, resulting in an indeterminate PPV. Those segments were excluded when computing the mean of F1 (and PPV), which explains why some methods (Martinez et al. and Camps et al.) showed low Se but high F1.

[3]https://physionet.org/content/nstdb/1.0.0/

Performance of the algorithm for the QT database is shown in Table II. It can be observed that Martinez et al. surpasses our proposal by 2.2 points for F1 and IOU, with similar QRS_{on}/QRS_{off} errors. This could be attributed to the fact that SoA algorithms were trained using the QT database. Regarding the deep learning-based algorithms, both Peimankar et al. and Camps et al. demonstrate poorer performance in both detection and delineation, probably due to overfitting with the IHCA database, resulting in a compromised performance on the QT database.

Errors in computing the HR and the QRS duration are shown for the IHCA and the QT datasets in Figure 3 and Figure 4, respectively. It can be observed that our proposal based on the U-Net provides smaller errors than other SoA solutions in IHCA, statistically significant ($p \leqslant 0.005$ Wilconxon test) for all solutions except for Peimankar with QRS width. Comparison with the QT dataset showed lower errors for Martinez et al. and Pilia et al., although not statistically significant in either HR or QRS duration.

Performance of the algorithm for different regular rhythms is shown in Figure 5. In overall, slightly higher performance was observed with PR segments. The mean (SD) values of F1/Se/PPV/IOU/QRS_{on}/QRS_{off} for PEA are 95.84 (7.62)/96.36 (13.51)/94.65 (11.82)/77.07 (15.88)/9.94 (12.59)/26.05 (22.34), while for PR segments, they are 98.47 (4.42)/97.84 (11.86)/98.17 (5.19)/79.72 (13.69)/8.03 (6.60)/23.02 (21.45). Similar results were obtained when comparing performance of the SoA algorithms with PEA and PR rhythms as shown in tables III and IV of the Appendix I. Slightly higher performance with PR rhythms could have been expected as these algorithms were designed with stable patients with

Model	TP	FP	FN	F1(%)	Se(%)	PPV(%)	IOU(%)	QRS_{on}/QRS_{off}(ms)
U-Net	**165302**	2305	**1250**	**97.03 (8.28)**	**97.69 (11.38)**	96.47 (9.92)	**79.09 (15.78)**	**8.56 (11.62)/25.11 (25.86)**
Martinez et al. [15]	106754	**556**	59798	93.80 (14.31)	63.96 (45.46)	**96.98(10.85)**	50.25 (38.11)	8.89 (15.38)/32.73 (34.94)
Pilia et al. [20]	162835	2678	3717	93.30 (13.49)	93.28 (17.84)	93.45(16.06)	61.88 (18.71)	22.92 (19.34)/38.98 (35.08)
Peimankar et al. [25]	163906	2883	2646	96.03 (9.38)	96.93 (12.10)	95.56 (11.20)	78.15 (16.58)	9.34 (14.39)/25.43 (26.14)
Camps et al. [14]	156945	10330	9607	89.55 (17.96)	84.47 (31.40)	92.47(14.32)	59.31 (28.48)	16.78 (22.31)/35.77 (35.71)

TABLE I: Performance of the QRS delineation methods for the IHCA database in terms of mean (SD) values of F1, Se, PPV, IOU and QRS_{on}/QRS_{off} errors.

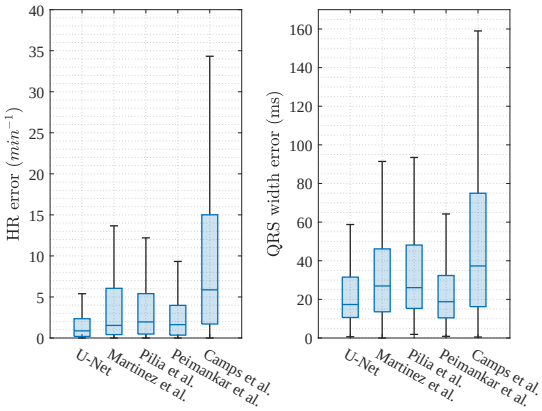

Fig. 3: Boxplots representing the errors of different methods for calculating HR (on the left) and QRS width (on the right) for the IHCA database in terms of median (IQR).

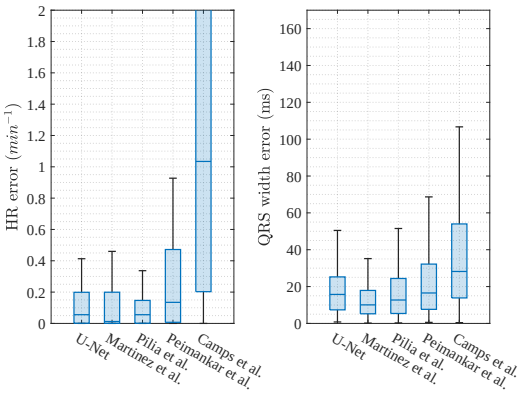

Fig. 4: Boxplots representing the errors of different methods for calculating HR (on the left) and QRS width (on the right) for the QT database in terms of median (IQR).

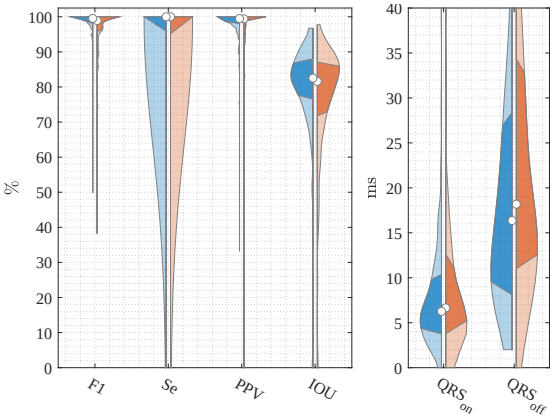

Fig. 5: Performance of the proposed method with PEA (orange) and PR (blue) rhythm segments in terms of F1, Se, PPV, IOU, QRS_{on}, and QRS_{off}. The white point in the middle of the distribution defines the median.

cardiac rhythms closer to PR in ECG waveform and regularity.

An additional independent analysis was conducted, wherein the model proposed in this study was trained using the QT database. The results presented in Appendix II reveal that when training the model with the QT database, the performance of the proposed model is similar to that of Martinez et al., which is the most effective within this particular database.

The performance analysis of the proposed method with different noises can be observed in Figure 6. With a different color line for each type of noise, the QRS detection error in terms of F1 is shown on the left, while the delineation error in terms of QRS_{on} and QRS_{off} are displayed on the center and right panels, respectively. As expected, all performance metrics deteriorate as SNR decreases. Baseline wondering is the most easily manageable noise, whereas electrode movement, white and pink noises are the most challenging, aligned with previous studies [39], [42]. Similar results were obtained in the noise analysis for the SoA methods as provided in Appendix III. They confirm the higher robustness of our proposal across all SNR values and types of noise.

VI. Discussion

The proposed method for QRS complex detection and delineation based on the U-Net architecture has surpassed SoA methods. For the IHCA database, it has demonstrated a mean (SD) QRS detection performance of 97.03 (8.28) %, 97.69 (11.38) % 96.47 (9.92) % in terms of F1, Se and PPV, respectively; a delineation error of 8.56 (11.62) ms for QRS_{on} and 25.11 (25.86) ms for QRS_{off}; and a IOU of 79.09 (15.78) %.

Model	TP	FP	FN	F1(%)	Se(%)	PPV(%)	IOU(%)	QRS_{on}/QRS_{off}(ms)
U-Net	107094	883	3783	97.37 (12.74)	96.39(16.92)	99.23(2.91)	77.11 (16.93)	16.78 (11.80)/11.25 (10.46)
Martinez et al. [15]	110323	**172**	554	**99.63 (1.05)**	99.48 (1.39)	**99.79 (0.86)**	**79.29 (7.03)**	**16.53 (8.74)/11.26 (9.33)**
Pilia et al. [20]	**110509**	850	**368**	99.40 (3.38)	**99.63 (1.28)**	99.32 (4.86)	72.11 (8.76)	16.89 (9.28)/23.33 (17.09)
Peimankar et al. [25]	90568	1198	20309	92.64 (22.49)	79.68 (38.28)	98.05 (11.43)	62.95 (32.21)	19.12 (13.23)/14.56 (14.56)
Camps et al. [14]	97912	8608	12965	86.96 (25.57)	85.92 (29.78)	95.08 (11.11)	61.31 (25.58)	25.34 (18.72)/18.43 (19.66)

TABLE II: Performance of the QRS delineation methods for the QT database in terms of mean (SD) values of F1, Se, PPV, IOU and QRS_{on}/QRS_{off} errors.

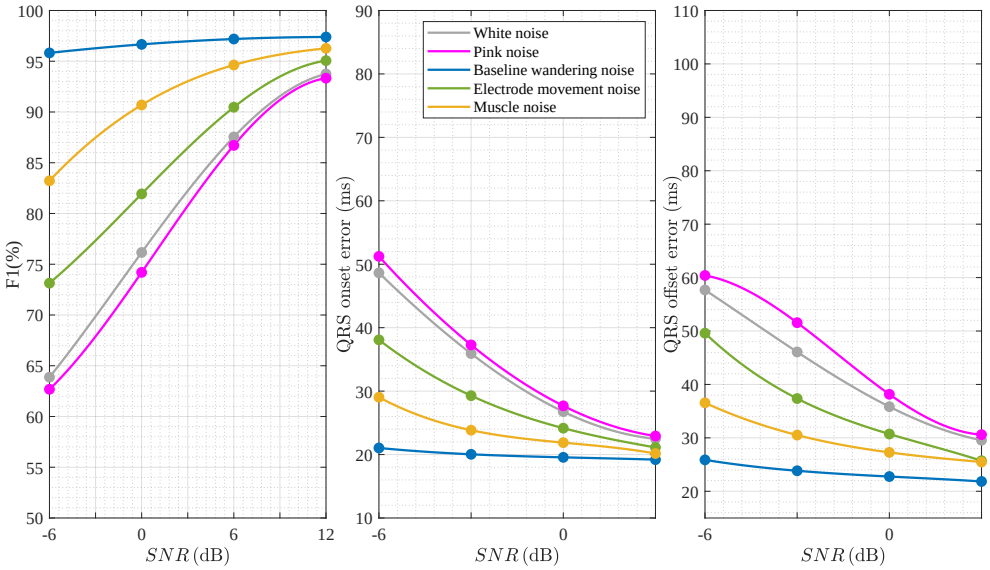

Fig. 6: Performance analysis of the algorithm for different types of noise: white, pink, baseline wandering, electrode motion and muscular. The F1 score, QRS_{on} and QRS_{off} errors are shown int the left, central and right panel, respectively.

The SoA algorithms compared in this study were designed using hemodynamically stable patients, which leads to algorithms that exhibit excellent performance with stable patients but considerably poorer performance when tested on CA patients, specially with PEA rhythms. In contrast, the proposed method demonstrates competency for both patient categories and efficacy with both PR and PEA rhythms, surpassing the SoA methods.

Regarding the deep learning-based methods, the number of trainable parameters was 540931 for the proposed U-Net, 1395038 for Peimankar et al., and 41672 for Camps et al. Consequently, the Peimankar et al. approach requires more time for both the training and testing phases in comparison to the other two methods. This is also attributed to the computational weight associated with the use of LSTM layers, which are inherently more demanding than the convolutional and fully connected layers featured in the alternative methods. It can also be observed in Table II that the Peimankar et al. method performs less effectively when tested on stable patients after being trained with IHCA patients. This may be attributed to overfitting, which seems to be affect less the proposed algorithm which keeps accurate when tested on a different datasets.

The potential applications of a QRS delineation during CA could be manifold in the optimization of the resuscitation therapy. Close relationship between the duration of the QRS complex and the HR with key aspects of CA arrest have been reported, mainly with the cardiac rhythm interpretation, outcome prediction, rearrest prediction, patient response to treatment, etc. [16], [18], [43]–[45]. Application of this algorithm for real-time delineation could be integrated in current monitors in order to monitor therapy and predict evolution through QRS complex features that are currently done using manual annotations [17], [46]–[48]. Additionally, retrospective analysis of massive CA episodes could benefit for the automated delineation of QRS and contribute to research studies of resuscitation therapy efficiency.

VII. Limitations

Algorithms proposed in this study were designed using 332 IHCA patients from three hospitals and 105 stable patients from various healthcare facilities. Diversity in hospitals and patient types contributes to a more comprehensive evaluation, preventing overfitting to a specific patient type or monitoring equipment. However, further assessment is needed for patients experiencing out-of-hospital CA, as such cases may vary slightly from those recorded within hospital settings, potentially affecting the performance of the methods.

VIII. Conclusion

A method employing SWT denoising and U-Net architecture has been introduced for QRS complex segmentation during CA. Demonstrating superiority over comparable SoA methods, it has proven to be reliable with stable patients and robust when exposed to various types of noise.

APPENDIX I
DELINEATION PERFORMANCE FOR PEA AND PR SEGMENTS

The delineation models were tested to analyze their performance with different types of organized rhythms present during CA, i.e. PEA and PR. The results of this analysis are presented in Tables III and IV for PEA and PR segments, respectively. It can be observed that the results for PR segments are slightly better than those for PEA segments.

APPENDIX II
TRAIN WITH QT DATABASE

An extensive analysis was undertaken where the models were trained utilizing the hemodynamically stable patients database (QT database). In Tables V and VI, the performance of this method is shown when tested on the QT and IHCA databases, respectively. The findings demonstrate that upon training the model with the QT database, the performance of U-Net model aligns comparably with that of Martinez et al.

APPENDIX III
NOISE ANALYSIS

Figures 7, 8, 9, and 10 display the performance of methods proposed by Martinez et al., Pilia et al., Peimankar et al., and Camps et al. across multiple noise types at SNR levels of -6 dB, 0 dB, 6 dB, and 12 dB. These comparisons, together with the results of the method proposed in this study depicted in Figure 6, offer valuable insights into the adaptability of these methods under diverse noise conditions.

REFERENCES

[1] J. Liu, Y. Jin, Y. Liu, Z. Li, C. Qin, X. Chen, L. Zhao, C. Liu, A novel p-qrs-t wave localization method in ecg signals based on hybrid neural networks, Computers in Biology and Medicine 150 (2022) 106110.

[2] M. Merah, T. Abdelmalik, B. Larbi, R-peaks detection based on stationary wavelet transform, Computer methods and programs in biomedicine 121 (3) (2015) 149–160.

[3] A. Karimipour, M. R. Homaeinezhad, Real-time electrocardiogram p-qrs-t detection–delineation algorithm based on quality-supported analysis of characteristic templates, Computers in biology and medicine 52 (2014) 153–165.

[4] J.-T. Gräsner, L. Bossaert, Epidemiology and management of cardiac arrest: what registries are revealing, Best practice & research Clinical anaesthesiology 27 (3) (2013) 293–306.

[5] C. Atwood, M. S. Eisenberg, J. Herlitz, T. D. Rea, Incidence of ems-treated out-of-hospital cardiac arrest in europe, Resuscitation 67 (1) (2005) 75–80.

[6] A. B. Rad, T. Eftestøl, K. Engan, U. Irusta, J. T. Kvaløy, J. Kramer-Johansen, L. Wik, A. K. Katsaggelos, Ecg-based classification of resuscitation cardiac rhythms for retrospective data analysis, IEEE Transactions on Biomedical Engineering 64 (10) (2017) 2411–2418.

[7] C. Mehta, W. Brady, Pulseless electrical activity in cardiac arrest: electrocardiographic presentations and management considerations based on the electrocardiogram, The American journal of emergency medicine 30 (1) (2012) 236–239.

[8] T. J. Mader, B. H. Nathanson, S. Millay, R. A. Coute, M. Clapp, B. McNally, Out-of-hospital cardiac arrest outcomes stratified by rhythm analysis, Resuscitation 83 (11) (2012) 1358–1362.

[9] P. A. Meaney, V. M. Nadkarni, K. B. Kern, J. H. Indik, H. R. Halperin, R. A. Berg, Rhythms and outcomes of adult in-hospital cardiac arrest, Critical care medicine 38 (1) (2010) 101–108.

[10] J. Urteaga, A. Elola, E. Aramendi, A. Norvik, E. Unneland, E. Skogvoll, Automated algorithm for qrs detection in cardiac arrest patients with pea, in: 2022 Computing in Cardiology (CinC), Vol. 498, IEEE, 2022, pp. 1–4.

[11] M. Bakke, A. Borgen, A. Norvik, G. W. Skjeflo, U. Irusta, T. Dybos Tannvik, D. Bergum, E. Aramendi, T. Eftestol, E. Skogvoll, Physiological effects of adrenaline in human cardiac arrest with pulseless electrical activity: A pilot study, Circulation 140 (Suppl_2) (2019) A166–A166.

[12] M. Hauck, J. Studnek, A. C. Heffner, D. A. Pearson, Cardiac arrest with initial arrest rhythm of pulseless electrical activity: do rhythm characteristics correlate with outcome?, The American Journal of Emergency Medicine 33 (7) (2015) 891–894.

[13] A. Norvik, E. Unneland, D. Bergum, D. Buckler, A. Bhardwaj, T. Eftestøl, E. Aramendi, T. Nordseth, B. Abella, J. Kvaløy, et al., Pulseless electrical activity in in-hospital cardiac arrest–a crossroad for decisions, Resuscitation (2022).

[14] J. Camps, B. Rodríguez, A. Mincholé, Deep learning based qrs multilead delineator in electrocardiogram signals, in: 2018 Computing in Cardiology Conference (CinC), Vol. 45, IEEE, 2018, pp. 1–4.

[15] J. P. Martínez, R. Almeida, S. Olmos, A. P. Rocha, P. Laguna, A wavelet-based ecg delineator: evaluation on standard databases, IEEE Transactions on biomedical engineering 51 (4) (2004) 570–581.

[16] D. Salcido, M. Sundermann, A. Koller, J. Menegazzi, Towards predicting the time and rhythm of rearrest after out-of-hospital cardiac arrest, Resuscitation 96 (2015) 10.

[17] A. Elola, E. Aramendi, E. Rueda, U. Irusta, H. Wang, A. Idris, Towards the prediction of rearrest during out-of-hospital cardiac arrest, Entropy 22 (7) (2020) 758.

[18] A. Norvik, J. Kvaløy, G. Skjeflo, D. Bergum, T. Nordseth, J. Loennechen, E. Unneland, D. Buckler, A. Bhardwaj, T. Eftestøl, et al., Heart rate and qrs duration as biomarkers predict the immediate outcome from pulseless electrical activity, Resuscitation 185 (2023) 109739.

[19] C. Li, C. Zheng, C. Tai, Detection of ecg characteristic points using wavelet transforms, IEEE Transactions on biomedical Engineering 42 (1) (1995) 21–28.

[20] N. Pilia, C. Nagel, G. Lenis, S. Becker, O. Dössel, A. Loewe, Ecgdeli-an open source ecg delineation toolbox for matlab, SoftwareX 13 (2021) 100639.

[21] N. Spicher, M. Kukuk, Delineation of electrocardiograms using multiscale parameter estimation, IEEE journal of biomedical and health informatics 24 (8) (2020) 2216–2229.

[22] J. M. Bote, J. Recas, F. Rincón, D. Atienza, R. Hermida, A modular low-complexity ecg delineation algorithm for real-time embedded systems, IEEE journal of biomedical and health informatics 22 (2) (2017) 429–441.

[23] C. Böck, P. Kovács, P. Laguna, J. Meier, M. Huemer, Ecg beat representation and delineation by means of variable projection, IEEE transactions on biomedical engineering 68 (10) (2021) 2997–3008.

[24] X. Wang, Q. Zou, Qrs detection in ecg signal based on residual network, in: 2019 IEEE 11th International Conference on Communication Software and Networks (ICCSN), IEEE, 2019, pp. 73–77.

[25] A. Peimankar, S. Puthusserypady, Dens-ecg: A deep learning approach for ecg signal delineation, Expert systems with applications 165 (2021) 113911.

[26] H. Chen, K. Maharatna, An automatic r and t peak detection method based on the combination of hierarchical clustering and discrete wavelet transform, IEEE journal of biomedical and health informatics 24 (10) (2020) 2825–2832.

[27] A. Elola, E. Aramendi, U. Irusta, J. Del Ser, E. Alonso, M. Daya, Ecg-based pulse detection during cardiac arrest using random forest classifier, Medical & biological engineering & computing 57 (2019) 453–462.

[28] P. Laguna, R. G. Mark, A. Goldberg, G. B. Moody, A database for evaluation of algorithms for measurement of qt and other waveform intervals in the ecg, in: Computers in cardiology 1997, IEEE, 1997, pp. 673–676.

[29] Z. Chen, M. Wang, M. Zhang, W. Huang, H. Gu, J. Xu, Post-processing refined ecg delineation based on 1d-unet, Biomedical Signal Processing and Control 79 (2023) 104106.

[30] X.-X. Yin, L. Sun, Y. Fu, R. Lu, Y. Zhang, et al., U-net-based medical image segmentation, Journal of Healthcare Engineering 2022 (2022).

[31] G. Du, X. Cao, J. Liang, X. Chen, Y. Zhan, Medical image segmentation based on u-net: A review., Journal of Imaging Science & Technology 64 (2) (2020).

[32] G. Jimenez-Perez, A. Alcaine, O. Camara, U-net architecture for the automatic detection and delineation of the electrocardiogram, in: 2019 Computing in Cardiology (CinC), IEEE, 2019, pp. Page–1.

[33] S. L. Oh, E. Y. Ng, R. San Tan, U. R. Acharya, Automated beat-wise arrhythmia diagnosis using modified u-net on extended electrocardiographic recordings with heterogeneous arrhythmia types, Computers in biology and medicine 105 (2019) 92–101.

Modelo	TP	FP	FN	F1(%)	Se(%)	PPV(%)	IOU(%)	QRS_{on}/QRS_{off}(ms)
U-Net	**16046**	540	**456**	96.23 (9.82)	**96.99 (13.22)**	95.67 (11.77)	**78.40 (17.85)**	**8.93 (13.21)/26.41 (27.82)**
Martinez et al. [15]	10798	**281**	5704	**98.46 (14.82)**	64.08 (45.86)	**95.98 (12.81)**	50.12 (38.16)	9.86 (17.77)/33.90 (34.41)
Pilia et al. [20]	15574	1093	928	91.25 (15.42)	91.45 (21.09)	90.95 (19.00)	60.66 (20.26)	23.89 (20.39)/40.73 (35.04)
Peimankar et al. [25]	16036	741	466	95.23 (10.88)	96.83 (13.03)	94.32 (13.53)	77.31 (18.12)	10.21 (16.89)/27.81 (28.67)
Camps et al. [14]	14107	1411	2395	89.92 (17.00)	81.92 (34.63)	91.51 (16.19)	56.37 (30.81)	18.55 (25.45)/38.14 (38.13)

TABLE III: Performance of the QRS delineation methods for PEA segments of the IHCA database in terms of mean (SD) values of F1, Se, PPV, IOU and QRS_{on}/QRS_{off} errors.

Modelo	TP	FP	FN	F1(%)	Se(%)	PPV(%)	IOU(%)	QRS_{on}/QRS_{off}(ms)
U-Net	**149256**	1765	**794**	**98.27 (4.85)**	**98.78 (7.58)**	97.77 (5.83)	**80.16 (11.81)**	8.01 (8.62)/22.39 (22.39)
Martinez et al. [15]	95956	**275**	54094	94.33 (13.48)	63.77 (44.86)	**98.49 (6.57)**	50.45 (38.05)	7.41 (10.58)/30.94 (35.68)
Pilia et al. [20]	147261	1585	2782	96.39 (9.06)	96.11 (10.49)	97.25 (8.82)	63.77 (15.84)	21.45 (17.56)/36.36 (35.00)
Peimankar et al. [25]	147870	2142	2180	97.27 (6.23)	97.07 (10.52)	97.48 (5.51)	79.44 (13.77)	**7.99 (9.18)/21.78 (21.18)**
Camps et al. [14]	142838	8919	7212	89.04 (19.21)	88.39 (25.14)	93.82 (11.07)	63.84 (23.76)	14.33 (16.70)/32.46 (31.78)

TABLE IV: Performance of the QRS delineation methods for PR segments of the IHCA database in terms of mean (SD) values of F1, Se, PPV, IOU and QRS_{on}/QRS_{off} errors.

Modelo	TP	FP	FN	F1(%)	Se(%)	PPV(%)	IOU(%)	QRS_{on}/QRS_{off}(ms)
U-Net	**110668**	1620	**209**	99.31 (2.89)	**99.78 (0.98)**	98.97 (4.54)	**92.88 (5.64)**	**4.98 (4.50)/5.11 (7.01)**
Martinez et al. [15]	110323	**172**	554	**99.63 (1.05)**	99.48 (1.39)	**99.79 (0.86)**	79.29 (7.03)	16.53 (8.74)/11.26 (9.33)
Pilia et al. [20]	110509	850	368	99.40 (3.38)	99.63 (1.28)	99.32 (4.86)	72.11 (8.76)	16.89 (9.28)/23.33 (17.09)
Peimankar et al. [25]	108763	885	2114	98.72 (5.46)	97.71 (12.01)	99.01 (3.06)	90.09 (14.50)	5.55(6.05)/6.58(10.61)
Camps et al. [14]	107942	6883	2935	95.82 (10.23)	97.08 (10.51)	95.44 (11.68)	81.25 (17.45)	12.74 (14.11)/12.81 (19.44)

TABLE V: Performance of the QRS delineation methods trained and tested using QT database in terms of mean (SD) values of F1, Se, PPV, IOU and QRS_{on}/QRS_{off} errors.

Model	TP	FP	FN	F1(%)	Se(%)	PPV(%)	IOU(%)	QRS_{on}/QRS_{off}(ms)
U-Net	161642	6175	4910	93.17 (12.42)	94.40 (17.49)	92.52 (13.99)	**71.75 (19.15)**	17.96 (16.72)/28.66 (27.85)
Martinez et al. [15]	106754	**556**	59798	**93.80 (14.31)**	63.96 (45.46)	**96.98(10.85)**	50.25 (38.11)	**8.89 (15.38)/32.73 (34.94)**
Pilia et al. [20]	**162835**	2678	**3717**	93.30 (13.49)	93.28 (17.84)	93.45(16.06)	61.88 (18.71)	22.92 (19.34)/38.98 (35.08)
Peimankar et al. [25]	161727	6620	4825	92.68 (12.31)	**94.76 (15.26)**	91.41 (15.15)	71.05 (17.96)	19.74 (18.63)/28.19 (26.81)
Camps et al. [14]	154846	11026	11706	87.65 (19.74)	83.84 (32.54)	90.01 (16.84)	57.07(28.38)	21.82 (22.21)/37.49 (37.03)

TABLE VI: Performance of the QRS delineation methods testing the IHCA database after being trained in QT database in terms of mean (SD) values of F1, Se, PPV, IOU and QRS_{on}/QRS_{off} errors.

[34] I. K. M. Jais, A. R. Ismail, S. Q. Nisa, Adam optimization algorithm for wide and deep neural network, Knowledge Engineering and Data Science 2 (1) (2019) 41–46.

[35] R. R. Shamir, Y. Duchin, J. Kim, G. Sapiro, N. Harel, Continuous dice coefficient: a method for evaluating probabilistic segmentations, arXiv preprint arXiv:1906.11031 (2019).

[36] B. Wang, X. Yan, Q. Jiang, Z. Lv, Generalized dice's coefficient-based multi-block principal component analysis with bayesian inference for plant-wide process monitoring, Journal of Chemometrics 29 (3) (2015) 165–178.

[37] Z. Zidelmal, A. Amirou, M. Adnane, A. Belouchrani, Qrs detection based on wavelet coefficients, Computer methods and programs in biomedicine 107 (3) (2012) 490–496.

[38] C. Meyer, J. F. Gavela, M. Harris, Combining algorithms in automatic detection of qrs complexes in ecg signals, IEEE Transactions on Information Technology in Biomedicine 10 (3) (2006) 468–475.

[39] R. Sameni, M. B. Shamsollahi, C. Jutten, G. D. Clifford, A nonlinear bayesian filtering framework for ecg denoising, IEEE transactions on Biomedical Engineering 54 (12) (2007) 2172–2185.

[40] A. K. Dohare, V. Kumar, R. Kumar, An efficient new method for the detection of qrs in electrocardiogram, Computers & Electrical Engineering 40 (5) (2014) 1717–1730.

[41] K.-M. Chang, S.-H. Liu, Gaussian noise filtering from ecg by wiener filter and ensemble empirical mode decomposition, Journal of Signal Processing Systems 64 (2011) 249–264.

[42] J. Eilers, J. Chromik, B. Arnrich, Choosing the appropriate qrs detector., in: BIOSIGNALS, 2021, pp. 50–59.

[43] T. P. Aufderheide, R. K. Thakur, H. A. Stueven, C. Aprahamian, Y.-R. Zhu, D. Fark, K. Hargarten, D. Olson, Electrocardiographic characteristics in emd, Resuscitation 17 (2) (1989) 183–193.

[44] G. W. Skjeflo, T. Nordseth, J. P. Loennechen, D. Bergum, E. Skogvoll, Ecg changes during resuscitation of patients with initial pulseless electrical activity are associated with return of spontaneous circulation, Resuscitation 127 (2018) 31–36.

[45] A. Bhardwaj, D. J. Ikeda, A. V. Grossestreuer, K. R. Sheak, G. Delfin, T. Layden, B. S. Abella, M. Leary, Factors associated with re-arrest following initial resuscitation from cardiac arrest, Resuscitation 111 (2017) 90–95.

[46] J. Urteaga, E. Aramendi, A. Elola, U. Irusta, A. Idris, A machine learning model for the prognosis of pulseless electrical activity during out-of-hospital cardiac arrest, Entropy 23 (7) (2021) 847.

[47] A. Elola, E. Aramendi, U. Irusta, P. O. Berve, L. Wik, Multimodal algorithms for the classification of circulation states during out-of-hospital cardiac arrest, IEEE Transactions on Biomedical Engineering 68 (6) (2020) 1913–1922.

[48] J. Urteaga, E. Aramendi, A. Elola, A. Norvik, E. Unneland, A. Bhardwaj, D. Buckler, B. Abella, E. Skogvoll, The prediction of pulseless electrical activity evolution during in-hospital cardiac arrest using machine learning, Circulation 146 (Suppl_1) (2022) A220–A220.

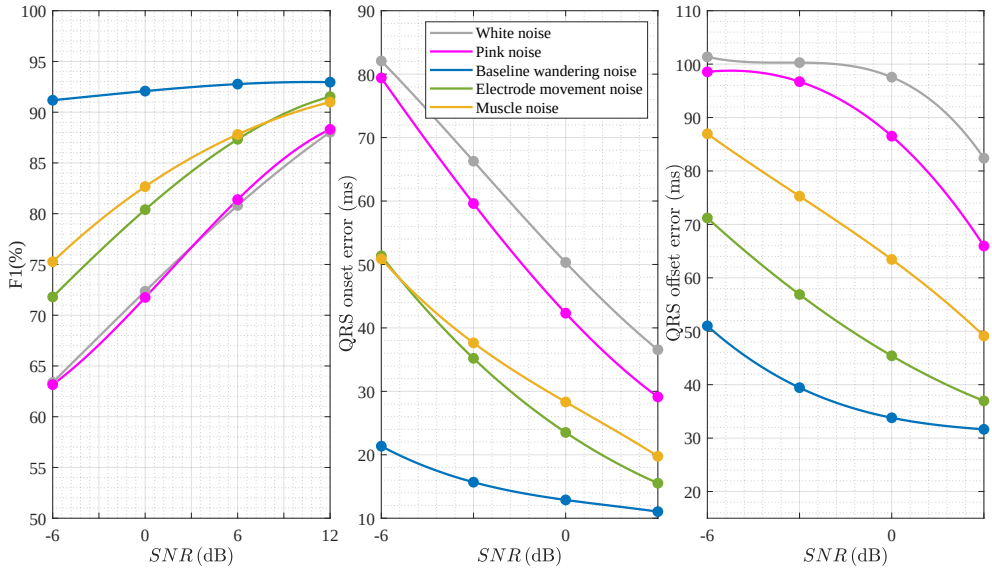

Fig. 7: Performance analysis of the Martinez et al. method for different types of noise: white (in gray), pink (in pink), baseline wandering (in blue), electrode motion (in green), and muscular (in yellow). The F1 score, QRS_{on} and QRS_{off} values are shown int the left, central and right panel, respectively.

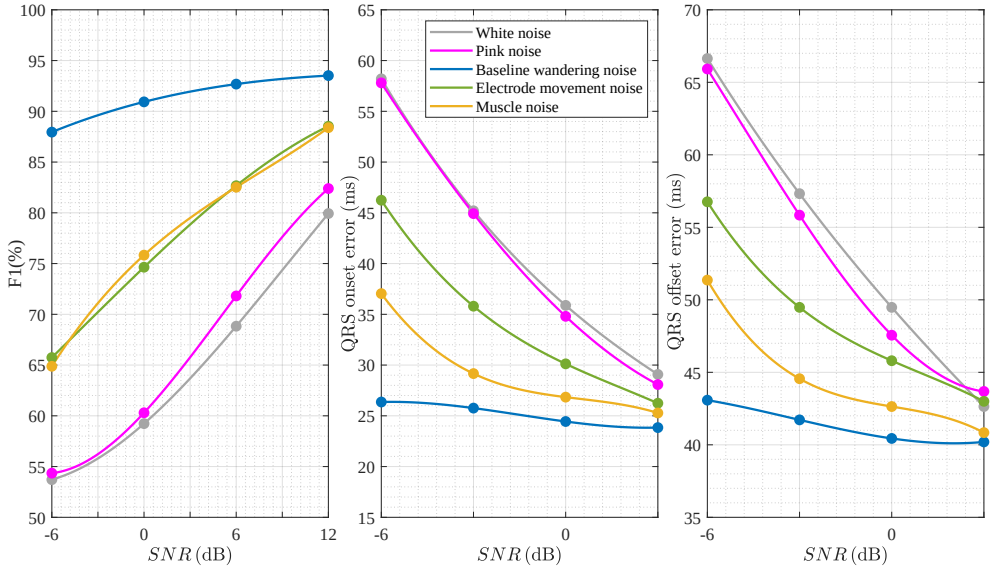

Fig. 8: Performance analysis of the Pilia et al. method for different types of noise: white (in gray), pink (in pink), baseline wandering (in blue), electrode motion (in green), and muscular (in yellow). The F1 score, QRS_{on} and QRS_{off} values are shown int the left, central and right panel, respectively.

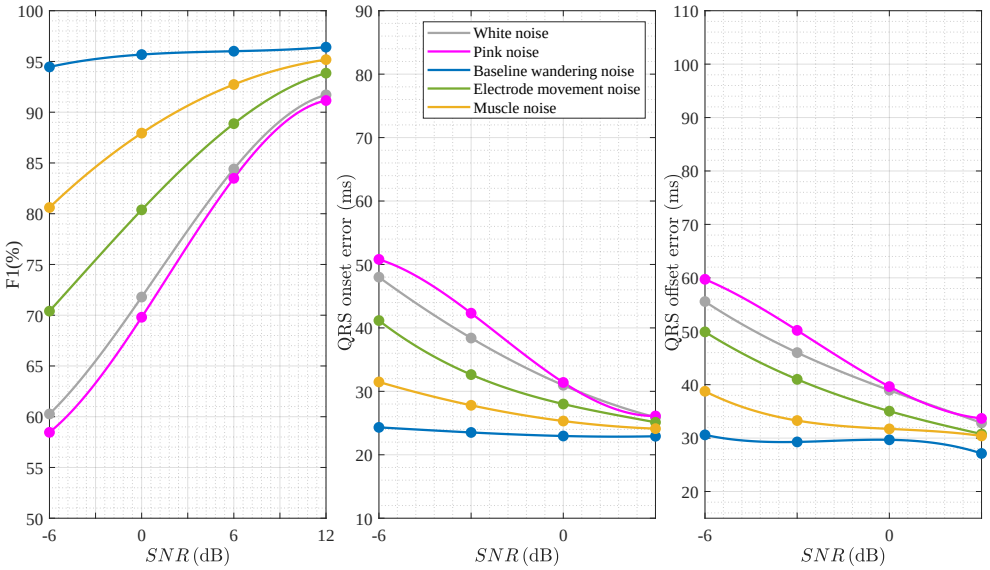

Fig. 9: Performance analysis of the Peimankar et al. method for different types of noise: white (in gray), pink (in pink), baseline wandering (in blue), electrode motion (in green), and muscular (in yellow). The F1 score, QRS_{on} and QRS_{off} values are shown int the left, central and right panel, respectively.

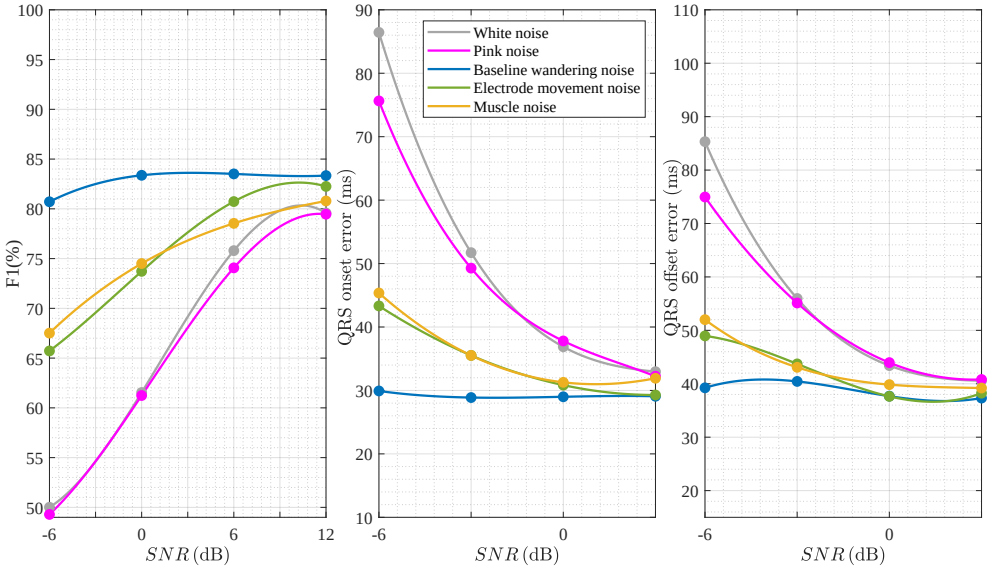

Fig. 10: Performance analysis of the Camps et al. method for different types of noise: white (in gray), pink (in pink), baseline wandering (in blue), electrode motion (in green), and muscular (in yellow). The F1 score, QRS_{on} and QRS_{off} values are shown int the left, central and right panel, respectively.